

FACULTY OF ENGINEERING SCIENCE  
DEPARTMENT OF CHEMICAL ENGINEERING  
Process Engineering for Sustainable Systems (ProcESS)  
Celestijnenlaan 200F - box 2424B-3001 HEVERLEEB,  
BELGIUM  
tel. + 32 48 79 98614  
ruijun.zhang@kuleuven.be  
www.website.kuleuven.be



Ruijun ZHANG

FABRICATION OF HIGH PERFORMANCE NANOFILTRATION MEMBRANES  
FOR WASTEWATER TREATMENT IN THE PETROLEUM INDUSTRY

June 2021

**KU LEUVEN**

ARENBERG DOCTORAL SCHOOL  
FACULTY OF ENGINEERING SCIENCE

# FABRICATION OF HIGH PERFORMANCE NANOFILTRATION MEMBRANES FOR WASTEWATER TREATMENT IN THE PETROLEUM INDUSTRY

**Ruijun ZHANG**

Supervisor:

Prof. Bart Van der Bruggen

Dissertation presented in partial  
fulfilment of the requirements for the  
degree of Doctor of Engineering  
Science (PhD): Chemical Engineering

June 2021

# FABRICATION OF HIGH PERFORMANCE NANOFILTRATION MEMBRANES FOR WASTEWATER TREATMENT IN THE PETROLEUM INDUSTRY

Ruijun ZHANG

Supervisor:

Prof. Bart Van der Bruggen

Members of the Examination committee:

Prof. Patrick Wollants (Chairman, KU Leuven)

Prof. Steffen Waldherr (KU Leuven)

Prof. Arne Verliefde (Ghent University)

Prof. Jo De Vrieze (KU Leuven)

Prof. Jiuyang Lin (Fuzhou University, China)

Dissertation presented in

partial fulfilment of the

requirements for the

degree of Doctor of Engineering

Science (PhD): Chemical Engineering

June 2021

© 2021 Ruijun ZHANG

Uitgegeven in eigen beheer, Ruijun ZHANG, Celestijnenlaan 200f - box 2424, 3001 Leuven

Alle rechten voorbehouden. Niets uit deze uitgave mag worden vermenigvuldigd en/of openbaar gemaakt worden door middel van druk, fotokopie, microfilm, elektronisch of op welke andere wijze ook zonder voorafgaandelijke schriftelijke toestemming van de uitgever.

All rights reserved. No part of the publication may be reproduced in any form by print, photoprint, microfilm, electronic or any other means without written permission from the publisher

## **Acknowledgements**

Just like a movie, so many important moments appear in my mind as I'm finishing the PhD thesis. When I was a high school student, an English teacher from Australia told me two things related to the water in my hometown. The first one was that he never drank the tap water in China because of the poor water quality. The second one was that once rain water in the school yard could be collected and treated, it can meet the water consumption of the swimming pool in the school, which was empty all the year due the water shortage. These two things shocked me so much. So from then on, I decided to engage in the career related to water treatment. From 2008 to 2014, I completed the undergraduate study and Master study successively. And also in 2014, I met Prof. Bart for the first time during an international conference held in China. Before the first meet, I saw "Bart Van der Bruggen" many times in the literatures when I was reading academic papers. I even thought this author must be an aged professor well-versed in membrane technology. I cannot believe this internationally renowned expert was so approachable and graceful, and the short communication between us made me so excited. Dear Prof. Bart, I still remember that "KU Leuven (1425)" was clearly printed on the card you gave me, which was carefully kept into the pocket of my suit jacket. Since then, to study with you in KU Leuven has become my dream. I'm so lucky that a chance hit me in 2017; China Scholarship Council (CSC) of the Ministry of Education agreed to fund my study abroad. So I immediately sent an email to you. I'm so grateful that you accepted me even without an interview. I still remember that wonderful moment; the moment when one's dream came true.

So first and foremost, I would like to present my extreme gratitude to my esteemed promoter, Prof. Bart Van der Bruggen, for his continuous support, invaluable advice, and patience during my PhD study both in and out of KU Leuven. The knowledge, plentiful experience as well as the life philosophy of Prof. Bart have enlightened me in all the time of my academic research and daily life. So becoming a man like you, who

can make contributions to his family, to the society, to the students and even to all the people around, is also my life pursuit.

My gratitude extends to Prof. Patrick Wollants from the Department of Materials Engineering, KU Leuven, for being the chairman of the jury for my PhD defense. I also would like to express my sincere gratitude to my assessors, Prof. Arne Verliefde (Ghent University) and Prof. Steffen Waldherr (Department of Chemical Engineering, KU Leuven) for their help, valuable comments and knowledgeable suggestions during my entire doctoral years. Without your help, I could not come to this part of my PhD. I express my deep appreciation to Prof. Jo De Vrieze (Department of Chemical Engineering, KU Leuven) and Prof. Jiuyang Lin (Fuzhou University, China) for agreeing to be my jury members and their enlightening advices. I'm also rather grateful to three special persons: Prof. Shuili Yu (Tongji University, China), Prof. Wenxin Shi (Chongqing University, China) and Prof. Jiayu Tian (Hebei University of Technology, China) for their trust and full support during my study, work and even life. I always consider why I can be so lucky that so many people would like to help me at different stages of my life.

There are so many people to thank for their help and accompany in Leuven. I would like to thank my friends, lab mates, colleagues and research team: Bin Liu, Junyong Zhu, Shushan Yuan, Jian Li, Miaomiao Tian, Xin Li, Yan Zhao, Zhijuan Zhao, Yi Li, Tim, Indah, and many other members for a cherished time spent together in the lab. I still remember it was Bin Liu who came to the railway station to pick me up in a cold morning when I arrived at Leuven. I still remember so many joyous parties held by Junyong, Shushan, Yan, Zhijuan and Indah, during which we talked freely and drank with pleasure. I still remember the lively and cheerful journeys together with Bin, Xin, Yan, Yi, and Zhijuan. I still remember that Tim usually told me to relax myself and took me to attend the local special activities in Belgium. I also would like to say thanks to my friends in Leuven: Wei Guo, Qinghua Tao and Zeyuan Xu. All the wonderful moments together with you in Leuven will stay in my memory forever. I hope all of you will have a bright future. I do believe the world today is small, so we will meet

again in a better state in the future.

My appreciation also goes to my colleagues which help me a lot during my PhD. First of all, I would like to express my sincere gratitude to Alena, Herman, Michele, Christine, Hannae and Jacques. PhD research is a complex process influenced by many factors, and it's your help from various aspects that promote the successful completion of my PhD. I gratefully acknowledge the China Scholarship Council (CSC) of the Ministry of Education for funding me to study in KU Leuven. It is a precious experience to look at China from the outside world. I would like to act as a small bridge to enhance the communication and cooperation between China and Belgium.

Last but not least, I would like to express my deepest gratitude to my families. Family is a source of unconditional love and a resource for all of us to weather life's changes and challenges. No matter the time and place, family is always the harbor waiting for me which can give me encouragement. It has been 19 years since I left home to study away from my parents. Thanks to my father and mother, your understanding and supporting are always the strongest power to support me through the tough time. I hope I can make you proud. Thanks to my brother and sister-in-law, you have assumed more responsibilities for me to take care of our parents, and also give me the care like parents as well as friends. Thanks to my son, thank you for your healthy growth. From your birth to now, four years of time, I have been more engaged with the PhD research, so I always feel guilty for my dereliction of a father. Finally, I would like to thank my wife, we have been together for nine years, but all kinds of difficulties cannot erase your smile. You look weak, but you give so much love, understanding, and support to me and our family.

Ruijun ZHANG

June 2021



## Abstract

With regard to the current situation of water shortage and increasingly strict environmental emission standards in petroleum industry, reusing petroleum wastewater after advanced treatment with nanofiltration (NF) technology becomes a reasonable choice, which can simultaneously decrease clean water consumption and wastewater discharge. However, the accessible commercial NF membranes in the market are not designed for the treatment of petroleum wastewater. Direct application of these ill-suited NF products will cause numerous problems including serious membrane fouling, improper foulant rejection and low water permeability. The inner structure and physicochemical features of a specific NF membrane are the main factors affecting membrane fouling, solute rejection and permeability. Therefore, this thesis intends to improve the performance of NF membranes from the perspective of membrane fabrication and modification aiming for the advanced treatment of wastewater in petroleum industry.

In order to improve the anti-fouling ability of the NF membranes used for the treatment of polymer flooding produced water, which is one important wastewater in petroleum industry, a novel thin film composite NF membrane was firstly prepared *via* the interfacial polymerization between serinol and trimesoyl chloride catalyzed by 4-dimethylaminopyridine (DMAP) on a flat-sheet polyether sulfone substrate membrane. The results showed that this novel NF membrane presented remarkable antifouling ability compared with the commercial product (NF90), due to its the stronger hydrophilicity, smoother surface structure and lower salt rejection. The optimized membrane fabricated with 0.05% (w/v) trimesoyl chloride (TMC), 1.0% (w/v) serinol, and 10% DMAP had a molecular weight cut-off (MWCO) of 474 Da and water permeability of  $6.0 \text{ L m}^{-2} \text{ h}^{-1} \text{ bar}^{-1}$ . The salt rejections followed the order of  $\text{Na}_2\text{SO}_4 > \text{MgSO}_4 > \text{NaCl} > \text{MgCl}_2$ , and the values were 96.27%, 83.92%, 58.68% and 28.76%,



respectively. It was inferred that the relatively low water permeability resulted from the support membrane pore blockage (SMPB).

In terms of the SMPB phenomenon, various conceptual models were proposed to expound it. SMPB was regulated by changing the monomer concentration, the pore size of the support membrane and the lag time after aqueous phase coating. The results indicate that SMPB can decrease the membrane water permeability. Nevertheless, the comparison between different interfacial polymerization techniques suggested that SMPB could improve the adhesion between support membrane and the selective layer through a “mechanical interlocking effect”, which should be rather meaningful to enhance the membrane long-term stability. It is expected to relieve SMPB by the proper selection of monomer concentration, lag time after aqueous phase coating and support membrane pore size. In order to prepare a NF membrane with desirable properties, SMPB should be alleviated on the premise of ensuring the membrane stability.

To make use of the antifouling ability of serinol and avoid the negative influence of SMPB, serinol was used to modify the piperazine based NF membrane through the acylation reaction between the amino group of serinol and the residual acyl chloride groups on the nascent membrane. Attenuated total reflection-Fourier transform infrared confirmed the successful covalent grafting of serinol on the nascent NF membrane. Atomic force microscope and Field emission scanning electron microscopy characterization suggested that this modification process did not change the membrane morphology. Contact angle goniometer, surface Zeta potential analyzer, and Toluidine blue O (TBO) technique indicated that the grafting process effectively improved the membrane hydrophilicity and decreased the surface carboxyl density. The results demonstrated that the modification of the active layer with serinol grafting can substantially improve the water permeability without sacrificing the desalting ability and rejection for neutral solutes. When treating the model PFPW, the serinol-grafted membrane showed excellent antifouling ability and satisfactory rejections against  $\text{Ca}^{2+}$ ,

Mg<sup>2+</sup>, SO<sub>4</sub><sup>2-</sup> and total organic carbon (TOC). This is rather meaningful in the case of treating polymerflooding produce water aiming for reuse in polymer flooding oil extraction.

In terms of the heavy metals presented in wastewater produced by petroleum refinery and petrochemical plants, research was further conducted to enhance the NF membranes' removing capacity against heavy metals, which would affect the petroleum wastewater reclamation. It was found that a NF membrane with desirable water permeability and high heavy metal removal could be fabricated by decreasing the TMC concentration to an exceptional low extent. The optimized NF membrane prepared with 0.6 w/v% PIP and 0.03 w/v% TMC had the smallest mean effective pore radius of 0.305 nm, weakened negative charge (isoelectric point =5.1) and moderate polyamide (PA) film thickness of 50 nm. All these features endowed its outstanding removal efficiency of about 98% against Ni<sup>2+</sup>, Zn<sup>2+</sup>, Cu<sup>2+</sup>, and more than 92.7% against Cd<sup>2+</sup>, and simultaneously keeping a high pure water permeability of 14.6 L m<sup>-2</sup> h<sup>-1</sup> bar<sup>-1</sup>. The simplicity, low cost and scaling up feasibility of the current strategy is expected to well meet the requirements of industrial production.

To further improve the water permeability and reduce the energy consumption during the treatment of petroleum wastewater with NF technology, a TFC NF membrane with ultrathin PA film was constructed by simultaneously optimizing the monomer concentration and substrate membrane selection. It was demonstrated that an ultrathin PA film can be directly generated on a commercial substrate membrane with in-situ interfacial polymerization (ISIP) technique by using the low piperazine concentration of 0.05 w/v% and high TMC concentration of 0.1 w/v%. Moreover, it was found that the commercial substrate membrane with strong hydrophilicity, smooth surface morphology and medium pore size could provide a homogeneous and intact "phase interface" for the stable interfacial polymerization during the ISIP process. Therefore, an ultrathin PA film (8.5 nm) with narrow pore size distribution can be directly

constructed on the substrate membrane. The resultant NF membrane successfully broke the trade-off between permeability and solute rejection, thus presenting an ultrahigh pure water permeability of  $46.6 \text{ L m}^{-2} \text{ h}^{-1} \text{ bar}^{-1}$  and a high  $\text{Na}_2\text{SO}_4$  rejection of 98.1%. The simplicity of fabrication may promote its industrialized application in the future. In conclusion, the outcome of this thesis is expected to improve the antifouling ability, solute rejection and permeability of the NF membranes that would be adopted in the treatment of petroleum wastewater in view of water recycling.

## Samenvatting

The translation will be done for the revised abstract in the final manuscript.

Gezien de huidige situatie van waterschaarste en steeds strengere milieu-emissienormen in de petroleumindustrie, wordt hergebruik van petroleumafvalwater na geavanceerde behandeling met nanofiltratie (NF) -technologie een redelijke keuze, die tegelijkertijd het verbruik van schoon water en de lozing van afvalwater kan verminderen. De in de handel verkrijgbare NF-membranen op de markt zijn echter niet ontworpen voor de behandeling van petroleumafvalwater. Directe toepassing van deze ongeschikte NF-producten zal tal van problemen veroorzaken, waaronder ernstige membraanvervuiling, onjuiste afstoting van vervuilende stoffen en lage waterdoorlatendheid. De inwendige structuur en fysisch-chemische kenmerken van een specifiek NF-membraan zijn de belangrijkste factoren die membraanvervuiling, selectiviteit en permeabiliteit beïnvloeden. Daarom is dit proefschrift bedoeld om de prestaties van NF-membranen te verbeteren vanuit het perspectief van membraanfabricage en -modificatie met als doel de geavanceerde behandeling van afvalwater in de petroleumindustrie.

Om het aangroeiwerende vermogen van de NF-membranen die worden gebruikt voor de behandeling van polymeeroverstromend geproduceerd water (PFPW), een belangrijk afvalwater in de aardolie-industrie, te verbeteren, werd eerst een nieuw dunne film composiet (TFC) NF-membraan bereid via de grensvlakpolymerisatie (IP) tussen serinol en trimesoylchloride (TMC) gekatalyseerd door 4-dimethylaminopyridine (DMAP) op een vlakke plaat polyethersulfon (PES) substraatmembraan. De resultaten toonden aan dat dit nieuwe NF-membraan een opmerkelijk antifouling-vermogen vertoonde in vergelijking met het commerciële product (NF90), vanwege de sterkere hydrofiliciteit, gladdere oppervlaktestructuur en lagere zoutafstoting. Het geoptimaliseerde membraan vervaardigd met 0.05% (w/v) TMC, 1.0% (w/v) serinol en 10% DMAP had een cut-off voor molecuulgewicht (MWCO) van 474 Da en een waterdoorlatendheid van  $6.0 \text{ L m}^{-2} \text{ h}^{-1} \text{ staaf}^{-1}$ . De zoutafwijzingen volgden de volgorde van  $\text{Na}_2\text{SO}_4 > \text{MgSO}_4 > \text{NaCl} > \text{MgCl}_2$ , en de waarden waren respectievelijk

96.3%, 83.9%, 58.7% en 28.8%. Hieruit werd geconcludeerd dat de relatief lage waterdoorlatendheid het gevolg was van de blokkering van de poriën van het steunmembraan (SMPB).

In termen van het SMPB-fenomeen werden verschillende conceptuele modellen voorgesteld om het uit te leggen. SMPB werd gereguleerd door de monomeerconcentratie, de poriegrootte van het dragermembraan en de vertragingstijd na het bekleden in de waterfase te veranderen. De resultaten geven aan dat SMPB de permeabiliteit van het membraanwater kan verminderen. Desalniettemin suggereerde de vergelijking tussen verschillende IP-technieken dat SMPB de adhesie tussen het ondersteunende membraan en de selectieve laag zou kunnen verbeteren door een "mechanisch in elkaar grijpend effect", wat nogal zinvol zou moeten zijn om de stabiliteit van het membraan op lange termijn te verbeteren. Verwacht wordt dat het SMPB verlicht door de juiste selectie van monomeerconcentratie, vertragingstijd na coating in de waterfase en poriegrootte van het ondersteunende membraan. Om een NF-membraan met gewenste eigenschappen te bereiden, moet SMPB worden verlicht op de premisse dat de membraanstabieliteit wordt gegarandeerd.

Om gebruik te maken van het aangroeiwerende vermogen van serinol en de negatieve invloed van SMPB te vermijden, werd serinol gebruikt om het op piperazine (PIP) gebaseerde TFC NF-membraan te modificeren door de acyleringsreactie tussen de aminogroep van serinol en de resterende acylchloridegroepen op de ontluikende membraan. ATR-FTIR bevestigde de succesvolle covalente transplantatie van serinol op het ontluikende NF-membraan. AFM- en FESEM-karakterisering suggereerden dat dit modificatieproces de membraanmorfologie niet veranderde. Contacthoekmeetapparaat, oppervlakte Zeta-potentiaalanalysator en TBO-techniek gaven aan dat het entproces de hydrofiliciteit van het membraan effectief verbeterde en de carboxyldichtheid aan het oppervlak verminderde. De resultaten toonden aan dat de modificatie van de actieve laag met serinol-enting duidelijk de waterdoorlaatbaarheid kan verbeteren zonder het ontzoutingsvermogen en de neutrale selectiviteit voor opgeloste stoffen op te offeren. Bij de behandeling van het model PFPW vertoonde het met serinol geënte membraan een uitstekend aangroeiwerend vermogen en bevredigende afstotingen tegen  $\text{Ca}^{2+}$ ,

Mg<sup>2+</sup>, SO<sub>4</sub><sup>2-</sup> en TOC. Dit is tamelijk zinvol in het geval van de behandeling van PFPW die gericht zijn op hergebruik bij oliewinning door overstromende polymeren.

Wat betreft de zware metalen die voorkomen in afvalwater dat wordt geproduceerd door aardolieraffinaderijen en petrochemische fabrieken, werd verder onderzoek uitgevoerd om de verwijderingscapaciteit van de NF-membranen tegen zware metalen te verbeteren, wat de terugwinning van aardolie-afvalwater zou beïnvloeden. Er werd gevonden dat een TFC NF-membraan met de gewenste waterdoorlatendheid en hoge verwijdering van zware metalen kon worden vervaardigd door de TMC-concentratie in een uitzonderlijk lage mate te verlagen. Het geoptimaliseerde NF-membraan bereid met 0.6 w / v% PIP en 0.03 w / v% TMC had de kleinste gemiddelde effectieve poriëradius van 0.305 nm, een verzwakte negatieve lading (IEP = 5,1) en een matige polyamide (PA) filmdikte van 50 nm. Al deze eigenschappen zorgden voor een uitstekende verwijderingsefficiëntie van ongeveer 98% tegen Ni<sup>2+</sup>, Zn<sup>2+</sup>, Cu<sup>2+</sup> en meer dan 92.7% tegen Cd<sup>2+</sup>, en tegelijkertijd een hoge permeabiliteit voor zuiver water van 14.6 L m<sup>-2</sup> h<sup>-1</sup> bar<sup>-1</sup> behouden. De eenvoud, lage kosten en schaalbaarheid van de huidige strategie zullen naar verwachting goed voldoen aan de eisen van industriële productie.

Om de waterdoorlatendheid verder te verbeteren en het energieverbruik te verminderen tijdens de behandeling van petroleumafvalwater met NF-technologie, werd een TFC NF-membraan met ultradunne PA-film geconstrueerd door tegelijkertijd de monomeerconcentratie en de substraatmembranselectie te optimaliseren. Er werd aangetoond dat een ultradunne PA-film direct kan worden gegenereerd op een commercieel substraatmembraan met in-situ grensvlakpolymerisatie (ISIP) -techniek door gebruik te maken van de lage PIP-concentratie van 0.05 w / v% en hoge TMC-concentratie van 0.1 w / v%. Bovendien werd gevonden dat het commerciële substraatmembraan met sterke hydrofiliteit, gladde oppervlaktemorfologie en gemiddelde poriëgrootte een homogene en intacte "fase-interface" zou kunnen verschaffen voor de stabiele grensvlakpolymerisatie tijdens het ISIP-proces. Daarom kan een ultradunne PA-film (8.5 nm) met een smalle poriëgrootteverdeling direct op het substraatmembraan worden geconstrueerd. Het resulterende TFC NF-membraan doorbrak met succes de trade-off tussen permeabiliteit en selectiviteit, waardoor het een ultrahoge permeabiliteit voor zuiver water van

46.6 L m<sup>-2</sup> h<sup>-1</sup> bar<sup>-1</sup> en een hoge Na<sub>2</sub>SO<sub>4</sub>-afstoting van 98.1% presenteerde. De eenvoudige fabricagemethode kan leiden tot industriële toepassingen.

Er kan worden besloten dat dit proefschrift het de weerstand tegen vervuiling, de selectiviteit en de permeabiliteit van de NF-membranen zal verbeteren voor toepassing bij de behandeling van petroleumafvalwater met het oog op water recyclage.

## List of Abbreviations

AAS	Atomic Absorption Spectrophotometer
AFM	Atomic force microscope
AOPs	Advanced oxidation processes
APAM	Anion polyacrylamide
AQPs	Aquaporins
ATR-FTIR	Attenuated total reflection Fourier transform infrared spectroscopy
BPA	Bisphenol A
BSA	Bovine serum albumin
CNTs	Carbon nanotubes
CP	Concentration polarization
DITC	Double interface thickness-controlling
DMAP	4-dimethylaminopyridine
DMF	N,N-dimethylformamide
EDS	Energy dispersive spectroscopy
ESIP	Ex-situ interfacial polymerization
FESEM	Field emission scanning electron microscopy
GD	Glutaraldehyde
GO	Graphene oxide
HA	Humic acid
IEP	Isoelectric point
IP	Interfacial polymerization
ISIP	In-situ interfacial polymerization
J	Water flux
$K_{KC}$	Kozeny-Carman coefficient
LDI	Limiting diffusion interface



MPD	m-phenylene diamine
MWCNTs	Multiwalled carbon nanotubes
MWCO	Molecular weight cut-off
NF	Nanofiltration
OSN	Organic solvent nanofiltration
PA	Polyamide
PAMAM	Poly (amidoamine) dendrimer
PAN	Polyacrylonitrile
PDA	Polydopamine
PEA	Polyesteramide
PEG	Poly ethylene glycol
PEI	Poly(ethyleneimine)
PES	Polyether sulfone
PFPW	Polymer flooding produced water
PIP	Piperazine
PRPP	Petroleum refinery and petrochemical plants
PS	Polysulfone
PTC	2,4,6-pyridinetricarboxylic acid chloride
PTFE	Polytetrafluoroethylene
PVA	Polyvinyl alcohol
PW	Produced water
PWP	Pure water permeability
$R_m$	Membrane hydraulic resistance.
RO	Reverse osmosis
$R_{RMS}$	Root-mean-squared roughness
SA	Sodium alginate
SFIP	Support-free interfacial polymerization
$S_m$	Specific surface area.

SMPB	Support membrane pore blockage
SWNTs	Single-walled carbon nanotubes
TA	Tannic acid
TBO	Toluidine blue O
TEA	Triethylamine
TEOA	Triethanolamine
TFC	Thin film composite
TMC	Trimesoyl chloride
TOC	Total organic carbon
UF	Ultrafiltration
WCA	Water contact angle
XPS	X-ray photoelectron spectroscopy
$\varepsilon$	Membrane porosity
$r_p$	Membrane pore radius
$\tau$	Membrane tortuosity
$l$	Thickness of the rejection layer
$\Delta P$	Trans-membrane pressure
$\eta$	Viscosity of water
$\Delta\pi$	Osmotic pressure difference



# Table of contents

<b>Acknowledgements</b> .....	<b>I</b>
<b>Abstract</b> .....	<b>V</b>
<b>Samenvatting</b> .....	<b>IX</b>
<b>Chapter 1 Introduction</b> .....	<b>1</b>
1.1 Background .....	1
1.2 Motivation and objective of the thesis.....	3
1.3 Overview of the petroleum industry wastewater .....	5
1.4 Basic theory of NF technology.....	8
1.4.1 Definition of NF .....	8
1.4.2 Separation mechanism of NF .....	8
1.4.3 Fabrication methods of NF membranes.....	10
1.5 Performance improvements of NF membrane.....	13
1.5.1 Membrane fouling control.....	14
1.5.2 Coordination between the water permeability and solute rejection.....	21
1.6 Thesis outline .....	33
<b>Chapter 2 Materials and Methods</b> .....	<b>37</b>
2.1 Materials .....	37
2.1.1 Membrane materials .....	37
2.1.2 Chemical reagents .....	38
2.2 Experimental apparatus and instruments.....	42
2.2.1 Cross-flow NF testing apparatus .....	42
2.2.2 Other instruments .....	42
2.3 Experimental methods .....	44
2.3.1 Interfacial polymerization method.....	44
2.3.2 Evaluation of membrane separation performance .....	45
2.3.3 Determination of oil content.....	46
2.3.4 Preparation of model petroleum wastewater .....	48
2.3.5 Evaluation of membrane antifouling ability .....	49

2.4 Membrane characterization .....	50
2.4.1 Analysis of material composition .....	50
2.4.2 Morphology analysis .....	50
2.4.3 Hydrophilicity analysis.....	51
2.4.4 Analysis of pore size distribution .....	51
2.4.5 Analysis of membrane charge property.....	52
2.4.6 Analysis of carboxyl density .....	52
2.4.7 Analysis of PA film thickness .....	53
<b>Chapter 3 Fabrication of antifouling NF membrane via interfacial polymerization of serinol and trimesoyl chloride catalyzed by 4-dimethylaminopyridine.....</b>	<b>55</b>
3.1 Introduction .....	55
3.2 Results and discussion.....	58
3.2.1 Optimization of the membrane fabrication conditions .....	58
3.2.2 Physicochemical properties of the optimized membrane .....	66
3.2.3 Separation performance of the optimized membrane.....	72
3.2.4 Anti-fouling properties of the PEA-TFC-NF membrane.....	74
3.3 Conclusions .....	76
<b>Chapter 4 Support Membrane Pore Blockage (SMPB): An Important Phenomenon during the Fabrication of Thin film Composite Membranes via Interfacial Polymerization .....</b>	<b>77</b>
4.1 Introduction .....	77
4.2 Results and discussion.....	79
4.2.1 Regulating SMPB by altering monomer concentration.....	79
4.2.2 Regulating SMPB by altering the pore size of the support membrane.....	88
4.2.3 Regulating SMPB by altering lag time after aqueous phase coating.....	90
4.2.4 Regulating SMPB by adopting different IP techniques.....	93
4.3 Conclusions .....	97
<b>Chapter 5 Surface modification of piperazine based nanofiltration membrane with serinol for reduced fouling in treatment of polymer flooding produced water.....</b>	<b>99</b>
5.1 Introduction .....	99
5.2 Results and discussion.....	101
5.2.1 Membrane physicochemical properties .....	101

5.2.2 Membrane permeation properties .....	106
5.2.3 Membrane performance in treating model PFPW .....	107
5.3 Conclusions .....	110
<b>Chapter 6 Fabrication of negatively charged NF membranes for heavy metal removal via the interfacial polymerization between PIP and TMC .....</b>	<b>111</b>
6.1 Introduction .....	111
6.2 Results and discussion.....	114
6.2.1 Influence of TMC concentration on membrane property evolution .....	114
6.2.2 Effect of operating conditions on heavy metal removal by NF-0.03 .....	123
6.2.3 Evaluation of the membrane long-term stability and performance comparison with other competitors .....	128
6.3 Conclusions .....	129
<b>Chapter 7 Direct Generation of an Ultrathin (8.5 nm) Polyamide Film with Ultrahigh Water Permeance via In-situ Interfacial Polymerization on a Commercial Substrate Membrane .....</b>	<b>131</b>
7.1 Introduction .....	131
7.2 Results and discussion.....	133
7.2.1 Thickness evolution of the PA film during the regulation of monomer concentration .....	133
7.2.2 Performance evaluation of the ultrathin PA film constructed on PSH-100 kDa. .	136
7.2.3 Impact of substrate membrane on TFC NF membrane with ultrathin PA film. ...	139
7.3 Conclusions .....	145
<b>Chapter 8 Conclusions and Recommendations for Future Research.....</b>	<b>147</b>
8.1 General conclusions.....	147
8.2 Recommendations for future research.....	149
<b>References: .....</b>	<b>153</b>
<b>Curriculum Vitae .....</b>	<b>181</b>



# Chapter 1 Introduction

## 1.1 Background

If one views from space, the most striking feature of our planet is water, as 70% of the Earth's surface is covered by water. However, more than 97% of the total water storage on Earth is seawater in the oceans, and two-thirds of the remaining is trapped in snowfields, Greenland and glaciers around polar regions [1]. Generally, only 0.8% of the total earth's water is fresh water available for human consumption [2]. As the most important substance for all life, the finite resources of fresh water are becoming more and more scarce. With the surge of population growth, climate change, and industrialization around the world, water shortage, to be classified as 'water crisis' has turned into one of the most critical concerns for global communities, especially for countries with large population, such as China and India. A report from UN indicates that two-thirds of the world population could face water stress by the year of 2025 [3]. Normally, water scarcity is in the form of quantity shortage, where water availability is not sufficient. However, it could also be in the form of quality-induced shortage, where although water is available, it is polluted and cannot meet the quality requirements, even after conventional treatment. As such, water pollution has become a prevalent problem threatening human health and the environment. For instance, a study suggests that 40% of rivers in China are severely contaminated and even 20% are so toxic that people cannot be in contact with river water [4]. Similarly, a report from an Indian scientific institute shows that ground water in India is severely polluted and the contamination depth is even up to 40 meters [5]. Human activities, especially the industrial production, are the most critical factor in aggravating water contamination. Different from domestic wastewater, industrial wastewater has a variable composition and presence of pollutants; it usually has a higher hazard [6]. Currently, direct discharge of industrial wastewater into the water environment has been legislatively banned by



## Chapter 1

most countries, but illegal emissions and insufficient treatment are still common.

Petroleum, which is known as the ‘black gold’, is not only the most important energy source in the world, but also the fundamental raw material of other industries including plastics, solvents, fertilizer, rubber, and many other chemical products [7]. Even though it is a much contested resource today, its impact is a reality, and reducing this impact at least helps to mitigate the adverse impacts of petroleum. The petroleum industry comprises crude oil exploration, refining, and petrochemical production [8]. Each process of the petroleum industry produces a large amount of wastewater with distinct pollution characteristics. For example, the produced water generated during crude oil exploration is one of the most important sources of industrial wastewater, of which the production was more than 397 million m<sup>3</sup>/d in 2015 [9]. This number increases with the growth of well life. As petroleum industry wastewater usually contains a wide array of contaminants including salts, oils, hydrocarbons, phenols, heavy metals and many other chemical additives [10], direct discharging would not only result in significant environment pollution, but also in a waste of water resources, especially for water-deficient areas. Therefore, properly managing industrial wastewater with an economically and technically acceptable strategy is of great significance for mitigating the negative impact of the sector, and for social development.

In order to reduce water scarcity and environment contamination, reclamation of industrial wastewater after proper treatment is a research challenge [9, 11, 12]. In this way, wastewater can be used as an unconventional but stable water resource to make up the water demand, and simultaneously avoiding pollution when discharging into the water environment, thus achieving a dual beneficial effect [13]. However, conventional water treatment processes such as coagulation, sedimentation, flotation, medium filtration, oxidation, precipitation and biodegradation are not sufficiently effective for the treatment of petroleum wastewater in view of reclamation as they are in treatment of municipal wastewater, due to the high salinity and toxicity [14-18]. It is common to use multiple treatment units in combination to meet the water reclamation requirements.

The expensive but inefficient wastewater treatment process severely limits the reclamation of petroleum wastewater.

In recent decades, alternative energy sources such as nuclear energy, and sustainable sources including solar energy, wind energy and geothermal energy have rapidly developed, but investments are too slow to satisfy the world energy consumption. As a consequence, petroleum still dominates the energy market and serves as the basis of the industrial economy, in spite of its prominent adverse effects [19]. Therefore, exploration of an economic and effective technology aiming at the reclamation of petroleum industry wastewater is of crucial significance for at least mitigating the impact of petroleum, and to recycle water resources.

### **1.2 Motivation and objective of the thesis**

In order to contribute to mitigate the current water crisis and to meet stringent environmental emission standards, reclamation of industrial wastewater related to petroleum, after advanced treatment, is thought a reasonable choice, which can simultaneously decrease clean water consumption and wastewater discharge. However, wastewater reuse usually raises a much higher requirement than emission in the environment. For instance, the *Daqing* oilfield in China plans to reuse their polymer flooding produced water for the preparation of the polymer flooding solution, but residual salts which could deteriorate the oil exploration efficiency cannot be easily removed. High-impact desalting processes such as ion exchange were adopted after a series of treatment processes including flotation, coagulation, sedimentation, sand filtration and ultrafiltration (UF) [20]. In addition, the heavy metals which may come from the oil reservoir or catalyzers used in petroleum refining and petrochemical production, as well as non-biodegradable organic matter are other typical contaminants to be removed before reuse [21-23]. All these contaminants cannot be sufficiently removed by conventional technologies employed in the treatment of municipal wastewater.

## Chapter 1

Nanofiltration (NF) membranes were first introduced in the late 1980s. They have pores around 1 nm and are usually charged in aqueous solution, which allows for separation by size exclusion and charge exclusion [24, 25]. NF is capable to effectively reject low molecular weight organics and multivalent ions, and partially remove monovalent ions. With all these features, NF is widely applied in water softening, brackish water desalination, municipal wastewater reuse, as well as food and medicine production etc. [26-30]. Preliminary explorations have confirmed the feasibility and potential for applying NF to manage petroleum industry wastewater. For instance, Su et al. employed NF to soften seawater for offshore oilfield polymer flooding [31]. Their results demonstrated that this technology could effectively meet water standards for polymer flooding and ensure stable oil production. Some other researchers also confirmed that advanced purification of petroleum wastewater with NF technology can meet the water reuse standards [32, 33].

However, the widely adopted NF membranes are commercial thin film composite (TFC) polyamide NF membranes, which are designed for the treatment of drinking water, municipal sewage water and brackish water. As commercial NF membranes are not optimized for the characteristics of petroleum wastewater, numerous problems would result, such as serious membrane fouling, improper foulant rejection and low water permeability. Notably, the membrane material is the core of NF technology. The inner structure and physicochemical features of a specific NF membrane are the main factors affecting membrane fouling, solute rejection and water permeability. Therefore, this thesis intends to improve the use of NF for advanced treatment and reclamation of petroleum wastewater from the perspective of membrane fabrication and modification. More specifically, the following three research objectives are set:

- To enhance the anti-fouling ability of the NF membranes aiming for a specific petroleum wastewater treatment.
- To promote the NF membranes' removing capacity for certain pollutants that would affect the petroleum wastewater reclamation.

- To increase the water flux of NF membranes and coordinate the trade-off effect between water permeability and solute rejection.

### 1.3 Overview of the petroleum industry wastewater

The petroleum industry is a wide-ranging industry related to petroleum exploration, petroleum refining, and petrochemical production, as illustrated in **Fig. 1.1**. Different types of wastewater would be generated in each process.

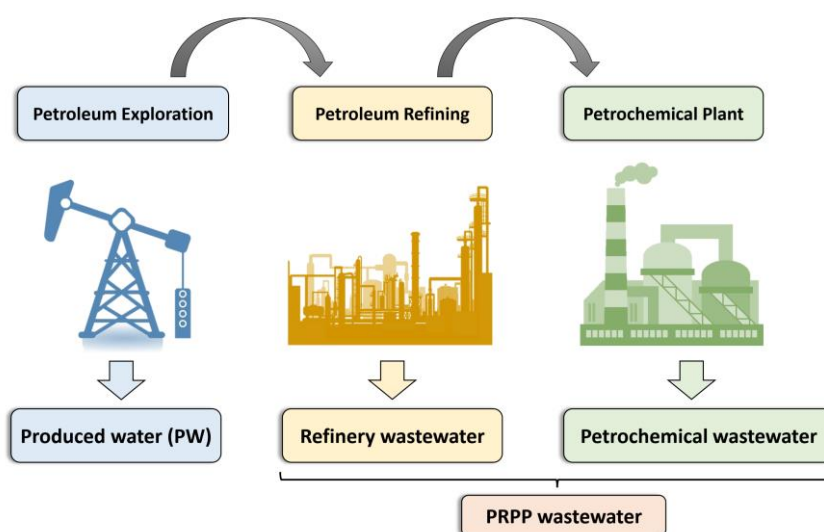


**Figure 1.1** Schematic diagram of petroleum industry configuration. The wastewater produced in petroleum refinery and petrochemical plants (PRPP) are collectively denoted as PRPP wastewater.

During oil exploration, fresh water is injected into the well to pump out the oil reserves. In this way, wastewater that is generally denoted as produced water (PW) will be generated as by-product after oil-water separation [34]. The constituents of PW are influenced by natural geological formation and minerals can be dissolved in the PW in addition to the crude oil. Moreover, novel oil flooding techniques introduce other chemicals into the PW and make it more complex. Taking polymer flooding as example, anion polyacrylamide (APAM) is added into the flooding water to increase the fluid viscosity and sweep efficiency [19, 35]. In this way, the oil production could be

increased by 5-30% [36]. However, residual APAM remains present in the PW and greatly increases the difficulty in wastewater treatment.

The crude oil separated from the oil-water mixture is processed in an oil refinery plant for refining using various processes such as distillation, coking, catalytic cracking. In these processes, the crude oil is separated into different fractions, upgraded and purified, while heavy fractions are converted to lighter and more useful fractions [37]. The products of the refinery plant can be directly used as energy resources such as gasoline and kerosene, or taken as raw materials for petrochemical plants. Petrochemical processes produce many important intermediates such as propylene, ethylene, benzene, toluene, and xylene, which can be further converted to other intermediates and final products for diverse applications [37]. All these processes in petroleum refinery and petrochemical plants (PRPP) produce wastewater with complex composition. According to an estimation made by Coelho et al. [38], the quantity of PRPP wastewater, comprising refinery wastewater and petrochemical wastewater, is around 0.4 to 1.6 times the quantity of PW. Furthermore, various toxic organic compounds that bring a great ecological threat to the environment are present in PRPP wastewater, as shown in **Fig. 1.2**. An overview of typical contaminants in PRPP wastewater, as well as their typical concentration ranges have been listed in **Table 1.1**.



**Figure 1.2** Contaminants resulting from various processes in PRPP [10].

**Table 1.1** An overview of typical contaminants in PRPP wastewater [39]

Parameters	Typical concentration range (mg/L)
Oil and grease (O&G)	12.5~20223
BOD	90~685
COD	300~600
TSS	28.9~950
Phenol	0.2~200
BTEX	1~100
Heavy metals	0.01~100

The treatment of petroleum wastewater aiming at reclamation may vary according to the specific quality of feed water and the reuse direction. In general, three treatment stages may be applied, including primary treatment, secondary treatment and tertiary treatment [10]. Suspended solids, turbidity and oil are mainly removed *via* the primary treatment [40]. Secondary treatment, or biological treatment, aims at degrading the nutrients, biodegradable organic pollutants and, partially, recalcitrant organic compounds [39]. Other contaminants such as non-biodegradable organic matter and ions are to be removed in the tertiary treatment, in order to meet the strict discharge or reuse standards. Chemical precipitation, adsorption, advanced oxidation processes (AOPs) and electro dialysis have been employed in tertiary treatment [41-44], but the production of sludge, the high treatment cost and low efficiency have limited their wide application. As tertiary treatment is the terminal process before wastewater reclamation, exploration of an economic and effective technology that can be used in tertiary treatment is of great importance.

## 1.4 Basic theory of NF technology

### 1.4.1 Definition of NF

NF is a separation process ranging between ultrafiltration (UF) and reverse osmosis (RO). The concept of NF was firstly proposed by the Filmtec Corporation when they developed RO membranes with a loose structure and pore size larger than 1 nm [45, 46]. Compared with UF membranes, NF membranes have a much lower molecular weight cut-off (MWCO) and can reject organic molecules, multivalent ions and colloidal particles. Different from RO membranes, NF membranes have a much higher water permeability and can selectively reject multivalent ions, while allowing most of the monovalent ions to pass through. Therefore, a typical feature of NF is that it can achieve a separation between different solutes, such as the separation of  $\text{Ca}^{2+}/\text{Na}^+$  or dyes/ $\text{Na}^+$  [47, 48]. Moreover, the low monovalent ion rejection of NF membranes can decrease the osmotic pressure difference across the membrane, thus improving the water recovery and mitigating concentration polarization. In spite of the wide concept range, a typical NF membrane should have the following four features:

- The membrane pore diameter is lower than 2 nm.
- Most of the monovalent ions can penetrate the membrane.
- The rejection of divalent and multivalent ions is apparently higher than that of monovalent ions.
- The MWCO for neutral solute ranges from 200 to 2000.

### 1.4.2 Separation mechanism of NF

NF is a separation process based on a driving force provided by the pressure difference between two sides of the membrane. NF is a very complex process, which is affected by interfacial interactions as well as micro fluid motions near the membrane surface and inside the membrane structure [49]. As the structural features of NF membrane are between UF and RO membranes, the separation mechanism of NF should fall between

that of UF and RO.

UF membranes have a porous structure and mass transfer through such membranes follow the “pore flow model”, which describes the convective mass transfer across the membrane pores driven by pressure. The separation in this process is determined by size exclusion due to the size difference between the target component and the membrane pores [50]. The water flux of a porous membrane can be calculated with the Hagen-Poiseuille equation or the Kozeny-Carman equation, as shown in equation (1-1) and equation (1-2), respectively [51].

$$J = \left( \frac{\varepsilon r_p^2}{8\tau l} \right) \left( \frac{\Delta P}{\eta} \right) = \frac{\Delta P}{\eta R_m} \quad (1-1)$$

where  $J$  is the water flux;  $\varepsilon$  is the membrane porosity;  $r_p$  is the membrane pore radius;  $\tau$  is the membrane tortuosity;  $l$  is the thickness of the rejection layer;  $\Delta P$  is the trans-membrane pressure;  $\eta$  is the viscosity of water and  $R_m$  is the membrane hydraulic resistance.

$$J = \left( \frac{\varepsilon^3}{K_{KC} l S_m^2 (1-\varepsilon)^2} \right) \left( \frac{\Delta P}{\eta} \right) \quad (1-2)$$

where  $K_{KC}$  is the Kozeny-Carman coefficient;  $S_m$  is the specific surface area.

RO membranes have a dense functional layer (rejection layer). As illustrated in **Figure 1.3**, the “Solution-diffusion model” is usually adopted to describe mass transfer through RO membranes, in which both the solute and solvent absorb into in the nonporous rejection layer, then diffuse across it driven by their respective concentration gradient and finally desorb at the permeate side. The separation is realized depending on solubility and diffusivity differences in RO membrane materials [52]. The mass transfer of water and solute in the “solution-diffusion model” can be described with equation (1-3) and (1-4), respectively.

$$J = A(\Delta P - \Delta\pi) \quad (1-3)$$

and

$$J_s = B\Delta C \quad (1-4)$$



where  $\Delta C$  is the concentration difference across the membrane;  $\Delta\pi$  is the osmotic pressure difference across the membrane; A and B are the water permeability coefficient and solute permeability coefficient, respectively.

The transport coefficients (A and B) can be calculated according to the membrane properties as illustrated in equation (1-5) and equation (1-6).

$$A = \frac{D_{wm}C_{wm}V_w}{R_g T l} \quad (1-5)$$

and

$$B = \frac{D_{sm}K_{sm}}{l} \quad (1-6)$$

where  $D_{wm}$  is the diffusion coefficient of water;  $D_{sm}$  is the diffusion coefficient of the solute inside the rejection layer;  $C_{wm}$  is the concentration of water inside the rejection layer;  $V_w$  is the molar volume of water;  $R_g$  is the universal gas constant ( $8.31 \text{ J mol}^{-1}\text{K}^{-1}$ );  $K_{sm}$  is the solute partitioning coefficient into the rejection layer

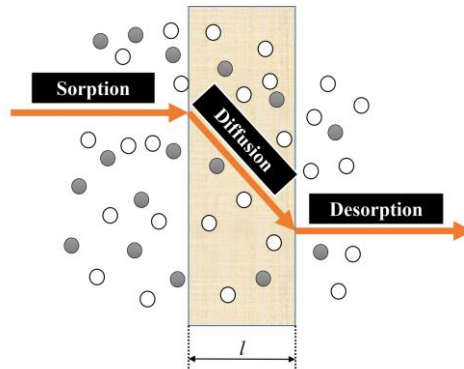


**Figure 1.3** Schematic diagram of the solution-diffusion mechanism

### 1.4.3 Fabrication methods of NF membranes

From the material point of view, NF membranes can be organic or inorganic. Inorganic NF membranes mainly refer to ceramic NF membranes, made of various metal oxides. Organic NF membranes are made of polymers such as polysulfone, sulfonated polysulfone, cellulose acetate and polyamide, etc. The fabrication process of a NF membrane aims at constructing pore structures with diameter below 2 nm on the surface

of a specific supporting material.

#### **1.4.3.1 Preparation methods of ceramic NF membranes**

The sol-gel method is the key to the preparation of ceramic NF membranes [53]. By taking a specific metal salt as precursor, the raw materials are firstly mixed in liquid phase to form a stable and transparent sol system. Subsequently, the sol system could transform to a gel system with three-dimensional network structure. Finally, a ceramic NF membrane can be obtained after drying and sintering the gel on the substrate structure. Researchers prepared ceramic NF membranes made of different metallic oxides such as Al<sub>2</sub>O<sub>3</sub> particles, TiO<sub>2</sub> particles, ZnO<sub>2</sub> and HfO<sub>2</sub> particles [54-57]. Ceramic NF membranes have numerous advantages such as a good chemical stability, a strong tolerance of high temperatures and an excellent organic solvent resistance, so they can be applied in a harsh environment [58]. However, ceramic NF membranes usually show a relatively low permeability, a poor solute rejection, a large MWCO as well as high manufacturing costs. For instance, the ceramic NF membrane reported by Guo et.al [56] had a MWCO of 620-850 Da, but its water permeability was lower than 0.2 L m<sup>-2</sup> h<sup>-1</sup> bar<sup>-1</sup>, and its Na<sub>2</sub>SO<sub>4</sub> rejection was below 40%. This performance lags far behind the typical organic NF membranes. Taking a commercial organic NF membrane (NF 270) as example, it has a MWCO lower than 300 Da and Na<sub>2</sub>SO<sub>4</sub> rejection over 96%, and simultaneously keeping a water permeability higher than 12 L m<sup>-2</sup> h<sup>-1</sup> bar<sup>-1</sup>. All these factors greatly limit the development and application of ceramic NF membranes.

#### **1.4.3.2 Preparation methods of organic NF membranes**

Organic or polymeric NF membranes can be prepared with various technologies including phase inversion, surface coating or grafting, layer-by-layer self-assembly, as well as interfacial polymerization.

● **Phase inversion.** As a technology mainly used for the preparation of porous UF and MF membranes, phase inversion can also be adapted to fabricate NF membranes. The main advantage of phase inversion is the asymmetric membrane structure with dense

selective layer and porous substrate, which can be obtained in one step. Most NF membranes prepared *via* phase inversion are used in organic solvent systems due to their good stability [59, 60].

● **Surface coating or grafting.** Organic NF membranes can also be prepared with surface coating technology, in which a dense polymer film can be constructed on the surface of a porous substrate [61]. The major advantage of this method is that the coating polymers with different functional groups can be selected according to different functional requirements [62]. The introduction of new functional groups on the surface of a porous substrate *via* grafting reaction is another way to fabricate NF membranes. A variety of techniques including ultraviolet radiation, low temperature plasma radiation, electron beam radiation and  $\gamma$  radiation can be adopted to produce the free radicals necessary in the grafting reaction [63, 64].

● **Layer-by-layer self-assembly.** In 1997, Decher firstly reported a polyelectrolyte film which was prepared *via* consecutive adsorption of polyanions and polycations, which was denoted as layer-by-layer self-assembly [65]. According to this mechanism, a membrane with multilayer structure and manipulated thickness can be obtained by selecting different polyanions and polycations with various functional groups. Inspired by this principle, a variety of composite NF membranes was fabricated with different combinations of polyelectrolytes [66, 67]. In spite of the simplicity and flexibility of this method, the drawback of the resultant membrane is the insufficient stability in many solutions.

● **Interfacial polymerization.** The polymerization reaction at the interface of two immiscible liquids, which contain two reactive monomers, is denoted as interfacial polymerization (IP), which can be used for the synthesis of ultrathin films, fibers or capsules [68]. Properties of the polymer generated in IP reaction are influenced by many factors, such as monomer reactivity, monomer concentration, number of reactive groups in the monomer, dissolution and diffusion rate of the monomer in the two phases, and interfacial stability of two phases [69, 70]. The monomers used in the IP reaction

usually include a nucleophile monomer (i.e., amines, alcohols, etc.) dissolved in aqueous phase and an electrophilic monomer (i.e., acid chlorides, isocyanates, etc.) dissolved in organic phase. As early as in 1969, Lonsdale et al. tried to prepare composite membranes with ethylenediamine and succinyl chloride as reactive monomers, but the resultant membranes did not have desalination capability. In 1973, Scala et al. applied a patent which recorded the synthesis of a composite membrane *via* the IP reaction between a disulfonyl halide compound and an amine compound, but the water permeability of this membrane was rather low [71]. The milestone achievement in the preparation of composite membranes with IP technology was taken by Cadotte, who prepared a RO membrane with high permeability and high salt rejection *via* the IP reaction between toluene diisocyanate and polyimide on a polysulfone substrate [72]. Similar to RO membranes, NF membranes can also be prepared with IP technology. Since it was created in the late 1980s, NF technology has experienced nearly 40 years of development. At present, thin film composite (TFC) polyamide (PA) NF membranes are playing a dominant role in the NF market due to their higher solute rejection and water productivity compared to other asymmetric membranes.

### **1.5 Performance improvements of NF membrane**

How to improve the membrane performance is a key topic for membrane researchers around the world. According to a survey [73], NF research has been steadily increasing since the year 2007. From 2007 to 2017, 1902 journal articles involving NF were published in *Science Direct*, 23.4% of which focused on membrane fabrication and modification. In order to meet the requirements of practical applications, three important directions have been explored by membrane researchers. The first one is to control membrane fouling, which could decrease the water flux, change the effluent quality, as well as increase the cleaning frequency and operating costs. The second one is to increase the membrane water permeability in order to decrease the energy consumption or improve the productivity. The third one is to enhance the removal

efficiency of a specific contaminant, such as heavy metals. However, one critical problem faced by researchers is the trade-off between water permeability and solute rejection, which embodies that an increased water permeability generally leads to a reduced solute rejection.

### 1.5.1 Membrane fouling control

Understanding the fouling mechanism is the basis of membrane fouling control. Membrane fouling is the deposition of foulants on the membrane surface or within the membrane pores. Different from porous membranes such as MF and UF, the formation of a fouling layer (cake layer or gel layer) on the NF membrane surface is the dominant fouling form because the pore size of NF membrane is too small to allow the foulants to penetrate. Generally, there are four categories of foulants in NF membrane fouling according to the material composition: colloidal foulants, organic foulants, inorganic foulants and biological foulants.

- **Colloidal fouling.** The accumulation of colloidal particles such as clays, colloidal silicon, metal oxides and organic macromolecules on the membrane surface induces colloidal fouling [74]. The size, concentration and charge characteristic of the colloidal particles affects the fouling behavior.

- **Organic fouling.** Organic fouling can be caused by the deposition or adsorption of dissolved organic matter on the membrane surface. The typical foulants reported in the literature include humic acid, natural organic matter, extracellular polymers, proteins and polysaccharides such as sodium alginate [75]. It should be noted that most of the target foulants in publications are typical foulants in drinking water treatment or domestic wastewater treatment. The composition of the organic matter in industrial wastewater differs a lot according to the specific product type and manufacturing process.

- **Inorganic fouling.** The dissolved salt ions that are rejected can be concentrated near the NF membrane surface. As a consequence, the ion concentration near the membrane

surface is higher than that in the bulk solution. This phenomenon is concentration polarization. Once the concentration of a sparingly soluble salt exceeds its equilibrium solubility product, precipitates will be formed and accumulate on the membrane surface, thus forming a scaling layer. Typical inorganic precipitates include calcium sulfate, calcium carbonate, and silicate [76].

● **Biological fouling.** Microorganisms associated with biological fouling in NF are bacteria and fungi. Biological fouling is initiated by the adsorption of microbial cells or flocs. Then the microorganisms attached on the membrane grow and secrete extracellular polymer. The extracellular polymer itself can foul the membrane and also strengthen the binding force between microorganisms and NF membrane [77]. Moreover, microorganisms may also degrade and destroy the membrane structure because of the organic nature of most NF materials, although this process is rather slow. Membrane fouling in NF is a complex physicochemical process, which is closely related to the interaction between foulants and the membrane surface. This interaction is mainly affected by three factors, i.e. the composition of the feed water, hydrodynamic conditions and the characteristics of the NF membrane [78]. Structural and physicochemical characteristics of a membrane, such as roughness, charge property, hydrophilicity and surface functional groups can fundamentally affect the interaction between foulants and the membrane surface. Many studies conclude that a rough membrane surface aggravates membrane fouling, but some studies have found that the membrane fouling can be mitigated by enhancing surface turbulence *via* constructing orderly rough structures on the membrane surface [79]. The electrostatic interaction between foulants and the membrane surface can strongly affect membrane fouling. Electrostatic attraction accelerates the fouling process, while electrostatic repulsive forces mitigate the accumulation of foulants on the membrane surface [80]. Since many foulants in feed water are hydrophobic, increasing the hydrophilicity of the membrane surface can generate a hydration layer and reduce the hydrophobic binding force between hydrophobic foulants and the membrane surface [81]. Functional groups on the membrane surface can also affect membrane fouling. For example, carboxyl groups on the surface of a polyamide NF membrane can aggravate membrane fouling by

combining with the carboxyl groups in foulants under the complexing bridging action of calcium [82]. Therefore, the development of NF membranes with antifouling ability can be promoted based on the above discussion.

During the past several decades, a variety of preparation or modification methods aiming to enhance the antifouling ability of NF membrane have been proposed. As shown in **Figure 1.4**, these strategies can be classified into four categories: selection of novel IP monomers, blending modification, surface coating modification and grafting modification.

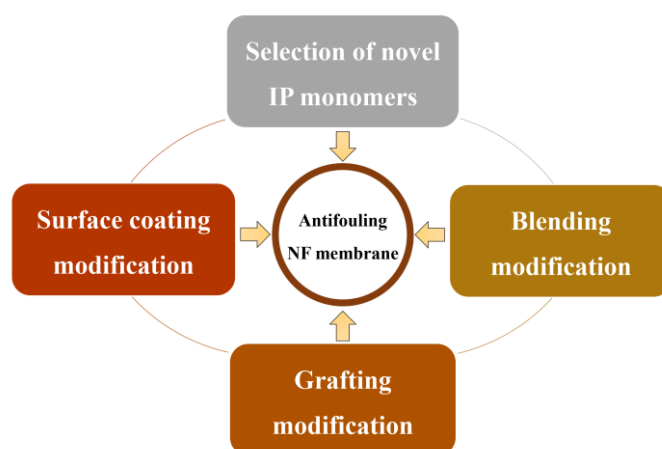


**Figure 1.4** Classification of fabrication technologies of NF membranes with antifouling ability

● **Selection of novel IP monomers.** For the NF membranes fabricated with IP technology, m-phenylene diamine (MPD) and piperazine (PIP) are the most commonly used water soluble monomers, while trimesoyl chloride (TMC) is the typical monomer dissolved in the organic phase. The selection or synthesis of novel IP monomers with specific structure and functional groups is a basic route to regulate the charge property, hydrophilicity and surface morphology of the resultant NF membranes [83]. In this way, the attracting interaction between foulants and membrane surface may be reduced, and the repulsive interaction between foulants and membrane surface may be enhanced. Therefore, the membrane antifouling ability could be improved. As illustrated in **Figure 1.5**, a novel NF membrane was fabricated by introducing a synthesized copolymer

monomer denoted as PEI-g-SBMA in the research of Ma et al. [84]. PEI-g-SBMA is a zwitterionic amine monomer, which can regulate the membrane charge. As a result, an electro-neutral NF membrane with enhanced antifouling property against bovine serum albumin (BSA), sodium alginate (SA) and humic acid (HA) was successfully obtained. The antifouling ability can also be enhanced by optimizing the monomer in the organic phase. In the study of Jewrajka et al. [85], 2,4,6-pyridinetricarboxylic acid chloride (PTC) was added into the organic phase together with TMC. Compared with the membrane prepared with TMC alone, the resultant membrane with 2:3-1:1 molar ratio of PTC to TMC showed a much lower tendency towards biological fouling.

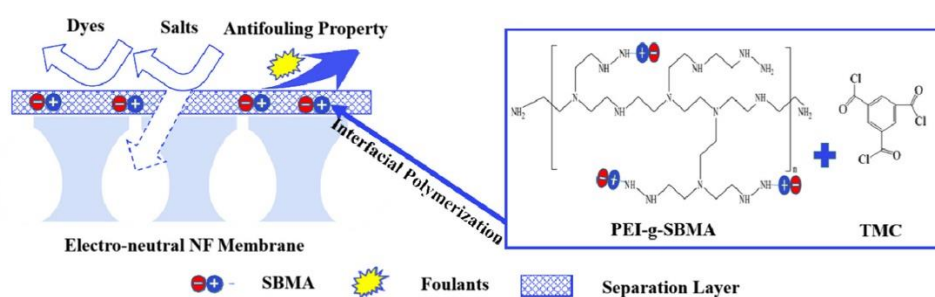


**Figure 1.5** Illustration the fabrication of NF membrane with antifouling property [84].

● **Blending modification.** Nanoparticles and hydrophilic macromolecules can be introduced into the separation layer of an NF membrane by blending modification. In this way, the roughness, hydrophilicity and surface charge can be regulated to improve the membrane antifouling performance. In a study by Vatanpour et al. [86], oxidized multiwalled carbon nanotubes (MWCNTs) were embedded in the asymmetric polyethersulfone (PES) NF membrane during the phase inversion process. It was found that the addition of 0.04 wt% MWCNT/PES can simultaneously decrease the surface roughness and improve the hydrophilicity of the resultant membrane, thus enhancing its antifouling property against BSA. Similarly, another study demonstrated that introducing a mixture of titanium dioxide and reduced graphene into the active layer of a polyamide TFC NF membrane could also improve the surface hydrophilicity of the membrane and reduce the surface roughness, resulting in an improved fouling resistance against BSA [87]. In order to improve the anti-biological fouling ability of



the NF membrane, Andrade et al. [88] prepared a NF membrane containing silver nanoparticles *via* wet phase inversion, as shown in **Figure 1.6**. Compared with the unmodified sample, the NF membrane with incorporated silver nanoparticles exhibited a decrease of 90% in *Escherichia coli* adhered cells. Although blending modification can improve the membrane flux and anti-fouling ability, it usually results in a loss of solute rejection [89].

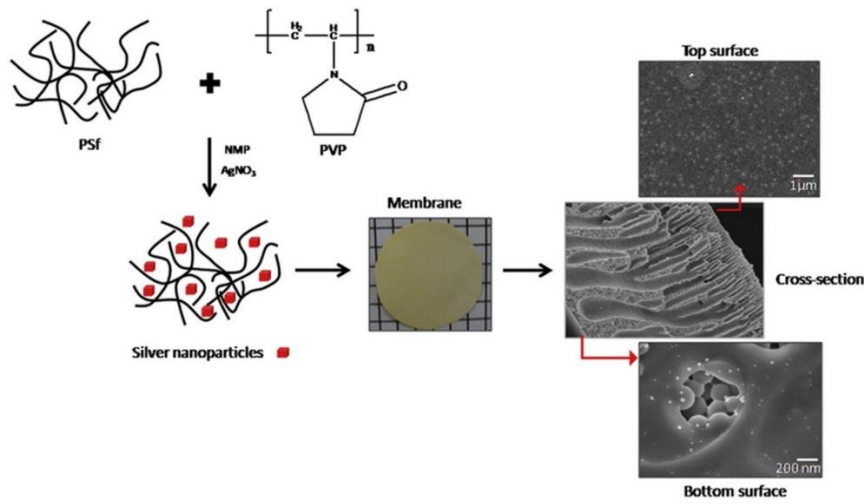


**Figure 1.6** Illustration of the preparation process of anti-biological fouling NF membranes [88].

● **Surface coating modification.** An additional coating layer covering the membrane surface may allow to decrease the interactions between foulants and the NF membrane matrix. It has been demonstrated that coating a hydrophilic and electrically neutral polyvinyl alcohol (PVA) on the surface of an NF membrane can effectively enhance its antifouling ability in the treatment of printing and dyeing wastewater [90]. In the study of Zhang et al. [91], the raw PVA was firstly sulfonated by an esterification reaction with sulfuric acid, and then the sulfonated polyvinyl alcohol (SPVA) was coated on the membrane surface by taking glutaraldehyde (GD) as the cross-linker. This is illustrated in **Figure 1.7**. The SPVA coated membrane showed an improved fouling resistance to BSA compared to the virgin membrane, with only 8% loss in flux after fouling for 12 h. Different from such PVA coating, McCloskey et al. proved that a simple dopamine coating on NF membranes could also effectively improve their antifouling property in

the treatment of oily wastewater [92]. It should be noted that the coating layer created in the modification process results in an additional mass transfer resistance for the passage of water molecules, thus reducing the membrane flux to varying degrees.

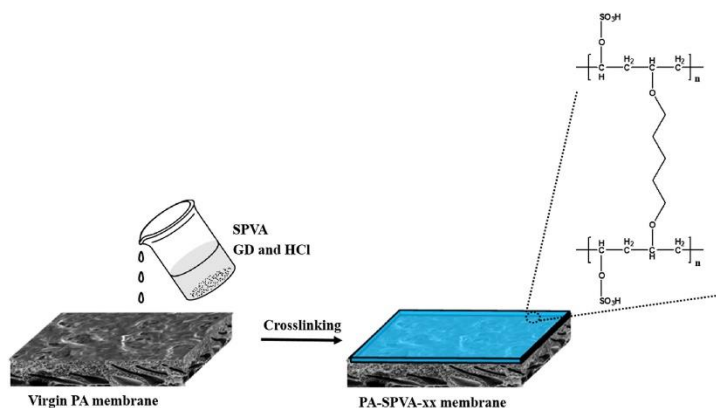


**Figure 1.7** Illustration of the surface coating modification of NF membrane with SPVA [91].

● **Grafting modification.** Both surface coating modification and grafting modification are carried out on the surface of an already formed NF membrane, but the mass transfer resistance induced by grafting modification is much lower than the additional resistance of a coating layer, so that surface grafting to improve the anti-fouling ability is an attractive route. In the research of Wagner et al. [93], a commercial NF membrane (NF90) was modified by grafting poly(ethylene glycol) (PEG) diglycidyl ether (PEGDE) onto the membrane top surface. It was confirmed that the membrane surface charge was reduced, so that the fouling resistance to charged surfactants and the flux recovery after membrane cleaning were improved. Recently, An et al. [94] reported a novel NF membrane grafted with hyperbranched polyglycerol (hPG) with superhydrophilicity and unique three-dimensional (3D) globular structure. As shown in **Figure 1.8**, this NF membrane was fabricated *via* the IP reaction between PIP and TMC on a carbon nanotubes (CNTs) deposited PES support, followed by the grafting modification with hPG. The resultant NF membrane had an outstanding hydrophilic surface, which greatly enhanced its fouling resistance against various foulants including

BSA, HA and SiO<sub>2</sub> colloidal particles.

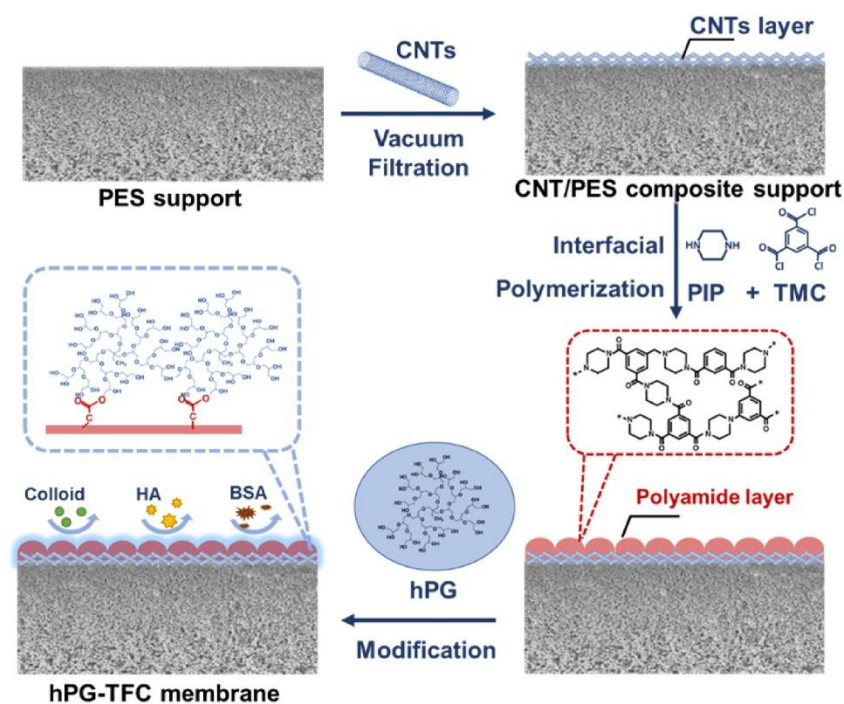


**Figure 1.8** Illustration of the fabrication of hPG modified TFC NF membranes [94].

Membrane fouling is a complex physicochemical process closely related to the foulant-membrane interactions, as well as the foulant-foulant interactions. However, the fabrication of antifouling membranes can only decrease the attractive interaction between foulant and membrane, or increase the repulsive interaction between foulant and membrane. The interaction between foulant and foulant cannot be changed by membrane modification. Therefore, the surface of an antifouling membrane would be covered by a foulant layer after a certain period. Henceforward, the membrane antifouling ability will not be functional.

Although membrane antifouling ability has a limited useful life, membrane modification aiming for an enhanced antifouling ability is still meaningful. This is because the membrane antifouling ability not only influences the flux decline rate, but also affects the difficulty of membrane cleaning. The fouling layer on a membrane with stronger antifouling ability would be more easily removed due to the smaller adhesion

between the foulant layer and the membrane matrix.

### **1.5.2 Coordination between the water permeability and solute rejection**

Another important research challenge related to NF membranes is to coordinate the trade-off between water permeability and solute rejection. During the past decade, numerous researchers have proposed a variety of solutions from different perspectives to coordinate the trade-off effect. By classifying and analyzing the membrane fabrication or modification methods in the literature, five technical approaches can be distinguished.

#### **1.5.2.1 Promoting water mass transfer by enhancing membrane surface hydrophilicity**

As water is a typical polar solvent, a hydrophilic membrane with high polarity can have a stronger affinity towards water molecules. The stronger affinity between an NF membrane and water is conducive to the mass transfer of water. Yet many researchers found that the salt rejection was sacrificed when improving the membrane hydrophilicity [95]. There are various reasons for this phenomenon. For instance, the addition of a co-solvent and nanoparticles is a strategy to enhance the membrane hydrophilicity and water permeability. However, the addition of a co-solvent in interfacial polymerization could influence the interface properties and the monomer solubility and diffusivity, thus making the polyamide layer looser and promote the generation of defect pores with different sizes [96, 97]. The embedding of nanoparticles might result in some tiny gaps at the polymer-inorganic interface [98]. A possible way that may avoid this problem is to hydrophilize the NF membrane by surface modification.

Surface coating, surface grafting and surface irradiation treatment are three commonly adopted surface modification methods. However, most surface coating processes decrease the water permeability because the coating layer can provide an additional barrier for water molecules to overcome. Thus, surface grafting and surface irradiation

are recommended. Recently, amphibian-inspired amino acid ionic liquid (AAIL) was grafted on the NF membrane to improve the membrane performance, as illustrated in **Figure 1.9** [99]. The authors found that surface grafting with 1.0 wt% AAIL can decrease the contact angle from 37.8 ° to 21.4 °. Due to the enhanced hydrophilicity and enlarged MWCO, the water permeability increased from 7.5 L m<sup>-2</sup> h<sup>-1</sup> bar<sup>-1</sup> to 12.6 L m<sup>-2</sup> h<sup>-1</sup> bar<sup>-1</sup>. Meanwhile, the Na<sub>2</sub>SO<sub>4</sub> rejection was unchanged, but the NaCl rejection was decreased, which were induced by the improved membrane negative charge and enlarged membrane pore size, respectively. As a consequence, the selectivity between Na<sub>2</sub>SO<sub>4</sub> and NaCl was increased.



**Figure 1.9** (a) Schematic diagram of an AAIL modified NF membrane, and (b) the reaction formula [99].

Membrane surface irradiation is another available technology to enhance the membrane hydrophilicity while maintaining a stable structure of the membrane matrix. In a study reported by Kim et al. [100], commercial NF membranes were modified with low-pressure NH<sub>3</sub> plasma. The water flux of the commercial membrane NF270 can be increased by 40% while keeping the salt rejection constant after 40 W plasma treatment for 10 minutes. This result was attributed to the enhanced membrane surface hydrophilicity and electronegativity. As water molecules adsorb better on a hydrophilic surface, the water permeability can be improved according to dissolution and diffusion mechanisms. Both surface grafting and surface irradiation are effective techniques for enhancing membrane surface hydrophilicity. The comparison between surface grafting

and irradiation is summarized in **Table 1.2**.

**Table 1.2** Comparison between surface grafting and irradiation

Technique types	Advantage(s)	Disadvantage(s)
Surface grafting	Simple operation; Low cost; High scalability.	Low grafting density; Membrane surface charge can be influenced.
Surface irradiation	Effective and rapid; Applicable to different materials.	Plasma reactor is expensive and energy-intensive; Defects may be produced; Difficult to scale up.

### 1.5.2.2 Introducing water molecule channels into the functional layer

Introducing water molecule channels into the functional layer of an NF membrane is another way to coordinate the trade-off between water permeability and salt rejection. Aquaporins (AQPs), graphene and carbon nanotubes (CNTs) are three typical choices to construct such water molecule channels.

● **Aquaporins (AQPs)**. AQPs are a kind of protein in the cytomembrane that can selectively promote the high-speed penetration of water molecules while efficiently rejecting salt ions. In 2007, Kumar et al. [101] anticipated that once AQPs can be incorporated into the polymeric membrane, it is expected that they dramatically improve the membrane permeability without compromising salt rejection. Inspired by this inference, researchers proposed various methods to make use of the special function of AQPs and obtained different membranes with inspiring features, such as imprinting vesicles containing AQPs onto the surface of a porous substrate [102, 103]. In order to reduce the defects in the functional layer, the vesicle including AQPs deposited on the substrate can be further covered by a polymer layer [104]. A typical example, illustrated in **Figure 1.10**, is to immobilize the AQPs-incorporated proteoliposomes on the inner surface of a hollow fiber membrane and subsequently cover a polyamide layer via interfacial polymerization [105]. The biomimetic membrane prepared in this way

showed a flux almost 200% as high as the flux of a typical commercial membrane without sacrificing NaCl rejection.

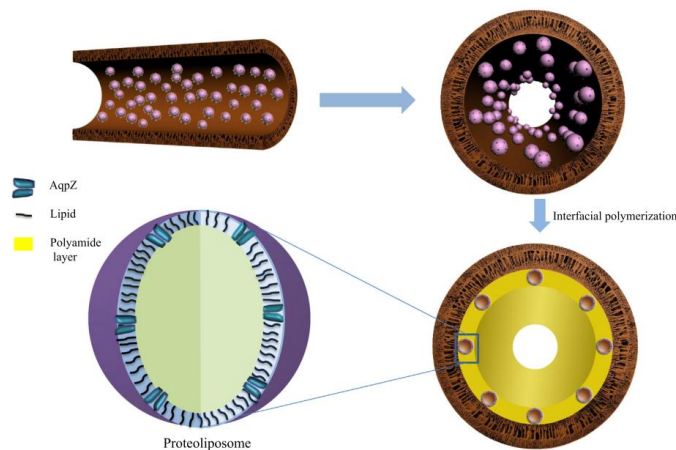


**Figure 1.10** Schematic representation of the preparation of AQP-based TFC composite membranes (not to scale) [105].

● **Graphene.** As the thinnest material (0.3 to 1.0 nm), graphene itself is impermeable due to its honeycomb lattice with high electron-density, strong structure with C-C bond energy and intrinsic strength [106]. There are two possible ways to construct water molecule channels with graphene. The first one is to create nano-pores in graphene sheets. If the pore size and functional groups can be precisely tuned to selectively allow water to permeate while rejecting dissolved salts, then the graphene sheets with nano-pores can be directly used as desalting membranes [107, 108]. However, how to produce pores with desirable size, and scaling up the membrane surface area are two main technique challenges. The second approach is to stack graphene oxide (GO) nanosheets and regard the interlamellar spacing as water molecule channels [109]. For this route, regulating the gap between GO nanosheets and keeping a stable stack structure during the cross flow desalination process are two critical problems to be solved before practical application. An alternative for making use of graphene is to introduce water molecule channels created by GO into the functional layer of polymeric membranes. In the research of Bano et al. [110], GO was embedded into the polyamide layer of an m-phenylenediamine (MPD) based NF membrane to improve its filtration

performance. The results indicate that incorporating 0.2 wt% GO may yield a 12 times increase in water flux while ensuring a non-decreased rejection for NaCl, Na<sub>2</sub>SO<sub>4</sub> and MgSO<sub>4</sub>.

● **Carbon nanotubes (CNTs)**. The smooth and hydrophobic inner hollow cavity at nanoscale makes CNTs to mimic the mass transfer characteristics of AQPs, which can selectively transport water molecules and reject other solutes [111]. In order to demonstrate the role of CNTs embedded in an NF membrane, different solutions were proposed to mix CNTs into the polyamide layer of NF membranes. Typically, raw CNTs should be first functionalized by, e.g., as poly(dopamine) coating, oxidation treatment, hydrothermal treatment, acid treatment, tannic acid (TA)-Fe complex coating and sulfonated treatment, aiming at promoting their dispersity in solvent and compatibility with the polymer matrix [112-116]. Then the functionalized CNTs can be added into the aqueous phase or organic phase together with reactive monomers, so that they can be introduced into the functional layer during interfacial polymerization. It should be noted that the packing density of CNTs in this method is very low, and the CNTs would be positioned randomly, rather than being well aligned. Even so, most researchers found that the addition of functionalized CNTs can effectively improve the water permeability and maintain a relatively stable salt rejection at optimized dosage. One possible reason for this phenomenon was that the embedded CNTs could provide fast transport channels for water molecules, although this was not directly evidenced. A comparison of the three materials is given in **Table 1.3**.



**Table 1.3** Comparison between surface grafting and irradiation

Material types	Advantage(s)	Disadvantage(s)
AQPs	<p>The compatibility between membrane matrix and AQPs incorporated vesicle is good, so defects are not easy to be produced;</p> <p>Rejections for all types of salts can be maintained when improving the water permeability, even for NaCl.</p>	<p>AQPs are not easy to obtain and preserve;</p> <p>AQPs need to be embedded into vesicles, and this process is complex;</p> <p>Difficult to scale up;</p> <p>May not be stable in harsh environment.</p>
GO	<p>Only a small dosage can achieve an obvious effect;</p> <p>GO is feasible to be functionalized to meet various requirements;</p> <p>Introducing GO into the selective layer may simultaneously enhance the membrane antifouling ability.</p>	<p>The distance between GO nanosheets is not easy to regulate;</p> <p>The stability of the stacked GO nanosheets cannot be ensured under high pressure;</p> <p>GO sheets may decrease the binding force between the substrate membrane and the polyamide layer;</p> <p>There may exist some potential toxicity once it was released into environment.</p>
CNTs	<p>The inner hollow cavity of CNTs is an inherent mass transfer channels for water molecules;</p> <p>Only a small dosage can achieve an obvious effect;</p> <p>Introducing CNTs into the selective layer may also enhance the membrane antifouling ability.</p>	<p>Raw CNTs need to be functionalized before use, and this process is complex;</p> <p>Difficult to scale up;</p> <p>Potential toxicity is higher than GO;</p> <p>How to align the CNTs is challenging;</p>

### 1.5.2.3 Increasing the effective membrane area by constructing a nano-wrinkled polyamide layer

The membrane area used in the calculation of the water permeability is essentially equal to the projected area of the flattened substrate membrane. If the functional layer of the TFC NF membrane can be folded on the substrate membrane, then the mass transfer regions can be enlarged to obtain a larger effective filtration area. The typical way to achieve this goal is to construct a nano-wrinkled polyamide layer *via* different techniques. In 2018, a paper published in *Science* reported a TFC NF membrane with “Turing structure” [117]. By adding hydrophilic polyvinyl alcohol (PVA) into the aqueous monomer solution during interfacial polymerization, the authors obtained a novel polyamide TFC NF membrane with nano-wrinkled surface morphology as shown in **Figure 1.11**. The increased effective filtration area made a great contribution in coordinating the trade-off between water permeability and salt rejection.

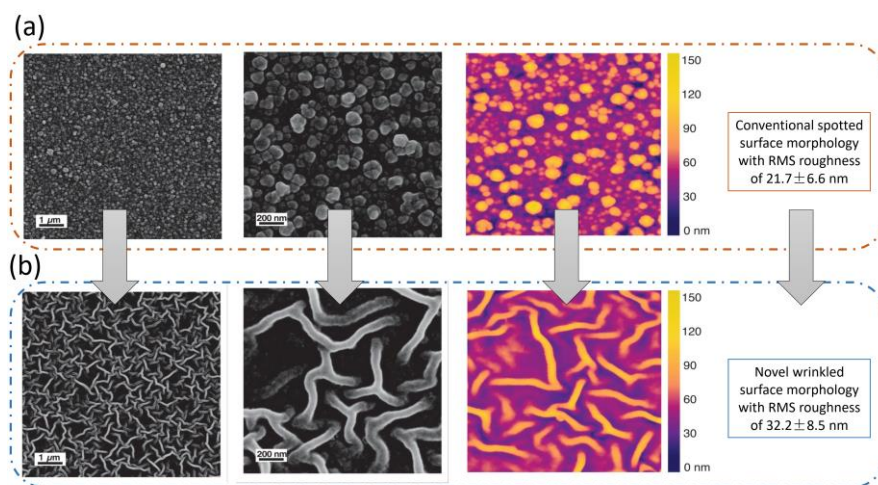


**Figure 1.11** Comparison between surface morphologies of conventional and novel wrinkled polyamide layer. (a) Conventional spotted surface morphology without polyvinyl alcohol addition. (b) Novel wrinkled surface morphology after adding polyvinyl alcohol in aqueous solution [117].

Almost at the same time, a nano-wrinkled polyamide active layer was constructed on the surface of a single-walled carbon nanotubes (SWNTs)/polyether sulfone composite

porous substrate membrane via another method by Wang et al. [118]. In this study, metal-organic framework nanoparticles (ZIF-8) were first deposited on the substrate membrane and used as a sacrificial templating material. Then the interfacial polymerization between PIP and TMC was conducted on the sacrificial layer, followed by removing the ZIP-8 particles *via* water dissolution. Finally, a TFC NF membrane with nano-wrinkled structure and outstanding performance was obtained, of which the water permeability and Na<sub>2</sub>SO<sub>4</sub> rejection reached 53.5 L m<sup>-2</sup> h<sup>-1</sup> bar<sup>-1</sup> and 95%, respectively.

### 1.5.2.4 Decreasing the thickness of NF membrane functional layer

The thickness of the membrane functional layer is an important parameter in both the solution-diffusion model and the pore flow model. According to these models, a reduction of the functional layer thickness can increase the water permeability, because a thinner functional layer would provide a shorter mass transfer distance. For TFC NF membranes, it is generally accepted that the thickness of the polyamide layer is between tens of nanometers and hundreds of nanometers [49].

From the perspective of reaction kinetics of interfacial polymerization, decreasing the monomer concentration is expected to yield a thinner polyamide layer. However, once the monomer concentration is decreased to a certain degree, the interfacial polymerization reaction on a conventional UF substrate membrane with low porosity, high roughness and poor wettability would promote the generation of many defects, which can obviously deteriorate the salt rejection. In order to solve this problem, Karan et al. presented a path-breaking study in 2015 [119]. The authors first prepared a special substrate by depositing cadmium hydroxide nanostrands on a conventional UF membrane. Then the interfacial polymerization reaction with extremely low monomer concentrations (0.1% MPD and 0.005% TMC) was carried out on this composite substrate. Benefiting from the low monomer concentration as well as the uniform and smooth surface of the substrate membrane, an integrated polyamide layer with sub-10 nm thickness was successfully produced, which promoted the ultrafast transport of

solvent while keeping the equivalent solute retention. Zhu et al. proposed another substrate membrane modification technique, in which polydopamine wrapped single-walled carbon nanotubes (SWCNT) were coated on a PES UF membrane [120]. Afterwards, a defect-free polyamide functional layer with thickness of 12 nm was fabricated on this substrate *via* the interfacial polymerization reaction between a low concentration of PIP (0.025%) and TMC (0.02%). The TFC NF membrane prepared with this technique showed ultrahigh water permeability of  $32 \text{ L m}^{-2} \text{ h}^{-1} \text{ bar}^{-1}$  and  $\text{Na}_2\text{SO}_4$  rejection of 95.9%. More recently, another controllable and scalable substrate membrane fabrication method as described in **Figure 1.12** was reported [121]. The ultrathin polyamide layer of only 15 nm formed on this substrate endowed the TFC NF membrane with high water permeability of  $40 \text{ L m}^{-2} \text{ h}^{-1} \text{ bar}^{-1}$  and  $\text{Na}_2\text{SO}_4$  rejection of 96.5%.

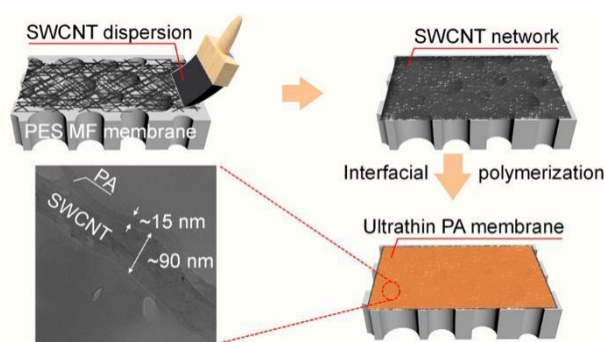


**Figure 1.12** Illustration of substrate membrane modification process via painting a SWCNT dispersion on a PES MF membrane and the fabrication of TFC NF membrane with an ultrathin polyamide layer [121].

In addition to decreasing the monomer concentration, other measures can also be taken to reduce the polyamide film thickness. For instance, Liu et al. tried to limit the transfer of PIP monomers into the organic reaction zone by decreasing the organic phase temperature [122]. It was found that the thickness of the polyamide film was reduced from 80.7 to 38.1 nm when decreasing the temperature from 25 °C to -10 °C. Spray technology is another useful tool for reducing the thickness of the polyamide layer. In

the work of Shan et al. [123], the authors proposed a novel microphase diffusion-controlled interfacial polymerization strategy by employing spray technology. Due to the unique micro-dispersion effect of liquid droplets in the spray process, fine polyamide matrices can be generated when the reactive monomer solution micro-droplets contact each other. Therefore, the thickness of the polyamide layer on the substrate membrane can be regulated by controlling spray cycles. Decreasing monomer concentration, reducing reaction temperature and spray technology are three typical methods to decrease the thickness of functional layer. The comparison of the three methods is summarized in **Table 1.4**.

**Table 1.4** Comparison between surface grafting and irradiation

Technical methods	Advantage(s)	Disadvantage(s)
Decreasing the monomer concentration	More effective than the other two methods in enhancing water permeability.	Special measures are necessary to mitigate the negative influence of substrate membrane; Binding force between the polyamide layer and substrate membrane may be reduced due the existence of interlayer made of nanomaterials; Difficult to scale up.
Decreasing the reaction temperature	Simple operation; Low cost; High scalability.	Effect is not obvious as other two methods.
Spray technology	The thickness of the polyamide layer can be precisely controlled by regulating the spray time or frequency.	Special spray equipment is necessary; Difficult to scale up; Desalting ability of the membranes prepared with this method is not high.

#### 1.5.2.5 Narrowing the pore size distribution of NF membranes

It is well recognized that the typical TFC NF membranes are non-isoporous membranes. The pore size distribution of these membrane follows a normal distribution within a certain size range. The usually mentioned pore size of a NF membrane is actually the

## Chapter 1

average pore size. It has been noted that the appearance of a trade-off effect was because it was difficult to increase the membrane pore size, while simultaneously narrowing the pore size distribution [124, 125]. Therefore, the water permeability can be improved without sacrificing salt rejection if one could simultaneously narrow the pore size distribution and increase the average pore size of a NF membrane. The most extreme strategy to achieve this objective is to fabricate an isoporous membrane. For instance, nano-sized pores with narrow size distribution (0.5~1 nm) were directly constructed on single-layer graphene by plasma etching in the work of Surwade et al. [108]. This nanoporous graphene membrane showed a high water permeability of over  $252 \text{ L m}^{-2} \text{ h}^{-1} \text{ bar}^{-1}$  and KCl rejection of almost 100%. However, only a micro-sized membrane sample can be obtained via this complex and expensive preparation method, which is far from the practical application. The self-assembly of block copolymers is another strategy to fabricate isoporous membranes. A typical example is the NF membrane prepared via the self-assembly of mixtures of two chemically interacting copolymers reported by the group of Peinemann [126]. The obtained NF membrane with pore size of 1.5 nm and MWCO of 600 presented a water permeability one order of magnitude higher than that of commercial NF membranes. However, the NF membrane fabricated in this way had no desalting ability due to its relatively large pore size.

Compared to the conventional phase inversion and interfacial polymerization methods, direct fabrication of an isoporous membrane *via* the above mentioned techniques (trepanning on single-layer graphene by plasma etching and the self-assembly of block copolymers) is much more expensive and complex. Therefore, the reconstruction of an existing NF membrane *via* post treatment seems to be a more feasible strategy for adjusting the membrane structure and narrowing the pore size distribution. Although there are many post treatment methods (such as acid treatment, base treatment and oxidation treatment) available [127], solvent activation may be the most promising one. This is because two effects may be resulted from solvent immersion. The first one is to heal the non-selective defects in the functional layer, while the second one is to unblock the permeation pathways by dissolving small polyamide fragments and other residual

reactants. In 2012, a paper published by Livingston's team first proposed the idea of activating the TFC organic solvent nanofiltration (OSN) membrane with strong solvent [128]. Another research finished by Razali et al. provided a more comprehensive results by analysing the influence of nine organic solvents on three different OSN membrane [129]. Although these two studies focused on OSN membranes, they were still enlightening for water treatment membranes. Recently, the study reported by Shin et al. confirmed the advantageous role of solvent activation in coordinating the trade-off between water permeability and salt rejection [130]. The authors found that solvent activation with benzyl alcohol after interfacial polymerization can improve the water permeability by 140%, while maintaining the same NaCl rejection (~99.6%) as that of the pristine sample. The performance of this post-treated membrane surpassed the current commercial products. It should be noted that the process conditions of solvent activation are critical to the resultant membrane performance. The trade-off between water permeability and salt rejection can only be coordinated under certain optimized conditions. For instance, the activation time could play an important role. An adequate solvent immersion time should be ensured to obtain the activation effect. However, an excessive activation time could usually deteriorate the membrane desalting ability.

According to the literature, there may exist three mechanisms for the defect-healing effect: 1) the polymer around the defects will swell during the solvent immersion. The rearrangement of the swelling polymer matrix could heal the non-selective pathways to some extent; 2) Secondly, some washed polymer fragments may be blocked in defects during the solvent immersion process, which could also heal the non-selective pathways; 3) the modulus of polymer network in the functional layer would be decreased after solvent activation, and then the chain flexibility would be improved. So some loosened sites without desalting ability could be eliminated after high pressure compaction during the filtration process. Although no direct evidence has been provided to support these explanations, they are still reasonable inferences. Based on the experimental results and reasonable inferences in the reported research, it is expected that this solvent activation process could heal the non-selective defects and simultaneously producing a

less dense polyamide layer. Preparing isoporous membranes and solvent activation are two promising techniques for narrowing the pore size distribution. A comparison of the two techniques is made in **Table 1.5**.

**Table 1.5** Comparison between surface grafting and irradiation

Technique types	Advantage(s)	Disadvantage(s)
Preparing isoporous membrane	High effectiveness;	Complex operation; High cost; Difficult to scale up.
Solvent activation	Simple operation; Low cost; High scalability.	Solvent selection is difficult; Substrate membrane should be solvent-resistant.

## 1.6 Thesis outline

The aim of this thesis is to explore nanofiltration as an advanced method for treatment and reclamation of petroleum wastewater from the perspective of membrane fabrication and modification. Accordingly, the chapters are organized as follows:

**Chapter 1** briefly describes the origin and characteristics of petroleum industry wastewater, followed by introducing the basic theory of NF technology including the definition, separation mechanism and fabrication methods. Furthermore, recent advances in NF membrane performance improvements are systematically reviewed from two aspects, i.e., membrane fouling control and the coordination between water permeability and solute rejection. **Chapter 2** lists the all the materials and chemicals used in the research. Procedures of different membrane fabrication/modification methods are described in detail. Membrane characterization methods and filtration performance testing devices are also systematically introduced.

**Chapter 3** aim to improve the anti-fouling ability of the NF membranes used for the treatment of polymer flooding produced water, which is one important wastewater in petroleum industry. More specifically, NF membranes are prepared by the interfacial



## Chapter 1

polymerization between serinol and TMC catalyzed by 4-dimethylaminopyridine (DMAP) on a flat-sheet PES substrate membrane. The membrane performance is maximized *via* optimization of the concentration of reactive monomers, the amount of DMAP, and reaction time of polymerization. The interfacial polymerization process is analyzed and divided in the four basic reaction patterns. The optimized NF membrane is characterized by XPS, ATR-FTIR spectroscopy, FESEM, AFM, contact angle meter, and electrokinetic analysis. Then, the desalting ability and molecular cut-off of the optimized NF membrane is assessed. Finally, the anti-fouling ability the novel NF membrane is evaluated.

In **Chapter 4**, an interesting phenomenon denoted as “support membrane pore blockage (SMPB)” which is found in the study of **Chapter 3** is systematically explored to understanding of the structure-property-performance relationship of TFC membranes. Herein, various experiments are designed to elaborate how SMPB impacted the TFC NF membrane performance by using piperazine (PIP) and trimesoyl chloride (TMC) as reactive monomers. A series of conceptual models are proposed to illustrate the SMPB phenomenon.

In order to make use of the antifouling ability of serinol and avoid the negative influence of “support membrane pore blockage (SMPB)”, in **Chapter 5**, serinol is used as a grafting monomer to modify the piperazine based TFC-NF membrane through the acylation reaction between the amino group of serinol and the residual acyl chloride groups on the nascent membrane. In this way, it is expected to decrease the number of residual carboxyl groups on the membrane surface and to enhance the membrane hydrophilicity. In order to demonstrate the effectiveness of this modification method, ATR-FTIR, AFM, FESEM, contact angle goniometer, surface Zeta potential analyzer, and the Toluidine blue O (TBO) technique are employed to study the unmodified membrane and the serinol-grafted membrane. Finally, the membrane performance including antifouling ability and solute rejection is evaluated.

In **Chapter 6**, research is conducted to enhance the NF membranes’ removing capacity

## Chapter 1

against heavy metals, which would affect the petroleum wastewater reclamation. A series of TFC NF membranes are prepared on the PES substrate by sharply decreasing TMC concentration. The physicochemical properties and microstructure of the resulted PA layers are comprehensively characterized, i.e., roughness, surface morphology, O/N, thickness, pore size, water contact angle and zeta potential. Meanwhile, membrane separation parameters are tested with a cross-flow filtration device. After analyzing all the statistic results, an optimized NF membrane with desirable performance is obtained. Then it was adopted to reject four heavy metal ions:  $\text{Ni}^{2+}$ ,  $\text{Zn}^{2+}$ ,  $\text{Cu}^{2+}$ , and  $\text{Cd}^{2+}$ . Furthermore, the effects of the operating factors on heavy metal removal, including metal ion concentration, cross-flow velocity, and pressure are investigated. Finally, the long-term operating stability and comparison with other reported results are provided. As increase the membrane water permeability is an effective way to decrease the energy consumption and operation cost during the reclamation of petroleum wastewater. In **Chapter 7**, the trade-off effect between solute rejection and water permeability is coordinated by regulating the thickness of the polyamide layer and optimizing the substrate membrane selection. The thickness variation of the PA film as well as the separation performance of the resultant TFC NF membranes when regulating the monomer (PIP and TMC) concentration are systematically explored. Five commercial UF membranes with different properties are used as the substrate to identify their impacts. Finally, general conclusions and future perspectives are proposed in **Chapter 8**.

## Chapter 1

# Chapter 2 Materials and Methods

## 2.1 Materials

### 2.1.1 Membrane materials

Two categories of commercial membranes, i.e., NF membranes and UF membranes, were used in this thesis. In order to evaluate the antifouling and separation performance of the NF membranes prepared in this thesis, commercial NF membranes including NF90 and NF270 provided by Filmtec Corporation were taken as comparison objects. Flat-sheet UF membranes with different structural and physicochemical properties manufactured by various companies were used the substrate membranes for interfacial polymerization reaction. The applied location, molecular weight cut-off (MWCO) and manufacturer information of the selected UF membranes are listed in **Table 2.1**.

**Table 2.1** Information of the selected UF membranes

Applied location	MWCO	Material	Manufacturer
Chapter 3/ Chapter 5	50 kDa	PES	Beijing Separate Equipment Co., Ltd.
Chapter 4	60 kDa	PS	Tangshan SEAPS Science and Technology Co., Ltd.
Chapter 5	30 kDa	PES	Beijing Separate Equipment Co., Ltd.
Chapter 5	80 kDa	PES	Beijing Separate Equipment Co., Ltd.
Chapter 6/ Chapter 7	100 kDa	PES	Microdyn-Nadir Co., Ltd.
Chapter 7	20 kDa	PES	Microdyn-Nadir Co., Ltd.
Chapter 7	50 kDa	Modified PES	Microdyn-Nadir Co., Ltd.
Chapter 7	150 kDa	PES	Microdyn-Nadir Co., Ltd.
Chapter 7	120 kDa	PES	Beijing OriginWater Membrane Technology Co., Ltd.

All the commercial membranes were thoroughly cleaned before use to remove the protective agents that may affect the experiments. The commercial NF membranes were immersed in ultrapure water for 24 hours and then flushed three times with ultrapure water before testing. However, for the commercial UF membranes, the cleaning procedure was more complicated as any residual agent on the membrane or inside its pores could influence the subsequent IP reaction. The UF membranes were immersed in 0.5% ethanol in water for 8 h and then transferred into ultrapure water for ultrasonic cleaning for 2 min. Subsequently, the substrate membranes were immersed in ultrapure water for another 12 h before use.

### 2.1.2 Chemical reagents

The chemical reagents used in this thesis can be classified into two categories according to their application. The first category is membrane preparation/modification, and the second category is membrane performance evaluation. All the chemicals and their related information are listed in **Table 2.2** and **Table 2.3**. All the reagents were used as received without further purification. In addition, the crude oil and anionic polyacrylamide (APAM) with molecular weight of 5 million Da used for preparing model PFPW were provided by the 5<sup>th</sup> Daqing oil production factory in China. The moisture content of the crude oil was less than 0.5%. The molecular structure of APAM is shown in **Figure 2.1**. Ultra-pure water was produced from a Milli-Q ultrapure water purification system. It should be noted that similar reagents produced by different manufacturers may be used because the research in this thesis was completed in different labs and countries.

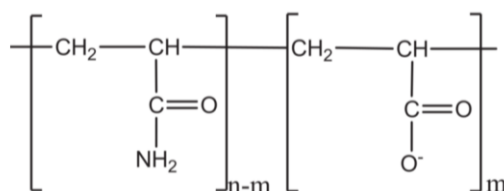


**Figure 2.1** Molecular structure of APAM

**Table 2.2** Chemicals used in membrane preparation/modification

Name	Specifications & Purity	Manufacturer
Serinol	>97.0%	Sinopharm Chemical Reagent Co., Ltd. (China)
n-hexane	>99%	Sinopharm Chemical Reagent Co., Ltd. (China)/ Sigma-Aldrich (Belgium)/ Aladdin Industrial Corporation (China)
Trimesoyl chloride (TMC)	>98.0%	Tokyo Chemical Industry (Japan)/ Sigma- Aldrich (Belgium)
4-dimethylaminopyridine (DMPA)	>99%	Aladdin Industrial Corporation Co., Ltd (China)
Triethylamine (TEA)	>99.5%	Aladdin Industrial Corporation Co., Ltd (China)
Piperazine (PIP)	>99%	Aladdin Industrial Corporation Co., Ltd (China)/ Sigma-Aldrich (Belgium)

**Table 2.3** Chemicals used in membrane performance evaluation

Name	Specifications & Purity	Manufacturer
NaCl	>99.5%	Sinopharm Chemical Reagent Co., Ltd. (China)/ Aladdin Industrial Corporation Co., Ltd. (China)
MgCl <sub>2</sub>	>99.5%	Sinopharm Chemical Reagent Co., Ltd. (China)/ Sigma-Aldrich (Belgium)/ Aladdin Industrial Corporation Co., Ltd. (China)

Table 2-3 (Continued)

Name	Specifications & Purity	Manufacturer
MgSO <sub>4</sub>	>99.5%	Sinopharm Chemical Reagent Co., Ltd. (China)/ Aladdin Industrial Corporation Co., Ltd. (China)
Na <sub>2</sub> SO <sub>4</sub>	>99.5%	Sinopharm Chemical Reagent Co., Ltd. (China)/ Sigma-Aldrich (Belgium)/ Aladdin Industrial Corporation Co., Ltd (China)/ Macklin Biochemical Co., Ltd. (China)
Polyethylene glycol (PEG) 200	average molar mass: 200 Da	Aladdin Industrial Corporation Co., Ltd. (China)/ Sinopharm Chemical Reagent Co., Ltd. (China)
Polyethylene glycol (PEG) 400	average molar mass: 400 Da	Aladdin Industrial Corporation Co., Ltd. (China)/ Sinopharm Chemical Reagent Co., Ltd. (China)
Polyethylene glycol (PEG) 600	average molar mass: 600 Da	Aladdin Industrial Corporation Co., Ltd. (China)/ Sinopharm Chemical Reagent Co., Ltd. (China)
Polyethylene glycol (PEG) 800	average molar mass: 800 Da	Aladdin Industrial Corporation Co., Ltd. (China)/ Sinopharm Chemical Reagent Co., Ltd. (China)
Polyethylene glycol (PEG) 1000	average molar mass: 1000 Da	Aladdin Industrial Corporation Co., Ltd. (China)/ Sinopharm Chemical Reagent Co., Ltd. (China)
Toluidine blue O (TBO)	>85%	J&K Scientific (China)

Table 2-3 (Continued)

Name	Specifications & Purity	Manufacturer
Diethylene glycol	>98%	Aladdin Industrial Corporation Co., Ltd. (China)
Triethylene glycol	>98%	Aladdin Industrial Corporation Co., Ltd. (China)
Glucose	>98%	Aladdin Industrial Corporation Co., Ltd. (China)
NiCl <sub>2</sub>	>99%	Aladdin Industrial Corporation Co., Ltd. (China)
ZnCl <sub>2</sub>	>98%	Aladdin Industrial Corporation Co., Ltd. (China)
CdCl <sub>2</sub>	>98%	Aladdin Industrial Corporation Co., Ltd. (China)
K <sub>2</sub> SO <sub>4</sub>	>99%	Aladdin Industrial Corporation Co., Ltd. (China)
CaCl <sub>2</sub>	>96%	Aladdin Industrial Corporation Co., Ltd. (China)
NaHCO <sub>3</sub>	>99%	Aladdin Industrial Corporation Co., Ltd. (China)
CuCl <sub>2</sub>	AR	Macklin Biochemical Co., Ltd. (China)
Methanol	>99%	Kemiou Chemical Reagent Co., Ltd. (China)
N,N-dimethylformamide (DMF)	>99%	Kemiou Chemical Reagent Co., Ltd. (China)



## 2.2 Experimental apparatus and instruments

### 2.2.1 Cross-flow NF testing apparatus

The separation performance and antifouling ability of different NF membranes were evaluated with a cross-flow NF testing apparatus as illustrated in **Figure 2.2**. The membrane cell of the cross-flow NF set-up was purchased from Sterlitech Corporation (CF016P, USA). The effective membrane surface area in this membrane cell was 20.4 cm<sup>2</sup>. The piston pump together with the frequency converter and pressure sensor could provide a relatively constant pressure of 1.5 MPa (pressure fluctuation  $\leq 0.01$  MPa). Electronic information of mass, pressure and temperature could be automatically controlled by the computer. The concentrates were recycled back into feed tank. The re-circulation flow rate was controlled by a rotameter to keep a constant cross-flow velocity. The capacity of feed tank was up to 30 L, and permeate water would be sent back to the feed tank once the accumulated volume was more than 100 mL. Therefore, the change of feed water caused by concentration effect could be ignored.

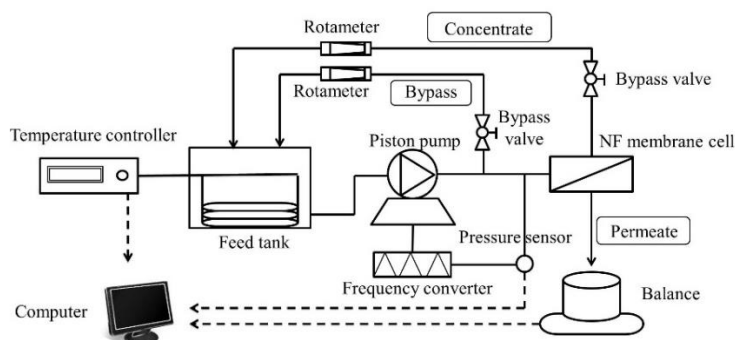


**Figure 2.2** Schematic diagram of the cross-flow NF testing apparatus used in this study

### 2.2.2 Other instruments

In this thesis, many other instruments were employed to analyse the water samples and to characterize the membrane properties. The name, model and manufacturer of all the used instruments are listed in **Table 2.4**. It should be noted that a similar characterization may be conducted with instrument with different models that produced

by different manufactures because the research in this thesis was completed in different labs and countries.

**Table 2.4** Other instruments used in experiments

Name	Model	Manufacturer
Attenuated total reflectance- Fourier transform infrared spectroscopy (ATR-FTIR)	Nicolet iS50	Thermo Scientific, USA
X-ray photoelectron spectroscopy (XPS)	ESCALAB 250Xi	Thermo Scientific, USA
Field emission scanning electron microscope (FESEM)	SUPRA 55	ZEISS, Germany
Atomic force microscope (AFM)	Bioscope	Veeco, USA
Electrokinetic analyzer	EKA	Anton Paar GmbH, Austria
Conductivity meter	DDSJ-308A	INESA Scientific Instrument, China
Total organic carbon analyzer	TOC-V <sub>CNP</sub>	Shimadzu, Japan
Contact angle goniometer	SL200B3	Solon, China
Spectrophotometer	DR5000	HACH, USA
Scanning electron microscope (SEM)	XL30 FEG	Philips, Netherlands
Conductivity meter	Orion Star A212	Thermo Scientific, USA
Scanning electron microscope	Nova Nano 450	FEI, USA
Atomic force microscopy (AFM)	Agilent 5500	Agilent, USA
Contact angle goniometer	OCA15EC	Dataphysics, Germany
Conductivity meter	ST3100C/F	Ohaus, USA
pH meter	DZS706	INESA Scientific Instrument, China
Atomic Absorption Spectrophotometer (AAS)	TAS-990	Beijin Purkinje, China

## 2.3 Experimental methods

### 2.3.1 Interfacial polymerization method

The NF membranes described in this thesis were thin film composite (TFC) NF membranes prepared with the interfacial polymerization technique. UF membranes listed in **Table 1.1** were used as the substrate membranes in interfacial polymerization (IP). The typical operation of this method consists of the following five steps, shown in **Figure 2.3**. All operations were performed in a clean room with a constant temperature and relative humidity. More detailed descriptions about the IP process, such as monomer concentration, coating time, heat treatment time and temperature, will be introduced in the specific chapter because they may differ from each other.

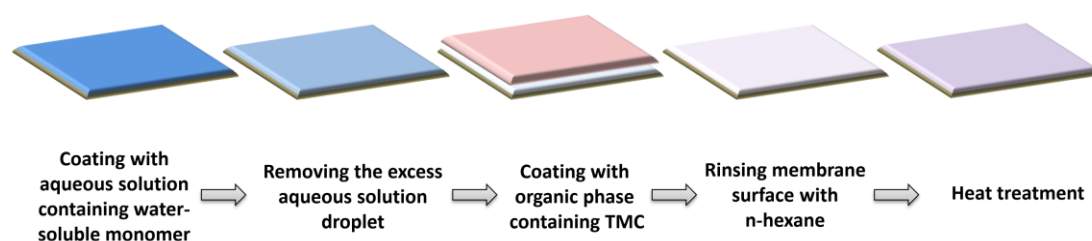


**Figure 2.3** Schematic diagram of the typical interfacial polymerization process

- **Aqueous phase immersion.** In this step, the cleaned substrate membrane was clamped in a polytetrafluoroethylene (PTFE) frame and coated with aqueous solution containing a certain amount of water-soluble monomer for a certain period of time. The PTFE frame can ensure only the top side of UF substrate can be coated with aqueous solution. The pH of the solution may be adjusted with base accordingly.

- **Removal of excess aqueous droplets.** Excess water droplets on the membrane surface should be removed to avoid its negative impact on interfacial polymerization. According to experience, the substrate surface should be kept in a state denoted as “moist but not watery” before coating with an organic phase. This condition could ensure the formation of a hydration layer containing water-soluble monomers on the

substrate surface, which is vitally important for the formation of a stable and intact interface. The time consumption of this step is defined as the lag time. If not specified, the lag time is fixed at 1 min to ensure the state of “moist but not watery”. Both filter paper and rubber scraper can be used to remove the excess water droplets. No matter which tool is adopted, the operation should be gentle to avoid scratching the surface of the substrate membrane.

● **Organic phase immersion.** After removing the residual aqueous droplets, the organic phase prepared by dissolving a certain amount of TMC into n-hexane was immediately poured onto the membrane surface and reacted for a certain period of time.

● **Rinsing the membrane surface with n-hexane.** Once the IP reaction time was up, the organic phase was poured off. Then the membrane surface was immediately rinsed with clean n-hexane to remove the residual TMC and terminate the IP reaction.

● **Heat treatment.** The above resultant membrane was positioned in an oven fixed at a certain temperature for a certain period of time. In this step, the residue n-hexane could evaporate and the newly formed polyamide film could be fixed on the substrate membrane. After heat treatment, the membranes were washed thoroughly with ultrapure water and stored in ultrapure water at 4 °C prior to use.

### 2.3.2 Evaluation of membrane separation performance

The water permeability and solute rejections of different NF membranes were evaluated with the cross-flow NF apparatus as illustrated in **Figure 2.2**. A constant trans-membrane pressure at a fixed temperature was always applied (details are indicated in the descriptions of specific experiments). Each new membrane was pre-pressurized with ultrapure water until the water flux was constant. The water permeability ( $P_0$ ) was subsequently measured using equation (2-1):

$$P_0 = \frac{V}{A \times \Delta t \times (\Delta P - \Delta \pi)} \quad (2-1)$$

## Chapter 2

where  $V$  is the permeate volume (L),  $A$  is the effective area of the membrane ( $m^2$ ),  $\Delta t$  is the time interval (h),  $\Delta P$  is the trans-membrane pressure, and  $\Delta\pi$  is the osmotic pressure difference. When membrane permeability was measured with ultrapure water, the osmotic pressure difference would be zero.

The salt rejection of a membrane was determined with a single-solute aqueous solution containing salts of NaCl, MgCl<sub>2</sub>, MgSO<sub>4</sub> or Na<sub>2</sub>SO<sub>4</sub>. The salt rejection was obtained by measuring the conductivity of aqueous solution using a conductivity meter. Neutral solutes including PEG of different molecular weight, diethylene glycol, triethylene glycol and glucose were used to determine the membrane molecular weight cut-off (MWCO). A rejection curve was plotted according to the different rejections of neutral solutes. The molar mass corresponding to a rejection of 90% was taken as the MWCO of the membrane [131]. As the solutions containing different neutral solutes were prepared by separately dissolving different neutral solutes (PEG, diethylene glycol, triethylene glycol and glucose) into ultrapure water, the rejections of different neutral solutes can be calculated according to the measurement of a TOC analyzer. The observed solute rejection  $R$  (%) was calculated according to equation (2-2). When studying the removal of heavy metals, concentrations of heavy metal ions were determined using an Atomic Absorption Spectrophotometer (see **Table 2.4**). The rejection was calculated according to equation (2-2).

$$R = \left(1 - \frac{C_p}{C_f}\right) \times 100\% \quad (2-2)$$

where  $C_p$  is the permeate concentration (mg/L) and  $C_f$  is the feed concentration (mg/L), respectively.

### 2.3.3 Determination of oil content

The oil content was measured by using the petroleum ether extraction method proposed by *Daqing* oilfield in China. The details of this method are as follows:

## Chapter 2

- **Establishment of the standard curve.** (1) Petroleum ether was used as the solvent to prepare a stock solution with an oil content of 20 mg/L. (2) A series of standard solutions with concentration gradient of 0 mg/L, 0.4 mg/L, 0.8 mg/L, 1.6 mg/L, 3.2 mg/L and 6.4 mg/L was prepared by diluting the crude oil stock solution with pure petroleum ether. (3) The absorbances of the six standard solution with concentration gradient were measured at the wavelength of 254 nm. Afterwards, the standard curve can be calculated. The standard curve is shown in equation (2-3):

$$y = 122.2311x + 0.0295 \quad (2-3)$$

$$R^2 = 0.9984$$

where  $x$  is the absorbance and  $y$  is the oil content (mg/L).

- **Operating steps.** (1) 20 ml of the water sample to be tested was added into a 125 ml separatory funnel with a pipette, followed by adding 3 ml of 1+1 hydrochloric acid and then mixing homogeneously. (2) 15 ml of pure petroleum ether was added into the separatory funnel, followed by shaking it up and down 300 times for full extraction. After standing for stratification, the aqueous solution in the lower layer was drained into a 50 ml colorimetric tube (A), and the petroleum ether with crude oil dissolved in the upper layer was drained into another 50 ml colorimetric tube (B) containing 5 g anhydrous  $\text{CaCl}_2$ . (3) 15 ml of pure petroleum ether was added into the colorimetric tube (A), followed by shaking to extract the oil in this water sample again. After standing for stratification, the petroleum ether with crude oil dissolved in the upper layer was also collected into the colorimetric tube (B). (4) Another 10 ml of petroleum ether was used to rinse the empty separatory funnel, and the rinse liquid was also collected into the colorimetric tube (B). (5) After shaking up the organic solution collected in the colorimetric tube (B), a 0.5 cm quartz cuvette was adopted to measure its absorbance at UV254. Finally, the oil content of the water sample can be calculated according to the standard curve.

### 2.3.4 Preparation of model petroleum wastewater

Model petroleum wastewater, more specific, polymer flooding produced water (PFPW), was prepared in laboratory to conduct the fouling related research. The ion composition and foulant concentration of the model solution were designated based on the analysis of the real wastewater in *Daqing* oilfield in China. As there were a mass of  $\text{HCO}_3^-$  in it, the buffering capacity of model PFPW was strong enough to keep its pH in 8.5-8.8. Therefore, the regulation of pH was not necessary in this work. Water quality of the model PFPW is illustrated in **Table 2.5**.

**Table 2.5** Water quality of the model PFPW

Parameter	Value
pH	8.5~8.8
TDS	5000 mg/L
$\text{Na}^+$	1442.6 mg/L
$\text{K}^+$	44.8 mg/L
$\text{Ca}^{2+}$	7.2 mg/L
$\text{Mg}^{2+}$	75.8 mg/L
$\text{Cl}^-$	1195.7 mg/L
$\text{HCO}_3^-$	2178.6 mg/L
$\text{SO}_4^{2-}$	55.2 mg/L
APAM	30.0 mg/L
Crude oil	1.5 mg/L

In order to prepare the model PFPW, the crude oil stock solution was firstly prepared using the following procedures: excessive crude oil, which had been melted at 60 °C, was added in flasks containing ultrapure water. Then ultrasonic dispersion and electric stirring were simultaneously lasted for 1 h. Subsequently, the oil slick in flasks was skimmed thoroughly and the oily solution was filtered by slow qualitative filter paper in order to remove dispersed oil. Eventually, a stock solution containing crude oil was prepared. The accurate crude oil concentration of the stock solution should be measured with the method described in **section 2.3.3**. Then a water solution with oil content of

1.50 mg/l was prepared by diluting the crude oil stock solution with ultrapure water. Finally, the model PFPW was obtained by dissolving calculated amount of salts and 30.00 mg/L APAM powder in the water solution with oil content of 1.50 mg/l. The salt amount that was added was 1.5800 g NaCl, 0.1000 g K<sub>2</sub>SO<sub>4</sub>, 0.0200 g CaCl<sub>2</sub>, 0.6408 g MgCl<sub>2</sub> • 6H<sub>2</sub>O, and 3.0000 g NaHCO<sub>3</sub> in every liter of water solution.

### 2.3.5 Evaluation of membrane antifouling ability

The model PFPW was used as the feed solution to evaluate the antifouling ability of different NF membranes. The new NF membranes were pre-pressurized with ultrapure water (temperature: 25 °C) until the water flux became constant. Then the baseline was obtained by treating ultrapure water (temperature: 25 °C, trans-membrane pressure: 5.0 bar and cross-flow velocity: 7.0 cm/s) for 2 h. Subsequently, the ultrapure water in the feed tank was replaced by the model PFPW. The filtration process was conducted for several cycles. Each cycle lasted for 8 h. After each cycle, the membrane was flushed with the feed water at a cross-flow velocity of 15.0 cm/s for 1 h. In order to avoid the influence of different initial fluxes on fouling evolution, the flux decline curve was obtained by treating model PFPW with the same starting water flux of 40 L•m<sup>-2</sup>•h<sup>-1</sup>. The flux decline rate and the flux recovery status after hydraulic cleaning can reflect the membrane anti-fouling ability. The flux recovery (FR) was calculated according to equation (2-3).

$$FR = \left( \frac{J_c - J_f}{J_0 - J_f} \right) \times 100\% \quad (2-3)$$

where  $J_c$  is the flux after hydraulic cleaning;  $J_f$  is the flux after fouling;  $J_0$  is the starting water flux.



## 2.4 Membrane characterization

### 2.4.1 Analysis of material composition

Attenuated total reflectance-Fourier transform infrared spectroscopy (ATR-FTIR) was used to analyze the chemical structure of different membranes. Samples were scanned in the range of 4000–650  $\text{cm}^{-1}$  with a resolution of 0.1  $\text{cm}^{-1}$  with air as the background. The element composition of the membrane surface was analyzed with X-ray photoelectron spectroscopy (XPS). Samples were scanned in the range of 0 to 5000 eV with a resolution of 1 eV. Shirley-type background was selected in the high-resolution spectra. Deconvolution with Gaussian-Lorentz peak was conducted to determine the binding energy shift of C (1s). All membrane samples used for ATR-FTIR and XPS analysis were firstly dried under vacuum at 30 °C for 24 h.

### 2.4.2 Morphology analysis

The surface morphologies and cross sections of membranes were visualized with a scanning electron microscope (SEM) equipped with an energy dispersive X-ray (EDX) detector that can be used to perform energy dispersive spectroscopy (EDS). The dried membrane samples were sputtered with gold before observation. Atomic force microscopy was used to analyze the 3D-morphologies and roughness of different membranes. The scanning pattern of probe was tapping mode in the air. The images were flattened with order 2 after scanning, so as to remove curvature and slope from the images. Then the RMS roughness (root-mean-squared roughness) was calculated according to equation (2-4):

$$R_{RMS} = \sqrt{\frac{\sum_{n=1}^N (z_n - \bar{z})^2}{N-1}} \quad (2-4)$$

where  $\bar{z}$  is the average of the z values within the given area,  $z_n$  is the current z value, and N is the number of data points within the given area [132].

### 2.4.3 Hydrophilicity analysis

Water contact angles of various membranes were measured with a contact angle goniometer by the sessile drop method at room temperature. Each contact angle value reported is the average of three different positions on the same membrane piece. Contact angles were calculated using the circle fitting method. In order to evaluate the hydrophilicity of different membranes more accurately, the model proposed by Wenzel was adopted to revise the measured contact angles to eliminate the influence of membrane roughness on water contact angles. The Wenzel model is expressed as equation (2-5) [133, 134]:

$$\cos \theta_w = r \cos \theta_0 \quad (2-5)$$

where  $\theta_w$  and  $\theta_0$  are the measured contact angle and intrinsic contact angle, respectively. The dimensionless roughness factor,  $r$ , is defined as the ratio of the actual solid surface area to the projected area of a rough surface. When the solid surface is relatively smooth with low roughness and a small  $r$  value ( $<1.7$ ), the  $r$  value can be calculated by AFM measurement [134-136]. The intrinsic contact angles ( $\theta_0$ ) were calculated according to the above equation.

### 2.4.4 Analysis of pore size distribution

To determine the pore size distribution of different membranes, a series of neutral organic solutions (200 mg/L) containing diethylene glycol, triethylene glycol, glucose, PEG with various molecular weight were used as markers. The concentrations of different organic solutes in feed and permeate solution were measured with a TOC analyzer. The geometric mean radius ( $\mu_s$ ) is defined as the Stokes-radius of a solute when the solute retention is 50%. The geometric standard deviation ( $\sigma_g$ ) is calculated from the ratio of stokes radius corresponding to the solute retention of 84.13% and 50%, respectively. By ignoring the dependence of solute separation on the steric and hydrodynamic interaction between solutes and pores, the mean effective pore radius

( $\mu_p$ ) and the geometric standard deviation ( $\sigma_p$ ) of the membrane can be considered to be the same as of  $\mu_s$  and  $\sigma_g$ . The relationship between pore size distribution and solute Stokes radius was mathematically fitted by an exponential probability density function (as shown in equation (2-6)) on the hypothesis that there are no hydrodynamic and electrostatic interactions between neutral solutes and membrane pores [137, 138].

$$\frac{df(r_p)}{dr_p} = \frac{1}{r_p \ln \sigma_p \sqrt{2\pi}} \exp \left[ -\frac{(\ln r_p - \ln \mu_p)^2}{2(\ln \sigma_p)^2} \right] \quad (2-6)$$

where  $r_p$  is the pore radius of the membrane.

The Stokes diameters of the different PEG solutes were calculated based on their molar mass with the following equations.

$$\text{Stokes diameter} = 33.46 \times 10^{-12} \times M^{0.557} \quad (2-7)$$

The Stokes diameters of other typical neutral solute used in the pore size distribution determination are listed in **Table 2.6**.

**Table 2.6** The Stokes radius (nm) of typical neutral solutes.

Type of organic solute	molar mass (Da)	Stokes diameter (nm)
Diethylene glycol	106.12	0.291
Triethylene glycol	150.17	0.334
glucose	180.16	0.365

#### 2.4.5 Analysis of membrane charge property

A SurPASS streaming potential analyzer was adopted to measure the membrane surface zeta potential using 1 mM KCl aqueous solution, and the pH was adjusted using 0.1 M of HCl or NaOH. The surface zeta potential was calculated from the measured streaming potential according to the Helmholtz-Smoluchowski equation [139].

#### 2.4.6 Analysis of carboxyl density

According to the method proposed by Tiraferri et al. [140], the density of negatively

charged functional groups on membrane surfaces can be quantification based on the adsorption of toluidine blue O (TBO). Briefly, the TFC NF membrane was sealed with a PTFE frame to leave only the active layer exposed. The exposed active layer was circular with a diameter of 9.0 cm. Then, the active layer of the TFC membrane was soaked in a freshly prepared TBO solution (2 mmol/L) for 30 min, which pH was adjusted to 11 using NaOH, so that the positively charged TBO molecules are bound to the deprotonated carboxylic acid groups on the TFC membrane surface. Then the TFC membrane surface was rinsed with a dye-free NaOH solution (pH 11) for 5 h to remove the unbound TBO molecules. At last, the TFC membrane was immersed into a NaCl solution for 30 min (pH was adjusted to 2 using HCl) to elute the bonded TBO dye from the active layer. The absorbance of the eluent was measured at a 630 nm wavelength to calculate the surface carboxyl group density [141].

### **2.4.7 Analysis of PA film thickness**

The thickness of the NF membrane functional layer is an important parameter that can affect its mass transfer process. In order to determine the PA film thickness, the PA film was peeled from the substrate with tape, tweezers, DMF solution and then transferred onto the silicon wafer [142]. More specific, the polyamide side of the TFC NF membrane was tightly pasted on the tape. Then the nonwoven fabric in the substrate membrane can be stripped with the tweezers. Afterwards, the substrate made of PES/PS was dissolved and thoroughly removed with DMF. Finally, the PA layer pasted on the tape can be taken down via flushing with methanol and then positioned onto the silicon wafer. After being dried in the air, it can be used in AFM detection. The drop between the silicon wafer surface and the PA film surface can be regarded as its thickness. The thickness data obtained from the AFM pictures were taken on the region close to the bound of silicon wafer and PA film [143, 144].

## Chapter 2

## Chapter 3

### **Fabrication of antifouling NF membrane *via* interfacial polymerization of serinol and trimesoyl chloride catalyzed by 4-dimethylaminopyridine**

Adapted from: *A novel polyesteramide thin film composite nanofiltration membrane prepared by interfacial polymerization of serinol and trimesoyl chloride (TMC) catalyzed by 4-dimethylaminopyridine (DMAP), Journal of Membrane Science, 542 (2017) 68-80.*

#### **3.1 Introduction**

One of the most prominent types of wastewater in the petroleum industry is polymer flooding produced water (PFPW). This is co-produced in the process of polymer flooding oil extraction. Previous research suggested to recycle PFPW for polymer flooding oil exploitation in an internal reuse pattern after advanced treatment with a commercial polyamide NF membrane [145]. However, the membrane fouling problem during this process is a challenge. The membrane material is the core of the membrane process, and the active layer synthesized *via* interfacial polymerization (IP) is crucial to enhance the performance of TFC NF membranes. The reactive monomers in IP and their chemical properties play the most important role to determine the pore dimensions, membrane thickness, roughness, hydrophilicity and chemical resistance of the active layer. Therefore, it is not surprising that various active monomers have been used for interfacial polymerization [146].

In recent decades, many researchers have tried to prepare novel TFC NF membranes with better performance by choosing different water-soluble monomers, such as polyamines, polyols, and polyphenols. Polyamide TFC NF membranes can be

obtained by choosing polyamines as water-soluble monomers. For instance, sulfonated monomers, melamine, ethylenediamine, fluoride monomers, zwitterionic amines as well as hyperbranched poly(ethyleneimine) have been used as water-soluble monomers to prepare polyamide TFC NF membranes [147-153]. Furthermore, polyester TFC NF membranes can be formed by employing polyols or polyphenols as water-soluble monomers. For example, bisphenol A (BPA), triethanolamine (TEOA), and tannic acid with abundant phenolic hydroxyl groups have been selected to prepare a polyester TFC NF membrane [154-156]. Generally, polyamide TFC NF membranes have higher salt rejections due to their higher cross-linked structure, while polyester TFC NF membranes have a stronger anti-fouling ability because of their abundant surface hydroxyl groups. An interesting area of research is focused on obtaining a TFC NF membrane that integrates the advantages of a polyamide membrane and a polyester membrane. In 2014, Zhou et al. [157] reported a novel TFC NF membrane formed with sericin that showed good anti-fouling ability. Sericin is a water-soluble globular protein with polar side groups, including hydroxyl, carboxyl and amino groups. The hydroxyl and amino groups in the sericin molecule have high reactivity, and they can both react with TMC and produce ester and amide bonds under normal conditions. Therefore, this kind of membrane is a polyesteramide (PEA) TFC NF membrane. However, as a water-soluble monomer, sericin has a rather high molecular weight of 10,000 g/mol, which would limit molecular diffusion. Therefore, the optimized membrane prepared with sericin has a relatively large MWCO of 880 g/mol. More recently, a poly(amide-co-ester) TFC NF membrane was formed through a two-step interfacial polymerization procedure using glucose and TMC on an ethylenediamine-cross-linked PEI support membrane [158]. This membrane exhibited a superior fouling resistance due to its highly hydrophilic and smooth surface.

Serinol (2-amino-1, 3-propanediol), which includes one amino group and two hydroxyl groups, is an important intermediate with good chemical stability and water solubility, which is widely used in medicine and in the chemical industry [159]. Serinol

is a small molecule with molecular weight of only 91 g/mol. If the amino and hydroxyl groups of serinol can react with TMC simultaneously, a PEA TFC NF membrane, which combines the advantages of polyamide membrane and polyester membrane, may be obtained. However, the acyl chloride of TMC would easily hydrolyze and limit the polymerization reaction at room temperature, as the reactivity of the hydroxyl groups is much lower than that of the amino group [160]. Moreover, due to the excellent hydrophilicity, serinol is difficult to transfer into the organic phase to react with TMC. Previous studies have demonstrated that 4-dimethylaminopyridine (DMAP) is an efficacious phase transfer catalyst as well as a nucleophilic acylation catalyst, which can obviously promote the interfacial polymerization reactions [158, 161, 162]. Therefore, DMAP is expected to facilitate the transport of serinol from an aqueous phase into an organic phase and accelerate the esterification of the hydroxyl group with acyl chloride.

Based on the above analysis, it can be anticipated that the hydrophilicity, roughness, carboxyl density and separation performance of a NF membrane would be regulated by selecting serinol as the reactive monomer for interfacial polymerization. Then the antifouling ability may be changed during the treatment of PFPW. Therefore, this chapter will try to fabricate a novel PEA TFC NF membrane *via* the interfacial polymerization between serinol and TMC catalyzed by DMAP on a flat-sheet PES substrate membrane. The membrane performance will be optimized by regulating the parameters of IP reaction, including the concentration of reactive monomers, the amount of DMAP, and the reaction time of polymerization. By taking a typical commercial NF product as reference, the structural and physicochemical features of the resultant NF membrane will be characterized by XPS, ATR-FTIR spectroscopy, FESEM, AFM, contact angle meter, and electrokinetic analyzer. Finally, the anti-fouling ability will be evaluated by taking model PFPW as feed solution.



## 3.2 Results and discussion

### 3.2.1 Optimization of the membrane fabrication conditions

The PEA TFC NF membranes were formed by interfacial polymerization between serinol and TMC on PES supporting membranes. The reaction mechanism and membrane preparation procedure is illustrated in **Figure 3.1**. The membrane performance is influenced by the preparation parameters, such as TMC and serinol concentrations, amount of catalyst, and reaction time, and these parameters were investigated to optimize the membrane fabrication conditions. Water permeability and the rejection of  $\text{Na}_2\text{SO}_4$ ,  $\text{NaCl}$ ,  $\text{MgSO}_4$  and  $\text{MgCl}_2$  were measured to evaluate the basic membrane performance.

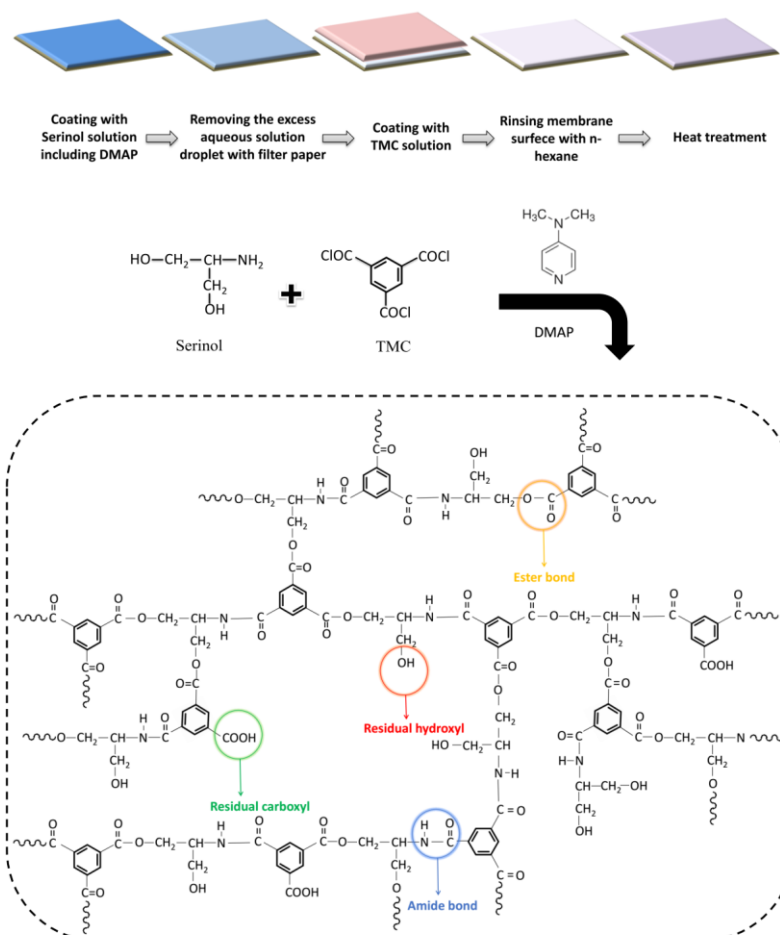


**Figure 3.1** Schematic representation of the reaction mechanism and membrane preparation procedure

### 3.2.1.1 Influence of TMC and serinol concentrations on membrane performance

As the reactive monomers, the concentrations of TMC and serinol have important impacts on the membrane performance. **Figure 3.2** shows the PEA TFC NF membranes fabricated using different concentrations of TMC with serinol concentration of 1.0% (w/v), DMAP equal to 10% the mass of serinol, and a reaction time of 70 s. **Figure 3.3** presents the PEA TFC NF membrane prepared using different concentrations of serinol with TMC concentration of 0.05% (w/v), DMAP equal to 10% the mass of serinol, and a reaction time of 70 s. Other conditions are discussed in Section 2.2.

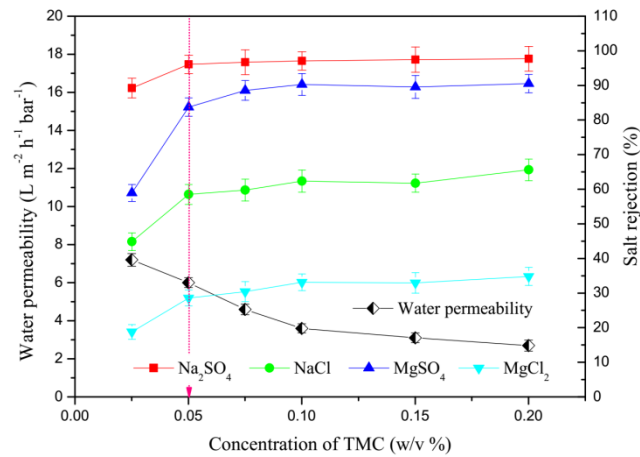


**Figure 3.2** Influence of TMC concentration on membrane performance at 0.5 MPa and 25 °C

As can be seen in **Figure 3.2**, the membrane water permeability continually decreased with increasing TMC concentration. This is because a higher concentration of TMC forms a denser and thicker active layer, thus improving the water mass transfer resistance [163]. As for the salt rejections, it can be seen that higher concentrations of TMC resulted in higher salt rejections. However, once the TMC concentration exceeded 0.05% (w/v), the improvement of salt rejections became unobvious. **Figure 3.3** shows that the membrane water permeability gradually decreased, while the salt rejections of Na<sub>2</sub>SO<sub>4</sub>, NaCl, MgSO<sub>4</sub> and MgCl<sub>2</sub> constantly improved as the serinol concentration increased from 0.25% to 2.5% (w/v). Nevertheless, when the serinol

concentration exceeded 2.5% (w/v), the membrane water permeability increased dramatically, while the membrane desalting ability sharply deteriorated. As DMAP adding amount was fixed at 10% the mass of serinol, the concentration of DMAP was increased with increasing the serinol concentration. When the concentration of serinol was higher than 2.5% (w/v), excessive DMAP would be harmful to the interfacial polymerization. This is because high concentration of DMAP in aqueous phase could promote the mass transfer of DMAP molecules into the organic phase. The DMAP molecules appearing in the organic phase would rapidly react with TMC and produce N-acylpyridinium salts, which are less soluble. This consequence would limit the interfacial polymerization between TMC and serinol. As a result, the membrane desalting ability sharply deteriorated. Therefore, in order to obtain relatively high water permeability and high salt rejections, the optimized concentrations of TMC and serinol were designated as 0.05% and 1.0% (w/v), respectively.

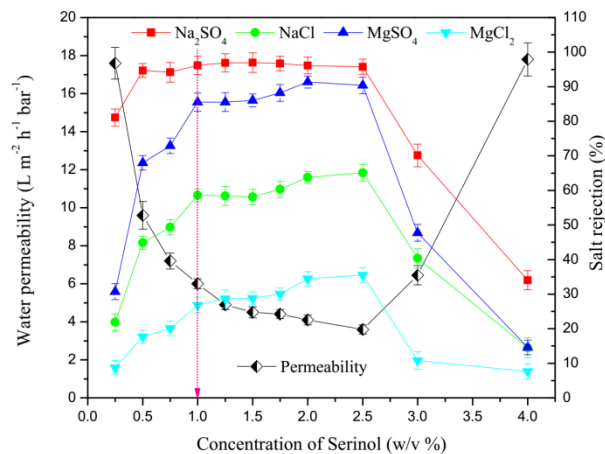


**Figure 3.3** Influence of serinol concentration on membrane performance at 0.5 MPa and 25 °C

Size exclusion and electrostatic repulsion are two main desalination mechanisms of NF membranes [164]. However, the dominant mechanism affects the relative rejections of different salts. **Figure 3.2** and **Figure 3.3** show that the relative rejections of the four salts always follows the order of  $\text{Na}_2\text{SO}_4 > \text{MgSO}_4 > \text{NaCl} > \text{MgCl}_2$ . This

particular order indicates that the TFC NF membranes prepared with serinol and TMC are negatively charged. Compared to  $\text{Cl}^-$  and  $\text{Na}^+$ , the membranes have a stronger repulsive force to  $\text{SO}_4^{2-}$  and a larger attractive force to  $\text{Mg}^{2+}$ . Although  $\text{Mg}^{2+}$  has a larger hydrated ionic radius, the rejection of  $\text{Na}_2\text{SO}_4$  was higher than that of  $\text{MgSO}_4$ . In addition, the rejection of  $\text{NaCl}$  was higher than that of  $\text{MgCl}_2$ . This phenomenon confirms that electrostatic repulsion is the dominant desalination mechanism of the PEA TFC NF membranes.

### 3.2.1.2 Influence of DMAP on membrane performance

Due to the limited catalytic capacity of the polymerization, it was necessary to optimize the amount of DMAP catalyst. Generally, it is necessary to use 0.05-0.2 mol of DMAP per mol of secondary or tertiary alcohol [161, 165]. For the convenience of calculations, the amount of DMAP in this study was determined based on its mass percentage accounting for serinol. **Figure 3.4** shows the influence of the amount of DMAP that was added on the membrane performance under the following conditions: TMC concentration of 0.05% (w/v), serinol concentration of 1.0% (w/v), and reaction time of 70 s.

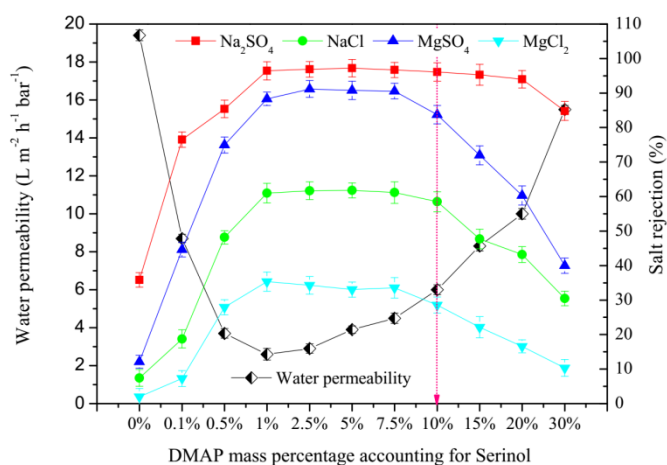


**Figure 3.4** Influence of DMAP on membrane performance tested at 0.5 MPa and 25 °C

The amount of DMAP added to the reaction had an obvious impact on the membrane performance. When the DMAP adding amount increased from 0 to 1%, the membrane water permeability dramatically decreased from 19.4 to 8.7 L m<sup>-2</sup> h<sup>-1</sup> bar<sup>-1</sup>, while the salt rejections improved. For instance, the Na<sub>2</sub>SO<sub>4</sub> rejection increased from 36.03% to 96.64%, and the NaCl rejection increased from 7.63% to 61.17%. This result suggests that DMAP effectively facilitated the interfacial polymerization between TMC and serinol. As the DMAP adding amount continually increased from 1% to 10%, the membrane water permeability increased from 2.6 to 6.0 L m<sup>-2</sup> h<sup>-1</sup> bar<sup>-1</sup> while the salt rejections remained relatively stable. A further increase of the DMAP concentration from 10% to 30% improved the water permeability, but the salt rejections deteriorated simultaneously.

In order to explain the influence of DMAP on the membrane performance, surface and cross-sectional images of the NF membranes prepared with different DMAP amount (0.1%, 1%, 10% and 30%, based on its mass percentage accounting for serinol) were analyzed with FESEM and shown in **Figure 3.5**. The surface FESEM images of the four PEA TFC NF membranes in **Figure 3.5 (a)**, **Figure 3.5 (c)**, **Figure 3.5 (e)** and **Figure 3.5 (g)** were used to estimate the particle size distribution. The particle size was measured with the *Nano Measurer 1.2* software. Two hundred surface particles were measured and analyzed statistically. The results are shown in **Figure 3.6**.

As shown in **Figure 3.5** and **Figure 3.6**, the mean size of the membrane surface particle gradually increased from 57.14 nm to 102.69 nm when the DMAP concentration was increased from 0.1% to 10%. This suggests that the molecular weight of the polymer formed in the polymerization reaction gradually increased. However, with small amounts of DMAP, such as 0.1%, no cross-linked thin film layer was found in the cross-section in **Figure 3.5 (b)**. Therefore, the membrane prepared under this condition had a very high water flux and a very low salt rejection. As the amount of DMAP increased to 1%, the membrane surface mean particle size increased to 85.21 nm, which implied that the molecular weight of the polymer increased.

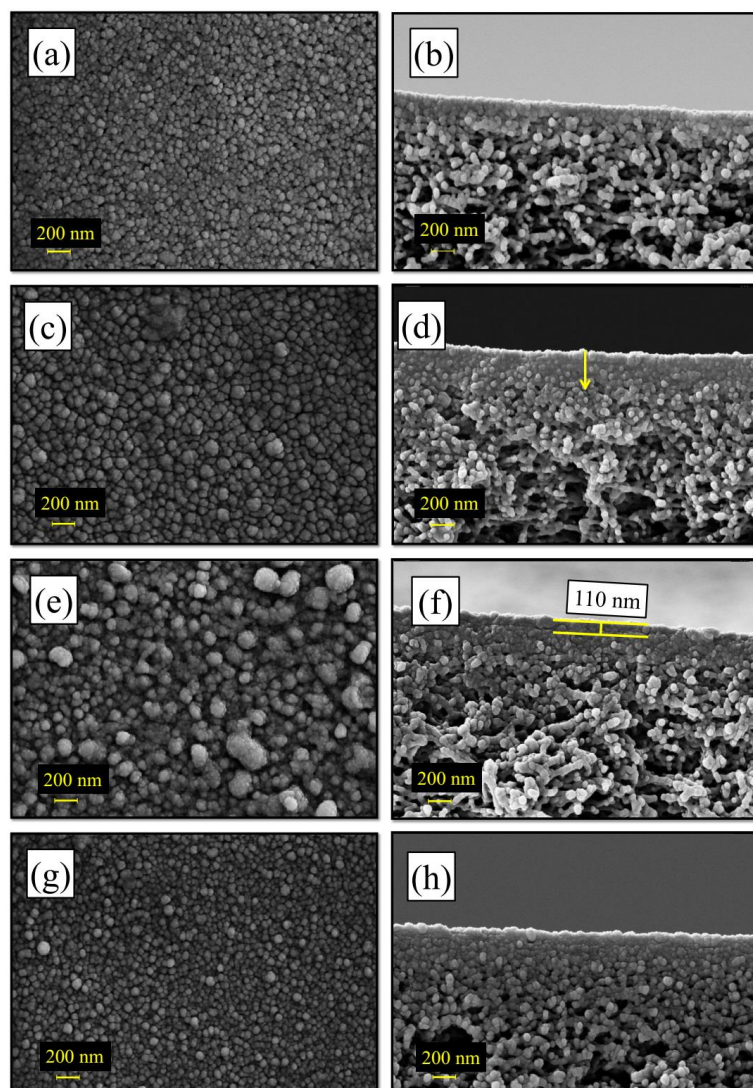


**Figure 3.5** FESEM images (a), (c), (e), and (g) show the top layers of the PEA TFC NF membranes with DMAP mass percentage accounting for serinol was 0.1%, 1%, 10% and 30%, respectively. FESEM images (b), (d), (f), and (h) show the cross-sections of the PEA TFC NF membranes when DMAP mass percentage accounting for serinol was 0.1%, 1%, 10% and 30%, respectively.

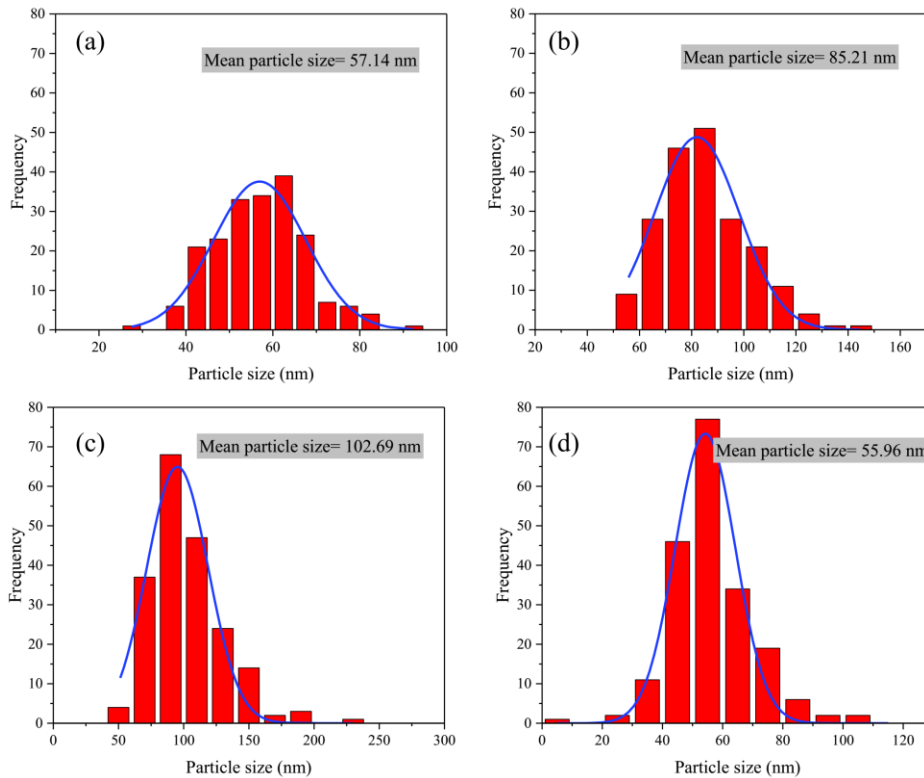


**Figure 3.6** The particle size distributions of (a), (b), (c), and (d) for the FESEM top layers of the PEA TFC NF membranes when DMAP mass percentage accounting for serinol was 0.1%, 1%, 10% and 30%, respectively.

Nevertheless, no obvious thin film layer can be found in **Figure 3.5 (d)**. Instead, the PES supporting membrane pores were filled. This suggests that the nascent polymer under this condition tended to enter the PES supporting membrane pores and block them, rather than forming a thin film layer. The polymer blocked in the supporting membrane pores can also endow the membrane desalting ability, but it will greatly increase the mass transfer resistance. Therefore, the membrane prepared under this condition had an extremely low water permeability. As the amount of DMAP increased to 10%, the molecular weight of the nascent polymer became large enough to form a thin film layer on the supporting membrane.

A thin film layer with thickness of about 110 nm can be seen in **Figure 3.5 (f)**. Therefore, the membrane water permeability was improved while maintaining a high

salt rejection. However, an excessive amount of DMAP (10% to 30%) would easily transform into the organic phase and rapidly react with TMC to produce N-acylpyridinium salts, which are less soluble [161]. This consequence would limit the interfacial polymerization between TMC and serinol. As shown in **Figure 3.6**, the membrane surface particle size dramatically decreased to 55.96 nm when the amount of DMAP was 30%. Consequently, no obvious cross-linked thin film layer can be found in the cross-section image in **Figure 3.5 (h)**. Therefore, the membrane prepared under this condition had a very high water flux and a very low salt rejection. Therefore, the optimized DMAP adding amount was determined to be 10%, accounting for the mass of serinol in order to acquire a relatively high water permeability and high salt rejections.

### 3.2.1.3 Influence of reaction time on membrane performance

The reaction time plays an important role in determining the degree of interfacial polymerization and, thus, the skin layer thickness and cross-linking extent [166]. Reaction times of polymerization from 15 s to 120 s were investigated under the following conditions: TMC concentration of 0.05% (w/v), serinol concentration of 1.0% (w/v), and the adding amount of DMAP equal to 10% of the mass of serinol. Other conditions are described in Section 2.2. The influence of reaction time on the membrane performance is presented in **Figure 3.7**.

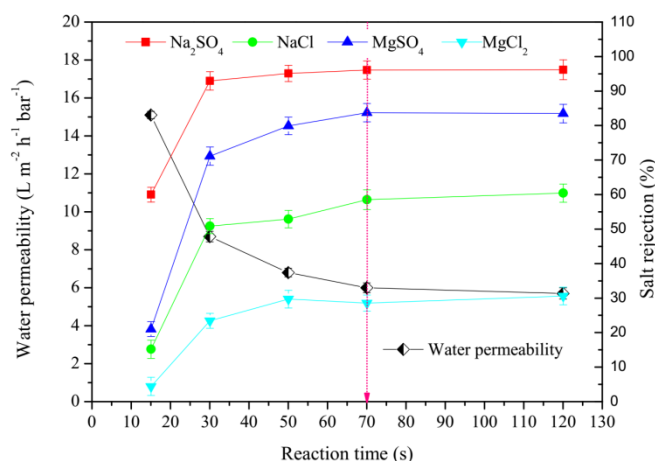


**Figure 3.7** Influence of reaction time on membrane performance tested at 0.5 MPa and 25 °C



As shown in **Figure 3.7**, the water permeability declined rapidly from 15.1 to 6.0 L m<sup>-2</sup> h<sup>-1</sup> bar<sup>-1</sup> when the reaction time increased from 15 s to 70 s. After 70 s, the permeability dropped slightly. Conversely, the salt rejection ability increased with prolonged reaction time from 15 s to 70 s. For example, the MgSO<sub>4</sub> rejection increased from 21.22% to 83.92%. Further increasing the reaction time from 70 s to 120 s did not obviously improve the salt rejections. The thickness of the skin layer of the composite NF membrane increased with prolonged reaction time [163]. Simultaneously, the degree of cross-linking also improved; therefore, the water permeability decreased, and the salt rejections increased. When the top layer is dense enough, the reactive monomers cannot diffuse across this layer and react with other monomers, so that the interfacial polymerization is a self-inhibiting reaction [164]. In this way, the thickness and cross-linking extent of the thin layer became stable after a reaction time of 70 s, which made the water permeability and salt rejections almost constant. Therefore, the optimized reaction time was determined to be 70 s.

#### 3.2.2 Physicochemical properties of the optimized membrane

According to the results presented in **Section 3.2.1**, the optimized membrane fabrication conditions are as follows: TMC concentration of 0.05% (w/v), serinol concentration of 1.0% (w/v), the amount of DMAP at 10% of the mass of serinol, and reaction time of 70 s. In the following sections, the NF membrane prepared under these optimized conditions is denoted as PEA-TFC-NF membrane. In order to evaluate the properties of the PEA-TFC-NF membrane, characterization was carried out with reference of a commercial polyamide NF membrane, NF90.

NF90 is a fully aromatic polyamide TFC NF membrane formed by the interfacial polymerization reaction between MPD and TMC. According to Tang et al. [167, 168], the molecular formula of the fully cross-linked polyamide membrane from TMC and MPD is C<sub>6</sub>H<sub>4</sub>ON with O/N of 1, while that of the fully linear one is C<sub>15</sub>H<sub>10</sub>O<sub>4</sub>N<sub>2</sub> with O/N of 2. Therefore, the O/N value of the NF membrane prepared with TMC and MPD

should range from 1 to 2. The lower the O/N value, the higher the cross-linking degree of the membrane. Different from the MPD molecule, serinol has three reactive groups, one amino and two hydroxyl groups. In this study, an evaluation method based on the reaction between serinol and TMC was established by employing a similar calculation to that of Tang. As the reaction rate constant of the amino group in the acylation reaction process is a few orders of magnitude higher than that of hydroxyl group [169], it can be assumed that the amino group in the serinol molecule must be able to react with TMC if any hydroxyl group in the same serinol molecule could react with TMC.

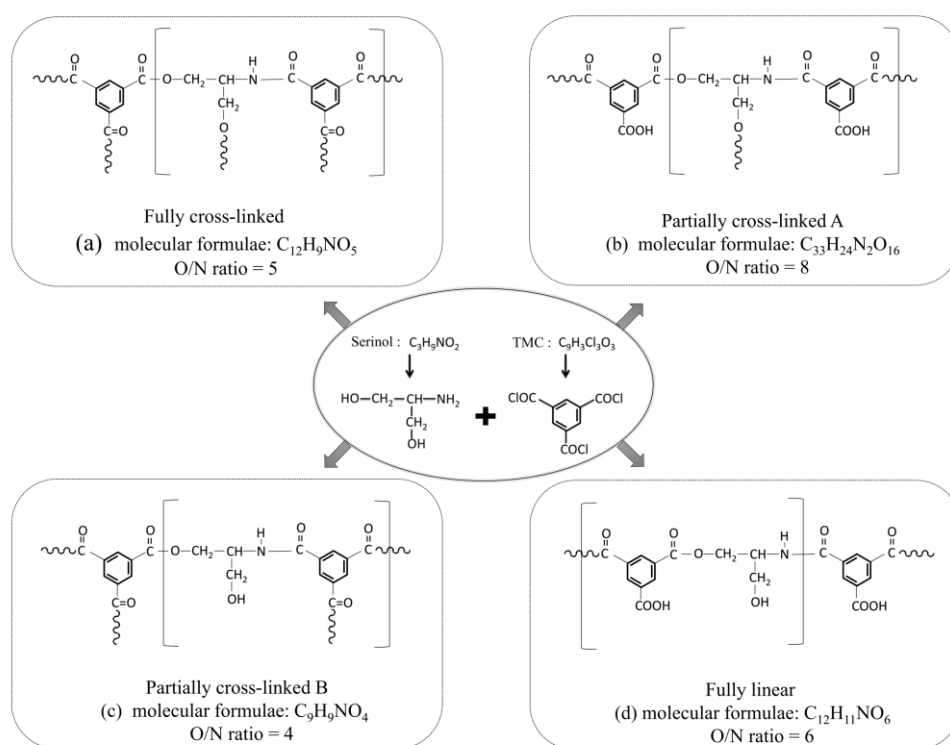


**Figure 3.8** Four basic reaction patterns of polyesteramide based on serinol and TMC

Based on this assumption, four kinds of basic reaction patterns are possible, as shown in **Figure 3.8**. They are named fully cross-linked pattern, partially cross-linked pattern A, partially cross-linked pattern B, and fully linear pattern, respectively. The molecular formulae of the four reaction patterns are  $C_{12}H_9NO_5$ ,  $C_{33}H_{24}N_2O_{16}$ ,  $C_9H_9NO_4$  and  $C_{12}H_{11}NO_6$ , respectively. The calculated O/N value of the four basic reaction patterns

are 5, 8, 4 and 6, respectively. It should be pointed out that the reaction patterns shown in **Figure 3.8** are four theoretically basic reaction patterns that may exist in the interfacial polymerization process between serinol and TMC. In reality, the actual reaction process should consist of more than one basic reaction pattern. The approach is to estimate to which reaction pattern the actual reaction process is closer according to the measured and theoretically calculated element compositions of different membranes.

**Table 3.1** XPS surface elemental analysis of the PA-TFC-NF and PEA-TFC-NF membranes

Membrane type	XPS surface elemental analysis			Relative ratio	
	C (%)	O (%)	N (%)	O/N	
NF90	Fully cross-linke <sup>d</sup>	75	12.5	12.5	1
	Fully linear <sup>a</sup>	71.41	19.06	9.53	2
	Measured value	73.9	14.0	12.1	1.16
PEA-TFC-NF membrane	Fully cross-linke <sup>d</sup>	66.4	28.0	5.6	5
	Partially cross-linked A <sup>a</sup>	63.9	31.2	3.9	8
	Partially cross-linked B <sup>a</sup>	64.5	28.4	7.1	4
	Fully linear <sup>a</sup>	62.9	31.8	5.3	6
	Measured value	65.45	27.82	6.73	4.13

<sup>a</sup> theoretically calculated value according to the molecular formula.

XPS was used to analyze the surface element composition of the PEA-TFC-NF and NF90 membranes. The measured and theoretically calculated element compositions of different membranes are shown in **Table 3.1**. By comparing the measured and theoretically calculated O/N value, it can be found that the cross-linking degree of NF90 is very high because its O/N value is 1.16. The O/N value of the PEA-TFC-NF membrane is 4.13, which is close to that of the partially cross-linked pattern B. This suggests that the cross-linking degree of the PEA-TFC-NF membrane is not very high. As the illustrated in **Figure 3.8**, there are residual hydroxyl groups in the partially cross-linked pattern B. The numerous residual hydroxyl groups in PEA-TFC-NF is expected

to enhance its hydrophilicity and promote its antifouling ability during the treatment of PFPW.

ATR-FTIR was employed to analyze the chemical structure of the PEA-TFC-NF membrane. For comparison, the PES supporting membrane and NF90 membrane were also studied. The results are presented in **Figure 3.9**. As the peak intensity in the high wave number region ( $> 3000\text{ cm}^{-1}$ ) is much lower than that in the low wave number region ( $< 2000\text{ cm}^{-1}$ ), the infrared spectra were divided into **Figure 3.9 (a)** and **Figure 3.9 (b)** in order to illustrate the peak difference more clearly.

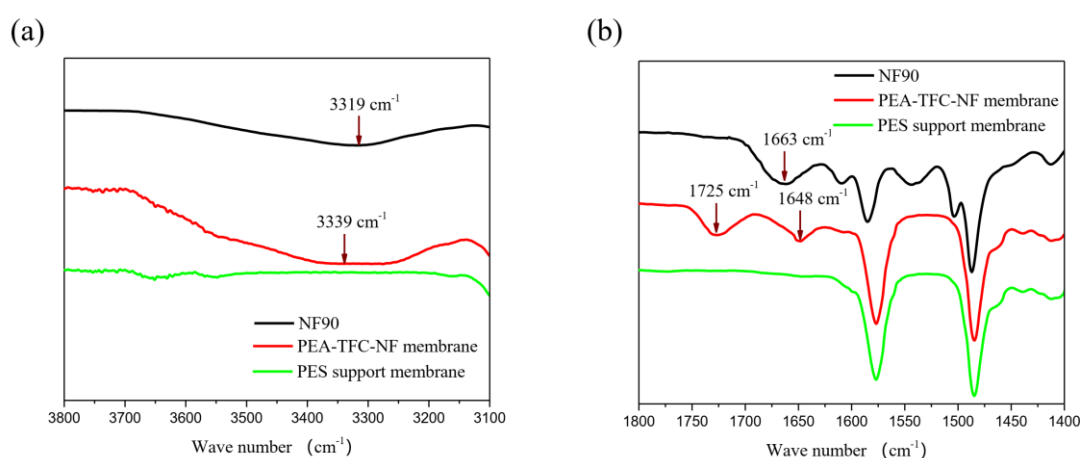


**Figure 3.9** ATR-FTIR spectra of different membranes

As indicated in **Figure 3.9 (a)** and **Figure 3.9 (b)**, three new peaks can be found at 3339  $\text{cm}^{-1}$ , 1725  $\text{cm}^{-1}$  and 1648  $\text{cm}^{-1}$  in the infrared spectrum of the PEA-TFC-NF membrane. The stretching vibration of hydroxyl groups produces a broad peak in the range of 3200-3500  $\text{cm}^{-1}$  [61, 170]. Therefore, the new peak at 3339  $\text{cm}^{-1}$  can be attributed to the unreacted hydroxyl groups of serinol in the PEA-TFC-NF membrane, which is consistent to the XPS data. These residual hydroxyl groups are expected to enhance the membrane hydrophilicity and suppress fouling by hydrophobic compounds. The presence of the new peak at 1648  $\text{cm}^{-1}$  and 1725  $\text{cm}^{-1}$  demonstrates the formation of amide bonds and ester bonds in the PEA-TFC-NF membrane [157, 171]. The absorption peak at 1663  $\text{cm}^{-1}$  in NF90 corresponds to the stretching vibration of C=O

in the amide I band, and the absorption peak at  $3319\text{ cm}^{-1}$  is related to characteristic absorption peak of N-H in the amide [167].

The surface morphology and roughness of PEA-TFC-NF membrane, NF90 and PES support membrane were characterized with AFM and shown in **Figure 3.10**. It can be found that the RMS roughness of the support membrane was only 6.1 nm. After the reaction between serinol and TMC, an active layer with granular surface structure and RMS roughness of 21.5 nm was formed on the support membrane. In contrast, NF90 was found to have a typical peak-valley structure with high RMS roughness of 46.7 nm. In comparison to NF90, the smoother surface feature and lower RMS roughness of PEA-TFC-NF membrane is beneficial to mitigate membrane fouling.

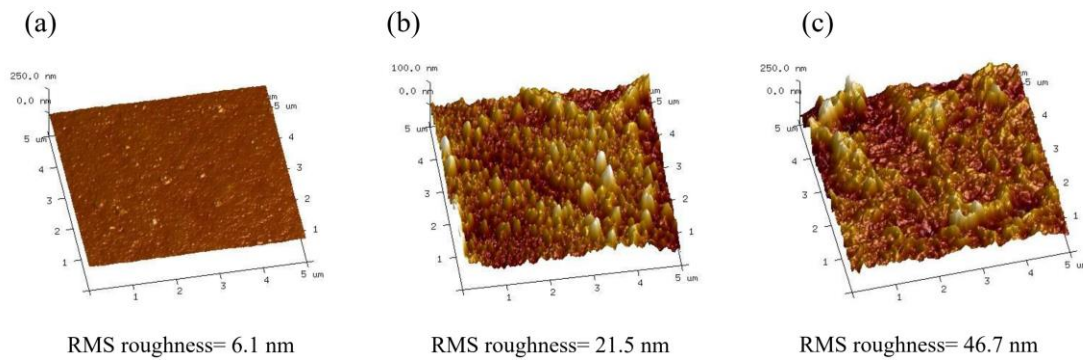


**Figure 3.10** AFM images of (a) the top layer of PES support membrane, (b) the top layer of PEA-TFC-NF membrane and (c) the top layer of NF90

The membrane hydrophilicity was evaluated by calculating the intrinsic water contact angles. The intrinsic water contact angles of the PES support membrane, the PEA-TFC-NF membrane, and the NF90 membrane were calculated according to the method described in Chapter 2. The results are displayed in **Figure 3.10**. The intrinsic water contact angle of the PES supporting membrane was  $58.12^\circ$ . After interfacial polymerization of serinol and TMC, the intrinsic contact angle of the PEA-TFC-NF membrane was only  $37.78^\circ$ , which was much lower than that of NF90 ( $61.16^\circ$ ). The FTIR spectra of the PEA-TFC-NF membrane in **Figure 3.8** indicate that there were unreacted, residual hydroxyl groups on the membrane surface. These hydroxyl groups

can effectively enhance the membrane hydrophilicity, which is beneficial to both water permeation and fouling resistance against hydrophobic foulants [172, 173].

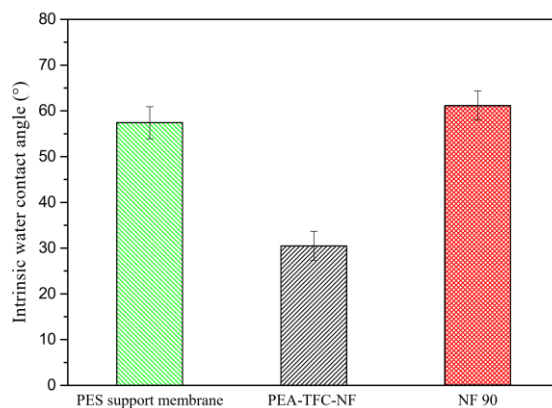


**Figure 3.11** Intrinsic water contact angles of different membranes

The surface charge of the membrane was evaluated by zeta-potential measurements. Surface zeta-potentials of the PEA-TFC-NF membrane and NF90 at different pH values are presented in **Figure 3.12**. It can be found that NF90 is an amphoteric membrane with isoelectric point at 4.35. It is negatively charged in a solution with pH higher than 4.35, and positively charged in a solution with pH lower than 4.35. Different from NF90, the zeta potential of the PEA-TFC-NF membrane was relatively stable, and negative across the entire pH range. The amphoteric surface characteristic of the typical polyamide composite membrane is due to its carboxyl groups and residual amino groups [139]. The more carboxyl groups, the more negative charge the membrane obtains. The more residual amino groups, the more positively charged the membrane surface. Similarly, the PEA-TFC-NF membrane in this study also has this feature. However, there is only one amino group and two hydroxyl groups in the serinol molecule. Additionally, the reactivity of the amino group is much stronger than that of hydroxyl groups in the interfacial polymerization process [160]; hence, most of the amino groups can effectively react with TMC. Therefore, the number of residual amino groups of PEA-TFC-NF membrane is small, contributing to the negative surface charge of the membrane across a wide pH range.

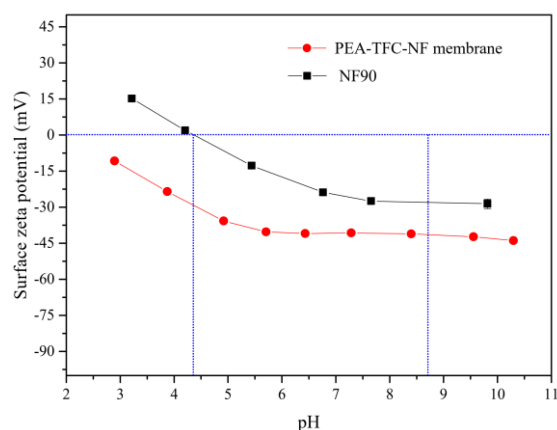


**Figure 3.12** Surface zeta-potentials of different membranes in 1 mM/L KCl solution with different pH values at 25 °C

In addition, the stronger negative charge of PEA-TFC-NF membrane compared to NF90 suggests that there are more residual carboxyl groups on the membrane surface of PEA-TFC-NF. The presence of numerous carboxyl groups on the membrane surface could bring two effects during the treatment of PFPW. On the one hand, the ionized carboxyl groups could enhance the electrostatic repulsion between the membrane surface and the negatively charge foulant (APAM), so membrane fouling could be mitigated due to this interaction. However, the electrostatic repulsion should be negligible because the high TDS of PFPW (5000 mg/L) would greatly screen the electrostatic effect. On the other hand, the interaction between APAM and membrane surface can be enlarged because of the complexation effect bridged by  $\text{Ca}^{2+}$ , which could enhance membrane fouling. Therefore, the high density of carboxyl groups on the PEA-TFC-NF membrane is harmful to the fouling control.

### 3.2.3 Separation performance of the optimized membrane

According to the testing results, the water permeability of the PEA-TFC-NF membrane was around  $6.0 \text{ L m}^{-2} \text{ h}^{-1} \text{ bar}^{-1}$ , while that of NF90 was  $7.6 \text{ L m}^{-2} \text{ h}^{-1} \text{ bar}^{-1}$ . Generally, the water permeability of a TFC NF membrane is determined by the active layer thickness, hydrophilicity and cross-linking degree. A lower active layer thickness, a

higher hydrophilicity and a lower cross-linking degree are expected to increase the water permeability. The thickness of the PA layer in NF90 was determined to be above 130 nm [174]. In comparison to NF90, the PEA-TFC-NF membrane has a lower active layer thickness (around 110 nm), a higher hydrophilicity and a lower cross-linking degree, but the water permeability of the PEA-TFC-NF membrane is lower. This unexpected behavior may result from the support membrane pore blockage induced by the oligomer produced by the polymerization between TMC and serinol with low reactivity. The pore blockage of the support membrane greatly increases the mass transfer resistance.

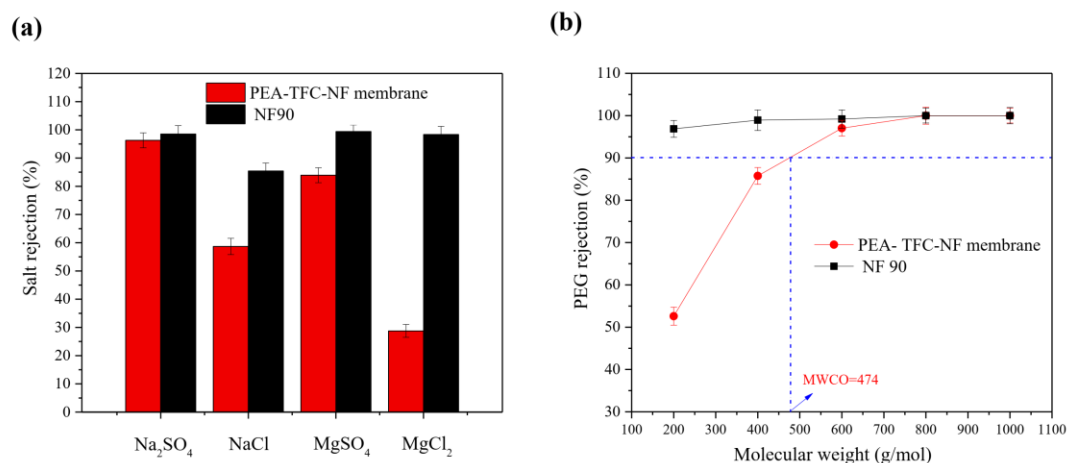


**Figure 3.13** Rejections to different salts and PEG solutions by the PEA-TFC-NF membrane and NF90 at 0.5 MPa and 25 °C

The rejections to different salts are shown in **Figure 3.13**. Molecular weight cut-off (MWCO) values of the membranes were determined based on the rejection of neutral solutes [175, 176]. Permeation experiments were conducted with feed solutions containing PEG 200, PEG 400, PEG 600, PEG 800 and PEG 1000. The PEG rejections are shown in **Figure 3.13 (b)**. The MWCO value is determined by the molecular weight of the solute whereby the rejection is equal to 90%. As indicated in **Figure 3.13 (a)**, the salt rejections of PEA-TFC-NF membrane followed the order of Na<sub>2</sub>SO<sub>4</sub> > MgSO<sub>4</sub> > NaCl > MgCl<sub>2</sub>, and the values were 96.3%, 83.9%, 58.7% and 85.4%, respectively. The MWCO of PEA-TFC-NF membrane was around 474 Da. Meanwhile, the salt rejections



of NF90 followed the order of  $\text{MgSO}_4 > \text{Na}_2\text{SO}_4 > \text{MgCl}_2 > \text{NaCl}$ , and the values were 99.4%, 98.5%, 98.3% and 85.4%, respectively. The MWCO of NF90 cannot be determined in **Figure 3.13 (b)** because its rejection to PEG200 was much higher than 90%. Size exclusion and electrostatic repulsion are two main desalination mechanisms of NF membranes; which one is dominant influences the rejection order of NaCl and  $\text{MgCl}_2$ . As indicated by the zeta-potential measurements, both the NF90 membrane and the PEA-TFC-NF membrane are negatively charged when the solution pH = 7. As the MWCO of NF90 is much lower than 200, size exclusion should be the dominant desalination mechanism.  $\text{Mg}^{2+}$  has a larger hydrated ionic radius than  $\text{Na}^+$ , so the  $\text{MgCl}_2$  rejection of NF90 is higher than the NaCl rejection. As for the PEA-TFC-NF membrane, it has a relatively high MWCO (about 474 Da). Thus, electrostatic repulsion should be the dominant desalination mechanism. In this case, the negatively charged PEA-TFC-NF membrane would have a larger attractive force to  $\text{Mg}^{2+}$  compared to  $\text{Na}^+$ , so its NaCl rejection is higher than its  $\text{MgCl}_2$  rejection. Besides, the number of residual amino groups in the PEA-TFC-NF membrane is very small. Therefore, this membrane does not have enough repulsive force to reject  $\text{Mg}^{2+}$ . Moreover, the XPS analysis suggests that the cross-linking degree of the PEA-TFC-NF membrane is relatively low. Therefore, the PEA-TFC-NF membrane has low rejections of  $\text{MgSO}_4$  and  $\text{MgCl}_2$ .

#### **3.2.4 Anti-fouling properties of the PEA-TFC-NF membrane**

In order to evaluate the antifouling ability during the treatment of PFPW, the NF90 and PEA-TFC-NF membranes were used to treat the model PFPW in this section. The treatment process was continuously operated for two cycles; each cycle was 8 hours. After the first cycle, the membrane was cleaned with high-speed hydraulic circulation. The flux decline curve and flux recovery after hydraulic cleaning can be used to evaluate the antifouling ability of the NF membranes. In order to avoid different hydrodynamic drag effects produced by permeate flux, the operation pressure was regulated to maintain the initial water flux at  $40 \text{ L/m}^2\cdot\text{h}$ .

As shown in **Figure 3.14**, the flux of NF90 quickly decreased during the treatment of model PFPW. The normalized flux decreased to 0.76 at the end of the first cycle. Even after the hydraulic cleaning for 1 hour, the flux recovery was rather low, and the normalized flux only recovered to 0.78. During the second cycle after hydraulic cleaning, the flux continues to decrease at a slower rate, indicating that the fouling layer had become relatively stable. The normalized flux after two operation cycles was 0.72.

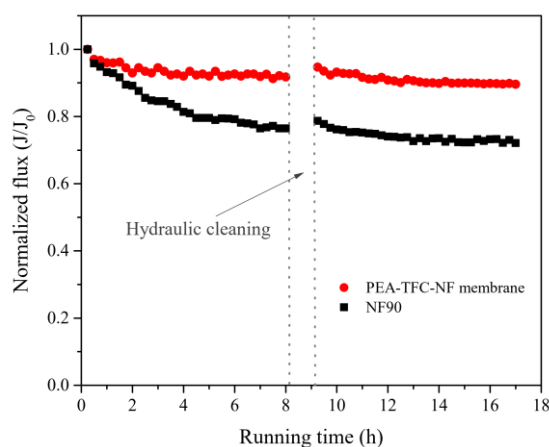


**Figure 3.14** Evaluation of NF membrane antifouling ability

Different from NF90, the novel PEA-TFC-NF membrane presented a different trend of membrane fouling. The membrane flux of PEA-TFC-NF only declined slightly during the first 3 h and then reached a relatively stable state. At the end of the first cycle, the normalized flux was still high (0.92). After hydraulic cleaning, the normalized flux recovered to 0.95. The normalized flux after two operation cycles was 0.89. These three values are much higher than for NF90, which demonstrates that the PEA-TFC-NF membrane showed a remarkable antifouling ability during the treatment of PFPW. According to the characterization results in the previous sections, the PEA-TFC-NF membrane fabricated via the IP reaction between serinol and TMC has a stronger hydrophilicity, smoother surface structure, stronger negative charge and lower salt rejection, in comparison to the commercial membrane NF90. A hydration layer can be formed on the hydrophilic membrane surface, which would prevent the adsorption of foulants on the membrane matrix. A smooth surface morphology could mitigate the accumulation of foulants on membrane surface. The stronger negative charge could

enhance the electrostatic repulsive between membrane matrix and the negatively charged APAM. The relatively low salt rejection could alleviate the concentration polarization, which is closely related to membrane fouling. All these property variations yielded the antifouling ability of the PEA-TFC-NF membrane.

### 3.3 Conclusions

In this chapter, a novel PEA-TFC-NF membrane was prepared by the interfacial polymerization between serinol and TMC catalyzed by DMAP on a flat-sheet PES substrate membrane. The results show that the optimized membrane fabrication conditions were as follows: TMC concentration of 0.05% (w/v), serinol concentration of 1.0% (w/v), the amount of DMAP at 10% of the mass of serinol, and reaction time of 70 s. The membrane has a MWCO of 474 Da and water permeability of  $6.0 \text{ L}\cdot\text{m}^{-2}\cdot\text{h}^{-1}\cdot\text{bar}^{-1}$  at 0.5 MPa and 25 °C. The membrane salt rejections followed the order of  $\text{Na}_2\text{SO}_4 > \text{MgSO}_4 > \text{NaCl} > \text{MgCl}_2$ , and the values were 96.3%, 83.9%, 58.7% and 28.8%, respectively. Compared with NF90, the stronger hydrophilicity, smoother surface structure and lower salt rejection of PEA-TFC-NF membrane endows its remarkable antifouling ability during the treatment of model PFPW. However, it should be noted that the PEA-TFC-NF membrane fabricated in this chapter is not optimal due to its low water permeability and poor rejection to divalent cations. Besides, the high density of residual carboxyl groups on membrane surface is not beneficial to the control of fouling.

## Chapter 4

### **Support Membrane Pore Blockage (SMPB): An Important Phenomenon during the Fabrication of Thin film Composite Membranes via Interfacial Polymerization**

Adapted from: *Support Membrane Pore Blockage (SMPB): An Important Phenomenon during the Fabrication of Thin film Composite Membrane via Interfacial Polymerization, Separation and Purification Technology, 215 (2019) 670-680.*

#### **4.1 Introduction**

The typical TFC membrane has a three-layer structure, which consists of a non-woven fabric, a polysulfone support layer and a selective layer made of polyamide (PA) [177]. As illustrated in the literature, there is a clear boundary between the support membrane and the PA thin film [178-181]. However, a growing number of studies indicates that the boundary is not so distinct as described in the conceptual models, especially for TFC membranes fabricated by *in-situ* IP reaction [182-186]. This is due to the possibility of polymer formation within the support membrane pores, although the bulk of polymer is on top of the support membrane. For instance, Singh et al. [187] found that the penetration of PA into the support membrane pores played an important role in the permeability and salt rejection of a TFC RO membrane. Similarly, Ghosh and Hoek [184] reported that PA formation deep within the support membrane deteriorated the TFC membrane permeability. The formation of PA layer inside the pores was also suggested by Misdan et al. [188] to explain the influence of the support membrane on the NF membrane performance. In the study of Zhang et al. [189], the PA structure could be found in the pores of a poly(ether sulfone) support membrane because of organic phase intrusion; this also resulted in a dramatic decrease in water flux. Jimenez-

Solomon et al.[190] demonstrated that PA penetration into the support layer should be well controlled to avoid a decrease in flux. Thus, they increased the solvent flux by impregnating the support membrane with polyethylene glycol and treating the TFC membrane with an “activating solvent”. An IP reaction may also occur in the pores of a support membrane, and block them [191]. The formed polymer causing the blockage within the support membrane pores will largely increase the mass transfer resistance. This phenomenon described in the literature is denoted as “support membrane pore blockage (SMPB)” in this study.

Apart from the *in-situ* IP reaction on a support membrane, a free-standing PA nanofilm can be directly formed at a free oil/water interface, followed by transferring onto the surface of a support membrane. This TFC membrane fabrication technique is expected to avoid SMPB. In the research of Karan and coworkers [192], a free-standing PA layer was created on a nanostrand sacrificial layer followed by acid dissolution of the sacrificial layer. This strategy enabled the attachment of a free-standing PA layer in the TFC membrane with ultrafast solvent transport. Recently, researchers in this group also prepared TFC RO membranes with higher permeability and comparable NaCl rejection by transferring a free-standing PA nanofilm onto different support membranes [193]. Park et al. [194] proposed the concept of support-free interfacial polymerization (SFIP) and prepared TFC RO membranes by directly attaching the PA layer onto a hydrolyzed polyacrylonitrile (HPAN) support membrane. Furthermore, they extended this concept with dual layer slot coating (DSC) equipment and successfully fabricated high performance TFC RO membranes with a facile and scalable method [195]. The higher permeability of TFC RO membranes produced with the SFIP and DSC technique was attributed to the thinner PA layer and less penetration of PA polymer into the pores of the support membrane.

It should be noted that SMPB is not always a negative factor for the membrane performance. Many researchers have mentioned that SMPB may enhance the adhesion force between the PA layer and the support membrane by mechanical interlocking,

which would be rather meaningful to obtain a good long-term stability of the membrane in view of practical application [194-197]. From this viewpoint, a drawback of the TFC membrane fabricated by the support-free technique is the relatively weak adhesion between the PA layer and the support membrane. Park et al. [194] found that such free-standing PA films are easily delaminated from the pristine PAN substrate after being soaked in water. The resulting TFC membrane only exhibited a NaCl rejection of only 17.2%. In this regard, the use of hydrolyzed polyacrylonitrile (HPAN) as a support can obviously improve the stability of the TFC membrane. This is mainly due to the formation of carboxyl groups after hydrolysis, which can result in ionic bonds through an acid-base interaction with the amine groups of the PA layer [198-200].

Although SMPB has been mentioned by many researchers, it is necessary to provide more evidence and expound it in a systematic way. Therefore, this chapter will explore the phenomenon denoted as “support membrane pore blockage (SMPB)”, and to identify the negative and positive influences on the performance of a TFC membranes. Based on this objective, various experiments were designed to elaborate how SMPB impacted the TFC NF membrane performance by using piperazine (PIP) and trimesoyl chloride (TMC) as reactive monomers. A series of conceptual models will be proposed to illustrate the SMPB phenomenon. The current study is expected to allow for a better understanding of the structure-property-performance relationship of TFC membranes.

## **4.2 Results and discussion**

### **4.2.1 Regulating SMPB by altering monomer concentration**

Based on the formation mechanism of the PA layer proposed by Xu et al. [201], oligomers are firstly produced at the initial stage of the IP reaction between monomers, and further laterally evolved into a continuous PA film which would be covered on the support membrane. This formation mechanism is built on the hypothesis that the IP

reaction occurs away from the surface of the support membrane. It is reasonable to infer that once the oligomers are formed within the pores of the support membrane, they will induce SMPB, rather than forming a continuous, defect-free PA film through the connection of oligomers. During the *in-situ* IP reaction, pores of the support membrane act as reservoirs of aqueous solution. If the monomer concentration in the aqueous solution or in organic phase is extremely low, the newly formed oligomers are too small in quantity to be timely connected. Thus the oligomers could be transferred into the support membrane pores and resulted in SMPB. In order to verify this inference, different TFC NF membranes were prepared by adjusting monomer concentrations (PIP in aqueous solution and TMC in n-hexane solution) separately or simultaneously.

#### 4.2.1.1 Adjusting TMC concentration

**Figure 4.1** (a) presents the influence of the TMC concentration on the membrane separation performance when the PIP concentration was fixed at 0.6%. The TMC concentration ranges from 0.00625% to 0.1%.

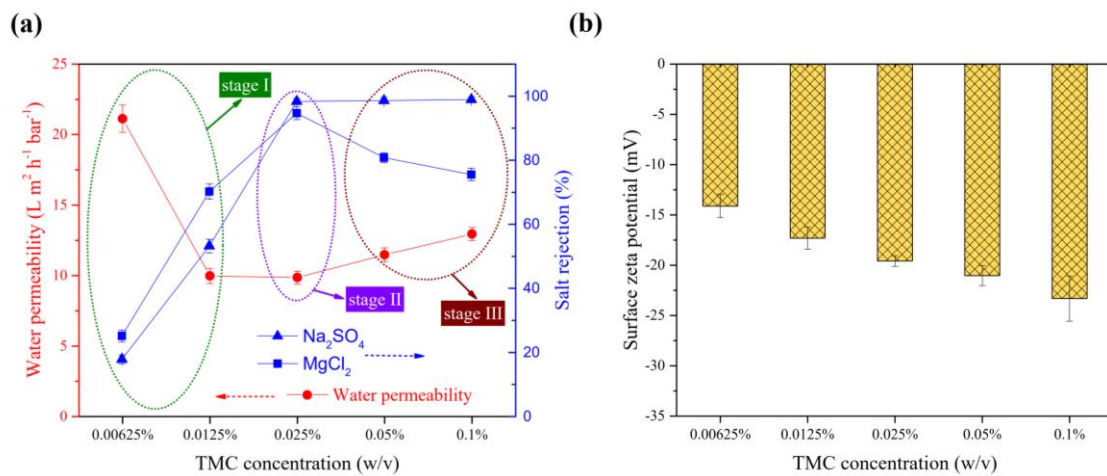


**Figure 4.1** Influence of TMC concentration on membrane separation performance tested at 0.5 MPa (a), and membrane surface zeta-potential measured at pH 7.0 (b)

Based on the five testing points related to different TMC concentrations, TMC concentration of 0.025% can be regarded as a “critical point” because the resultant NF membrane at this point showed the lowest water permeability and highest  $Na_2SO_4$  and  $MgCl_2$  rejection. Taking this point as boundary line, **Figure 4.1** (a) can be divided into

three stages. **Stage II** corresponds to the “critical point” of 0.025% TMC. TMC concentration lower than 0.025% can be taken as **stage I**, in which the water permeability decreases while salt rejections increase when increasing the TMC concentration from 0.00625% to 0.025%. Moreover, the  $\text{MgCl}_2$  rejection was higher than the  $\text{Na}_2\text{SO}_4$  rejection in this stage. TMC concentration higher than 0.025% can be taken as **stage III**, in which the  $\text{MgCl}_2$  rejection was lower than the  $\text{Na}_2\text{SO}_4$  rejection. The water permeability increases, while the  $\text{MgCl}_2$  rejection decreases when increasing the TMC concentration from 0.025% to 0.1%. As shown in **Figure 4.1 (b)**, the surface zeta-potentials of different NF membranes gradually decrease from -14.1 mV to -23.3 mV when TMC concentration increase from 0.00625% to 0.1%, indicating that the negative charge of the membrane can be enhanced with higher TMC concentration.

SEM images in **Figure 4.2 (b)** and **Figure 4.2 (f)** show the surface morphology and the cross-section of NF-0.6-0.00625-30 kDa. Some defects can be observed on the membrane surface. This result demonstrates that the continuous coverage of a PA film without defects cannot be obtained in **Stage I**. Moreover, as shown in **Figure 4.2 (f)**, the pores of the porous support membrane were filled with oligomers, which can induce SMPB. Therefore, compared with the 30 kDa PES support membrane (water permeability around  $180 \text{ L m}^{-2} \text{ h}^{-1} \text{ bar}^{-1}$ ), NF-0.6-0.00625-30 kDa has a water permeability of only  $21.1 \text{ L m}^{-2} \text{ h}^{-1} \text{ bar}^{-1}$  and a poor desalting ability (18.1% for  $\text{Na}_2\text{SO}_4$  and 25.3% for  $\text{MgCl}_2$ ). The higher rejection of  $\text{MgCl}_2$  compared to  $\text{Na}_2\text{SO}_4$  was a result of the extremely large PIP/TMC ratio (96:1), which can endow the membrane with more residual amino groups and a lower negative charge (only -14.12 mV for NF-0.6-0.00625-30 kDa.). In conclusion, severe SMPB without continuous PA layer coverage is a proper description for the TFC membranes in **Stage I**.

As for **Stage II**, the structural features of NF-0.6-0.025-30 kDa in **Figure 4.2(c)** and **Figure 4.2(g)** provide an appropriate description. That is severe SMPB and continuous PA layer coverage. The severe SMPB in NF-0.6-0.025-30 kDa resulted in its lowest



water permeability, while the continuous PA layer coverage endowed its highest salt rejection, as shown in **Figure. 4.1 (a)**.

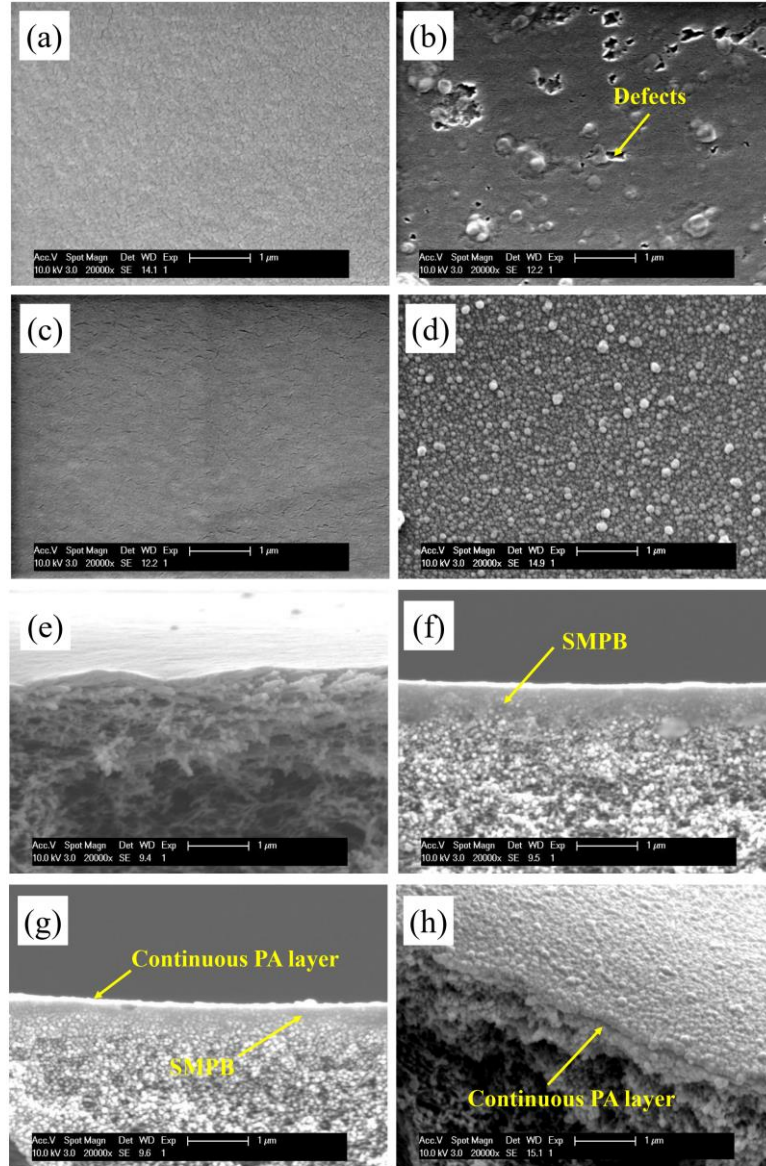


**Figure 4.2** SEM images (a), (b), (c), and (d) show the surfaces of 30 kDa PES support membrane, NF-0.6-0.00625-30 kDa, NF-0.6-0.025-30 kDa and NF-0.6-0.1-30 kDa, respectively. SEM images (e), (f), (g), and (h) show the cross-sections of 30 kDa PES support membrane, NF-0.6-0.00625-30 kDa, NF-0.6-0.025-30 kDa and NF-0.6-0.1-30 kDa, respectively.

In **stage III** with higher TMC concentrations, the IP reaction between PIP and TMC was accelerated, so the nascent oligomers would tend to connect and form a PA layer on the support membrane surface, rather than penetrating into the pores of the support membrane. In this stage, SMPB was alleviated. Thus, the resultant NF membranes in **stage III** have a higher water permeability, as shown in **Figure 4.1 (a)**. The SEM images in **Figure 4.2(d)** and **Figure 4.2(h)** confirm that there is a continuous PA layer coverage on the support membrane. However, due to the enhanced negative charge of the NF membranes in **stage III** (as shown in **Figure 4.1(b)**), the  $\text{MgCl}_2$  rejections of these membrane are lower than NF-0.6-0.025-30 kDa. The general description of **Stage III** is slight SMPB and with continuous PA layer coverage.

#### 4.2.1.2 Adjusting PIP concentration

**Figure 4.3 (a)** indicates the influence of the PIP concentration on the membrane separation performance when fixing the TMC concentration at 0.1%. Different from the complex variation trend in **Figure 4.1 (a)**, the sustainable decrease of water permeability with increasing PIP concentration from 0.1% to 2.4% is consistent to the findings of other researchers [202]. As shown in **Figure 4.3 (b)**, when increasing PIP concentration from 0.1% to 2.4%, the negative charge property was reduced as the residual amino groups increased (from -28.4 mV to -17.4 mV).

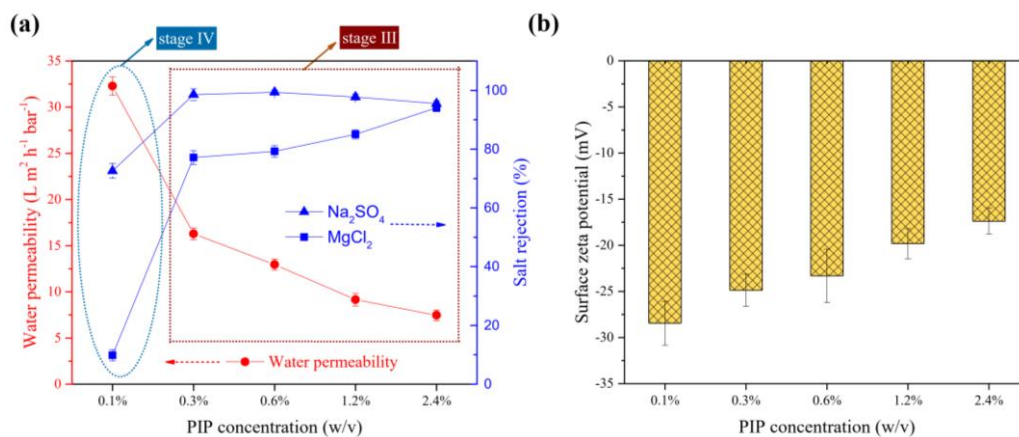


**Figure 4.3** Influence of PIP concentration on membrane separation performance tested at 0.5 MPa (a), and membrane surface zeta-potential measured at pH 7.0 (b)

Meanwhile, the PA selective layer became thicker, as shown in **Figure 4.4**.

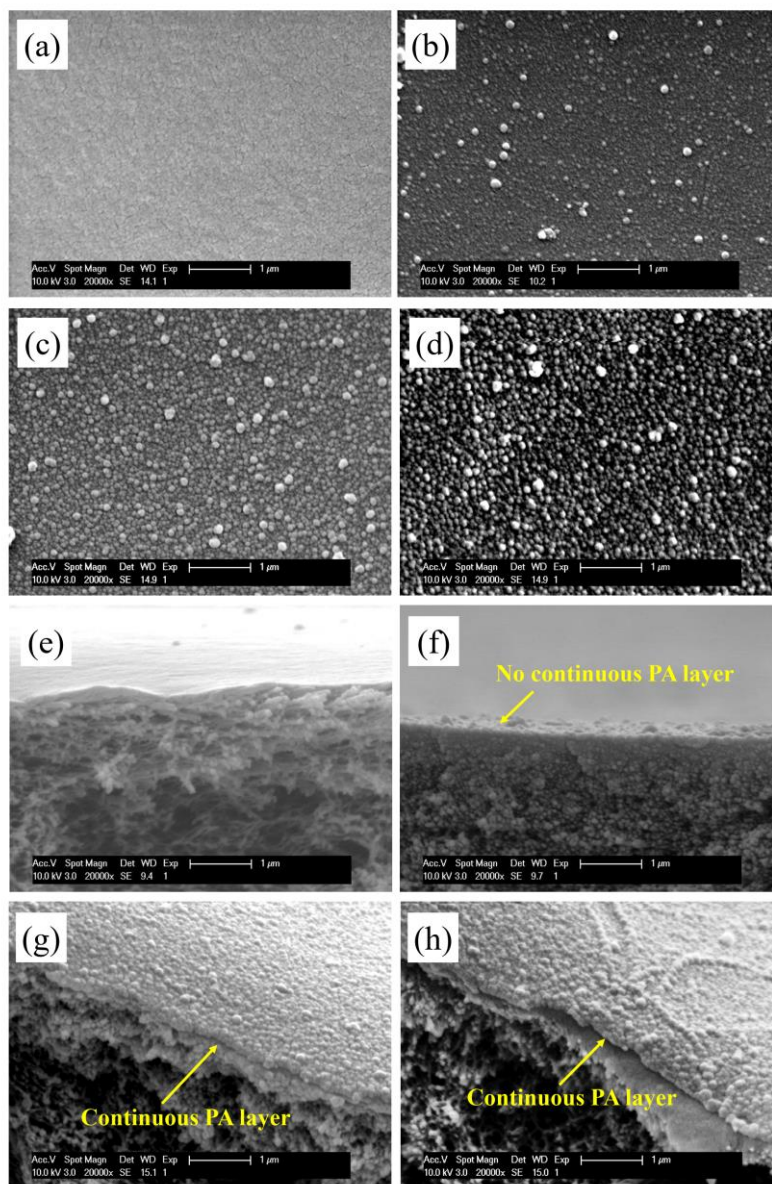


**Figure 4.4** SEM images (a), (b), (c), and (d) show the surfaces of 30k Da PES support membrane, NF-0.1-0.1-30 kDa, NF-0.6-0.1-30 kDa and NF-2.4-0.1-30 kDa, respectively. SEM images (e), (f), (g), and (h) show the cross-sections of 30k Da PES support membrane, NF-0.1-0.1-30 kDa, NF-0.6-0.1-30 kDa and NF-2.4-0.1-30 kDa, respectively.

As a consequence, the  $\text{Na}_2\text{SO}_4$  rejection declined slightly, while the  $\text{MgCl}_2$  rejection and the water transfer resistance continuously increased when the PIP concentration

increased from 0.3% to 2.4%. When the PIP concentration was 0.1%, the PA layer was so thin that defects were easily produced (as shown in **Figure 4.4(b)** and **Figure 4.4(f)**). The ultrathin PA layer with defects allowed NF-0.1-0.1-30 kDa to have a high water permeability and a low salt rejection. The structure and separation performance of this membrane is rather different from other membrane samples which are described in **Stage I**, **Stage II** and **Stage III** in **Section 4.2.1.1**. Therefore, NF-0.1-0.1-30 kDa can be classified into another new stage (**Stage IV**), which is characterized with slight SMPB without continuous PA layer coverage. Other TFC membranes illustrated in **Figure 4.4** (PIP concentration ranging between 0.3% and 2.4%) can be put into **Stage III** of which the description is slight SMPB with continuous PA layer coverage. **Figure 4.5** schematically depicts possible structural differences among the TFC NF membranes obtained in the four different stages concluded in **Section 4.2.1.1** and **Section 4.2.1.2**.

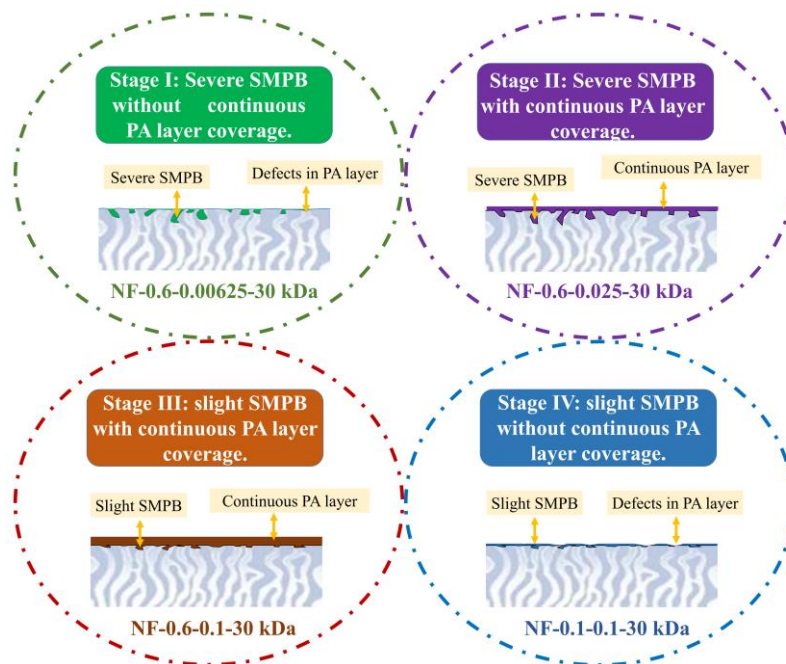


**Figure 4.5** Schematic of membrane structural distinction in different stages

### 4.2.1.3 Adjusting the concentration of TMC and PIP simultaneously

The membrane performance was further studied by simultaneously adjusting the concentration of TMC and PIP. As NF-0.6-0.025-30 kDa was taken as the “critical point” in the stage classification, the monomer concentration of this membrane was set as the baseline in this section. Four other membranes including NF-0.15-0.00625-30 kDa, NF-0.3-0.0125-30 kDa, NF-1.2-0.05-30 kDa and NF-2.4-0.1-30 kDa were prepared and characterized. The separation performances of these membranes are shown in **Figure 4.6**.

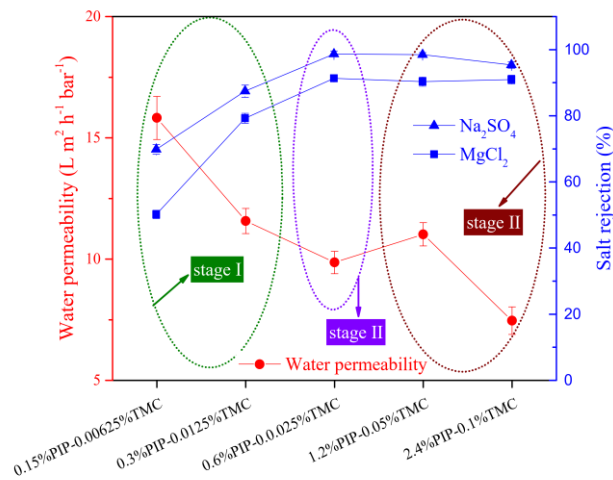


**Figure 4.6** Membrane performance when adjusting the concentration of TMC and PIP simultaneously

Similar to **Figure 4.1 (a)**, **Figure 4.6** can also be divided into **Stage I**, **Stage II** and **Stage III** as illustrated in **Figure 4.3**. For instance, NF-0.15-0.00625-30 kDa in **Stage I** has a relatively low water permeability and poor salt rejection due to the severe SMPB and the loose PA selective layer, which can be found in **Figure 4.7 (b)** and **Figure 4.7 (f)**. The higher water permeability of NF-1.2-0.05-30 kDa compared to NF-0.6-0.025-30 kDa further demonstrates that SMPB can be alleviated by increasing the monomer concentration. However, an excessive monomer concentration would increase the thickness of the PA selective layer. As shown in **Figure 4.7 (h)**, a continuous and thick PA layer with grainy surface can distinctly enhance the membrane mass transfer resistance. Additionally, the comparable salt rejections of NF-1.2-0.05-30 kDa and NF-

0.6-0.025-30 kDa further indicate that the continuous PA selective layer is the critical factor for salt removal.

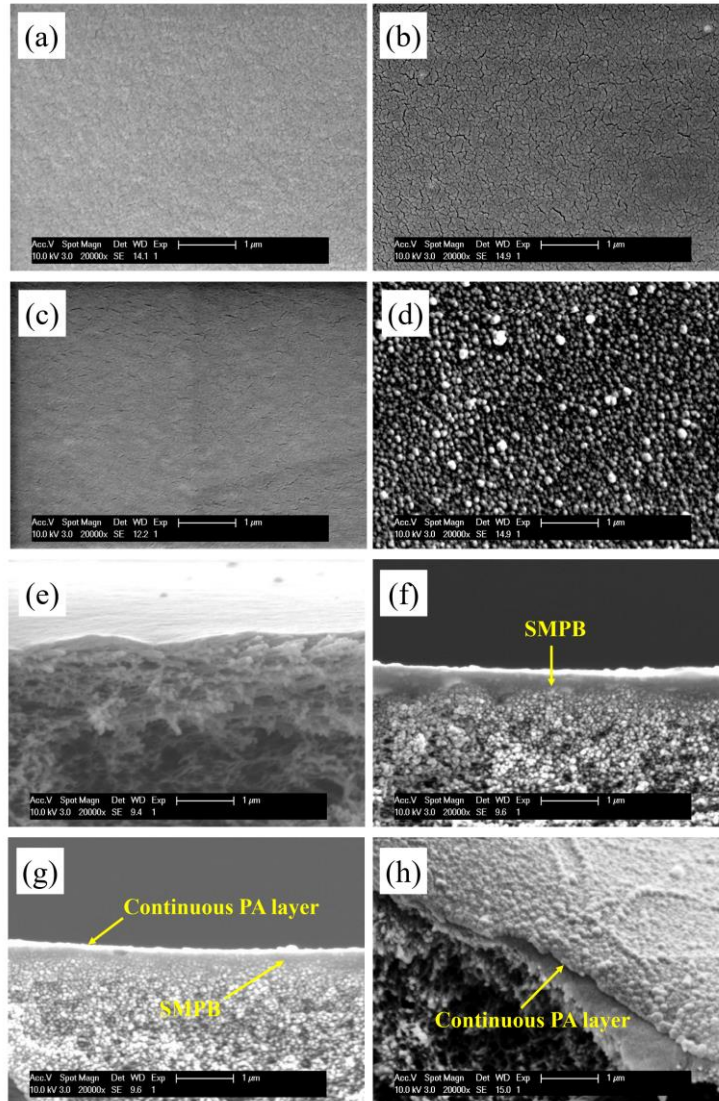


**Figure 4.7** SEM images (a), (b), (c), and (d) show the surfaces of 30k Da PES support membrane, NF-0.15-0.00625-30 kDa, NF-0.6-0.025-30 kDa and NF-2.4-0.1-30 kDa, respectively. SEM images (e), (f), (g), and (h) show the cross-sections of 30k Da PES support membrane, NF-0.15-0.00625-30 kDa, NF-0.6-0.025-30 kDa and NF-2.4-0.1-30 kDa, respectively.

### 4.2.2 Regulating SMPB by altering the pore size of the support membrane

Although many studies have focused on the importance of IP reaction conditions on the performance of a TFC membrane [83, 203, 204], more and more researchers begin to realize that the properties of the support membrane can also influence the TFC membrane water permeability, solute rejection and even antifouling ability [185, 186]. The pore structure and pore chemistry of the support membrane can affect the TFC membrane performance by influencing the *in-situ* IP reaction [184, 205]. Therefore, SMPB can be regulated by altering the pore size of the support membrane. In order to verify this hypothesis, PES UF membranes with similar chemistry but different MWCOs (30 kDa, 50 kDa and 80 kDa) were used as support membranes. In this section, the concentrations of PIP and TMC were fixed at 0.6% and 0.025%, respectively. The TFC membrane performance is shown in **Figure 4.8**. SEM images of different membranes are presented in **Figure 4.9**.

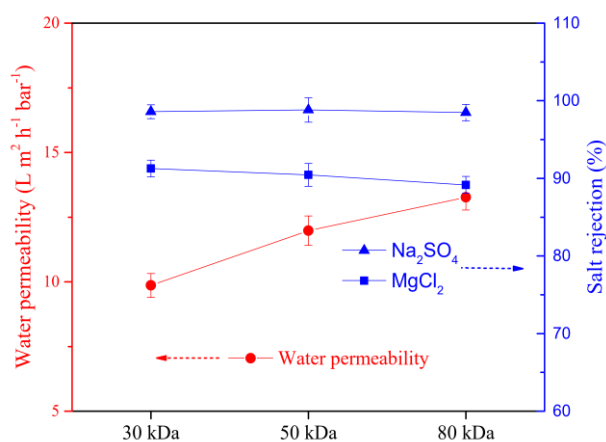


**Figure 4.8** Influence of support membrane pore size on membrane performance at 0.5 MPa and 20 °C

As shown in **Figure 4.8**, the water permeability continuously increases, while the salt rejection remains relatively stable when shifting the MWCO of the support membrane from 30 kDa to 80 kDa. The results suggest that a continuous PA selective layer is formed on each support membrane with different MWCO, which is confirmed by the surface morphologies of the different TFC membranes in **Figure 4.9 (g)**, **Figure 4.9 (h)**

and **Figure 4.9 (i)**. However, the cross-section images in **Figure 4.9 (j)**, **Figure 4.9 (k)** and **Figure 4.9 (l)** present some difference in SMPB. When a 50 kDa PES UF membrane and a 80 kDa PES UF membrane were used as support membranes, no obvious SMPB can be found in the support membrane pores.

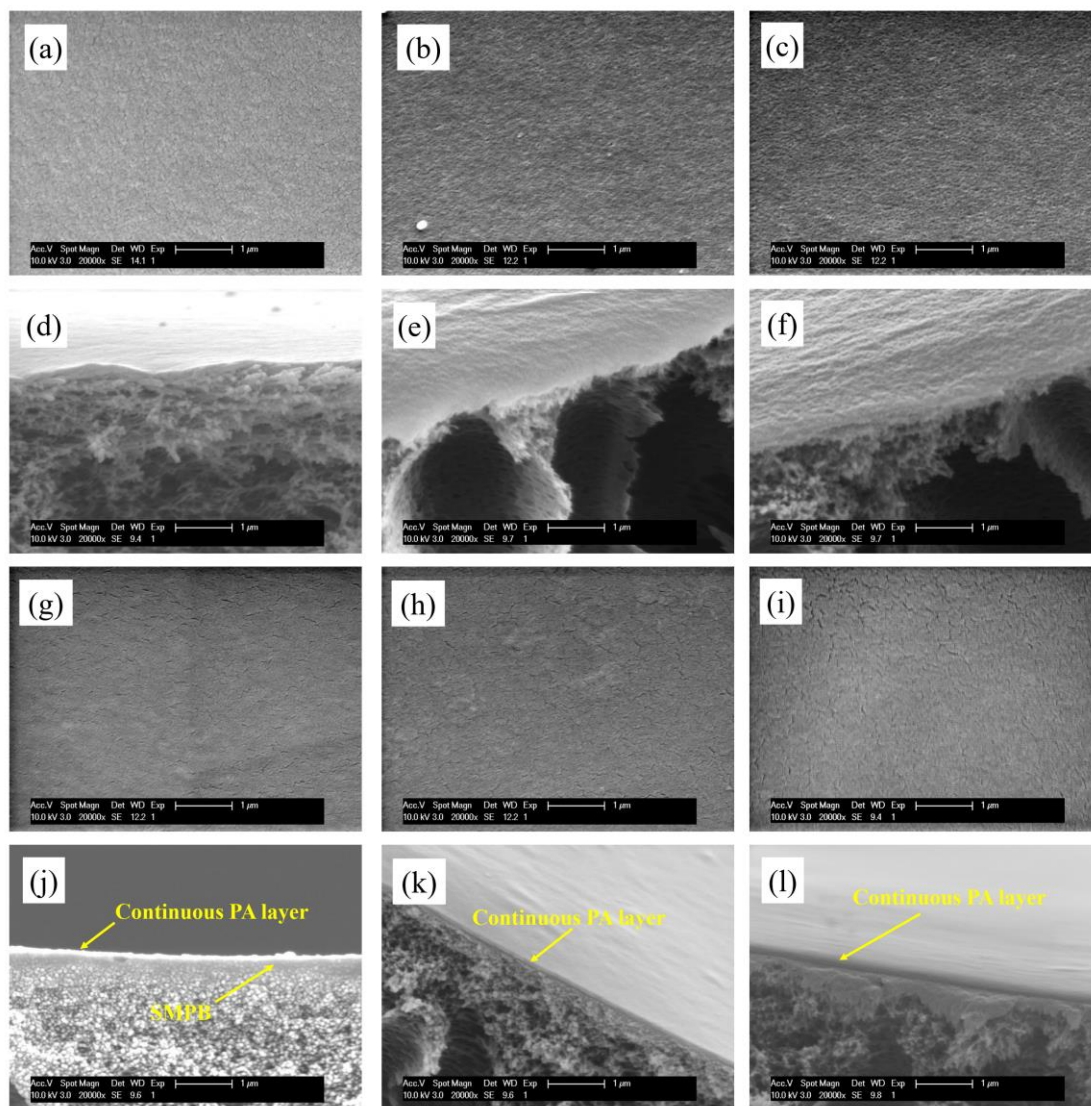


**Figure 4.9** SEM images (a), (b) and (c) show the surfaces of 30k Da PES support membrane, 50k Da PES support membrane and 80k Da PES support membrane, respectively. SEM images (d), (e), and (f) show the cross-sections of 30k Da PES support membrane, 50k Da PES support membrane and 80k Da PES support membrane, respectively. SEM images (g), (h) and (i) show the surfaces of NF-0.6-0.025-30 kDa,



NF-0.6-0.025-50 kDa and NF-0.6-0.025-80 kDa, respectively. SEM images (j), (k), and (l) show the cross-sections of NF-0.6-0.025-30 kDa, NF-0.6-0.025-50 kDa and NF-0.6-0.025-80 kDa, respectively

As illustrated in **Figure 4.10**, SMPB can be relieved when increasing the pore size of support membrane. Compared with the support membrane with larger pore size, the liquid level within the support membrane pores with smaller size (after removing the excess water droplets on the membrane surface with filter paper) should be lower because of its smaller aqueous solution storage amount. In addition, a support membrane with larger pore size has a lower possibility to be completely blocked. This may be another reason for the higher water permeability when choosing a support membrane with large MWCO, although the porosity and mass transfer resistance of the support membrane itself may also influence the final performance of the TFC membrane.

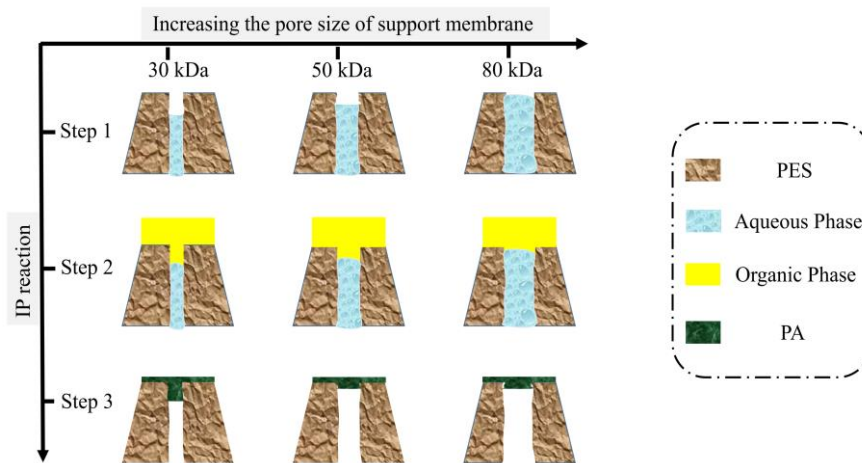


**Figure 4.10** Schematic representation of the structural differences in the membrane when altering the pore size of the support membrane.

### 4.2.3 Regulating SMPB by altering lag time after aqueous phase coating

The removal of the excess water droplets after aqueous phase coating is a necessary step when preparing a TFC membrane with an *in-situ* IP technique [206]. Various

methods including rollers or wiping with filter paper, air knife sweep, vertical drainage and evaporation in air have been used alone or in combination [206-210]. All these methods are normally operated in air, so the water can easily evaporate during the process, especially for a low humidity and high flow velocity air environment. In this study, the time span from the start of removing the water droplets to contacting the organic is defined as the lag time. **Fig. 4.11** presents how the lag time influences the membrane performance, and **Fig. 4.12** shows the surface morphologies and cross-sections of TFC membranes with different lag times. All the TFC membranes in this section were prepared with a PIP concentration of 0.6% and a TMC concentration of 0.025% on 80 kDa PES support membranes. The four membranes fabricated with lag time ranging from 1 min to 20 min are referred to as NF-lag-1, NF-lag-10, NF-lag-15 and NF-lag-20, respectively.

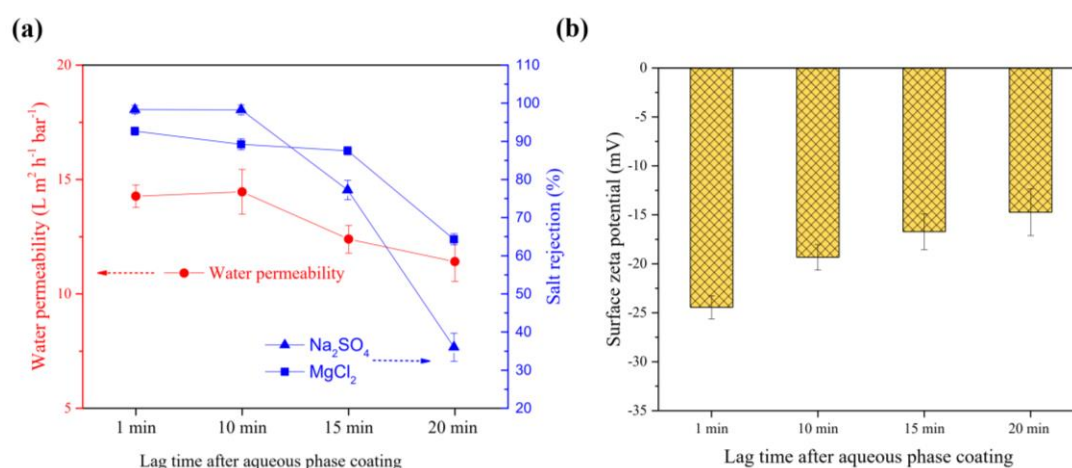


**Figure 4.11** Influence of lag time after aqueous phase coating on membrane separation performance tested at 0.5 MPa (a), and membrane surface zeta-potential measured at pH 7.0 (b)

As shown in **Figure 4.11 (a)**, water permeability and salt rejection decrease both when increasing the lag time. Another interesting phenomenon is that the MgCl<sub>2</sub> rejection becomes higher than the Na<sub>2</sub>SO<sub>4</sub> rejection when the lag time is longer than 15 min. During fabricating of a TFC membrane with an *in-situ* IP technique, the support membrane acts as the PIP solution reservoir. As illustrated in **Figure 4.13**, the pores of

the support membrane was filled with PIP solution after aqueous phase coating. When prolonging the lag time from 1 min to 20 min, the liquid level would gradually decrease due to water evaporation. After pouring the TMC n-hexane solution on the surface of support membrane, the TMC solution will invade and react with PIP in the pore structure. Then the PA polymer is produced in the pores, which induces severe SMPB. The PA layer would be thinner and thinner.

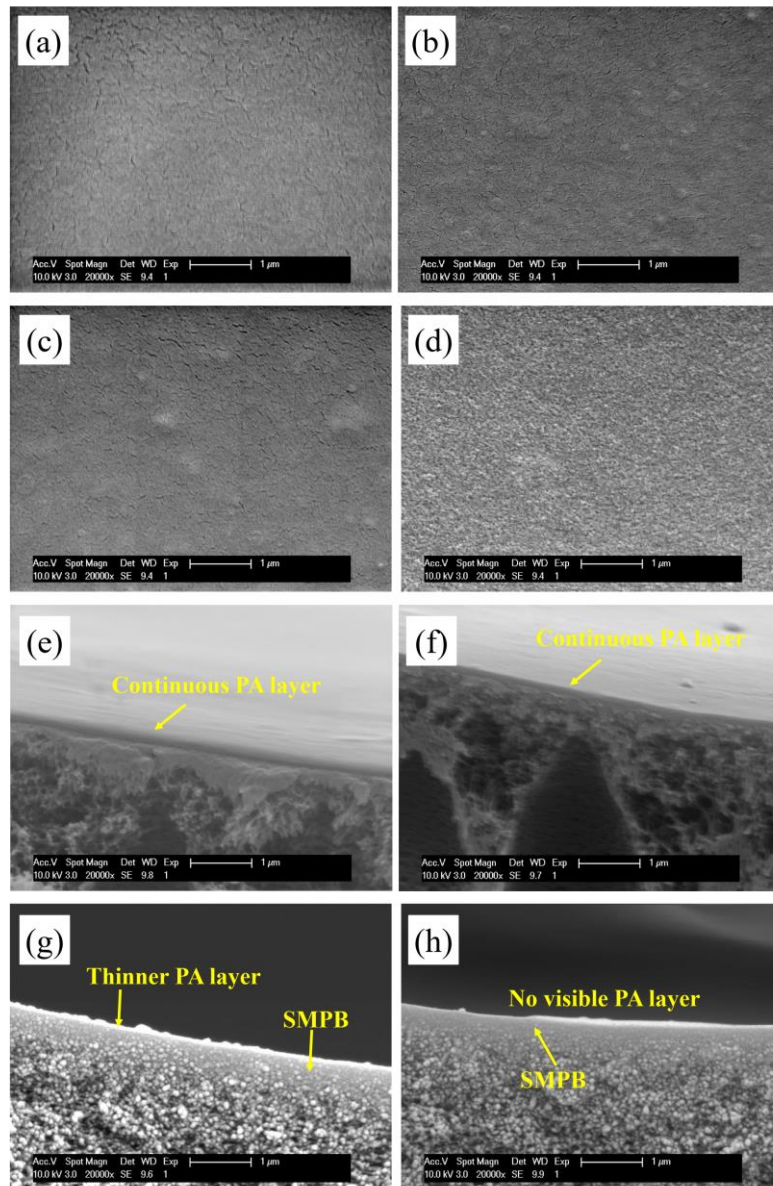


**Figure 4.12** SEM images (a), (b), (c), and (d) show the surfaces of NF-lag-1, NF-lag-10, NF-lag-15 and NF-lag-20, respectively. SEM images (e), (f), (g), and (h) show the cross-sections of NF-lag-1, NF-lag-10, NF-lag-15 and NF-lag-20, respectively.

SEM images in **Figure 4.12** further confirm this conclusion. Therefore, the water permeability drops down with increasing lag time. As SMPB can hinder PIP from diffusing out of the pores, no visible PA layer can be formed over the surface of support membrane when the lag time was prolonged to 20 min (as shown in **Figure 4.12 (d)** and **Figure 4.12 (h)**), which can account for the decreased salt rejection. In addition, the PIP concentration is expected to become much higher after water evaporates out from the pores of the support membrane, thus the PIP/TMC ratio would be improved. A high PIP/TMC ratio could increase the number of residual amino groups and decrease the negative charge of the membrane, which results in the  $\text{MgCl}_2$  rejection higher than  $\text{Na}_2\text{SO}_4$  rejection. This can be confirmed by **Figure 4.11 (b)**, which shows that the membrane surface zeta-potential increases from  $-24.4$  mV to  $-14.7$  mV when prolonging lag time from 1 min to 20 min. Therefore, the removal of the excess water droplets after aqueous phase immersion should be completed within 1 min to alleviate SMPB and obtain a desirable water flux and salt rejection.

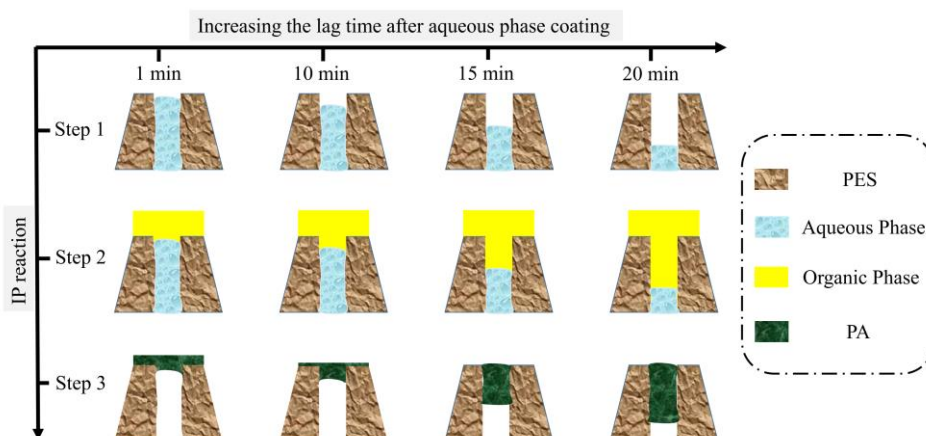


**Figure 4.13** Schematic representation of the membrane structure in three different stages.

#### 4.2.4 Regulating SMPB by adopting different IP techniques

As discussed in the **Introduction** part, support-free interfacial polymerization (SFIP) is expected to avoid SMPB. In this study, two TFC NF membranes (named NF-ISIP and NF-SFIP) were prepared with *in-situ* interfacial polymerization (ISIP) and SFIP. The support-free interfacial polymerization (SFIP) process consists of the following

steps: (a) the cleaned support membrane was fixed on a seat in a glass tank and immersed in the PIP solution. The liquid level should be 1 cm higher than the support membrane surface. (b) TMC n-hexane solution was gently added into the tank to react with the PIP solution at the interface for 50 s and then covered on the support membrane surface by regulating the drainage valve. (c) Rinsing the membrane surface thoroughly with clean n-hexane, followed by heat treatment at 60 °C for 10 min to evaporate the solvent. A detailed description of the SFIP process can be found elsewhere [194]. The PIP concentration was fixed at 0.6%, while the TMC concentration was fixed at 0.025%. An 80 kDa PES UF membrane was used as the support membrane. In order to verify the influence of SMPB on the stability of TFC membranes, NF-ISIP and NF-SFIP were further immersed in ethanol for 5 min. The water permeability and salt rejection of NF-ISIP and NF-SFIP before and after ethanol immersion are presented in **Figure 4.14 (a)** and **Figure 4.14 (b)**. **Figure 4.15** shows the surface morphologies and cross-sections of NF-ISIP and NF-SFIP before and after ethanol immersion. **Figure 4.14** shows that NF-SFIP resulted in a ~13 % improvement in water permeability and equivalent salt rejections compared with NF-ISIP. SEM images of the cross-section in **Figure 4.15 (f)** show that there is a relatively distinct boundary between the support membrane and the PA selective layer of NF-SFIP. This demonstrates that no SMPB can occur when using the SFIP technique to prepare a TFC membrane. Therefore, it can be further confirmed that avoiding SMPB is beneficial to enhance the water permeability. Park et al. found that RO membranes prepared with the SFIP technique have a higher NaCl rejection than the ISIP technique due to the absence of interference with the support membrane [194]. Jiang et al. observed that an RO membrane fabricated with the SFIP technique has a smoother surface, and they attributed this result to the more rapid heat dissipation when producing the PA layer at a free aqueous solution interface [193]. However, no obvious difference in salt rejection and surface roughness was found in this study. This may be induced by the difference in chemical properties of PIP and MPD.

## Chapter 4

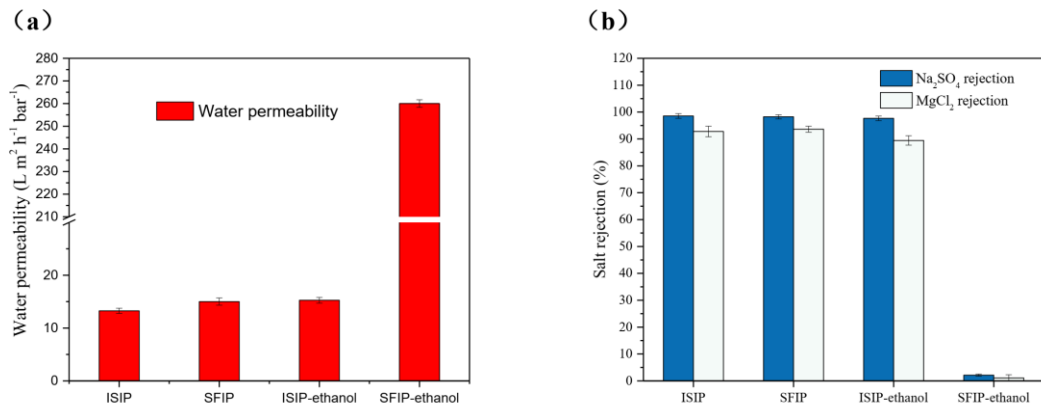


**Figure 4.14** Membrane performance before and after ethanol immersion tested at 0.5 MPa and 20 °C

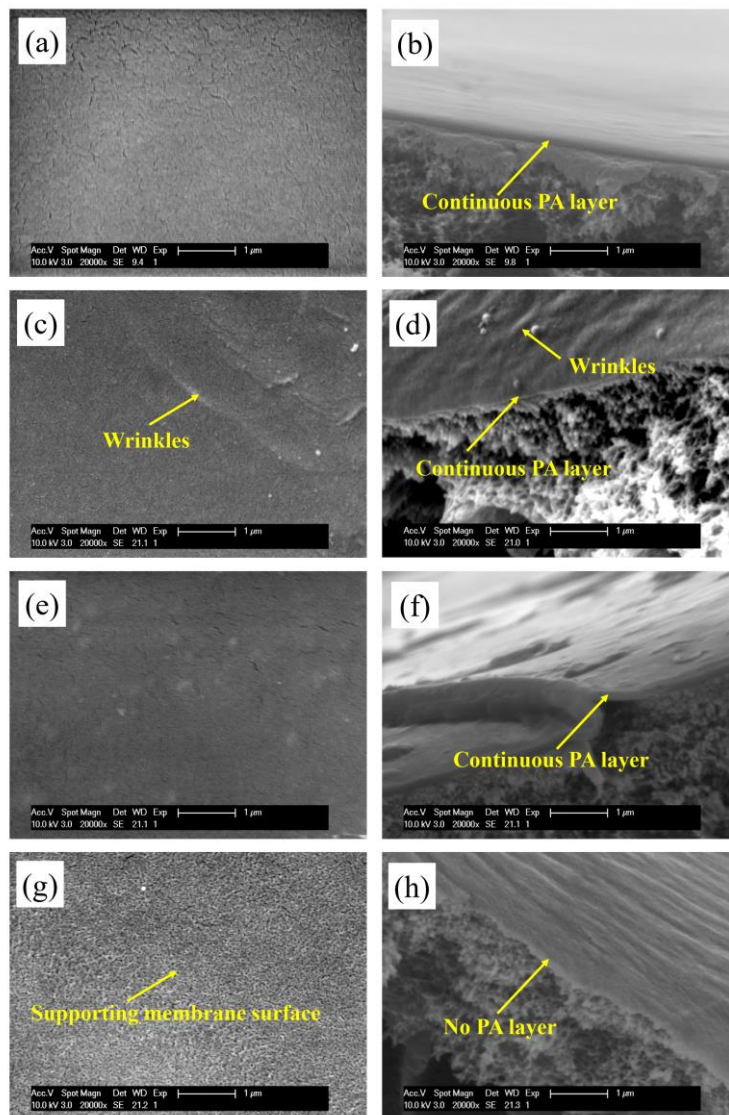


**Figure 4.15** SEM images (a) and (e) respectively show the surfaces of NF-ISIP and NF-SFIP before ethanol immersion. SEM images (c) and (g) respectively show the surfaces of NF-ISIP and NF-SFIP after ethanol immersion. SEM images (b) and (f) respectively show the cross-sections of NF-ISIP and NF-SFIP before ethanol immersion. SEM images (d) and (h) respectively show the cross-sections of NF-ISIP and NF-SFIP after ethanol immersion

**Figure 4.14** also indicates the separation performance of NF-ISIP and NF-SFIP after ethanol immersion. The structure difference between NF-ISIP and NF-SFIP before and after ethanol immersion is illustrated in **Figure 4.16**.

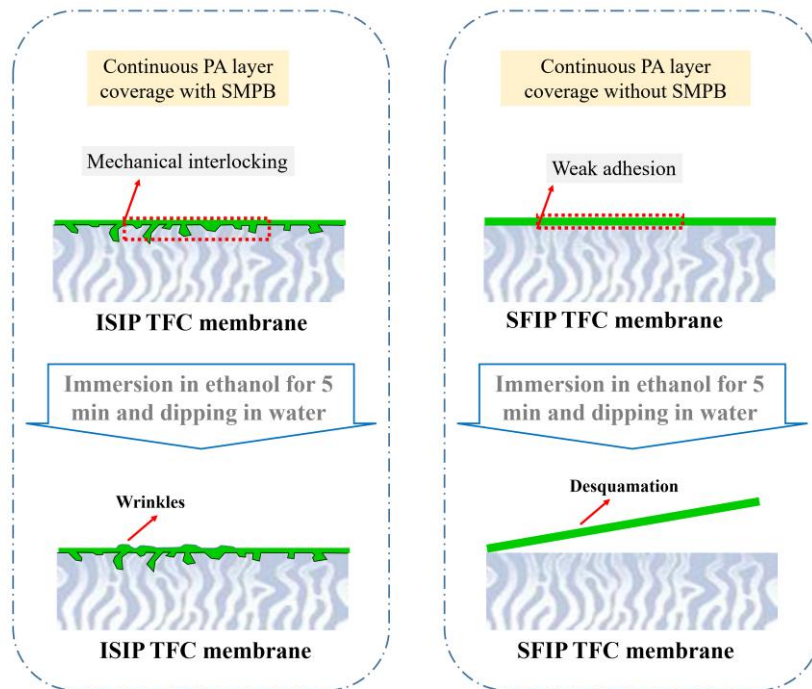


**Figure 4.16** Schematic of membrane structure difference between NF-ISIP and NF-SFIP before and after ethanol immersion

Compared with the PES support membrane, the PA layer has higher organic solvent resistance because of its crosslinking structure [211]. Thus the swelling of the PES support membrane should be more severe than that of the PA layer when the TFC membranes are immersed in ethanol. The difference in swelling extent between PES

support membrane and the PA layer is expected to damage the TFC membrane structure and worsen the membrane separation performance, especially when the adhesion between the PA layer and the support membrane is weak. Therefore, it is reasonable to evaluate the stability of the TFC membrane by testing the membrane separation performance after ethanol immersion.

As shown in **Figure 4.14**, ethanol immersion of NF-ISIP results in a ~15 % improvement in water permeability, a ~0.9% decline in Na<sub>2</sub>SO<sub>4</sub> rejection and a ~3.6% decrease in MgCl<sub>2</sub> rejection. A far more serious deterioration of the TFC membrane separation performance was observed when immersing NF-SFIP in ethanol for 5 min: the PA selective layer was desquamated off the support membrane when dipping into water again, which made the membrane permeability jump to ~260 L m<sup>-2</sup> h<sup>-1</sup> bar<sup>-1</sup>; the membrane had lost its desalting ability completely. **Figure 4.15 (g)** and **Figure 4.15 (h)** demonstrate that the PA layer was completely removed, so that the membrane has the characteristic of the 80 kDa PES support membrane. The difference in performance change after ethanol immersion indicates that NF-ISIP has a stronger stability which can be ascribed to the SMPB. As illustrated in **Figure 4.16**, SMPB can produce a “mechanical interlocking effect” and enhance the adhesion between the PA layer and the PES support membrane. As for NF-SFIP, the adhesion between the PA layer and the PES support membrane is relatively weak. Because of the inconsonant swelling of the PES support membrane and the PA layer when TFC membranes were immersed in ethanol, only some “wrinkles” can be created in NF-ISIP (as shown in **Figure 4.15 (c)** and **Figure 4.15 (d)**), while desquamation of the PA layer can be induced in NF-SFIP.

### 4.3 Conclusions

As a general phenomenon in *in-situ* interfacial polymerization, support membrane pore blockage (SMPB) has been systematically studied in this chapter. Various conceptual models were proposed to expound SMPB in a comprehensive way. By changing the monomer concentration, the pore size of support membrane and the lag time after



## Chapter 4

aqueous phase coating, SMPB was proved to be a negative factor that can severely decrease the TFC membrane water permeability. Nevertheless, the comparison between different IP techniques, including ISIP and SFIP, suggested that SMPB could improve the adhesion between support membrane and the PA layer through a “mechanical interlocking effect”, which should be rather meaningful to enhance the TFC membrane long-term stability. In order to prepare a TFC membrane with desirable properties, SMPB should be alleviated on the premise of ensuring the membrane stability. It is expected to relieve SMPB by the proper selection of monomer concentration, lag time after aqueous phase coating and support membrane pore size, as well as using the SFIP technique. However, other measures should be taken to enhance the membrane stability when adopting the SFIP technique.

## Chapter 5

### **Surface modification of piperazine based nanofiltration membrane with serinol for reduced fouling in treatment of polymer flooding produced water**

Adapted from: *Surface modification of piperazine-based nanofiltration membranes with serinol for enhanced antifouling properties in polymer flooding produced water treatment*, *RSC Advances*, 7(77) (2017) 48904-48912.

#### **5.1 Introduction**

According to previous research about the treatment of PFPW with NF membrane,  $\text{Ca}^{2+}$  in the feed solution could act as a “bridge” by complexation interaction between the carboxyl groups of the membrane surface and those present in APAM, as well as different APAM molecules, thus enhancing membrane fouling [145, 212]. Surface modification through grafting has been explored to modify the membrane surface, and to improve the antifouling properties of the membrane [213, 214]. In consideration of the fact that the carboxyl groups of the polyamide composite NF membrane surface arise from the hydrolysis of the unreacted acyl chloride groups, covalent grafting using these unreacted acyl chloride groups before their hydrolysis and turning the carboxyl groups to other hydrophilic groups is expected to yield improved NF membranes.

Some studies have been conducted to modify the polyamide membrane with different monomers; these studies suggest the effectiveness of this method in improving the membrane performance. For instance, Yan et al. [173] studied the grafting of triethanolamine (TEOA) on a nascent polyamide NF membrane through esterification reaction between the hydroxyl groups of TEOA and the residual acyl chloride groups on the membrane. The modified membrane had a higher hydrophilicity, a higher water

flux, and a better antifouling ability against hydrophobic foulants. Zhu et al. [215] made use of the grafting reaction between the poly (amidoamine) dendrimer (PAMAM) and the residual acyl chloride groups on a nascent membrane. The PAMAM grafting can decrease the membrane pore size and provide positively charged functional groups, thus making the membrane positively charged. In this way, the membrane hydrophilicity and water permeability is improved. Furthermore, the modified membrane has higher rejections of most tested heavy metals. In the study of Wang et al. [216], poly(ethyleneimine) (PEI) was used to graft with the residual acyl chloride after the reaction between trimesoyl chloride (TMC) and polydopamine (PDA). The deposition of PEI effectively decreases the membrane pore size and surface roughness. In addition, the membrane long-term stability was also confirmed. The above research results indicate that it is possible to tailor a membrane in view of enhancing its antifouling properties in PFPW treatment through the grafting of a well-chosen monomer with the residual acyl chloride groups on the nascent membrane.

Serinol which includes one amino group and two hydroxyl groups, is an important intermediate with good chemical stability and water solubility that is widely used in medicine and chemical industries [159]. As the reaction rate constant of amino group is a few orders of magnitude higher than that of the hydroxyl group [169], the amino and hydroxy groups present in serinol cannot simultaneously react with the acyl chloride groups under a relatively mild condition without a catalyst.

In **Chapter 3**, serinol has been used as a water soluble monomer to prepare TFC NF membranes with 4-dimethylaminopyridine (DMAP) as catalyst, which has demonstrated that a polymerization reaction cannot happen without a catalyst. In this chapter, serinol will be used to modify a piperazine based TFC-NF membrane through the acylation reaction between the amino group of serinol and the residual acyl chloride groups on the nascent membrane. In this way, it is expected to make use of the antifouling ability of serinol and avoid the negative influence of “support membrane pore blockage (SMPB)”. As illustrated in **Figure 5.1**, the number of residual carboxyl

groups of the resultant membrane may be decreased, and the membrane hydrophilicity may be enhanced simultaneously. In order to confirm the effectiveness of this modification method, ATR-FTIR, AFM, FESEM, contact angle geometer, surface zeta potential analyzer, and the toluidine blue O (TBO) technique were employed to study the unmodified TFC-NF membrane and the serinol-grafted TFC-NF membrane. Finally, the membrane performance including antifouling ability and solute rejection was evaluated by treating model PFPW.

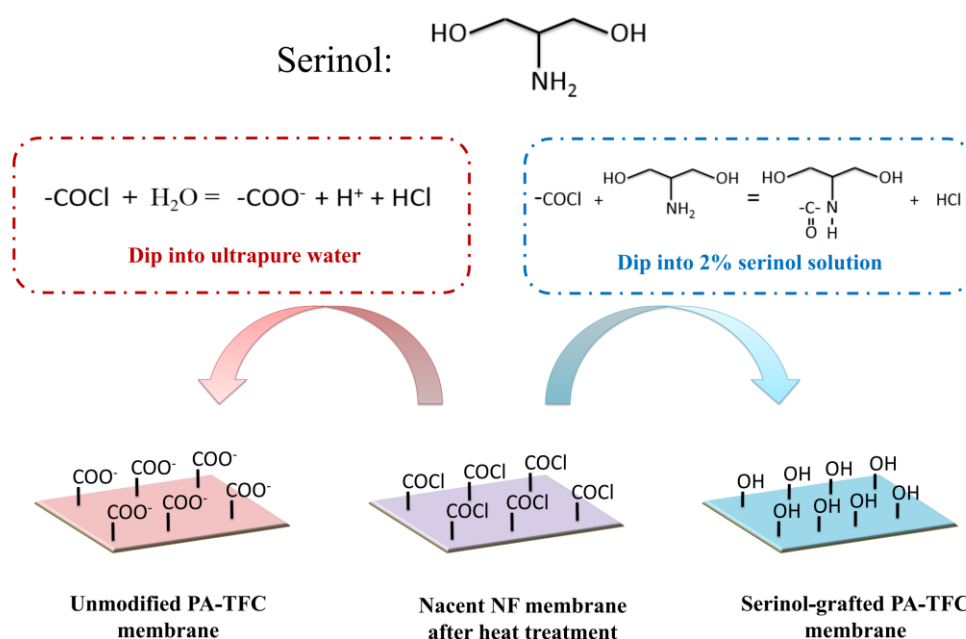


**Figure 5.1** Schematic diagram of the surface modification process with serinol

## 5.2 Results and discussion

### 5.2.1 Membrane physicochemical properties

ATR-FTIR was employed to analyze the chemical structure of the PS support membrane, the unmodified PA-TFC membrane and the serinol-grafted PA-TFC membrane. The results are presented in **Figure 5.2**. Compared with the PS support membrane, the new peak at  $1630\text{ cm}^{-1}$  was related to stretching vibration of carbonyls in amide bonds present in the unmodified PA-TFC membrane. As for the serinol-

grafted PA-TFC membrane, the peak related to the stretching vibration of carbonyl groups in amide bonds shifted to  $1634\text{ cm}^{-1}$  because the secondary amide formed by primary amino group in serinol molecule can result in shifts to higher wave numbers [167, 196, 217]. No new peak appears around  $1725\text{ cm}^{-1}$ , which implies that the hydroxyl group cannot react with the acyl chloride and form ester bonds [157, 218]. Moreover, the new peak at  $3340\text{ cm}^{-1}$  can be attributed to the hydroxyl groups of serinol, which were successfully grafted on the modified membrane, because the stretching vibration of hydroxyl groups can produce a broad peak in the range of  $3200\text{--}3500\text{ cm}^{-1}$  [61, 170]. The grafted hydroxyl groups are expected to decrease the number of carboxyl groups and enhance the membrane hydrophilicity.

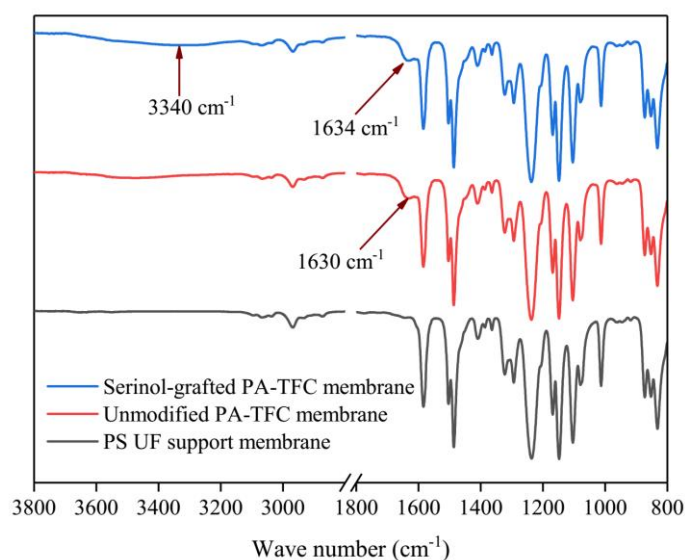


**Figure 5.2** ATR-FTIR spectra of different membranes

The morphology of the unmodified PA-TFC membrane and the serinol-grafted PA-TFC membrane was investigated by AFM and FESEM. Additionally, the RMS roughness of the two membranes was obtained from the AFM images with the Nanoscop Analysis software 1.40. The results are presented in **Figure 5.3** and **Figure 5.4**. The AFM images in **Figure 5.3** imply that the surface of the serinol-grafted PA-TFC membrane and of the unmodified PA-TFC membrane were both rather smooth. The average RMS roughness only increased to 5.1 nm from 4.5 nm after grafting. The

RMS roughness difference is so small that it should be within the experimental error. Therefore, it can be stated that the grafting process with serinol did not substantially change the membrane morphology. Similar to the results of AFM, the FESEM images further confirmed the above conclusion, suggesting that the modification process would not influence the membrane surface structure. The above phenomenon is because no cross-linking reaction could occur during the grafting process with serinol, as there was only one reactive group (the amino group) in the serinol molecule that could react with the residual acyl chloride groups on the nascent membrane. This is also the difference between the modification process described here and modifications proposed by other researchers [173, 215].

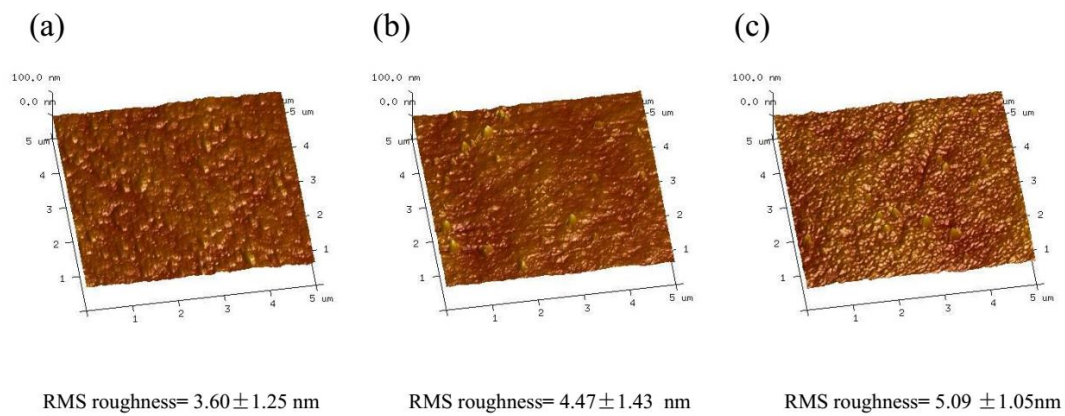


**Figure 5.3** AFM images of (a) UF substrate membrane, (b) the top layer of unmodified PA-TFC membrane and (c) the top layer of serinol-grafted PA-TFC membrane

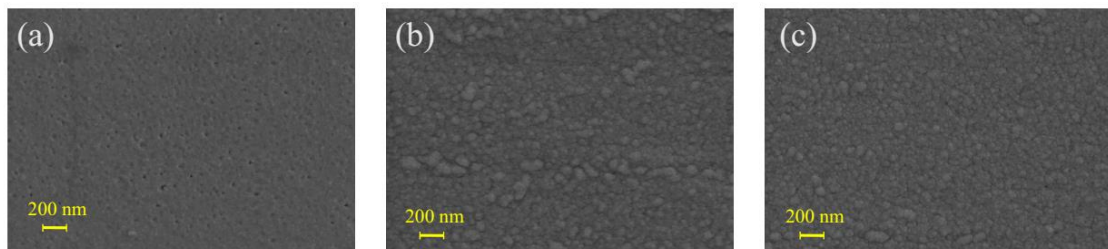


**Figure 5.4** FESEM images of (a) UF substrate membrane, (b) the top layer of unmodified PA-TFC membrane and (c) the top layer of serinol-grafted PA-TFC membrane

The membrane hydrophilicity was evaluated by measuring the water contact angles. The contact angles of the PS UF support membrane, the unmodified PA-TFC membrane, and the serinol-grafted PA-TFC membrane are shown in **Figure 5.5**. The water contact angle of the PS supporting membrane was  $69.2^\circ$ , while that of the unmodified PA-TFC membrane was  $45.8^\circ$ . After modification with serinol, the water contact angle of the serinol-grafted PA-TFC membrane decreased to  $35.2^\circ$ . The FTIR spectra of the serinol-grafted PA-TFC membrane in **Figure 5.2** indicate that serinol has been successfully grafted on the PA-TFC membrane. The hydroxyl groups in the serinol molecule can effectively enhance the membrane hydrophilicity, which is beneficial to both water permeation and fouling resistance against hydrophobic foulants.

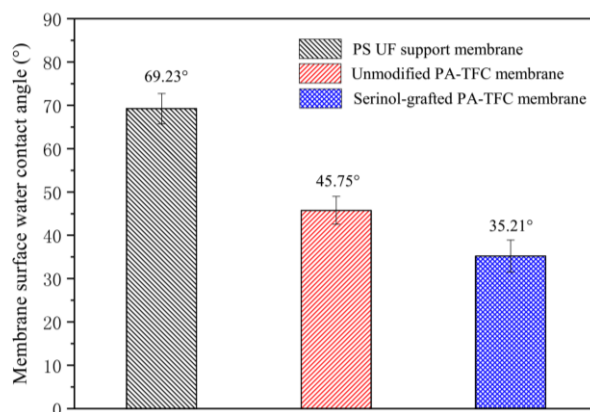


**Figure 5.5** Membrane surface water contact angles of different membranes

The surface charge of the unmodified PA-TFC membrane and serinol-grafted PA-TFC membrane were evaluated by zeta-potential measurements. Surface zeta-potentials at different pH are shown in **Figure 5.6**. It can be seen that the grafting process with serinol decreased the absolute value of the PA-TFC membrane's negative charge. The amphoteric surface characteristic of the typical PA-TFC membrane is due to its residual carboxyl groups and amino groups [139]. The measured zeta potential should be the tradeoff between carboxyl groups and residual amino groups. Theoretically, the amino group number of the modified and unmodified PA-TFC membranes should be the same, so the change of the serinol-grafted PA-TFC membrane's surface zeta-potential should result from the number of residual carboxyl groups. The isoelectric points of the

modified and unmodified membrane were both between 4 and 5. When the solution pH was under 5, the surface charge of these two membranes was similar, taking the experimental error into consideration. When the solution pH was higher than 5, the absolute value of the serinol-grafted PA-TFC membrane's negative charge was smaller than that of the unmodified membrane, which should result from the reaction between serinol and acyl chloride, as illustrated in **Figure 5.1**. Furthermore, based on the proposed fouling and cleaning mechanism previously described [145, 212],  $\text{Ca}^{2+}$  in feed solution could act as a “bridge” by complexation interaction between the carboxyl groups of the membrane surface and those of APAM, as well as different APAM molecules, thus enhancing membrane fouling. Therefore, the decrease of the number of carboxyl groups is expected to improve the membrane antifouling property when treating PFPW.

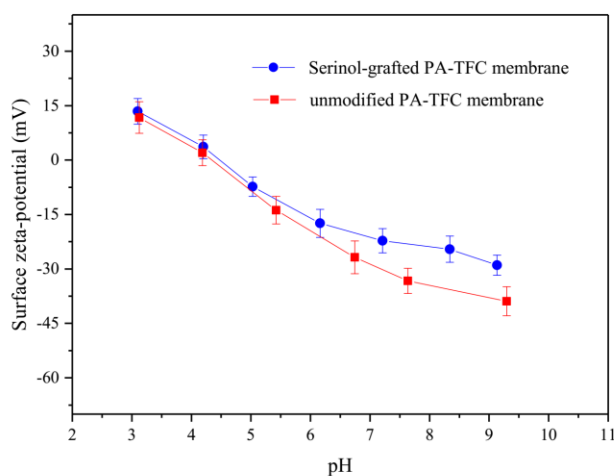


**Figure 5.6** Surface zeta-potentials of different membranes in 1 mM/L KCl solution with different pH values at 25 °C

The TBO technique was used to quantify the density of carboxyl groups on the membrane surface. As shown in **Figure 5.7**, the grafting process with serinol decreased the density of carboxyl groups on the membrane surface from  $29.96 \text{ nm}^{-2}$  to  $20.14 \text{ nm}^{-2}$ . The results are consistent with membrane zeta-potential measurements, which demonstrates the successful modification by serinol grafting. The decreased surface



carboxyl density is beneficial to mitigate the complexation interaction between the carboxyl groups of the membrane surface and those of APAM induced by  $\text{Ca}^{2+}$  in the feed solution.

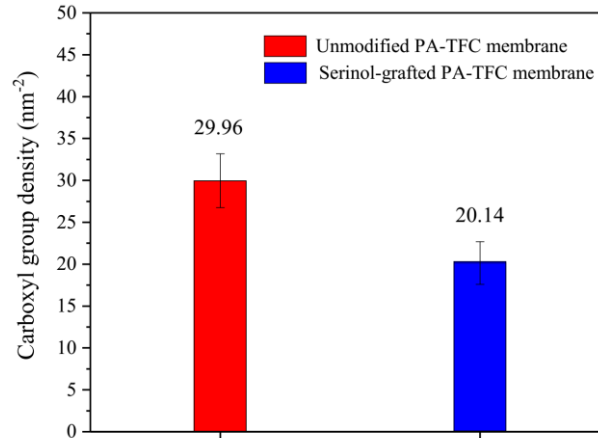


**Figure 5.7** Surface carboxyl group density of different membranes

### 5.2.2 Membrane permeation properties

The permeation through the membrane, i.e., pure water permeability, salt rejections and molecular weight cut-off (MWCO) of the unmodified PA-TFC membrane and the serinol-grafted PA-TFC membrane are shown in **Figure 5.8 (a)**, **Figure 5.8 (b)** and **Figure 5.8 (c)**, respectively. The MWCO of the two membranes was determined based on the rejection of neutral solutes [175, 176].

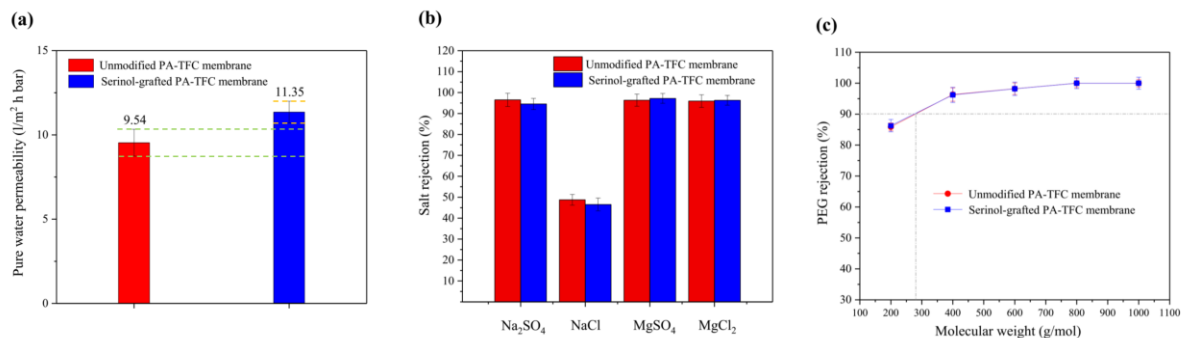


**Figure 5.8** Permeation properties: (a) pure water permeability, (b) salt rejections and (c) PEG rejections of different membranes tested at 0.5 MPa and 25 °C

As indicated in **Figure 5.8 (a)**, the unmodified PA-TFC membrane has an average pure water permeability of  $9.5 \text{ L m}^{-2} \text{ h}^{-1} \text{ bar}^{-1}$ . After modification by serinol grafting, the average pure water permeability increased to  $11.3 \text{ L m}^{-2} \text{ h}^{-1} \text{ bar}^{-1}$ . It was demonstrated (see section 3.1) that the serinol grafting process can enhance the membrane hydrophilicity while retaining a similar active layer structure. Thus, the improved pure water permeability was a result of the stronger hydrophilicity because the enhanced hydrophilicity is favorable for transport of water molecules across the active layer [219]. **Figure 5.8 (b)** indicates that there was no significant difference in the salt rejections of the unmodified PA-TFC membrane and the serinol modified PA-TFC membrane in consideration of the error bar. **Figure 5.8 (c)** suggests that both the unmodified PA-TFC membrane and the serinol-grafted PA-TFC membrane had a MWCO around 275 Da. This confirms that the modification process did not influence the active layer's compactness and pore size because only one reactive group (the amino group) in the serinol molecule could react with the residual acyl chloride groups on the nascent membrane. **Figure 5.8 (a)**, **Figure 5.8 (b)** and **Figure 5.8 (c)** show that modification of the active layer with serinol grafting enhances the water permeability, while maintaining its desalting ability and neutral solute removal.

### 5.2.3 Membrane performance in treating model PFPW

The unmodified PA-TFC membrane and the serinol-grafted PA-TFC membrane were used to treat the model PFPW. The filtration process was conducted for four cycles. Each cycle lasted for 8 h. After each cycle, the membrane was flushed with the feed water at a cross-flow velocity of  $15.0 \text{ cm/s}$  for 1 h. The total operation time was 36 h. The flux decline curve was obtained and shown in **Figure 5.9 (a)**. The rejection of different solutes, including  $\text{Ca}^{2+}$ ,  $\text{Mg}^{2+}$ ,  $\text{Na}^+$ ,  $\text{K}^+$ ,  $\text{SO}_4^{2-}$ ,  $\text{Cl}^-$  and organic solutes represented by the TOC, were measured and illustrated in **Figure 5.9 (b)**. As shown in **Figure 5.9 (a)**, the flux of unmodified PA-TFC membrane continuously decreased during the filtration process. Although the hydraulic cleaning can recover the flux to

some extent, yet the recovery rate was rather low. At the end of the operation, the normalized flux had decreased to 0.84. Different from the unmodified PA-TFC membrane, the serinol-grafted PA-TFC membrane showed a clear antifouling ability. The normalized flux of the serinol-grafted PA-TFC membrane remained relatively stable and had only a small decline throughout the filtration process, still reaching 0.98 at the end.

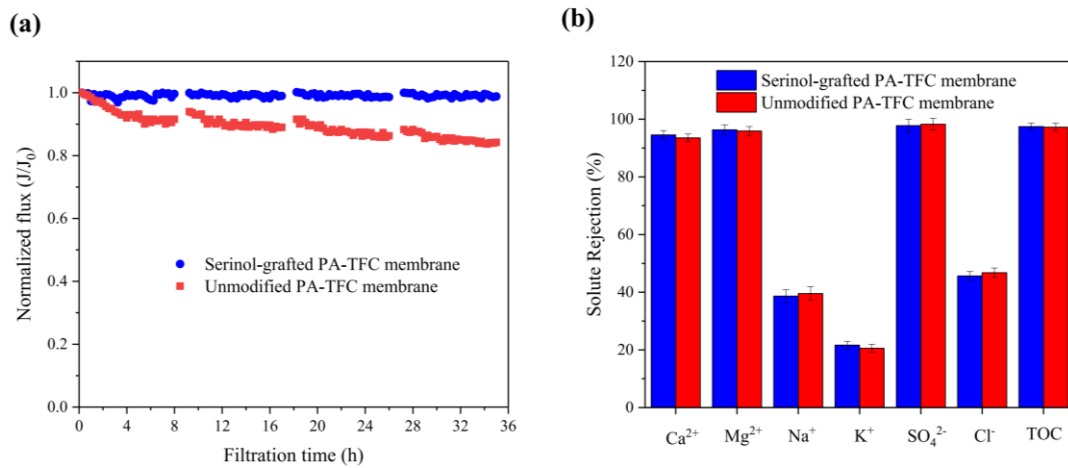


**Figure 5.9** Membrane performance in treating model PFPW: (a) normalized flux decline curve and (b) different solute rejections of different membranes

The excellent antifouling ability of the serinol-grafted PA-TFC membrane can be ascribed to its enhanced hydrophilicity and decreased membrane surface carboxyl group density. Furthermore, as the serinol-grafted PA-TFC membrane had a higher water permeability, its operational pressure was lower than that of the unmodified PA-TFC membrane in order to keep the same starting flux. The lower operational pressure was also beneficial to mitigate membrane fouling because of its reduced compaction effect. ATR-FTIR was used to analyse the different NF membranes. The fouled membranes were thoroughly flushed with deionized water before drying. Infrared spectroscopy of the virgin modified membrane, the modified membrane fouled by model PFPW, the virgin unmodified membrane and the unmodified membrane fouled

by model PFPW are shown in **Figure 5.10**. As indicated in **Figure 5.10**, there are four new peaks in the infrared spectroscopy of the unmodified membrane fouled by model PFPW. The peaks at  $3354\text{ cm}^{-1}$  and  $3198\text{ cm}^{-1}$  can be attributed to APAM [212], while the peaks at  $2925\text{ cm}^{-1}$  and  $2857\text{ cm}^{-1}$  can be related to the crude oil [212]. The new peaks involving APAM and crude oil suggest that the unmodified membrane was substantially fouled by model PFPW. As a consequence, the membrane flux decreased. For the modified membrane, no obvious peaks related to APAM and crude oil were observed after filtrating the model PFPW for 32 h. The ATR- FTIR measurements further confirmed the modification process can effectively improve the membrane antifouling ability.

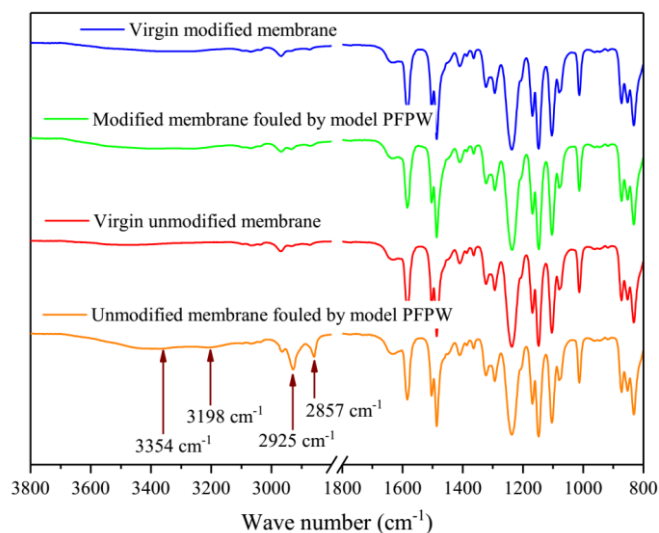


**Figure 5.10** The change of infrared spectroscopy after membrane fouling

**Figure 5.9 (b)** indicates that both the unmodified PA-TFC membrane and the serinol-grafted PA-TFC membrane can effectively reject  $\text{Ca}^{2+}$ ,  $\text{Mg}^{2+}$ ,  $\text{SO}_4^{2-}$  and TOC. The high  $\text{Ca}^{2+}$  and  $\text{Mg}^{2+}$  rejections are beneficial to the treatment of PFPW aiming for reuse in polymer flooding oil extraction, because divalent cations would severely cause the shielding of APAM's negative charge, lead to the coiling up of the linear polymer, and eventually decrease the recovery of crude oil [19, 220]. Moreover, scale control is also very important for oil extraction because the scale formation would block the oil wells

and decrease the crude oil recovery. Therefore, the high  $\text{SO}_4^{2-}$  rejection is also beneficial to the wastewater reuse in polymer flooding oil extraction.

### 5.3 Conclusions

In this chapter, a surface modification method with serinol was proposed to enhance the antifouling property of the TFC NF membrane applied for treatment of polymer flooding produced water treatment. ATR-FTIR confirmed the successful covalent grafting of serinol on the nascent PIP and TMC based NF membrane. AFM and FESEM characterization suggested that the modification process did not change the membrane morphology. Contact angle geometry, surface zeta potential analysis, and the TBO technique indicated that the grafting process effectively improved the membrane hydrophilicity and decreased the density of carboxyl groups on the membrane surface. The modification of the active layer with serinol grafting can obviously improve the water permeability, while maintaining its desalting ability and neutral solute rejection. When treating the model PFPW, the serinol-grafted PA-TFC membrane showed an excellent antifouling ability and satisfactory rejections of  $\text{Ca}^{2+}$ ,  $\text{Mg}^{2+}$ ,  $\text{SO}_4^{2-}$  and TOC, which is important in the case of treating PFPW aiming for reuse in polymer flooding oil extraction.

## Chapter 6

### **Fabrication of negatively charged NF membranes for heavy metal removal via the interfacial polymerization between PIP and TMC**

Adapted from: *How to fabricate a negatively charged NF membrane for heavy metal removal via the interfacial polymerization between PIP and TMC? Desalination, 491 (2020) 114499.*

#### **6.1 Introduction**

As important water contaminants produced in petroleum refinery and petrochemical plants (PRPP) [221-224], heavy metals, such as nickel, zinc, copper, and cadmium, etc., can not only directly damage the water ecosystem but also bring a great threat to human health because they are usually toxic, persistent, non-biodegradable and accumulating in the food chain [225-227]. Therefore, the removal of heavy metals from PRPP wastewater before discharging or reclamation has become an important social concern to be solved. Compared with conventional ion removing technologies, NF is an environmentally friendly and low energy consuming process with no phase change and less chemical addition, which also allows to recover useful resources under certain conditions [164, 228]. All these features have made NF a feasible and promising option for removing heavy metals from wastewater in comparison with traditional methods such as chemical precipitation, ion exchange, adsorption, or coagulation and flocculation [229].

At present, the mainstream NF membranes are PA TFC membranes prepared by interfacial polymerization (IP) with two reactive monomers on top of a substrate. Trimesoyl chloride (TMC) including three acyl chloride groups is the most usually

adopted monomer in the organic phase. Acyl chloride groups in some TMC molecules could transform into carboxyl groups either during or after the IP process. During the IP process, some TMC molecules may contact with the aqueous solution via molecular diffusion driven by a concentration gradient. After IP process, some residual acyl chloride groups transform into carboxyl groups when the membrane is immersed in water. The carboxyl groups produced in both ways can make the resulting membrane electronegative in neutral solution, which is not beneficial for heavy metal removal because of the electrostatic attraction [230]. Therefore, weakening the membrane electronegativity or even making the membrane positively charged is a reasonable strategy for enhancing the heavy metal removal capacity of NF membranes. For instance, polyethyleneimine (PEI), which has abundant active amide groups, was employed to fabricate positively charged NF membranes via various techniques, e.g., interfacial polymerization, chemical cross-linking, and layer-by-layer self-assembly [231-233]. In addition, surface grafting [234], dually charged composite layer [235], introducing charged-nanoparticles or zwitterions [236, 237] have also been proved to be effective methods of regulating membrane charge property. However, it should be noted that although a positively charged NF membrane can effectively reject multivalent cations, the membrane fouling problem should be equally considered. As many pollutants in aqueous solution are negatively charged, such as silica, humic acid, polysaccharides and bacteria, membrane fouling may be accelerated because of the electrostatic attraction between the positively charged membrane and negatively charged foulants [238]. Besides, the complex fabrication process and high manufacturing costs of these membranes are also obstacles for commercialized production and application.

Size exclusion is another important separating mechanism of the NF process; therefore, decreasing the pore size of the NF membrane is another technical route for enhancing the rejection of heavy metals. A fully-aromatic polyamide NF membrane prepared with *m*-phenylenediamine (MPD) and TMC was found to have a satisfactory rejection of

metal cation due to its stronger steric hindrance effect, due to its relatively thick and dense PA film [239, 240]. The commercial NF membrane NF90, produced by Dow, is such a typical example showing a high cation rejection, even for monovalent ions [164]. However, the problem is its relatively low water flux and rough surface morphology, resulting from the reaction between MPD and TMC. Piperazine (PIP) is another widely used aqueous monomer with desirable film forming characteristics and relatively low cost. TFC NF membranes prepared with PIP and TMC typically have a high water flux and a low monovalent ion rejection. However, because of its intrinsic loose structure and the electronegativity, PIP-based NF membranes are generally considered unsuitable for removing divalent cations. Taking  $Mg^{2+}$  ( $MgCl_2$ ) as an example, most of the reported membranes report a rejection of only 70~80% [241]. NF270, another well-known commercial product from Dow, also has a  $Ca^{2+}$  rejection of only 40~60% [242]. Therefore, the fabrication of a NF membrane with high water flux for efficient heavy metal removal via a facile and economical method seems an attractive topic. As discussed above, MPD-based NF membranes would effectively reject all the multivalent cations due to the strong size exclusion effect, but this also results in a low water permeability. On the other hand, most PIP-based NF membranes show an insufficient rejection of divalent cations because of their loose structure and negatively charged PA layer, resulting from the hydrolysis of acyl chloride groups in TMC, despite its higher water permeability. The adopted TMC concentration in most studies was in the range of 0.1~0.15 w/v % [243, 244]. In fact, the concentration of TMC in the organic phase could greatly affect the molecular diffusion and residual monomer amount, and further impact the PA layer structure and surface charge.

Based on the above analysis, it is expected to simultaneously adjust the PA layer structure and surface charge by sharply decreasing the TMC concentration when using PIP as aqueous monomer. If so, then a NF membrane with a high water flux as well as an efficient heavy metal removal may be obtained. Therefore, in this chapter, a series of TFC NF membranes will be prepared on a polyethersulfone (PES) UF substrate by



decreasing the TMC concentration from 0.12 w/v% to 0.00075 w/v%. The physicochemical properties and microstructure of the resulting PA layers will be comprehensively characterized, i.e., roughness, surface morphology, O/N, thickness, pore size, water contact angle and zeta potential. Membrane separation parameters will be tested with a cross-flow filtration device. After analyzing all these characterization and testing results, an optimized NF membrane with desirable performance could be obtained. Then the membrane will be used to study the rejection of four heavy metal ions including  $\text{Ni}^{2+}$  ( $\text{NiCl}_2$ ),  $\text{Zn}^{2+}$  ( $\text{ZnCl}_2$ ),  $\text{Cu}^{2+}$  ( $\text{CuCl}_2$ ), and  $\text{Cd}^{2+}$  ( $\text{CdCl}_2$ ). Furthermore, the effects of the operating factors on heavy metal removal, including metal ion concentration (50-1000 mg/L), cross-flow velocity (0.15-0.56 m/s), and pressure (3-7 bar) will be investigated. Finally, the long-term operating stability will be studied and compared with literature results.

## **6.2 Results and discussion**

### **6.2.1 Influence of TMC concentration on membrane property evolution**

Five TFC NF membranes were prepared by interfacial polymerization between 0.6 w/v% PIP and (0.0075~0.12 w/v%) TMC on the PES substrate membrane. To explore the effect of the TMC concentration on the physicochemical properties of the TFC NF membranes, the polyamide layer of all prepared NF membranes was comprehensively characterized, including surface morphology, thickness, element composition, surface charge and contact angle determination. Afterwards, the separation performance of the five membrane samples was measured by determining the MWCO, pore size distribution, pure water permeability (PWP) and rejection of  $\text{MgCl}_2$ ,  $\text{Na}_2\text{SO}_4$ ,  $\text{MgSO}_4$  and  $\text{NaCl}$ . To reveal the evolution mechanism when decreasing the TMC concentration, the variation of physical features, physicochemical properties and the separation performance were comprehensively taken into consideration

#### **6.2.1.1 Physical features of different NF-TMC membranes**

**Figure 6.1 (a-e)** presents the SEM images of the NF membranes prepared with different TMC concentrations. It was observed that the membrane surface morphology changed when decreasing the TMC concentration from 0.12 w/v% to 0.0075 w/v%. A PA film with nodular surface morphology can be obtained at the highest TMC concentration of 0.12 w/v% (as shown in **Figure 6.1 (a)**), which is similar to other reported results [245-247]. However, the nodular structure gradually vanishes when decreasing the TMC concentration from 0.12 w/v% to 0.015 w/v%. The membrane surface becomes smoother, as demonstrated by the RMS roughness characterized by AFM (**Figure 6.1 (f-i)**). For instance, the RMS roughness of NF-0.015 was only 4.53 nm, which was much lower than that of NF-0.12 (18.86 nm).

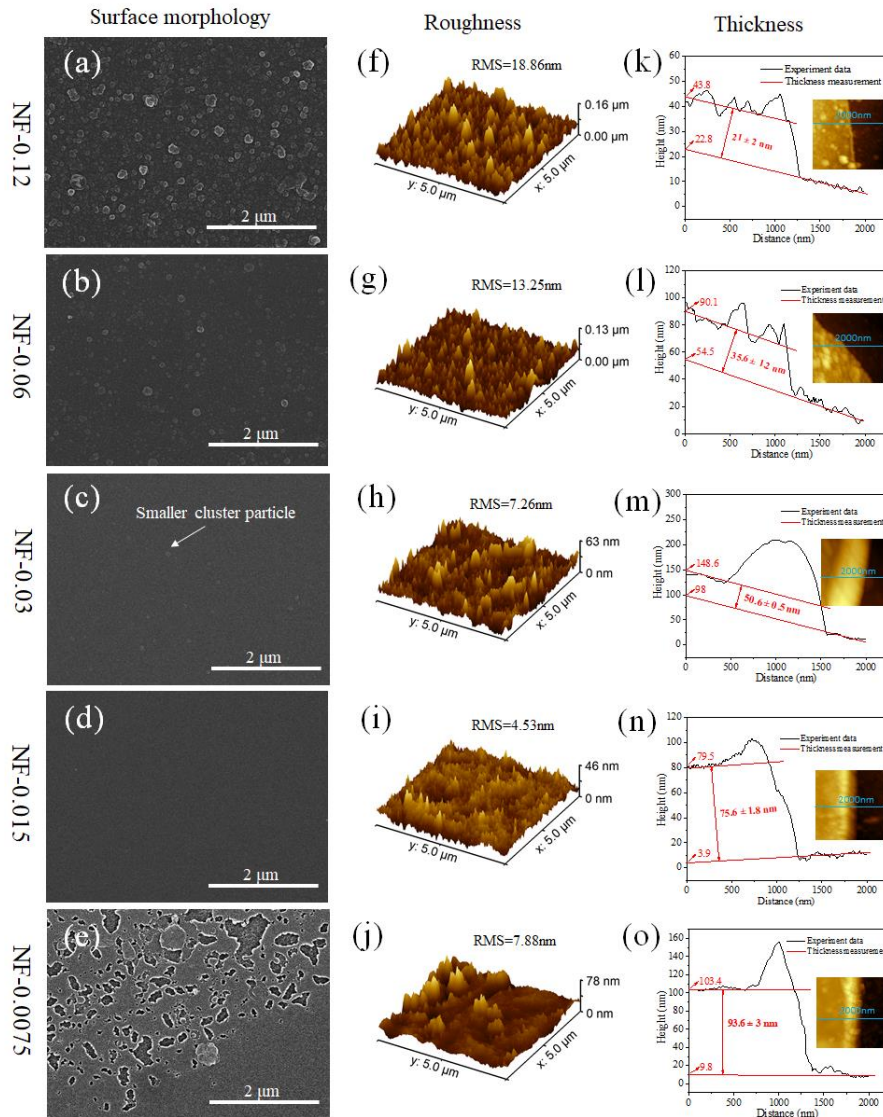


**Figure 6.1** Microscopic image and thickness measurement of polyamide film fabricated using 0.6 w/v% PIP and 0.12%-0.0075% w/v% TMC. SEM images (a-e) show the surface morphology of PA nano-films. AFM micrographs (f-j) show the surface roughness. Fig (k-o) shows the AFM height images and thickness measurement of the stripped PA nanofilm transferred onto a silicon wafer.

However, at the lowest TMC concentration (0.0075 w/v%), many crack-like defects were generated in the PA film (as shown in **Figure 6.1 (e)**). Compared with NF-0.015, the defects of NF-0.0075 increased its RMS roughness from 4.53 nm to 7.88 nm. The analytical results of SEM and RMS roughness confirm that the PA film surface morphology can be regulated by controlling the TMC concentration. A smooth PA layer can be constructed on the substrate membrane by decreasing the TMC concentration. Such a smooth surface is considered to be beneficial for mitigating membrane fouling [248]. As shown in **Figure 6.1 (c)**, a TMC concentration of 0.03 w/v% can be taken as the critical point for transforming a rough surface to a smooth one. Some small cluster particles can be observed in NF-0.03. Once the TMC concentration is lower than 0.03 w/v%, a smooth surface without observable cluster particles can be obtained. Inversely, a nodular surface morphology is produced.

The thickness of the NF membrane functional layer is an important parameter that can affect the mass transfer process. In order to investigate the influence of the TMC concentration on the PA film thickness, the PA film was successfully detached from the PES substrate membrane and then transferred onto a silicon wafer in order to conduct AFM analyses. The drop between the silicon wafer surface and the PA film surface can be regarded as its thickness. As shown in **Figure 6.1 (k-o)**, the thickness of the PA films increased when decreasing the TMC concentration from 0.12 w/v% to 0.0075 w/v%. The highest TMC concentration of 0.12 w/v% resulted in the thinnest PA film, with a thickness of around 21 nm. The lowest TMC concentration of 0.0075 w/v% resulted in the thickest PA film, with a thickness of over 90 nm. Interfacial polymerization is a self-limiting process controlled by monomer diffusion near the interface between water and

hexane. The reaction between PIP and TMC would stop once the mass transfer resistance of the generated PA layer is high enough to prevent the monomer diffusion across this layer [249]. Monomer diffusion is closely related to its concentration. A high concentration of TMC could accelerate the IP process and promptly produce a PA layer that is dense enough to stop the contact and reaction between PIP and TMC. Therefore, a thinner PA film can be obtained in this fast process. However, as the TMC concentration was decreased, the IP process would be prolonged because more time was needed for the diffusion of TMC molecules to react with PIP. The prolonged IP process could not create a PA layer that is dense enough to stop monomer diffusion. Instead, a thicker and looser PA film was generated. According to the solution-diffusion model and pore flow model, a higher thickness of the PA film would increase the mass transfer resistance of both solute and solvent [250]. On the other hand, a looser PA structure is expected to increase the membrane water flux and decrease solute rejection.

### 6.2.1.2 Physicochemical properties of different NF-TMC membranes

SEM and AFM characterization confirmed that the surface morphology and thickness of the PA film can be regulated by decreasing the TMC concentration. For the inner chemical structure of the PA film, XPS was employed to investigate the variation of the element content and functional groups. The C, O and N element composition and O/N are listed in **Table 6.1**.

**Table 6.1** XPS scanning results of the different NF-TMC membranes

Type of membrane	C (%)	O (%)	N (%)	O/N
NF-0.12	71.25	15.69	13.06	1.21
NF-0.06	71.24	15.52	13.24	1.17
NF-0.03	71.33	15.38	13.29	1.16
NF-0.015	71.28	14.78	13.94	1.06
NF-0.0075	71.01	14.70	14.29	1.03

As O1s in XPS relates to the binding energy of the electrons in the 1s orbit of oxygen atom, the narrow scan spectrum of O1s can provide more detailed information about the chemical state of oxygen atoms. According to the deconvolution of narrow scan spectrum of O1s, one can calculate the percentage of different oxygen-containing functional groups. Therefore, the O1s narrow scan spectrum of NF-0.12, NF-0.06, NF-0.03, NF-0.015, NF-0.0075 were further deconvoluted into two peaks at  $\sim 531.6$  eV (N-C=O) and  $\sim 533.5$  eV (O-C=O) as illustrated in **Figure 6.2 (a-e)**.

As analyzed in **Figure 6.2 (f)**, there is a correlation between the TMC concentration and the O/N ratio, as well as the relative percentage of carboxylic acid groups. The  $R^2$  of the linearly correlation between TMC concentration and O/N value is 0.8, while that of the linearly correlation between TMC concentration and -COOH content is 0.9. A lower concentration of TMC can decrease the O/N ratio and the residual carboxylic acid groups of the PA film. According to the theory proposed by Tang et al. [248], the O/N ratio of a PA film can be used to estimate the crosslinking degree between PIP and TMC. Normally, the calculated value of O/N ranges between 1 and 2. A lower O/N value indicates a higher crosslinking degree. From this point of view, decreasing the concentration of TMC could seemingly improve the crosslinking degree. However, it should be noted that the evaluation of the crosslinking degree with O/N tested with XPS is under the assumption that all the amino groups in PIP have reacted with acyl chloride groups in TMC. When the concentration of PIP is much higher than the concentration of TMC, such as sample NF-0.0075 (0.6 w/v% PIP, 0.0075 w/v% TMC, the ratio of PIP to TMC dosage was 80), some unreacted amino groups may remain in the PA film. The unreacted amino groups are expected to decrease the O/N value. An excessive PIP dosage could promote the reaction rate of acyl chloride groups in TMC, so the number of unreacted acyl chloride groups could be decreased. Thus, the relative percentage of carboxylic acid groups was decreased when reducing the TMC concentration. For example, the percentage of carboxylic acid groups of NF-0.12 was 20.64% (**Figure 6.2 (a)**), while that of NF-0.0075 was only 12.0% (**Figure 6.2 (e)**).

Surface charge and surface hydrophilicity play an important role in the salt rejection and water permeance of the NF membrane. The number of residual amino groups and carboxylic acid groups in the PA film is closely related to the charge property and surface hydrophilicity. The zeta potential, isoelectric point (IEP) and water contact angle of the different membranes are shown in **Figure 6.2 (g)** and **Figure 6.2 (h)**.

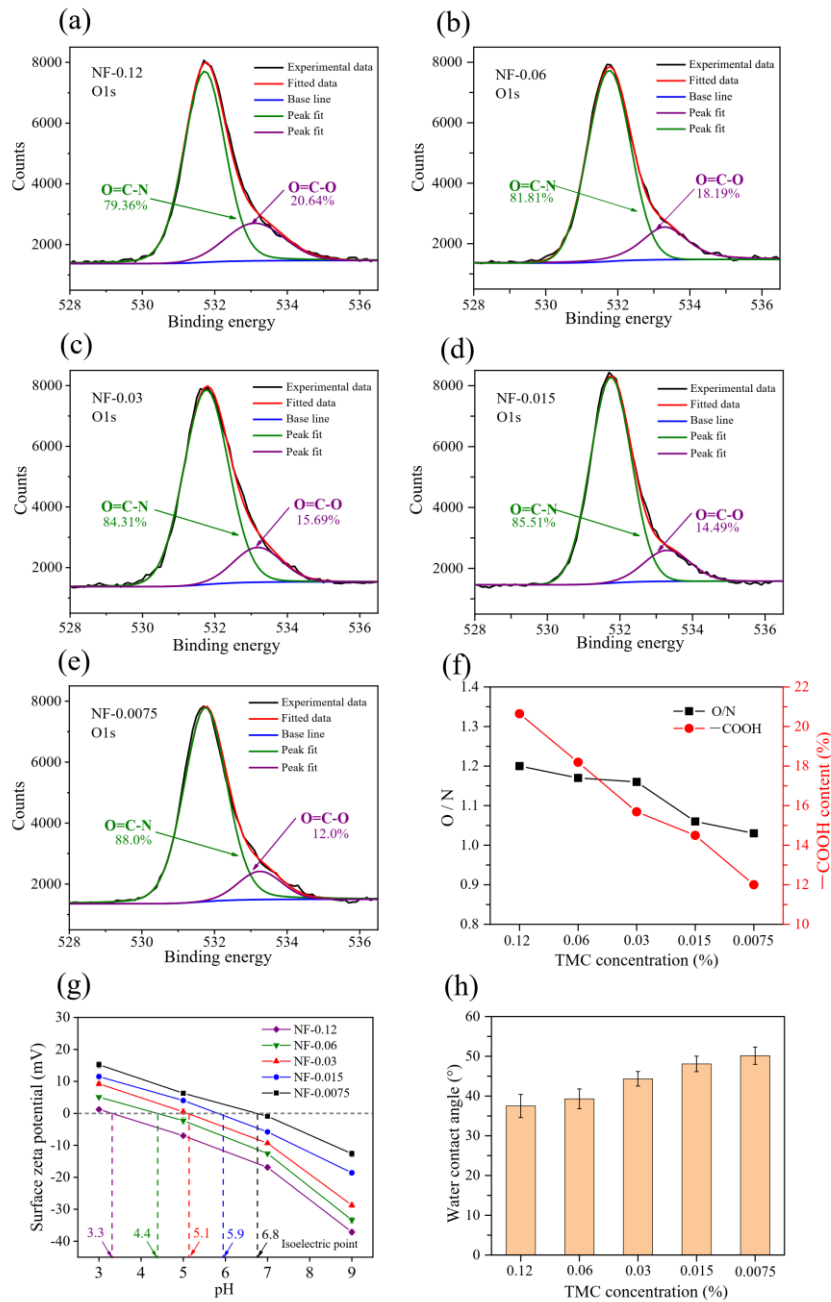


**Figure 6.2** (a-e) XPS narrow scan spectra of O1s measured from the surfaces of different NF-TMC membranes and the deconvoluted spectra for the probable chemical

species: NF-0.12, NF-0.06, NF-0.03, NF-0.015, NF-0.0075, representatively. (f) The influence of TMC concentration on O/N and -COOH content of PA film. (e) Zeta potential and isoelectric point of NF-(0.12-0.0075) membrane. (g) Water contact angle of NF-(0.12-0.0075) membrane.

It can be found that the IEP of the PA film increased from pH=3.3 to pH=6.8 when decreasing the TMC concentration from 0.12 w/v% to 0.0075 w/v%, demonstrating that the surface charge of the PA film transferred from strongly negative to weakly negative, or even near electric neutrality. This change resulted from the functional groups at membrane surface. As analyzed by XPS, the residual amino groups can be increased while the residual carboxylic acid groups can be decreased when reducing the TMC concentration in the IP reaction. A membrane surface with more polar functional groups or charged functional groups shows a stronger hydrophilicity. Therefore, the water contact angles gradually increased when decreasing the TMC dosage, indicating that the hydrophilicity was lower. Apparently, the decreased number of carboxylic acid groups in the PA film is the main reason. On the other hand, the smoother membrane surface with lower RMS roughness is another cause, according to the Wenzel model [251]. All these characterization results provide strong evidence that can support the speculation that it is possible to simultaneously adjust the PA layer structure and charge property by sharply decreasing the TMC concentration when using PIP as aqueous monomer.

### **6.2.1.3 Separation performance of different NF-TMC membranes**

The physicochemical structure of the PA film determines the separation performance of a TFC NF membrane; therefore the separation performance, including molecular weight cut-off (MWCO), pore size distribution, pure water permeability (PWP) and salt rejection, were further analyzed. The MWCO was determined using neutral organic solutes of different molecular weight; the MWCO was recorded when the solute rejection rate was 90%. Pore size and pore size distribution were calculated based on the Stokes radius of diethylene glycol, triethylene glycol and glucose. Four prepared

NF membranes were characterized; NF-0.0075 was not included, because the extremely low TMC concentration of 0.0075 w/v% cannot form a continuous PA film without defects on the PES substrate (as shown in **Figure 6.1 (c)**). The measured MWCO and pore size distribution are illustrated in **Figure 6.3 (a)** and **Figure 6.3 (b)**, respectively. An interesting observation is that the MWCO and mean pore radius decreased when the TMC concentration was reduced from 0.12 w/v% to 0.03 w/v%, which is inconsistent with the traditional expectation. However, this trend is consistent with that of the PA film thickness and the crosslinking degree (the value of O/N), as discussed in **section 6.2.1.1 and 6.2.1.2**. Further decreasing the TMC concentration to 0.015 w/v% promoted the generation of a looser PA structure, so the MWCO of NF-0.015 increased to 271, and the mean pore radius to 0.334 nm, although NF-0.015 presented a smooth surface without visible defects (**Figure 6.1(d)**).

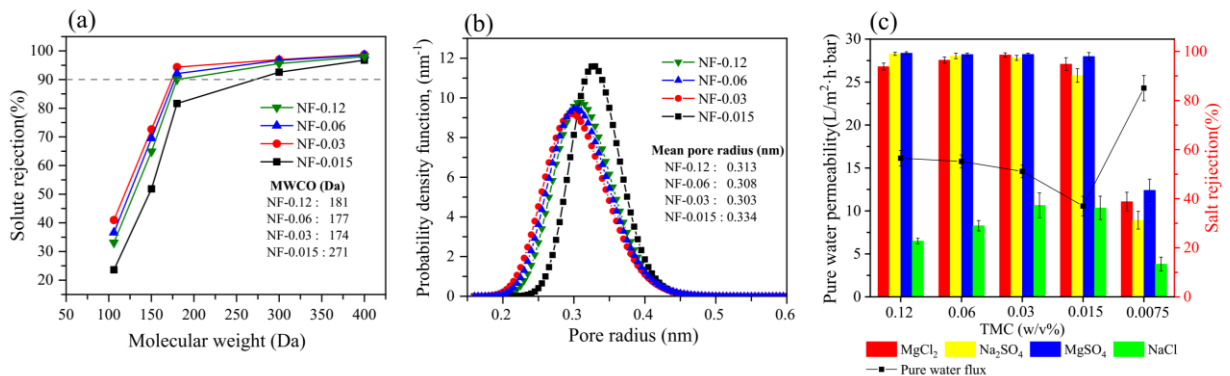


**Figure 6.3** (a) MWCO and (b) pore size distribution curves of the NF-0.12, NF-0.06, NF-0.03 and NF-0.015 membranes. (c) Pure water permeability and desalting performance of all prepared NF membranes

**Figure 6.3 (c)** presents the PWP and salt rejection of the five membrane samples prepared with different TMC concentrations. The PWP of these NF membranes continually decreased from 16.2 to 10.7 L m<sup>-2</sup> h<sup>-1</sup> bar<sup>-1</sup> when decreasing the TMC concentration from 0.12% to 0.015%. According to the data in **Figure 6.3 (a)** and **Figure 6.3 (b)**, NF-0.015 has a larger MWCO and mean pore radius than NF-0.12, NF-0.06 and NF-0.03, but its PWP is the lowest. This probably resulted from its higher PA



film thickness as shown in **Figure 6.1**. A thicker PA film would greatly increase the mass transfer resistance. NF-0.0075 presented the highest PWP (up to  $24.3 \text{ L m}^{-2} \text{ h}^{-1} \text{ bar}^{-1}$ ) and the poorest desalination performance due to the numerous defects in the PA film (as shown in **Figure 6.1 (e)**). The four other samples, including NF-0.12, NF-0.06, NF-0.03 and NF-0.015, all exhibited a high desalination efficiency for divalent electrolytes solution, and their rejections for  $\text{MgCl}_2$ ,  $\text{MgSO}_4$  and  $\text{Na}_2\text{SO}_4$  were 93.8-98.6%, 97.8-99.3% and 90.2-99.0%, respectively. Previous studies concluded that the original negative electricity of polyamide membranes fabricated with PIP and TMC resulted in a higher rejection of  $\text{Na}_2\text{SO}_4$  than of  $\text{MgCl}_2$  due to charge exclusion [252]. As shown in **Figure 6.3 (c)**, NF-0.12 and NF-0.06 in this study have a higher rejection of  $\text{Na}_2\text{SO}_4$  than of  $\text{MgCl}_2$ . However, this order was reversed when the TMC concentration was adjusted to a lower level. NF-0.03, NF-0.015 and NF-0.0075 all presented a higher rejection for  $\text{MgCl}_2$  than for  $\text{Na}_2\text{SO}_4$ . This is because the lower TMC dosage decreased the negative charge of the resulting NF membrane (as indicated in **Figure 6.2 (g)**), which could alleviate the attraction between the membrane matrix and cations in the feed solution.

Overall, NF-0.03 exhibited the best desalting ability with the highest rejections for all the four salts ( $\text{MgCl}_2$ ,  $\text{MgSO}_4$ ,  $\text{Na}_2\text{SO}_4$  and  $\text{NaCl}$ ), and simultaneously keeping a relatively high PWP of  $14.6 \text{ L m}^{-2} \text{ h}^{-1} \text{ bar}^{-1}$ . The desirable desalting performance of NF-0.03 can be attributed to its small mean effective pore size of 0.305, weakened negative charge (IEP=5.1) and moderate PA film thickness of 50 nm. In this case, size exclusion is expected to play a more important role in removing divalent ions. Furthermore, its lower negative charge is beneficial for mitigating the electrostatic attraction between cations and the membrane matrix. Therefore, the rejections of NF-0.03 for  $\text{MgCl}_2$ ,  $\text{Na}_2\text{SO}_4$  and  $\text{MgSO}_4$  are all higher than 98%, demonstrating its excellent ability to remove both divalent anions and cations. Compared with MPD-based TFC NF membranes, the relatively low  $\text{NaCl}$  rejection of 37.3% suggests that the PA structure of NF-0.03 is not so dense to effectively remove monovalent ions with smaller hydrated

radius. This yields a higher PWP. All these features of NF-0.03, including its efficient rejection for  $Mg^{2+}$ , high PWP and smooth surface structure, indicate it would be an outstanding candidate for heavy metal removal from wastewater.

### 6.2.2 Effect of operating conditions on heavy metal removal by NF-0.03

According to the results presented in **section 6.2.1**, NF-0.03, the sample prepared with a decreasing TMC concentration down to 0.03 w/v%, showed promising features fitting for removing heavy metal ions from water. In the following section, four commonly used heavy metal ions, including  $Ni^{2+}$ ,  $Zn^{2+}$ ,  $Cu^{2+}$  and  $Cd^{2+}$ , were employed to evaluate the heavy metal removal capacity of NF-0.03. The influence of operating conditions, including ion concentration, pressure and cross-flow velocity on heavy metal removal were systematically assessed with the cross-flow filtration device. The results are presented in **Figure 6.4**.

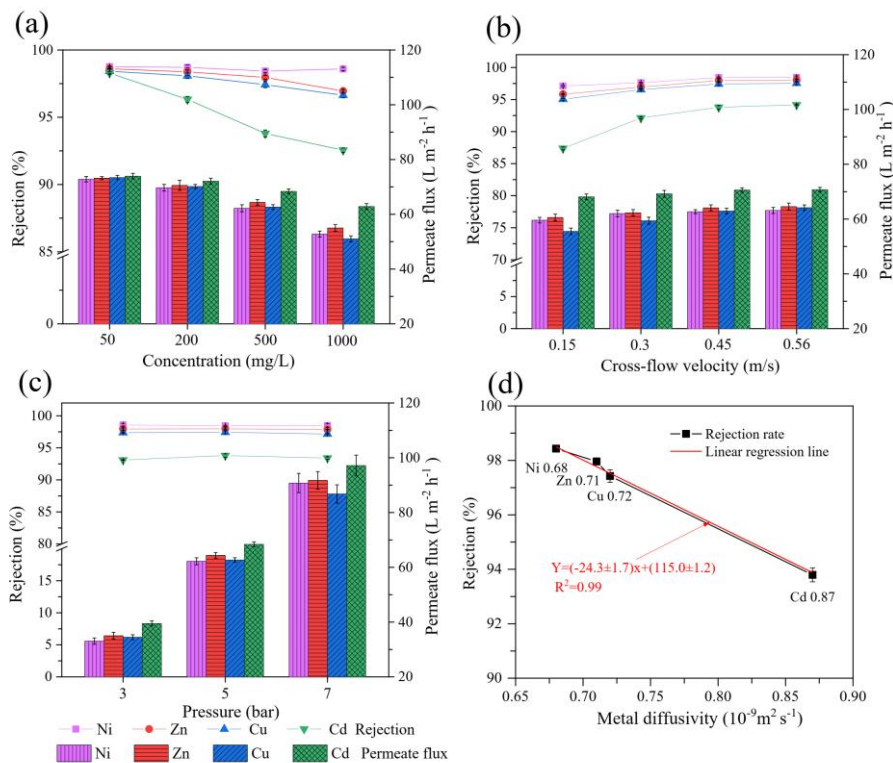


**Figure 6.4** (a) Effect of ion concentration (50~1000 mg/L) on rejection and permeate flux of NF-0.03, testing conditions: pH=5, pressure=5 bar, cross-flow velocity=0.45 m/s, temperature=25°C. (b) Effect of cross-flow velocity (0.15~0.56 m/s) on rejection

and permeate flux of NF-0.03, testing conditions: pH=5, pressure =5 bar, ion concentration=500 mg/L, temperature=25°C. (c) Effect of pressure (3 ~ 7 bar) on rejection and permeate flux of NF-0.03, testing conditions: pH=5, cross-flow velocity=0.45 m/s, ion concentration=500 mg/L, temperature=25°C. (d) Correlativity between ion diffusivity and ion rejection. The ion rejection was obtained under the condition: ion concentration=500 mg/L, pH=5, pressure=5 bar, cross-flow velocity=0.45 m/s, temperature=25°C.

### 6.2.2.1 Effect of heavy metal ion concentration

The ion rejection and permeate flux as a function of ion concentration ( $\text{Ni}^{2+}$ ,  $\text{Zn}^{2+}$ ,  $\text{Cu}^{2+}$  and  $\text{Cd}^{2+}$ ) is presented in **Figure 6.4 (a)**. An obvious phenomenon is that all the heavy metal ion rejections and corresponding permeate fluxes decreased when increasing the ion concentration from 50 to 1000 mg/L. However, for  $\text{Ni}^{2+}$ ,  $\text{Zn}^{2+}$  and  $\text{Cu}^{2+}$ , the rejections decreased only slightly from 98.8 to 97.3%, from 98.6 to 97.0%, and from 98.4 to 96.7%, demonstrating the excellent heavy metal removal capacity of NF-0.03. Different from the other three ions, the  $\text{Cd}^{2+}$  rejection presented a relatively distinct drop at high feed solution concentration. It was 98.3% when the feed solution concentration was 50 mg/L, but decreased to 92.7% when the feed solution concentration was 1000 mg/L. Concentration polarization (CP) is a natural phenomenon in the membrane separation process that is closely related to permeate flux, solute rejection and membrane fouling [253, 254]. At constant cross-flow velocity, CP can be intensified by increasing the ion concentration, because more ions can be transported to the membrane surface in the same time interval and enlarge the concentration difference between the membrane surface and the bulk solution. On the other hand, the ion concentration gradient across the NF membrane was larger, which can allow more ions to penetrate through the membrane. In addition, the osmotic pressure difference between the feed and permeate side would be increased, thus partially counteracting the transmembrane pressure. As a consequence, the heavy metal removal and the permeate flux were simultaneously reduced when increasing the ion

concentration in feed solution. Other researchers also found that both rejection and permeate flux decreased as the concentrations of heavy metal ions were increased, although the prepared NF membranes were positively charged [215, 255].

Another interesting phenomenon in **Figure 6.4 (a)** is that the permeate flux of a  $\text{Cu}^{2+}$  solution sharply decreased to the lowest level, much lower than with other three heavy metals, when increasing the ion concentration from 50 to 1000 mg/L. During this variation process, the permeating flux decrease extent of  $\text{Cu}^{2+}$  solution is up to 31%, while those of other three ions ( $\text{Ni}^{2+}$ ,  $\text{Zn}^{2+}$  and  $\text{Cd}^{2+}$ ) ranges between 15% and 23%. When the membrane sample was taken out of the membrane cell after filtrating  $\text{Cu}^{2+}$  solution, a cake layer consisting of blue precipitates can be seen on the membrane surface. This indicates that membrane fouling occurred during the filtration of the  $\text{Cu}^{2+}$  solution. The pH of the permeate water in this process was measured. Its pH was around 4 after operating for one hour and continued to decline over time; this was much lower than the feed solution (pH=5). This can be explained with the Donnan effect. The heavy metal salts used in this study are chlorides. Compared with the heavy metal ions,  $\text{H}^+$  with smaller size and higher diffusivity would preferably pass through the NF membrane together with  $\text{Cl}^-$  to close the charge balance. Therefore, more  $\text{OH}^-$  and  $\text{Cu}^{2+}$  can be rejected and accumulated near the membrane surface. Once reaching the solubility product of  $\text{Cu}(\text{OH})_2$ ,  $\text{Cu}(\text{OH})_2$  precipitates would be generated; this leads to membrane fouling. Compared to the other three heavy metals, the solubility product of  $\text{Cu}(\text{OH})_2$  is the lowest (as shown in **Table 6.2**), so  $\text{Cu}(\text{OH})_2$  precipitates are the easiest to be generated. Thus, membrane fouling together with CP at high ion concentration of 1000 mg/L resulted in the observed sharp decrease of permeate flux. Al-Rashdi et al. [256] reported similar findings, indicating that  $\text{Cu}^{2+}$  can be adsorbed or deposited onto NF270, thus leading to the most obvious flux decline compared with other tested heavy metals.

**Table 6.2**  $K_{sp}$  of the hydroxide related to four heavy metal ions [257].

Type of ions	$K_{sp}$
Ni(OH) <sub>2</sub>	$2.0 \times 10^{-15}$
Zn(OH) <sub>2</sub>	$2.09 \times 10^{-16}$
Cu(OH) <sub>2</sub>	$4.8 \times 10^{-20}$
Cd(OH) <sub>2</sub>	$7.5 \times 10^{-15}$

### 6.2.2.2 Effect of cross-flow velocity and operating pressure

Cross-flow filtration is an important method to alleviate CP [258], and the cross-flow velocity is a decisive factor to be considered. The ion rejection and permeate flux when regulating the cross-flow velocity is presented in **Figure 6.4 (b)**. It can be found that cross-flow velocity has a notable influence on the  $Cd^{2+}$  rejection. The rejection of  $Cd^{2+}$  increased from 87.4% to 93.8% when increasing the cross-flow velocity from 0.15 to 0.45 m/s. Meanwhile, the cross-flow velocity shows more influence on the permeate flux of  $Cu^{2+}$  solution. At the lowest cross-flow velocity of 0.15 m/s, the permeating flux of  $Cu^{2+}$  solution is around  $55 \text{ L m}^{-2} \text{ h}^{-1}$ , but it was improved to about  $62 \text{ L m}^{-2} \text{ h}^{-1}$  when the cross-flow velocity is enlarged to 0.45 m/s. The lowest permeate flux of a  $Cu^{2+}$  solution at a cross-flow velocity of 0.15 m/s is explained by CP and membrane fouling as explained in **Section 6.2.2.1**. The above results suggest that the enhancement of cross-flow is beneficial for promoting ion removal, as well as mitigating membrane fouling. However, further increasing the cross-flow velocity above 0.45 m/s cannot give an additional enhancement. The observed plateau has also been confirmed by other researchers [259]. Besides, excessive cross-flow is also a waste of energy. Thus cross-flow velocity of 0.45 m/s can be regarded as an optimized choice.

**Figure 6.4 (c)** shows the ion rejection and permeate flux when regulating the operating pressure from 3 to 7 bar. The permeate flux almost linearly increased with the operating pressure, while a relatively stable ion rejection was observed. This linear relation between operating pressure and permeate flux confirms the good stability of NF-0.03 under high pressure. The stable ion rejection is somewhat different from previous studies. For instance, Gherasim et Al. [260] found that the rejection of  $Pb^{2+}$

showed a slight increase when the operating pressure was increased from 10 bar to 50 bar. The authors inferred that the larger solvent flux at higher pressure could dilute the permeate solution, thus enlarging the ion rejection. In the current study, the pressure variation range is small (from 3 to 7 bar). Therefore, the dilution effect was negligible. In another study of Al-Rashdi et.al [256], the rejection of  $Pb^{2+}$  and  $Cd^{2+}$  fluctuated when the pressure increased from 3 bar to 5 bar, which may explained by concentration polarization. The cross-flow velocity in this study was fixed at a relatively high value of 0.45 m/s, thus pressure-induced concentration polarization could be eliminated by the strong flow disturbance. Therefore, the heavy metal removal of NF-0.03 maintained relatively stable when regulating the pressure.

As summarized in **Table 6.3**, the hydrated radius of the four heavy metal ions follow the order:  $Zn^{2+} > Cd^{2+} > Cu^{2+} > Ni^{2+}$ . According to the size exclusion mechanism, the removal of the four ions should also follow the same order. For example,  $Ni^{2+}$  with minimum hydration radius was expected to have the poorest removal.

**Table 6.3** Hydrated radius and diffusion coefficient of different heavy metal ions [215].

Type of ions	Hydrated radius (nm)	Diffusivity ( $10^{-9} \text{ m}^2 \text{ s}^{-1}$ )
$Ni^{2+}$	0.404	0.68
$Zn^{2+}$	0.43	0.71
$Cu^{2+}$	0.419	0.72
$Cd^{2+}$	0.426	0.87

However, the experimental results in **Figure 6.4 (a)**, **Figure 6.4 (b)** and **Figure 6.4 (c)** all provide a rejection order:  $Ni^{2+} > Zn^{2+} > Cu^{2+} > Cd^{2+}$ . Therefore, other factors should be taken into consideration. Based on the mechanism of solution-diffusion model, solute diffusivity is another important factor affecting the solute mass transfer across membrane [261]. The diffusivities of the four heavy metals are listed in **Table 6.3**. After the comparison between ion diffusivity and ion rejection, a remarkable negative correlation was discovered and illustrated in **Figure 6.4 (d)**. The linear correlation analysis between the ion diffusivity and ion rejection shows that the  $R^2$  is high: 0.99,

As shown in **Figure 6.4 (b)**, the mean pore radius of NF-0.03 was only 0.303 nm, which is much lower than the hydrated radii of the four heavy metal ions, so the size difference of the four heavy metal ions cannot determine the overall rejection. Therefore, ion diffusivity is thought to play a dominant role in removing heavy metals by NF-0.03. Ions with stronger diffusivity are more likely to diffuse across the PA film and be present in the permeate water. In another study, the lower rejection of  $\text{Cd}^{2+}$  with a positively charged NF membrane was ascribed to the fact that Cd has both anions and cations forms in aqueous solution, including  $\text{Cd}^{2+}$ ,  $\text{CdCl}^+$ ,  $\text{CdCl}^{3-}$ ,  $\text{CdCl}_4^{2-}$  [215, 255]. These negatively charged components could lead to electrostatic attraction and promote ion penetration.

### **6.2.3 Evaluation of the membrane long-term stability and performance comparison with other competitors**

As explained in **Section 6.2.2**,  $\text{Cd}^{2+}$  with the highest diffusivity is the most difficult to be removed by NF-0.03. Therefore,  $\text{Cd}^{2+}$  can reflect the membrane performance change. In order to evaluate the long-term stability on NF-0.03, a solution with 200 mg/L  $\text{CdCl}_2$  was used as feed solution for continuous filtration for 48 hours. The  $\text{Cd}^{2+}$  rejection and permeate flux are shown in **Figure 6.5 (a)**. It can be found that both  $\text{Cd}^{2+}$  rejection and permeate flux were rather stable during the filtration process. The average  $\text{Cd}^{2+}$  rejection was high, at 96.2%. This result reflects the good durability of NF-0.03 to some extent, although 48 h is not long enough. The desirable long-term stability of NF-0.03 can be attributed to its moderate PA film thickness (50 nm) and high crosslinking degree (O/N=1.16) as discussed in **Section 6.2.1**.

The performance in terms of permeation flux and heavy metal rejection of the NF-0.03 is compared with other state-of-art NF membranes reported in the literature. The comparison results are presented in **Figure 6.5 (b)**. It is apparent that NF-0.03 shows an outstanding performance for heavy metal removal, with much higher water permeability and comparative heavy metal removal efficiency, especially for  $\text{Ni}^{2+}$ ,  $\text{Zn}^{2+}$

and  $\text{Cu}^{2+}$ , of which rejections are all over 98%. The comparison suggests that the performance of the fabricated NF-0.03 in our research exceeds the majority of currently reported NF membranes aiming for heavy metal removal. More importantly, NF-0.03 was fabricated only by decreasing the TMC concentration, which is a strategy with simplicity, low cost and scaling up feasibility.

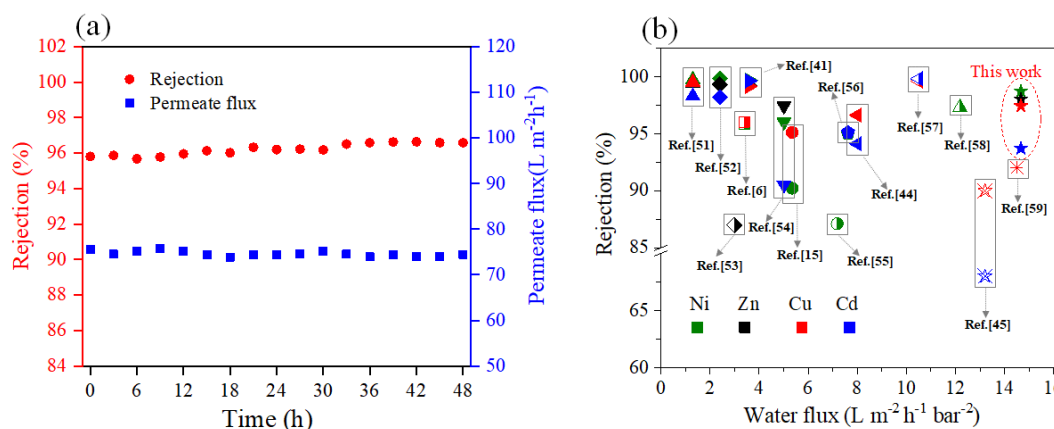


**Figure 6.5** (a) The long-term separation performance of NF-0.03, testing conditions: 200 mg/L  $\text{CdCl}_2$ , pH=5, pressure=5 bar, cross-flow velocity=0.45 m/s, temperature=25°C. (b) Performance comparison with other reported results.

### 6.3 Conclusions

The preparation of a TFC NF membrane with desirable rejection of heavy metal ions is a promising route to deal with the wastewater produced in petroleum refineries and petrochemical plants. However, conventional TFC NF membranes prepared with PIP and TMC usually have an insufficient ability to remove heavy metal ions from water because of their loose structure and negatively charged surface. In this chapter, a TFC NF membrane with good water permeability and high heavy metal removal was fabricated by decreasing the TMC concentration to an exceptionally low extent. The physicochemical properties and microstructure of the resulting PA layers, as well as the NF membrane separation parameters when regulating the TMC concentration were comprehensively characterized and analyzed. The optimal NF membrane (NF-0.03) prepared with 0.6 w/v% PIP and 0.03 w/v% TMC had the smallest mean effective pore



## Chapter 6

radius of 0.305 nm, low negative charge (IEP=5.1) and moderate PA film thickness of 50 nm. All these features endowed its outstanding removal efficiency of about 98% against  $\text{Ni}^{2+}$ ,  $\text{Zn}^{2+}$ ,  $\text{Cu}^{2+}$ , and more than 92.7% for  $\text{Cd}^{2+}$ , simultaneously keeping a high pure water permeability of  $14.6 \text{ L m}^{-2} \text{ h}^{-1} \text{ bar}^{-1}$ . The systematical exploration of the IP reaction between PIP and TMC suggests that this is a good strategy for fabricating a negatively charged NF membrane for heavy metal removal. The simplicity, low cost and scaling up feasibility of the current strategy is expected to meet the requirements of industrial production.

## Chapter 7

### **Direct Generation of an Ultrathin (8.5 nm) Polyamide Film with Ultrahigh Water Permeance via In-situ Interfacial Polymerization on a Commercial Substrate Membrane**

Adapted from: *Direct generation of an ultrathin (8.5 nm) polyamide film with ultrahigh water permeance via in-situ interfacial polymerization on commercial substrate membrane. Journal of Membrane Science, 634 (2021) 119450.*

#### **7.1 Introduction**

The moderate water permeance of conventional NF membranes, together with the prevalent “trade-off” effect between water permeability and solute rejection, has plagued its further development for a long time. Engineering the molecular and structural properties of the PA layer is of paramount significance for promoting the membrane performance. Based on the classical theories of hydrodynamics and solution diffusion<sup>[262][263]</sup>, decreasing the thickness of the PA film is expected to be an effective strategy for enhancing the water flux and coordinating the trade-off between water permeance and solute rejection, which was also verified by many experimental results<sup>[263-265]</sup>. However, the conventional NF membranes fabricated with *in situ* interfacial polymerization (ISIP), in which the interfacial polymerization reaction directly proceeds on the substrate membrane, usually have a PA film thickness of 30-100 nm<sup>[266-270]</sup>. Although many other strategies have been proposed to enhance the membrane performance, such as constructing a nano-wrinkled PA structure<sup>[271, 272]</sup>, embedding additional water channels<sup>[273, 274]</sup> and strengthening the hydrophilicity of the material<sup>[275]</sup>, the performance improvement was found not sufficient. As a consequence, the water permeance of NF membranes prepared with ISIP generally ranges between

5-30 L m<sup>-2</sup> h<sup>-1</sup> bar<sup>-1</sup>.

Recently, some pioneering studies reported that an ultrathin PA film with thickness below 10 nm can be constructed on a substrate membrane *via* other novel techniques [264] [276]. These novel techniques can be classified into two categories. The first is to introduce a sacrificial or intermediate layer of nanomaterials between the PA film and the substrate membrane [121, 277-279]. The second is to synthesize an ultrathin PA film *via* support-free interfacial polymerization and then transferring it onto the substrate membrane [265, 280] [281]. As interfacial polymerization reactions did not directly proceed on the substrate membrane, these novel techniques can be denoted as *ex situ* interfacial polymerization (ESIP). During ESIP, the monomer solution can be more homogeneously distributed, thus enabling a rapid and controllable IP reaction [121, 281]. TFC NF membranes with ultrathin PA film fabricated with ESIP can dramatically shorten the mass transfer distance and reduce the mass transfer resistance, thus achieving an ultrafast separation and an ultrahigh water permeance over 30 L m<sup>-2</sup> h<sup>-1</sup> bar<sup>-1</sup>. In terms of operational procedures, ISIP is a simple, mature and reliable technique, which has been adopted to manufacture TFC membranes in industrialized production. In contrast, ESIP is complex and expensive, thus only feasible in laboratory scale up today. Therefore, combining the advantage of ISIP and that of ESIP, and directly synthesize an ultrathin PA film on substrate membranes with the ISIP technique may allow to greatly improve the performance of TFC NF membranes and promote their applications.

In order to achieve this goal, two critical issues should be considered. The first one is to control the interfacial polymerization reaction; the second one is to select a proper substrate membrane. For the first issue, research about the construction of an ultrathin PA film with ESIP may provide useful information. For instance, Zhu et al. [282] obtained a PA film with a thickness of 12 nm by using a low piperazine (PIP) concentration of 0.025 w/v%. Similarly, in the study of Niu et al. [281], the thickness of PA film was further decreased to 3-4 nm by reducing PIP concentration to 0.001

w/v%. It was previously found that increasing the trimesoyl chloride (TMC) concentration could reduce the thickness of the PA film [283]. These results imply that the thickness of PA film can be controlled by regulating the monomer concentrations. However, the influence of the monomer concentration on the thickness of the PA film in ISIP has not been systematically analyzed up to now. For the second issue, the properties of the sacrificial or intermediate layer created in some ESIP reactions may be enlightening, as the sacrificial or intermediate layer is usually hydrophilic, porous and smooth<sup>[276, 284, 285]</sup>. Nevertheless, the necessary characteristics of a proper substrate membrane for constructing ultrathin PA film in ISIP are still unknown and controversial [286-288], although there have been some theoretical models describing the influence of substrate membrane on the interfacial polymerization reaction [289-292].

The objective of this chapter is to coordinate the trade-off between membrane water permeability and solute rejection by decreasing the thickness of PA film. Based on the above analysis, it can be anticipated that a TFC NF membrane with ultrathin PA film may be fabricated *via* ISIP by simultaneously optimizing the monomer concentration and the selection of a substrate membrane. Therefore, this chapter will explore the PA film thickness variation, as well as the separation performance of the resultant TFC NF membranes when regulating the monomer (PIP and TMC) concentration. Five commercial UF membranes with different properties will be used as the substrate to identify their impacts. The current research is expected to provide a deeper insight in manufacturing high-performance TFC NF membranes.

## **7.2 Results and discussion**

### **7.2.1 Thickness evolution of the PA film during the regulation of monomer concentration**

In order to understand the influence of the monomer concentration on the thickness of the PA film, 15 TFC NF membranes with a gradient variation of PIP and TMC

concentration (as listed in **Table 7.1**) were fabricated *via* ISIP strategy on a commercial UF substrate denoted as PSH-100 kDa. The properties of PSH-100 kDa can be found in **Table 7.2**. The PA films on the substrate membranes were isolated and then transferred onto the silicon wafer, so the vertical drop characterized with AFM between the surface of PA film and that of silicon wafer can be regarded as the thickness of the PA film [264, 265, 281, 293]. The evolution of PA film thickness are shown in **Figure 7.1**.

**Table 7.1** Monomers concentration of the fabricated TFC NF membrane

Monomers concentration		Monomers concentration		Monomers concentration	
(w/v %)		(w/v %)		(w/v %)	
PIP	TMC	PIP	TMC	PIP	TMC
1	0.03	1	0.06	1	0.1
0.6	0.03	0.6	0.06	0.6	0.1
0.3	0.03	0.3	0.06	0.3	0.1
0.1	0.03	0.1	0.06	0.1	0.1
0.05	0.03	0.05	0.06	0.05	0.1

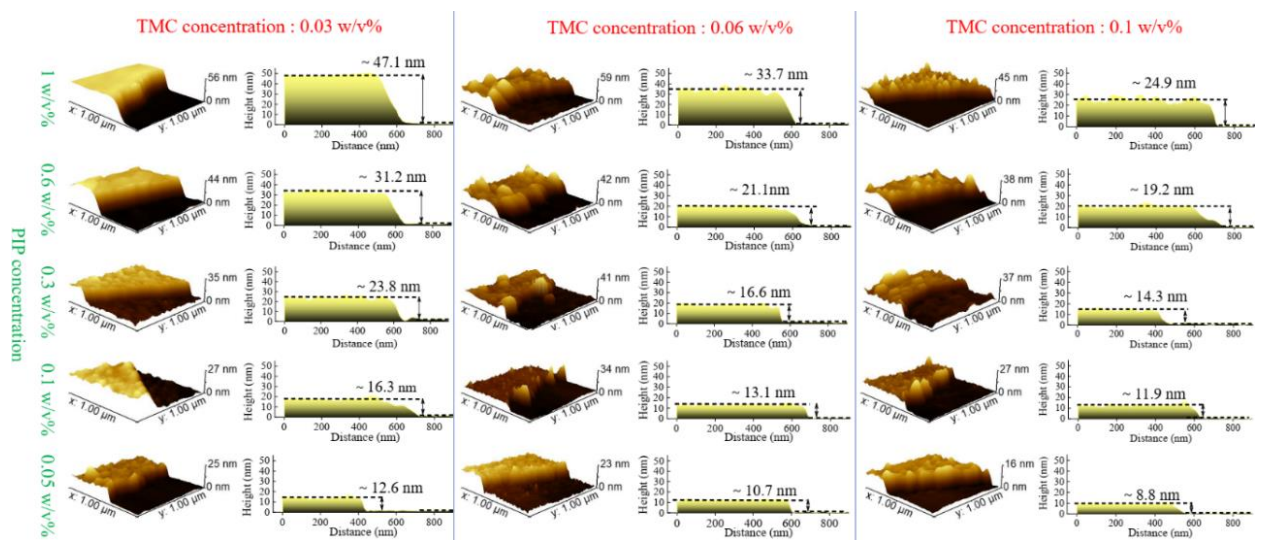


**Figure 7.1** Evolution of PA film thickness versus the monomer concentration. The PA

film with different monomers concentration was fabricated on PSH-100 kDa membrane

As indicated in **Figure 7.1** and **Figure 7.2 (b)**, the thickness of the PA film is closely related to the monomer concentration. An obvious variation trend can be found, i.e., reducing the PIP concentration or increasing the TMC concentration can decrease the PA film thickness. For instance, when fixing the TMC concentration at 0.06 w/v%, the thickness of the PA film can be sharply decreased from 33.7 nm to 10.7 nm by reducing the PIP concentration from 1 w/v% to 0.05 w/v%. On the other hand, when fixing the PIP concentration at 0.3 w/v%, the thickness of the PA film can be gradually decreased from 23.8 nm to 14.3 nm by increasing the TMC concentration from 0.03 w/v% to 0.1 w/v%. Therefore, a conclusion can be obtained that the PA film thickness of the TFC NF membranes prepared with the ISIP strategy can be flexibly manipulated by regulating the PIP or TMC concentration. Why can a lower PIP concentration combined with a higher TMC concentration decrease the PA film thickness? To answer this question, a model is proposed, denoted as “Double interface thickness-controlling (DITC) theory”. This model is illustrated in **Figure 7.2 (a)**.

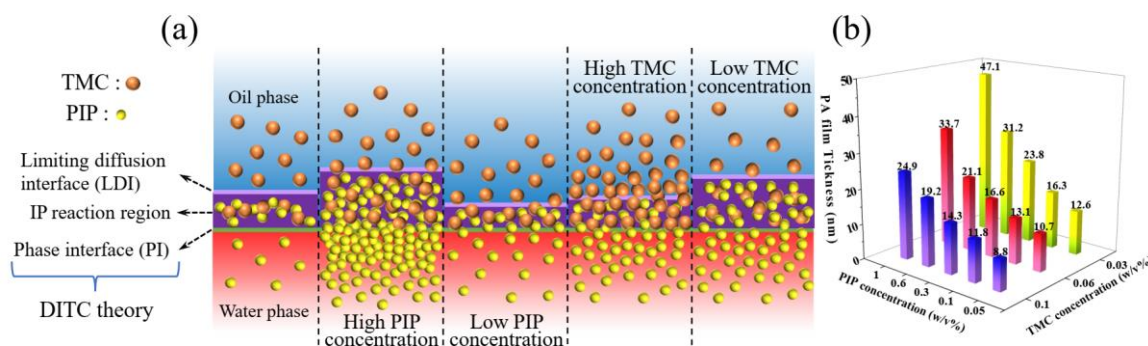


**Figure 7.2** (a) Illustration of the DITC theory. (b) Evolution of PA film thickness versus the monomer concentration

According to the classical interfacial polymerization theory, there is an interface between the water phase and oil phase (the green line in **Figure 7.2 (a)**). It is widely accepted that the polymerization between PIP and TMC would proceed on the side of

the oil phase, because the solubility of PIP in the organic solvent is greater than that of TMC in water [294-297]. Thus, PIP molecules break through the phase interface and enter into the oil phase. The TMC molecules “waiting” in the oil phase collide and react with the “arriving” PIP molecules. So there is a “driving force” and a “resistance” for the diffusion of PIP molecules above the green line (interface). The “driving force” is governed by the concentration gradient between the aqueous phase and the oil phase, so the higher the PIP concentration, the larger the “driving force”. The “resistance” is controlled by the numbers of TMC in oil phase. So the higher the TMC concentration is, the larger the “resistance” is. As a result of the interaction between the “driving force” and “resistance”, there is a maximum diffusion distance away from the phase interface. The interface determined by the maximum diffusion distance is denoted as “Limiting diffusion interface of water phase monomer (LDI)” (the pink line in **Figure 7.2 (a)**).

Based on the above assumptions, there are no PIP molecules above the LDI. In other words, the polymerization between PIP and TMC only proceeds in the space between the two interfaces (phase interface and LDI). So the thickness of the PA layer produced by the reaction between PIP and TMC is determined by the distance between the two interfaces. A higher PIP concentration gives a stronger “driving force” and a larger maximum diffusion distance, while a higher TMC concentration yields a larger “resistance” and a smaller maximum diffusion distance. Thus, reducing the PIP concentration but increasing the TMC concentration decreases the PA film thickness (as shown in **Figure 7.2 (b)**). On the basis of this DITC theory, an ultrathin PA film with thickness of 8.8 nm can be directly generated on a substrate membrane with the ISIP technique by using a low PIP concentration of 0.05 w/v% and a high TMC concentration of 0.1 w/v%. This thickness is comparable to other reported ultrathin PA films in the literature.

### **7.2.2 Performance evaluation of the ultrathin PA film constructed on PSH-100 kDa.**

It is widely accepted that decreasing the thickness of the PA film is an effective strategy

for enhancing the membrane water permeance, as a thinner PA film can reduce the mass transfer distance and resistance. In order to verify this inference, the pure water permeability of all the TFC NF membranes fabricated in last section was measured. The results are presented in **Figure 7.3 (a)** by taking the PA film thickness as horizontal axis. It can be clearly observed that the PWP of the resultant TFC NF membrane increased sharply for a thinner PA film. For instance, the TFC NF membrane with PA film of 47.1 nm had a PWP of  $8.2 \text{ L m}^{-2} \text{ h}^{-1} \text{ bar}^{-1}$ , while the TFC NF membrane with PA film of 12.6 nm had a much higher PWP of  $46.1 \text{ L m}^{-2} \text{ h}^{-1} \text{ bar}^{-1}$  (460% higher). Notably, the TFC NF membrane with the thinnest PA film of only 8.8 nm showed the highest PWP of  $55.1 \text{ L m}^{-2} \text{ h}^{-1} \text{ bar}^{-1}$ .

As the trade-off between water permeability and solute rejection is a challenge, the separation performance of the TFC NF membrane with the thinnest PA film (8.8 nm) was further evaluated. **Figure 7.3 (b)** indicates that this TFC NF membrane had a MWCO of 613 Da and a mean pore diameter of 0.707 nm. Although the mean pore diameter was below 1 nm, the pore size distribution was relatively wide. A large proportion of the PA region with pore size over 1 nm can be found in **Figure 7.3 (b)**. As pores with a diameter over 1 nm cannot effectively reject dissolved ions, they can be regarded as micro defects, which decrease the membrane salt rejection. Therefore, the 8.8 nm PA film provided a desalting performance as shown in **Figure 7.3 (c)**: the rejections for  $\text{MgCl}_2$  and  $\text{NaCl}$  were less than 10%; the  $\text{Na}_2\text{SO}_4$  rejection of ~92% was higher than the  $\text{MgSO}_4$  rejection of ~55% due to the electrostatic interaction between ions and the charged PA film. This suggests that the ultrathin (8.8 nm) PA film constructed on PSH-100 kDa can greatly promote the mass transfer of water molecules, but its desalting ability was insufficient.

The surface morphology of the substrate (PSH-100 kDa) and that of the TFC NF membrane with 8.8 nm PA film were characterized with SEM and illustrated in **Figure 7.3 (d)**. The relatively rough pore structure of PSH-100 kDa can be seen in the SEM image. Once the ultrathin PA film was produced after the ISIP between PIP and TMC,



the pore structure of the substrate was fully covered, and the TFC NF membrane presented a rather smooth surface morphology. Although no visible defects can be found in the SEM image, there may exist some micro defects which cannot be observed due to the limited resolution. As the ultrathin PA film of 8.8 nm was so vulnerable, it was rather sensitive to the substrate properties. Any structure defect can deteriorate the desalting ability of the TFC NF membrane. Therefore, in order to promote the desalination performance of the TFC NF membrane with an ultrathin PA film (8.8 nm), the selection of the substrate membrane should be further optimized.

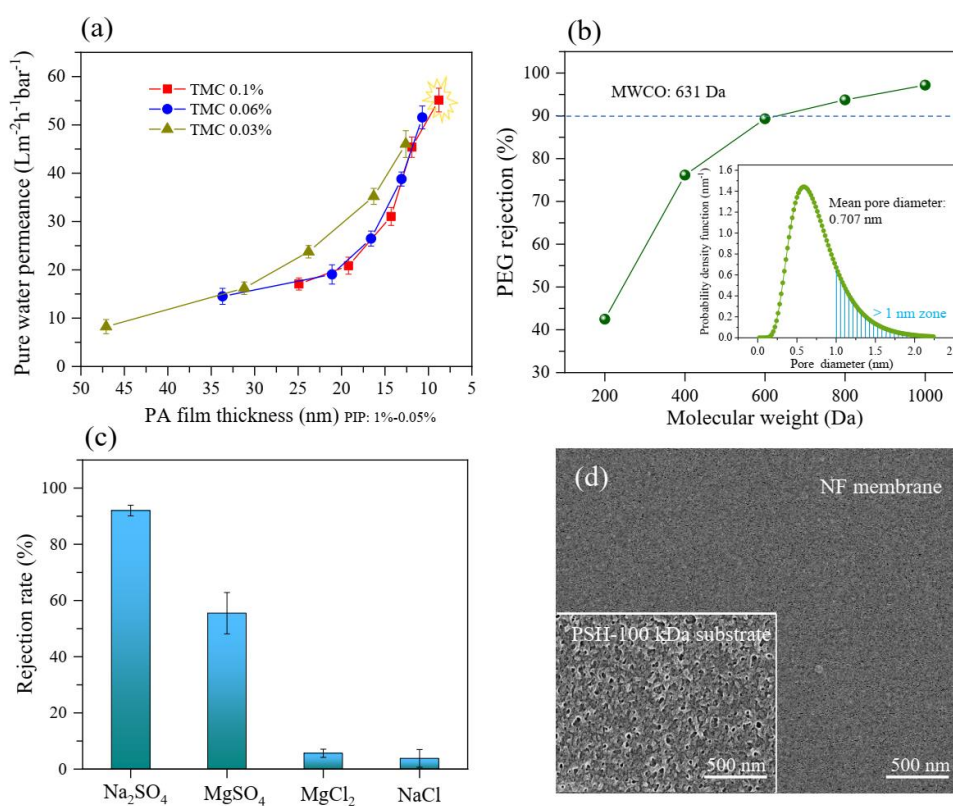


**Figure 7.3** (a) Evolution of the NF membrane PWP versus the thickness of the composed PA film (TMC: 0.03%, 0.06%, 0.1%, PIP: 1%, 0.6%, 0.3%, 0.1%, 0.05%). (b) MWCO and pore size distribution curves of the NF membrane. (c) Desalination performance of the NF membrane for  $\text{Na}_2\text{SO}_4$ ,  $\text{MgSO}_4$ ,  $\text{MgCl}_2$ ,  $\text{NaCl}$  solution. (d) Surface morphology of the NF membrane and the PSH-100 kDa substrate. The NF membrane for the above (b-d) cited was fabricated by monomers concentration of TMC: 0.1% and PIP: 0.05% on PSH-100 kDa substrate.

### 7.2.3 Impact of substrate membrane on TFC NF membrane with ultrathin PA film.

In order to optimize the desalination performance of the TFC NF membrane with ultrathin PA film, another four commercial UF membranes in addition to the PSH-100 kDa were selected for applying the same ISIP reaction with 0.05 w/v% PIP and 0.1 w/v% TMC. All the five commercial substrate membranes (denoted as PES-20 kDa, PESH-50 kDa, PSH-100 kDa, PES-150 kDa and PS-OW) are made of PES (polyether sulfone) but having different structure characteristics, as listed in **Table 7.2**. It should be noted that the measured MWCO of PES-20 kDa, PESH-50 kDa, PSH-100 kDa, PES-150 kDa were somewhat different from the manufacturer-marked values, which may be due to the different calculation methods. Nevertheless, the orders of MWCO, mean effective pore diameter and PWP were consistent. A larger MWCO and mean effective pore diameter were found corresponding to a higher PWP. Furthermore, the RMS roughness of the five substrates also showed an increasing trend with larger MWCO, so the pore structures were more and more obvious, as shown in **Figure 7.4**.

**Table 7.2** Structural parameters testing results of the five commercial UF substrates

Type of substrate	MWCO (kDa)	Mean effective pore diameter (nm)	RMS roughness (nm)	PWP ( $\text{L m}^{-2} \text{bar}^{-1} \text{h}^{-1}$ )
PES-20 kDa	8.7	3.2	3.51	121 ± 10
PESH-50 kDa	68.9	8.5	5.10	172 ± 12
PSH-100 kDa	113.5	11.81	7.45	259 ± 7
PES-150 kDa	187.9	14.51	11.10	563 ± 23
PS-OW	142.5	12.91	8.56	301 ± 13

After the ISIP reaction was completed on the above different substrate membranes, the thickness of the resultant PA films was determined with AFM; the membrane surface morphologies before and after ISIP were characterized with SEM. As shown in **Figure 7.4 (a)~(d)**, an ultrathin PA film with thickness lower than 10 nm can all be constructed

on the four alternative substrates PES-20 kDa, PESH-50 kDa, PSH-100 kDa, PES-150 kDa. The PA films formed on these four substrates all presented smooth surface morphology as indicated in **Figure 7.4 (f)~(i)**. However, different from the other four candidates, the substrate denoted as PS-OW presented a distinct influence on the formation of the PA film. As shown in **Figure 7.4 (e)**, the thickness of the PA film generated on PS-OW was up to 22.1 nm, which cannot be classified as “ultrathin”. In addition, the surface of NF-OW presented numerous granular structures (**Figure 7.4 (j)**) that were not found in the other four samples as illustrated in **Figure 7.4 (f)~(i)**. This remarkable observation cannot be ascribed to the structural difference among the five substrates, because both the substrate with lower structural parameter values (PES-20 kDa, PES-50kDa, PSH-100 kDa) and that with higher structural parameter values (PES-150kDa) can all be used for the construction of an ultrathin and smooth PA film. In addition, the surface morphology of PS-OW measured by SEM also did not present any abnormalities in comparison to the other four substrates.

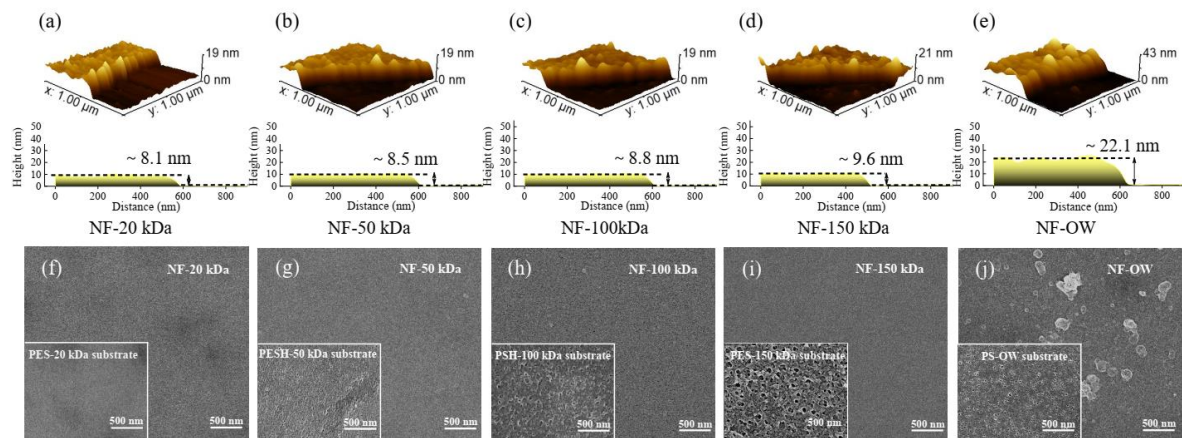


**Figure 7.4** (a-e) Thickness of the PA films formed on five different substrate membranes. The TFC NF membranes prepared on the five substrates are respectively denoted as NF-20 kDa, NF-50 kDa, NF-100 kDa, NF-150 kDa and NF-OW. (f-j) SEM images of the surface morphology of five substrates and five TFC NF membranes.

In order to understand which critical factor affects the formation of an ultrathin PA film, the pore size distributions and dynamic water contact angles (WCA) of the five

commercial substrates were determined; they are provided in **Figure 7.5 (a)** and **Figure 7.5 (b)**. It can be found that the pore size distribution of PS-OW is in between the series of five candidate membranes. PES-20 kDa has a narrower pore size distribution, and PES-150 kDa has a wider pore size distribution. As a consequence, the pore size distribution can be excluded. Notably, the dynamic WCA measurements provided enlightening information. As shown in **Figure 7.5 (b)**, the WCA of PS-OW was much higher than the WCA of the other four candidates. Specifically, the WCA of PS-OW was relatively stable and higher than  $77^\circ$  during the entire measurement process of 60 s. In contrast, the WCA of the other four samples was lower than  $70^\circ$ , and continuously decreased during 60 s. Especially for the PSH-50 kDa, the dynamic WCA was  $58.7^\circ$  at the beginning and then sharply declined to  $29.8^\circ$  after 60 s. Therefore, it can be concluded that the WCA or hydrophilicity of the substrate membrane is the critical factor that essentially affects the formation of an ultrathin PA film.

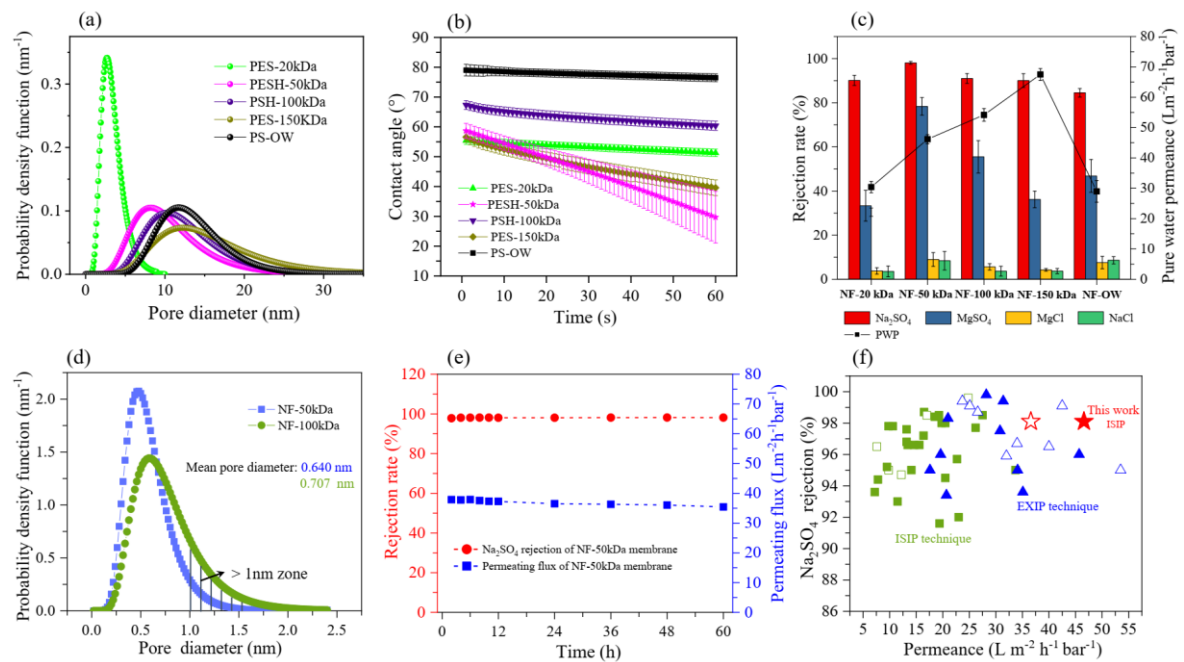


**Figure 7.5** (a) The pore size distribution of the five substrates. (b) The dynamic WCA of the substrate membrane in the test time of 60s. (c) PWP and desalination performance of the five fabricated NF-(20 kDa-150 kDa, OW) membranes. (d) The comparison of the NF-100 kDa and the NF-50 kDa in terms of the pore size and pore size distribution.

(e) Performance stability of the optimized NF-50 kDa during continues operation of 60 h. (Feed solution: 1000 mg/L Na<sub>2</sub>SO<sub>4</sub>, Pressure: 2 bar, cross-flow velocity: 0.45 m/s).

(f) Performance comparison of the NF-50 kDa with the state-of-the-art NF membranes fabricated by ISIP (marked with green block) and EXIP (marked with blue trigon) techniques reported recent 5 years. In consideration of the different reported results in the literature, both pure water permeance and permeating flux of Na<sub>2</sub>SO<sub>4</sub> solution are shown here. The solid shape color represents PWP while the hollow shape color represents the permeating flux of Na<sub>2</sub>SO<sub>4</sub> solution.

During the fabrication of TFC NF membranes with ISIP technology, the aqueous solution containing PIP monomers should be removed after aqueous phase immersion. According to experience, the substrate surface should be kept in a state denoted as “moist but not watery” before contacting with the organic phase containing TMC. This special state could ensure the formation of a hydration layer containing PIP monomers on the substrate surface, which was vitally important for the formation of a stable and intact interface as shown in **Figure 7.2 (a)**. The stable and intact interface on the substrate membrane is crucial for the ISIP reaction and the construction of an ultrathin PA film without defects. In fact, this is also the essential reason for many researchers who created a sacrificial or intermediate layer of nanomaterials on the surface of other substrate membranes. The large WCA or low hydrophilicity of PS-OW indicate that the affinity between water molecules and the membrane surface was rather poor. Therefore, it cannot produce a stable and intact interface. Moreover, the water molecules in the incomplete hydration layer tended to evaporate into the air during the operation process, thus resulting in an increase of the PIP concentration. It was the unstable IP reaction and increased PIP concentration that resulted in the thick and rough PA film on PS-OW shown in **Figure 7.4 (e)** and **Figure 7.4 (j)**. The PWP and salt rejections of the TFC NF membranes constructed on the five commercial substrates were tested and provided in **Figure 7.5 (c)**. Undoubtedly, NF-OW with the thickest and defective PA film showed the lowest PWP (only 28.9 L m<sup>-2</sup> h<sup>-1</sup> bar<sup>-1</sup>) and the poorest salt rejection. Even for

Na<sub>2</sub>SO<sub>4</sub>, the rejection was just around 84.5%.

Different from NF-OW, the other four TFC NF membranes with ultrathin PA films (NF-20 kDa, NF-50 kDa, NF-100 kDa and NF-150 kDa) presented an increasing PWP with larger substrate membrane pore size, which suggests that the mass transfer resistance of the substrate membrane would play an important role in the permeance of the composite NF membrane with ultrathin PA film. The substrate with larger pore size and higher permeance contributed a lower resistance both for water lateral mass transfer and water pore-flow mass transfer [265, 281, 291]. NF-150 kDa exhibited the highest PWP of 67.5 L m<sup>-2</sup> h<sup>-1</sup> bar<sup>-1</sup>, while NF-20 kDa had the lowest PWP of 30.4 L m<sup>-2</sup> h<sup>-1</sup> bar<sup>-1</sup>. However, the salt rejections of these two samples were not high. The Na<sub>2</sub>SO<sub>4</sub> rejections of NF-150 kDa and NF-20 kDa were both around 90%, which indicates that some micro defects should be formed in the ultrathin PA film, although they cannot be observed in the SEM images. Thus, substrate membranes with either too small pore size or too large pore size are not beneficial for the formation of a non-defective PA film. During the fabrication process of TFC NF membranes with ISIP technique, the pores of the substrate membrane virtually act as numerous reservoirs that can store the PIP solution. The PIP solution in these pores will provide the aqueous solution for the formation of phase interface. If the pores of the substrate membrane were too small, the PIP solution storage amount would be very small. In this condition, the phase interface cannot be well formed. As a result, it cannot form a non-defective PA film. As for the substrate membrane with too large pores, the PIP storage amount is large enough to ensure the formation of a complete phase interface. However, the large voids of the membrane pores cannot provide a stable support for the ultrathin PA film with low strength. Consequently, the PA film across the large void would be easily destroyed under pressure in testing, thus producing defects.

NF-50 kDa, which was fabricated on the PESH-50 kDa with medium pore size, smooth surface and strong hydrophilicity, showed the best desalting ability: it has a Na<sub>2</sub>SO<sub>4</sub> rejection of 98.1 % and MgSO<sub>4</sub> rejection of 78.3%. This performance was much better

the than other four samples. In addition, NF-50 kDa could maintain a high PWP up to  $46.6 \text{ L m}^{-2} \text{ h}^{-1} \text{ bar}^{-1}$ . The pore size of NF-50 kDa was further characterized and compared with NF-100 kDa, as shown in **Figure 7.5 (d)**. In comparison to NF-100 kDa, NF-50 kDa had a lower MWCO (518 Da) and a mean pore diameter of 0.640 nm. Furthermore, NF-50 kDa presented a much narrower pore size distribution. The proportion of the PA region with pore size over 1 nm was reduced. It was the ultrathin PA film as well as the narrow pore size distribution that gave NF-50 kDa a high permeability as well as a high  $\text{Na}_2\text{SO}_4$  rejection. The NaCl and  $\text{MgCl}_2$  rejections of these membranes are all lower than 10%, which is much lower than the optimized NF membrane in **Chapter 6**, of which NaCl and  $\text{MgCl}_2$  rejection are 40% and 98%, respectively. The rejection of NaCl is mainly based on size exclusion, while the rejection of  $\text{MgCl}_2$  relied on charge exclusion. The optimized NF membrane in **Chapter 6** has a MWCO of 174 Da and a surface zeta potential around -10 mV at pH 7. Taking NF-50 kDa in this chapter as example, its MWCO is 518 Da and its surface zeta potential is around -40 mV at pH 7. Thus, the NF membranes in this chapter have larger pore size and stronger negative charge, and the size exclusion and charge exclusion against NaCl and  $\text{MgCl}_2$  are greatly weakened. Therefore, the removal capacity of NaCl and  $\text{MgCl}_2$  is low.

By taking 1000 mg/L  $\text{Na}_2\text{SO}_4$  solution as feed water, a continuous operation for 60 hours at low-pressure of 2 bar was conducted to evaluate the stability of NF-50 kDa. As indicated in **Figure 7.5 (e)**, the permeating flux of  $36.6 \text{ L m}^{-2} \text{ h}^{-1} \text{ bar}^{-1}$  and the  $\text{Na}_2\text{SO}_4$  rejection of ~98% was steadily maintained in the operation, which confirmed the stability of NF-50 kDa. The performance of NF-50 kDa in terms of  $\text{Na}_2\text{SO}_4$  rejection and PWP is compared with the “state-of-the-art” NF membranes recently reported in the literature. According to the definition in the **Introduction**, the reported NF membranes in literature were classified into two categories, i.e., *in situ* interfacial polymerization (ISIP) and *ex situ* interfacial polymerization (ESIP). These are denoted as green squares and blue triangles, respectively, in **Figure 7.5 (f)**. The comparison suggests that the performance of NF-50 kDa is superior to all the reported NF

membranes fabricated with ISIP techniques, and surpassed most of the NF membranes prepared with the expensive and complicated ESIP techniques. The excellent performance of NF-50 kDa membrane confirms that an ultrathin PA film with desirable permeability and Na<sub>2</sub>SO<sub>4</sub> rejection can be directly constructed on a commercial UF membrane with medium pore size and strong hydrophilicity.

### 7.3 Conclusions

In this chapter, a TFC NF membrane with ultrathin PA film was fabricated with ISIP by simultaneously optimizing the monomer concentration and the selection of a substrate membrane. Firstly, it was demonstrated that the thickness of PA film formed in ISIP process can be manipulated by regulating the monomer concentration: a higher TMC concentration and lower PIP concentration lead to a thinner PA film, which was explained by the proposed DITC model. On this basis, an ultrathin PA film with thickness of 8.8 nm was directly generated on a commercial substrate membrane with the ISIP technique by using a low PIP concentration of 0.05 w/v% and a high TMC concentration of 0.1 w/v%. The resulting TFC NF membrane showed an extremely high PWP of 55.1 L m<sup>-2</sup> h<sup>-1</sup> bar<sup>-1</sup> and a Na<sub>2</sub>SO<sub>4</sub> rejection of 92%. In order to improve the Na<sub>2</sub>SO<sub>4</sub> rejection and minimize the defects induced by the substrate membrane, five commercial substrate membranes with different features were studied to understand the role of the substrate membrane in determining the performance of a TFC NF membrane. It was found that a commercial substrate membrane (PESH-50 kDa) with strong hydrophilicity, smooth surface morphology and medium pore size could provide a homogeneous and intact interface for a stable interfacial polymerization during the ISIP process. Therefore, an ultrathin PA film (8.5 nm) with narrow pore size distribution can be directly constructed on the substrate membrane. The eventual TFC NF membrane showed an excellent balance between permeability and solute rejection, thus presenting an ultrahigh PWP of 46.6 L m<sup>-2</sup> h<sup>-1</sup> bar<sup>-1</sup> and a high Na<sub>2</sub>SO<sub>4</sub> rejection of 98.1%. This performance is superior to most of the “state-of-the-art” NF membranes prepared with



## *Chapter 7*

other advanced materials and complex methods. Furthermore, the confirmed critical role of monomer concentration and substrate membrane in ISIP process provided a deeper insight in manufacturing high-performance TFC NF membranes, of which the simplicity and feasibility is expected to promote its industrialized application in the future.

## Chapter 8

### Conclusions and Recommendations for Future Research

#### 8.1 General conclusions

Reclamation after advanced treatment has become the most promising choice to properly manage the wastewater produced in petroleum industry, in order to simultaneously decrease the clean water consumption and wastewater discharge. Previous explorations have confirmed the feasibility and potential for applying NF technology in the advanced treatment of petroleum wastewater, but the widely adopted commercial NF membranes are facing numerous problems such as membrane fouling, insufficient foulant rejection and low water permeability. As the membrane material is the core of NF technology, this thesis intends to improve the performance of NF membranes from the perspective of membrane fabrication and modification. The outcome of this thesis is expected to provide technical support for promoting the benign circulation of petroleum wastewater. The detailed conclusions are as follows:

- (1) A novel NF membrane can be prepared by interfacial polymerization between serinol and TMC catalyzed by DMAP. The optimized membrane fabricated with 0.05% (w/v) TMC, 1.0% (w/v) serinol, and 10% DMAP has a MWCO of 474 Da and a water permeability of  $6.0 \text{ L}\cdot\text{m}^{-2}\cdot\text{h}^{-1}\cdot\text{bar}^{-1}$ . The salt rejections followed the order of  $\text{Na}_2\text{SO}_4 > \text{MgSO}_4 > \text{NaCl} > \text{MgCl}_2$ , and the values were 96.3%, 83.9%, 58.7% and 28.8%, respectively. Compared with a commercial product (NF90), the stronger hydrophilicity, smoother surface structure and lower salt rejection of the newly developed membrane was found to have a remarkable antifouling ability during the treatment of model PFPW.
- (2) As a general phenomenon in *in situ* interfacial polymerization, support membrane pore blockage (SMPB) could improve the adhesion between support membrane and the PA layer through a “mechanical interlocking effect”, which should be meaningful to

enhance the TFC membrane long-term stability. In order to prepare a TFC membrane with desirable properties, SMPB should be alleviated on the premise of ensuring the membrane stability. It is expected to relieve SMPB by the proper selection of monomer concentration, lag time after aqueous phase coating and support membrane pore size.

(3) Surface modification with serinol can enhance the antifouling property of the TFC NF membrane applied in polymer flooding produced water treatment. The modification of the active layer with serinol grafting can obviously improve the water permeability, while maintaining its desalting ability and neutral solute rejection. When treating the model PFPW, the serinol-grafted NF membrane showed an excellent antifouling ability and satisfactory rejections of  $\text{Ca}^{2+}$ ,  $\text{Mg}^{2+}$ ,  $\text{SO}_4^{2-}$  and TOC.

(4) A TFC NF membrane with desirable water permeability and high heavy metal removal can be fabricated by decreasing the TMC concentration to an exceptional low extent. The optimized NF membrane prepared with 0.6 w/v% PIP and 0.03 w/v% TMC had the smallest mean effective pore radius of 0.305 nm, weakened negative charge (IEP=5.1) and moderate PA film thickness of 50 nm. All these features endowed its outstanding removal efficiency of about 98% for  $\text{Ni}^{2+}$ ,  $\text{Zn}^{2+}$ ,  $\text{Cu}^{2+}$ , and more than 92.7% for  $\text{Cd}^{2+}$ , with a high pure water permeability of  $14.6 \text{ L m}^{-2} \text{ h}^{-1} \text{ bar}^{-1}$ . The simplicity, low cost and scaling up feasibility of the new strategy is expected to meet the requirements of industrial production.

(5) A TFC NF membrane with ultrathin PA film can be fabricated with ISIP by simultaneously optimizing the monomer concentration and the selection of a substrate membrane. Firstly, it was demonstrated the thickness of the PA film formed in the ISIP process can be manipulated by regulating the monomer concentration: a higher TMC concentration and a lower PIP concentration yield a thinner PA film. An ultrathin PA film can be directly generated on a commercial substrate membrane with the ISIP technique by using a low PIP concentration of 0.05 w/v% and a high TMC concentration of 0.1 w/v%. Moreover, it was found that the commercial substrate

membrane (PESH-50 kDa) with strong hydrophilicity, smooth surface morphology and medium pore size could provide a homogeneous and intact “phase interface” for the stable interfacial polymerization during the ISIP process. Therefore, an ultrathin PA film (8.5 nm) with narrow pore size distribution can be directly constructed on the substrate membrane. The resultant TFC NF membrane showed an excellent balance between permeability and solute rejection, thus presenting an ultrahigh PWP of 46.6 L m<sup>-2</sup> h<sup>-1</sup> bar<sup>-1</sup> and a high Na<sub>2</sub>SO<sub>4</sub> rejection of 98.1%.

However, it should be noted that the five experimental chapters in this thesis are only on the level of laboratory testing. There is still a long distance from the current study to practical application in the petroleum industry. The key challenge is to convert the membrane preparation and modification techniques in this thesis into industrial manufacturing procedures, because the manual operation in the lab is rather different from the production flow in actual plants. A technical cooperation with NF membrane manufacturers may be necessary. Besides, the five experimental chapters of this thesis related to membrane fouling mitigation, foulant removal capacity enhancement and water permeability improvement were studied separately. However, in the application process, these three factors can influence each other. Therefore, a systematical pilot-scale study is also important before the practical scale application.

### **8.2 Recommendations for future research**

In consideration of the experiments and conclusions in this thesis, several recommendations are provided for future research.

(1) The macroscopic filtration efficiency, represented by the water permeability and salt rejection, is the joint result of many microstructure characteristics, including membrane hydrophilicity, charge property, surface morphology, functional layer thickness, pore size distribution, etc. A butterfly effect usually exists since these parameters could influence each other when regulating one of them. For instance, when the membrane surface hydrophilicity is enhanced by surface grafting, the membrane surface charge

would be simultaneously changed due the reaction between the grafting monomer and membrane surface chemical groups. Therefore, the coordination of the relationship among various microstructure characteristics is a significant topic for further study.

(2) The structure of NF membranes, especially the inner structure, is in the scale of nanometer or sub-nanometer. Many current available instruments have an insufficient ability to accurately analyze some parameters. More microscopic characterization methods with higher resolution should be developed in order to better understand the structure-property-performance relationship, which is the foundation of rational design and fabrication of desirable NF membranes.

(3) Computational chemistry is a branch of theoretical chemistry, aiming for calculating the properties of molecules via mathematical approximations and computer programs. It has been proved to be a useful tool assisting understanding reaction mechanisms and regulating reaction conditions. If some coefficients related to interface polymerization can be estimated via the application of computational chemistry, then the reaction process can be understood more accurately. Thus, more efforts should be paid in order to apply these tools in promoting the development of NF technologies at the molecular and atomic scales.

(4) There is a gap between lab-scale preparation and industrialized production. Although the separation performance including water permeability and salt rejection of NF membrane is important, other factors such as cost and stability should be equally considered, because they are all critical to the practical application of NF technology. Taking the NF membrane with ultrathin PA film (8.5 nm) in Chapter 7 as example, its separation performance is much better than that of many other commercial products. Its stability is also confirmed by a continuous testing of 60 hours. However, the stability of 60 hours is not sufficient for practical application. Although the ultrathin PA film shows an extremely high water permeability, yet the ultrathin PA also makes it easily abraded and destroyed. This should be one important factor to be considered before commercialization. Due to the limitation of the study in laboratory, more evaluation

related to this issue are not given in this thesis. More research as well as pilot scale testing is necessary in the future.

(5) During the application of NF technology, a certain amount of concentrated solution (brine) which is often more harmful and difficult to deal with would be co-produced. Therefore, more research focusing on the proper treatment of this concentrated wastewater is of great significance.

(6) A problem in the current membrane research field is that different studies and publications usually adopt different testing devices and testing conditions. The inconsistent testing brings difficulties in the comparison of different membrane samples. A standard membrane testing principle is necessary to be accepted and used by membrane researchers. And membrane studies should report their results based on this similar testing principle.

## Chapter 8

## References:

- [1] V. Ayyam, S. Palanivel, S. Chandrakasan, Water resources and the changing needs, Coastal Ecosystems of the Tropics-Adaptive Management, (2019) 153-173.
- [2] L.F. Greenlee, D.F. Lawler, B.D. Freeman, B. Marrot, P. Moulin, Reverse osmosis desalination: Water sources, technology, and today's challenges, Water Research, 43 (2009) 2317-2348.
- [3] R.F. Service, Desalination freshens up, Science, 313 (2006) 1088-1090.
- [4] X. Miao, Y. Tang, C.W.Y. Wong, H. Zang, The latent causal chain of industrial water pollution in China, Environmental Pollution, 196 (2015) 473-477.
- [5] S. Kumar, H.M. Meena, K. Verma, Water pollution in India: Its impact on the human health: Causes and remedies, International Journal of Applied Environmental Sciences, 12 (2017) 275-279.
- [6] A. Shahedi, A.K. Darban, F. Taghipour, A. Jamshidi-Zanjani, A review on industrial wastewater treatment via electrocoagulation processes, Current Opinion in Electrochemistry, 22 (2020) 154-169.
- [7] M. Rusin, J. Gospodarek, A. Nadgórska-Socha, G. Barczyk, Effect of petroleum-derived substances on life history traits of black bean aphid (*Aphis fabae* Scop.) and on the growth and chemical composition of broad bean, Ecotoxicology, 26 (2017) 308-319.
- [8] G. Hu, J. Li, G. Zeng, Recent development in the treatment of oily sludge from petroleum industry: A review, Journal of Hazardous Materials, 261 (2013) 470-490.
- [9] F.L.R. Ahmadun, A. Pendashteh, L.C. Abdullah, D.R.A. Biak, S.S. Madaeni, Z.Z. Abidin, Review of technologies for oil and gas produced water treatment, Journal of Hazardous Materials, 170 (2009) 530-551.
- [10] M. Jain, A. Majumder, P.S. Ghosal, A.K. Gupta, A review on treatment of petroleum refinery and petrochemical plant wastewater: A special emphasis on constructed wetlands, Journal of Environmental Management, 272 (2020) 111057.
- [11] A. Yusuf, A. Sodiq, A. Giwa, J. Eke, O. Pikuda, G.D. Luca, J.L.D. Salvo, S. Chakraborty, A review of emerging trends in membrane science and technology for sustainable water treatment,



## References

Journal of Cleaner Production, 266 (2020) 121867.

[12] S. Bauer, H.J. Linke, M.D Wagner, Combining industrial and urban water-reuse concepts for increasing the water resources in water : carce regions, *Water Environment Research*, 92 (2020) 1027-1041.

[13] X. Huo, L. Huang, Q. Zhang, Z. Yang, Impact of greening of wastewater reuse from gas purification plant on soil environment, *Environmental Science and Management*, 44 (2019) 25-29.

[14] H. Altaher, E. Elqada, W. Omar, Pretreatment of wastewater streams from petroleum/petrochemical industries using coagulation, *Advances in Chemical Engineering and Science*, 01 (2011) 245-251.

[15] L.N. Butseva, L.V. Gandurina, B.M. Ustinov, P.P. Pridatkin, Flotation treatment of wastewater using cationic flocculants, *Chemistry and Technology of Fuels and Oils*, 22 (1986) 313-315.

[16] C.M. Able, J.P. Trembly, Advanced supercritical water-based process concepts for treatment and beneficial reuse of brine in oil/gas production, *Desalination*, 481 (2020) 114334.

[17] P. Stepnowski, E.M. Siedlecka, P. Behrend, B. Jastorff, Enhanced photo-degradation of contaminants in petroleum refinery wastewater, *Water Research*, 36 (2002) 2167-2172.

[18] A. Neisi, S. Afshin, Y. Rashtbari, A.A. Babaei, Y.O. Khaniabadi, A. Asadi, M. Shirmardi, M. Vosoughi, Efficiency of sequencing batch reactor for removal of organic matter in the effluent of petroleum wastewater, *Data in Brief*, 19 (2018) 2041-2046.

[19] D.A.Z. Wever, F. Picchioni, A.A. Broekhuis, Polymers for enhanced oil recovery: A paradigm for structure–property relationship in aqueous solution, *Progress in Polymer Science*, 36 (2011) 1558-1628.

[20] H. Guo, L. Xiao, S. Yu, H. Yang, J. Hu, Gui. Liu, Y. Tang, Analysis of anion exchange membrane fouling mechanism caused by anion polyacrylamide in electro dialysis, *Desalination*, 346 (2014) 46-53.

[21] H.I Mustapha, J.J.A.V. Bruggen, P.N.L Lens, Fate of heavy metals in vertical subsurface flow constructed wetlands treating secondary treated petroleum refinery wastewater in Kaduna, Nigeria, *International journal of phytoremediation*, 20 (2018) 44-53.

[22] P.L. Dold, Current practice for treatment of petroleum refinery wastewater and toxics removal,

## References

- Water Pollution Research Journal of Canada, 24 (1989) 363-390.
- [23] A. Coelho, A.V. Castro, M. Dezotti, G.L. Sant'Anna Jr, Treatment of petroleum refinery sourwater by advanced oxidation processes, *Journal of Hazardous Materials*, 137 (2006) 178-184.
- [24] A. Escoda, P. Fievet, S. Lakard, A. Szymczyk, S. D'ón, Influence of salts on the rejection of polyethyleneglycol by an NF organic membrane: Pore swelling and salting-out effects, *Journal of Membrane Science*, 347 (2010) 174-182.
- [25] M. Nilsson, G. Trägårdh, K. Östergren, The influence of pH, salt and temperature on nanofiltration performance, *Journal of Membrane Science*, 312 (2008) 97-106.
- [26] B.M. Jun, H.K. Lee, Y.N. Kwon, Acid-catalyzed hydrolysis of semi-aromatic polyamide NF membrane and its application to water softening and antibiotics enrichment, *Chemical Engineering Journal*, (2018) 419-430.
- [27] W.L. Ang, A.W. Mohammad, A. Benamor, N. Hilal, Hybrid coagulation–NF membrane processes for brackish water treatment: Effect of pH and salt/calcium concentration, *Desalination*, 390 (2016) 25-32.
- [28] S.M. Abtahi, S. Ilyas, C. Joannis Cassan, C. Albasi, W.M. de Vos, Micropollutants removal from secondary-treated municipal wastewater using weak polyelectrolyte multilayer based nanofiltration membranes, *Journal of Membrane Science*, 548 (2018) 654-666.
- [29] M.G. Buonomenna, J. Bae, Organic solvent nanofiltration in pharmaceutical industry, *Separation and Purification Reviews*, 44 (2015) 157-182.
- [30] F. Salehi, Current and future applications for nanofiltration technology in the food processing, *Food and Bioproducts Processing*, 92 (2014) 161-177.
- [31] B. Su, M. Dou, X. Gao, Y. Shang, C. Gao, Study on seawater nanofiltration softening technology for offshore oilfield water and polymer flooding, *Desalination*, 297 (2012) 30-37.
- [32] S. Alzahrani, A.W. Mohammad, N. Hilal, P. Abdullahe, O. Jaafara, Comparative study of NF and RO membranes in the treatment of produced water—Part I: Assessing water quality, *Desalination*, 315 (2013) 18-26.
- [33] S. Alzahrani, A.W. Mohammad, N. Hilal, P. Abdullahe, O. Jaafara, Comparative study of NF and RO membranes in the treatment of produced water II: Toxicity removal efficiency, *Desalination*,

## References

315 (2013) 27-32.

[34] E.T. Igunnu, G.Z Chen, Produced water treatment technologies, *International Journal of Low Carbon Technologies*, 9 (2012) 157-177.

[35] G.A. Bartelds, J. Bruining, J. Molenaar, The modeling of velocity enhancement in polymer flooding, *Transport in Porous Media*, 26 (1997) 75-88.

[36] A.Z. Abidin, T. Puspasari, W.A. Nugroho, Polymers for enhanced oil recovery technology, *Procedia Chemistry*, 4 (2012) 11-16.

[37] K.Y. AlkMahtani, A. Elkamel, *Petroleum refining and petrochemical industry overview*[M], Wiley-VCH Verlag GmbH & Co. KGaA, (2010).

[38] A. Coelho, A.V. Castro, M. Dezotti, G.L. Sant'Anna, Treatment of petroleum refinery sourwater by advanced oxidation processes, *Journal of Hazardous Materials*, 137 (2006) 178-184.

[39] S. Jafarinejad, S.C. Jiang, Current technologies and future directions for treating petroleum refineries and petrochemical plants (PRPP) wastewaters, *Journal of Environmental Chemical Engineering*, 7 (2019) 103326.

[40] D.A.D.A. Aljuboury, P. Palaniandy, A.H.B. Abdul, S. Feroz, Treatment of petroleum wastewater by conventional and new technologies A review, *Global Nest Journal*, 19 (2017) 439-452.

[41] Y. Nurdogan, Iron coprecipitation for selenium removal from petroleum refinery wastewater : Waste management and remediation in oil production, upgrading and refining processes, *Preprints-American Chemical Society. Division of Petroleum Chemistry*, 43 (1998) 480-483.

[42] M.H. El-Naas, M.A. Alhaija, S. Al-Zuhair, Evaluation of a three-step process for the treatment of petroleum refinery wastewater, *Journal of Environmental Chemical Engineering*, 2 (2014) 56–62.

[43] A.K. Hassan, M.M.A. Hassan, A.F. Hasan, Treatment of iraqi petroleum refinery wastewater by advanced oxidation processes, *Journal of Physics Conference*, 1660 (2020) 012071.

[44] T. Sirivedhin, J. Mccue, L. Dallbauman, Reclaiming produced water for beneficial use: salt removal by electrodialysis, *Journal of Membrane Science*, 243 (2004) 335-343.

[45] T.D. Waite, A.G. Fane, A.I. Schäfer, *Nanofiltration: Principles and applications*, *Journal*

## References

- American Water Works Association, 97 (2005) 121-122.
- [46] M. Paul, S.D. Jons, Chemistry and fabrication of polymeric nanofiltration membranes: A review, *Polymer*, 103 (2016) 417-456.
- [47] R. Malaisamy, A. Talla-Nwafo, K.L. Jones, Polyelectrolyte modification of nanofiltration membrane for selective removal of monovalent anions, *Separation and Purification Technology*, 77 (2011) 367-374.
- [48] Q. Li, Z. Liao, X. Fang, J. Xie, J. Li, Tannic acid assisted interfacial polymerization based loose thin-film composite NF membrane for dye/salt separation, *Desalination*, 479 (2020) 114343.
- [49] A.W. Mohammad, Y.H. Teow, W.L. Ang, Y.T. Chung, D.L. Oatley-Radcliffe, N. Hilal, Nanofiltration membranes review: Recent advances and future prospects, *Desalination*, 356 (2015) 226-254.
- [50] S. Lee, B. Kwon, M. Sun, J. Cho, Characterizations of NOM included in NF and UF membrane permeates, *Desalination*, 173 (2005) 131-142.
- [51] M. Mulder, *Basic Principles of Membrane Technology*[M], Springer Netherlands, (1996).
- [52] J.G. Wijmans, R.W. Baker, The solution-diffusion model: A review, *Journal of Membrane Science*, 107 (1995) 1-21.
- [53] Q. Xu, M.A. Anderson, Sol–Gel route to synthesis of microporous ceramic membranes: Preparation and characterization of microporous TiO<sub>2</sub> and ZrO<sub>2</sub> xerogels, *Journal of the American Ceramic Society*, 77 (1994) 1939-1945.
- [54] A. Larbot, S. Alami-Younssi, M. Persin, J. Sarrazin, L. Cot, Preparation of a  $\gamma$ -alumina nanofiltration membrane, *Journal of Membrane Science*, 97 (2018) 167-173.
- [55] Y. Cai, Y. Wang, X. Chen, M. Qiu, Y. Fan, Modified colloidal sol–gel process for fabrication of titania nanofiltration membranes with organic additives, *Journal of Membrane Science*, 476 (2015) 432-441.
- [56] H. Guo, S. Zhao, X. Wu, H. Qi, Fabrication and characterization of TiO<sub>2</sub>/ZrO<sub>2</sub> ceramic membranes for nanofiltration, *Microporous and Mesoporous Materials*, 260 (2018) 125-131.
- [57] P. Blanc, A. Larbot, J. Palmeri, M. Lopez, L. Cot, Hafnia ceramic nanofiltration membranes. Part I: Preparation and characterization, *Journal of Membrane Science*, 149 (1998) 151-161.

## References

- [58] T.V. Gestel, C. Vandecasteele, A. Buekenhoudt, C. Dotremont, J. Luyten, R. Leysen, B.V. Bruggen, G. Maes, Alumina and titania multilayer membranes for nanofiltration: preparation, characterization and chemical stability, *Journal of Membrane Science*, 207 (2002) 73-89.
- [59] A. Holda, Preparation of polysulfone solvent resistant nanofiltration membranes via phase inversion[M], (2013).
- [60] A.K. Holda, I.F.J. Vankelecom, Understanding and guiding the phase inversion process for synthesis of solvent resistant nanofiltration membranes, *Journal of Applied Polymer Science*, 132 (2015) 42130.
- [61] J.M. Gohil, P. Ray, Polyvinyl alcohol as the barrier layer in thin film composite nanofiltration membranes: Preparation, characterization, and performance evaluation, *Journal of Colloid and Interface Science*, 338 (2009) 121-127.
- [62] F. Peng, Z. Jiang, E.M.V. Hoek, Tuning the molecular structure, separation performance and interfacial properties of poly(vinyl alcohol)–polysulfone interfacial composite membranes, *Journal of Membrane Science*, 368 (2011) 26-33.
- [63] M. Homayoonfal, A. Akbari, M.R. Mehrnia, Preparation of polysulfone nanofiltration membranes by UV-assisted grafting polymerization for water softening, *Desalination*, 263 (2010) 217-225.
- [64] R. Bernstein, E. Antón, M. Ulbricht, Tuning the nanofiltration performance of thin film strong polyelectrolyte hydrogel composite membranes by photo-grafting conditions, *Journal of Membrane Science*, 427 (2013) 129-138.
- [65] G. Decher, Fuzzy nanoassemblies: Toward layered polymeric multicomposites, *Science*, 277 (1997) 1232-1237.
- [66] J. Shi, W. Zhang, Y. Su, Z. Jiang, Composite polyelectrolyte multilayer membranes for oligosaccharides nanofiltration separation, *Carbohydrate Polymers*, 94 (2013) 106-113.
- [67] S. Rajabzadeh, C. Liu, L. Shi, R. Wong, Preparation of low-pressure water softening hollow fiber membranes by polyelectrolyte deposition with two bilayers, *Desalination*, 344 (2014) 64-70.
- [68] M.J.T. Raaijmakers, N.E. Benes, Current trends in interfacial polymerization chemistry, *Progress in Polymer Science*, 63 (2016) 86-142.

## References

- [69] A.K. Ghosh, B.H. Jeong, X. Huang, E.M.V. Hoek, Impacts of reaction and curing conditions on polyamide composite reverse osmosis membrane properties, *Journal of Membrane Science*, 311 (2008) 34-45.
- [70] Y.C. Chiang, Y.Z. Hsub, R.C. Ruaan, C.J. Chuang, K.L. Tung, Nanofiltration membranes synthesized from hyperbranched polyethyleneimine, *Journal of Membrane Science*, 326 (2009) 19-26.
- [71] L.C. Scala, D.F. Ciliberti, D. Berg, Interface condensation desalination membranes, CA, CA1000135 A, 1973.
- [72] J.E. Cadotte, Reverse osmosis membrane, US, US4039440 A, 1975.
- [73] D.L. Oatley-Radcliffe, M. Walters, T.J. Ainscough, P.M. Williams, A.W. Mohammad, N. Hilal, Nanofiltration membranes and processes: A review of research trends over the past decade, *Journal of Water Process Engineering*, 19 (2017) 164-171.
- [74] K. Boussu, A. Belpaire, A. Volodin, C.V. Haesendonck, P.V.D. Meeren, C. Vandecasteele, B.V.D. Bruggen, Influence of membrane and colloid characteristics on fouling of nanofiltration membranes, *Journal of Membrane Science*, 289 (2007) 220-230.
- [75] C. Jarusutthirak, G. Amy, J-P. Croué Fouling characteristics of wastewater effluent organic matter (EfOM) isolates on NF and UF membranes, *Desalination*, 145 (2002) 247-255.
- [76] S. Shirazi, C. J. Lin, D. Chen, Inorganic fouling of pressure-driven membrane processes — A critical review, *Desalination*, 250 (2010) 236-248.
- [77] H. Ivnitsky, I. Katz, D. Minz, G. Volvovic, E. Shimoni, E. Kesselman, R. Semiat, C. G. Dosoretz, Bacterial community composition and structure of biofilms developing on nanofiltration membranes applied to wastewater treatment, *Water Research*, 41 (2007) 3924-3935.
- [78] C. Y. Tang, T. H. Chong, A. G. Fane, Colloidal interactions and fouling of NF and RO membranes: A review, *Advances in Colloid and Interface Science*, 164 (2011) 126-143.
- [79] S. H. Maruf, A. R. Greenberg, J. Pellegrino, Y. Ding, Fabrication and characterization of a surface-patterned thin film composite membrane, *Journal of Membrane Science*, 452 (2014) 11-19.
- [80] T. Chidambaram, Y. Oren, M. Noel, Fouling of nanofiltration membranes by dyes during brine recovery from textile dye bath wastewater, *Chemical Engineering Journal*, 262 (2015) 156-168.
- [81] Y. Kang, M. Obaid, J. Jang, I.S. Kim, Sulfonated graphene oxide incorporated thin film

## References

nanocomposite nanofiltration membrane to enhance permeation and antifouling properties, *Desalination*, 470 (2019) 114125.

[82] M. Elimelech], S. Hong, Chemical and physical aspects of natural organic matter (NOM) fouling of nanofiltration membranes, *Journal of Membrane Science*, 132(1997)159-181..

[83] G. D. Kang, Y. M. Cao, Development of antifouling reverse osmosis membranes for water treatment: A review, *Water Research*, 46 (2012) 584-600.

[84] T. Ma, Y. Su, Y. Li, R. Zhang, Z. Jiang, Fabrication of electro-neutral nanofiltration membranes at neutral pH with antifouling surface via interfacial polymerization from a novel zwitterionic amine monomer, *Journal of Membrane Science*, 503 (2016)101-109.

[85] S. K. Jewrajka, A. V. R. Reddy, H. H. Rana, S. Mandal, S. Khullar, S. Haldar, N. Joshi, P.K. Ghosh, Use of 2,4,6-pyridinetricarboxylic acid chloride as a novel co-monomer for the preparation of thin film composite polyamide membrane with improved bacterial resistance, *Journal of Membrane Science*, 439 (2013) 87-95.

[86] V. Vatanpour, S. S. Madaeni, R. Moradian, S. Zinadini, B. Astinchap, Fabrication and characterization of novel antifouling nanofiltration membrane prepared from oxidized multiwalled carbon nanotube/polyethersulfone nanocomposite, *Journal of Membrane Science*, 375 (2011) 284-294.

[87] M. Safarpour, V. Vatanpour, A. Khataee, M. Esmaeili, Development of a novel high flux and fouling-resistant thin film composite nanofiltration membrane by embedding reduced graphene oxide/TiO<sub>2</sub>, *Separation and Purification Technology*, 154 (2015) 96-107.

[88] P. F. Andrade, A. F. De Faria, S. R. Oliveira, M. A. Zezzi Arruda, M. D. C. Goncalves, Improved antibacterial activity of nanofiltration polysulfone membranes modified with silver nanoparticles, *Water Research*, 81 (2015) 333-342.

[89] J. Zhu, M. Tian, Y. Zhang, H. Zhang, J. Liu, Fabrication of a novel "loose" nanofiltration membrane by facile blending with Chitosan–Montmorillonite nanosheets for dyes purification, *Chemical Engineering Journal*, 265 (2015)184-193.

[90] I. C. Kim, K. H. Lee, Dyeing process wastewater treatment using fouling resistant nanofiltration and reverse osmosis membranes, *Desalination*, 192 (2006) 246-251.

[91] Y. Zhang, Y. Wan, G. Pan, H. Shi, Y. Liu, Surface modification of polyamide reverse osmosis membrane with sulfonated polyvinyl alcohol for antifouling, *Applied Surface Science*, 433 (2018) 139-

## References

148.

[92] B. D. McCloskey, H. B. Park, H. Ju, B. W. Rowe, D. J. Miller, B. D. Freeman., A bioinspired fouling-resistant surface modification for water purification membranes, *Journal of Membrane Science*, 413-414 (2012) 82-90.

[93] E. M. V. Wagner, A. C. Sagle, M. M. Sharma, Y. H. La, B. D. Freeman, Surface modification of commercial polyamide desalination membranes using poly(ethylene glycol) diglycidyl ether to enhance membrane fouling resistance, *Journal of Membrane Science*, 367 (2011) 273-287.

[94] X. An, K. Zhang, Z. Wang, Q.V. Ly, Y. Hu, C. Liu, Improving the water permeability and antifouling property of the nanofiltration membrane grafted with hyperbranched polyglycerol, *Journal of Membrane Science*, 612 (2020) 118417.

[95] M. Qasim, M. Badrelzaman, N. N. Darwish, N.A. Darwish, N. Hilal, Reverse Osmosis Desalination: A State-of-the-Art Review, *Desalination*, 459 (2019) 59-104.

[96] M. Duan, Z. Wang, J. Xu, J. Wang, S. Wang, Influence of hexamethyl phosphoramidate on polyamide composite reverse osmosis membrane performance, *Separation and Purification Technology*, 75 (2010) 145-155.

[97] C. Kong, T. Shintani, T. Kamada, V. Freger, T. Tsuru, Co-solvent-mediated synthesis of thin polyamide membranes, *Journal of Membrane Science*, 384 (2011) 10-16.

[98] H. Dong, L. Zhao, L. Zhang, H. Chen, C. Gao, W.S. Winston Ho, High-flux reverse osmosis membranes incorporated with NaY zeolite nanoparticles for brackish water desalination, *Journal of Membrane Science*, 476 (2015) 373-383.

[99] H. F. Xiao, C. H. Chu, W. T. Xu, B. Z. Chen, X. H. Ju, W. Xing, S. P. Sun, Amphibian-inspired amino acid ionic liquid functionalized nanofiltration membranes with high water permeability and ion selectivity for pigment wastewater treatment, *Journal of Membrane Science*, 586 (2019) 44-52.

[100] E. S. Kim, Q. Yu, B. Deng, Plasma surface modification of nanofiltration (NF) thin-film composite (TFC) membranes to improve anti organic fouling, *Applied Surface Science*, 257 (2011) 9863-9871.

[101] M. Kumar, M. Grzelakowski, J. Zilles, M. Clark, W. Meier, Highly permeable polymeric membranes based on the incorporation of the functional water channel protein Aquaporin Z, *Proceedings of the National Academy of Sciences of the United States of America*, 104 (2008) 20719-20724.

[102] S. Z. Pei, T. S. Chung, K. Jeyaseelan, A. Armugam, Aquaporin-embedded biomimetic membranes



## References

- for nanofiltration, *Journal of Membrane Science*, 407-408 (2012) 27-33.
- [103] W. Xie, F. He, B. Wang, T. S. Chung, K. Jeyaseelan, A. Armugam, Y. W. Tong, An aquaporin-based vesicle-embedded polymeric membrane for low energy water filtration, *Journal of Materials Chemistry A*, 1 (2013) 7592.
- [104] Y. Li, S. Qi, M. Tian, W. Widjajanti, R. Wang, Fabrication of aquaporin-based biomimetic membrane for seawater desalination, *Desalination*, 467 (2019) 103-112.
- [105] X. Li, S. Chou, R. Wang, L. Shi, W. Fang, G. Chaitra, C.Y. Tang, J. Torres, X. Hu, A. G. Fane, Nature gives the best solution for desalination: Aquaporin-based hollow fiber composite membrane with superior performance, *Journal of Membrane Science*, 494 (2015) 68-77.
- [106] V. Berry, Impermeability of graphene and its applications, *Carbon*, 62 (2013) 1-10.
- [107] D. Cohen-Tanugi, J. C. Grossman, Water Desalination across Nanoporous Graphene, *Nano Letters*, 12 (2012) 3602-3608.
- [108] S. P. Surwade, S. N. Smirnov, I. V. Vlassiok, R. R. Unocic, G. M. Veith, S. Dai, S. M. Mahurin, Water desalination using nanoporous single-layer graphene, *Nature Nanotechnology*, 10 (2015) 459-464.
- [109] X. Yang, H. Dai, Z. Xu, Water Permeation and Ion Rejection in Layer-by-Layer Stacked Graphene Oxide Nanochannels: A Molecular Dynamics Simulation, *Journal of Physical Chemistry C*, 39 (2016) 22585-22596.
- [110] S. Bano, A. Mahmood, S. J. Kim, K. H. Lee, Graphene oxide modified polyamide nanofiltration membrane with improved flux and antifouling properties, *Journal of Materials Chemistry A*, 3 (2015) 1-1.
- [111] M. Majumder, N. Chopra, R. Andrews, B. J. Hinds, Enhanced flow in carbon nanotubes, *Nature*, 438 (2005) 44-44.
- [112] F. Zhao, Y. Ji, X. D. Weng, Y. Mi, C. Gao, High-Flux Positively Charged Nanocomposite Nanofiltration Membranes Filled with Poly(dopamine) Modified Multiwall Carbon Nanotubes, *Acs Applied Materials & Interfaces*, 8 (2016) 6693-6700.
- [113] S. M. Xue, Z. L. Xu, Y. J. Tang, C. H. Ji, Polypiperazine-amide nanofiltration membrane modified by different functionalized multiwalled carbon nanotubes (MWCNTs), *ACS applied materials & interfaces*, 8 (2016) 19135-19144.
- [114] I. W. Azelee, P. S. Goh, W. J. Lau, A. F. Ismail, M. Rezaei-Dashtarzhandi, K. C. Wong, M. N.

## References

- Subramaniam, Enhanced desalination of polyamide thin film nanocomposite incorporated with acid treated multiwalled carbon nanotube-titania nanotube hybrid, *Desalination*, 409 (2017) 163-170.
- [115] H. Wu, H. Sun, W. Hong, L. Mao, Y.J. Liu, Improvement of polyamide thin film nanocomposite membrane assisted by tannic acid-Fe<sup>III</sup> functionalized multiwall carbon nanotubes, *ACS Applied Materials & Interfaces*, 9 (2017) 32255-32263.
- [116] J. Zheng, M. Li, K. Yu, J. Hu, X. Zhang, L. Wang, Sulfonated multiwall carbon nanotubes assisted thin-film nanocomposite membrane with enhanced water flux and anti-fouling property, *Journal of Membrane Science*, 524 (2016) 344-353.
- [117] Z. Tan, S. Chen, X. Peng, L. Zhang, C. Gao, Polyamide membranes with nanoscale Turing structures for water purification, *Science*, 360 (2018) 518-521.
- [118] Z. Wang, Z. Wang, S. Lin, H. Jin, S. Gao, Y. Zhu, J. Jin, Nanoparticle-templated nanofiltration membranes for ultrahigh performance desalination, *Nature Communications*, 9 (2018) 3251-3256.
- [119] S. Karan, Z. Jiang, A. G. Livingston, Sub-10 nm polyamide nanofilms with ultrafast solvent transport for molecular separation, *Science*, 348 (2015) 1347.
- [120] Y. Zhu, W. Xie, S. Gao, F. Zhang, W. Zhang, Z. Liu, J. Jin, Single-walled carbon nanotube film supported nanofiltration membrane with a nearly 10 nm thick polyamide selective layer for high-flux and high-rejection desalination, *Small*, 12 (2016) 5034-5041.
- [121] S. Gao, Y. Zhu, Y. Gong, Z. Wang, W. Fang, J. Jin, Ultrathin polyamide nanofiltration membrane fabricated on brush-painted single-walled carbon nanotube network support for ion sieving, *ACS Nano*, 13 (2019) 5278-5290.
- [122] S. Liu, C. Wu, W. S. Hung, X. Lu, K. R. Lee, One-step constructed ultrathin Janus polyamide nanofilms with opposite charges for highly efficient nanofiltration, *Journal of Materials Chemistry A*, 5 (2017) 22988-22996.
- [123] L. Shan, J. Gu, H. Fan, S. Ji, G. Zhang, Microphase diffusion-controlled interfacial polymerization for an ultrahigh permeability nanofiltration membrane, *ACS Applied Materials & Interfaces*, 9 (2017) 44820-44827.
- [124] H. B. Park, C. H. Jung, Y. M. Lee, A. J. Hill, S. J. Pas, S. T. Mudie, E. V. Wagner, B. D. Freeman, D. J. Cookson, Polymers with Cavities Tuned for Fast Selective Transport of Small Molecules and Ions, *Science*, 318 (2007) 254-258.

## References

- [125] H. B. Park, J. Kamcev, L. M. Robeson, M. Elimelech, B. D. Freeman, Maximizing the right stuff: The trade-off between membrane permeability and selectivity, *Science*, 356 (2017) 1138-1148.
- [126] H. Yu, X. Qiu, N. Moreno, Z. Ma, V. M. Calo, S. P. Nunes, K. V. Peinemann, Self-assembled asymmetric block copolymer membranes: bridging the gap from ultra-to nanofiltration, *Angewandte Chemie*, 127 (2015) 14143-14147.
- [127] Z. Yang, H. Guo, C. Y. Tang, The upper bound of thin-film composite (TFC) polyamide membranes for desalination, *Journal of Membrane Science*, 590 (2019) 117297.
- [128] M. F. Jimenez Solomon, Y. Bhole, A. G. Livingston, High flux membranes for organic solvent nanofiltration (OSN)—Interfacial polymerization with solvent activation, *Journal of Membrane Science*, 423-424 (2012) 371-382.
- [129] M. Razali, C. Didaskalou, J. F. Kim, M. Babaei, E. Drioli, Y. M. Lee, G. Szekely, Exploring and Exploiting the Effect of Solvent Treatment in Membrane Separations, *ACS Applied Materials & Interfaces*, 9 (2017) 11279-11289.
- [130] M. G. Shin, S. H. Park, S. J. Kwon, H. E. Kwon, J. B. Park, J. H. Lee, Facile performance enhancement of reverse osmosis membranes via solvent activation with benzyl alcohol, *Journal of Membrane Science*, 578 (2019) 220-229.
- [131] P. M. Williams, N. F. Membrane Characterization Methods, *NF Membrane Characterization Methods*, 2016.
- [132] K. Boussu, B. V. D. Bruggen, A. Volodin, J. Snauwaert, C. V. Haesendonck, C. Vandecasteele, Roughness and hydrophobicity studies of nanofiltration membranes using different modes of AFM, *Journal of Colloid & Interface Science*, 286 (2005) 632-638.
- [133] R. N. Wenzel, Resistance of Splid Surfacef to Wetting by Water, *American Chemical Society*, 28 (1936) 988-994.
- [134] H. Ai, X. Li, S. Shi, Y. Zhang, T. Liu, Measurement of Wenzel roughness factor by laser scanning confocal microscopy, *RSC Advances*, 7 (2017) 7052-7059.
- [135] K. R. Khedir, G. K. Kannarpady, H. Ishihara, J. Woo, C. Ryerson, A. S. Biris, Design and Fabrication of Teflon-Coated Tungsten Nanorods for Tunable Hydrophobicity, *Langmuir*, 27 (2011) 4661-4668.
- [136] A. Qu, X. Wen, P. Pi, J. Cheng, Z. Yang, Studies on gradient distribution of the hydrophobic

## References

segment and surface microstructure of the fluoro-silicon-containing methacrylate super hydrophobic coatings, *Acta Polymerica Sinica*, 12 (2007) 1176.

[137] Y. Li, E. Wong, A. Volodine, C.V. Haesendonck, K. Zhang, B.V.D. Bruggen, Nanofibrous hydrogel composite membranes with ultrafast transport performance for molecular separation in organic solvents, *Journal of Materials Chemistry A*, 7 (2019) 19269-19279.

[138] Y. Li, E. Wong, Z. Mai, B.V.D. Bruggen, Fabrication of composite polyamide/Kevlar aramid nanofiber nanofiltration membranes with high permselectivity in water desalination, *Journal of Membrane Science*, 592 (2019) 117396.

[139] A.E. Childress, M. Elimelech, Effect of solution chemistry on the surface charge of polymeric reverse osmosis and nanofiltration membranes, *Journal of Membrane Science*, 119 (1996) 253-268.

[140] A. Tiraferri, M. Elimelech, Direct quantification of negatively charged functional groups on membrane surfaces, *Journal of Membrane Science*, 389 (2012) 499-508.

[141] X. Lu, L.H. Arias Chavez, S. Romero-Vargas Castrillón, J. Ma, M. Elimelech, Influence of active layer and support layer surface structures on organic fouling propensity of thin-film composite forward osmosis membranes, *Environmental science & technology*, 49 (2015) 1436-1444.

[142] B. Yuan, H. Sun, S. Zhao, H. Yang, P. Wang, P. Li, H. Sun, Q. Jason Niu, Semi-aromatic polyamide nanofiltration membranes with tuned surface charge and pore size distribution designed for the efficient removal of Ca<sup>2+</sup> and Mg<sup>2+</sup>, *Separation and Purification Technology*, 220 (2019) 162-175.

[143] J. Zhu, J. Hou, R. Zhang, S. Yuan, J. Li, M. Tian, P. Wang, V. Alexander, Y. Zhang, VDB.Bart, Rapid water transport through controllable, ultrathin polyamide nanofilms for high-performance nanofiltration, *Journal of Materials Chemistry A*, 32 (2018) 15701-15709.

[144] Z. Jiang, S. Karan, A.G. Livingston, Water transport through ultrathin polyamide nanofilms used for reverse osmosis, *Advanced Materials*, 30 (2018) 1705973.

[145] R. Zhang, W. Shi, S. Yu, W. Wang, Z. Zhang, B. Zhang, L. Li, X. Bao, Influence of salts, anion polyacrylamide and crude oil on nanofiltration membrane fouling during desalination process of polymer flooding produced water, *Desalination*, 373 (2015) 27-37.

[146] A.F. Ismail, M. Padaki, N. Hilal, T. Matsuura, W.J. Lau, Thin film composite membrane — Recent development and future potential, *Desalination*, 356 (2015) 140-148.

[147] W. Xie, G.M. Geise, B. D. Freeman, H. S. Lee, G. Byun, J. E. Mcgrath, Polyamide interfacial

## References

composite membranes prepared from *m*-phenylene diamine, trimesoyl chloride and a new disulfonated diamine, *Journal of Membrane Science*, s 403–404 (2012) 152-161.

[148] R. Han, Formation and characterization of (melamine–TMC) based thin film composite NF membranes for improved thermal and chlorine resistances, *Journal of Membrane Science*, s 425–426 (2013) 176-181.

[149] Y. Hai, J. Zhang, C. Shi, A. Zhou, C. Bian, W. Li, Thin film composite nanofiltration membrane prepared by the interfacial polymerization of 1,2,4,5-benzene tetracarboxyl chloride on the mixed amines cross-linked poly(ether imide) support, *Journal of Membrane Science*, 520(2016)19-28.

[150] D. Hu, Z. L. Xu, Y. M. Wei, S. Cao, W. D. Chen, X. H. Qian, A Novel Composite Nanofiltration Membrane Prepared by Interfacial Polymerization of 2,2'-Bis(1-Hydroxyl-1-trifluoromethyl-2,2,2-trifluoroethyl)-4,4'-methylenedianiline and Trimesoyl Chloride, *Separation Science & Technology*, 48 (2013) 554-563.

[151] J. Hu, Z. Lv, Y. Xu, Z. Xuan, L. Wang, Fabrication of a high-flux sulfonated polyamide nanofiltration membrane: Experimental and dissipative particle dynamics studies, *Journal of Membrane Science*, 505 (2016) 119-129.

[152] Q.F. An, W.D. Sun, Q. Zhao, Y.L. Ji, C.J. Gao, Study on a novel nanofiltration membrane prepared by interfacial polymerization with zwitterionic amine monomers, *Journal of Membrane Science*, 431 (2013) 171-179.

[153] X.D. Weng, Y.L. Ji, R. Ma, F.Y. Zhao, Q.F. An, C.J. Gao, Superhydrophilic and antibacterial zwitterionic polyamide nanofiltration membranes for antibiotics separation, *Journal of Membrane Science*, 510 (2016) 122-130.

[154] M.N. Abu Seman, M. Khayet, N. Hilal, Nanofiltration thin-film composite polyester polyethersulfone-based membranes prepared by interfacial polymerization, *Journal of Membrane Science*, 348 (2010) 109-116.

[155] H. Wu, B. Tang, P. Wu, Preparation and characterization of anti-fouling  $\beta$ -cyclodextrin/polyester thin film nanofiltration composite membrane, *Journal of membrane science*, 428 (2013) 301-308.

[156] Y. Zhang, Y. Su, J. Peng, X. Zhao, J. Liu, J. Zhao, Z. Jiang, Composite nanofiltration membranes prepared by interfacial polymerization with natural material tannic acid and trimesoyl chloride, *Journal of Membrane Science*, 429 (2013) 235-242.

## References

- [157] C. Zhou, Y. Shi, C. Sun, S. Yu, M. Liu, C. Gao, Thin-film composite membranes formed by interfacial polymerization with natural material sericin and trimesoyl chloride for nanofiltration, *Journal of Membrane Science*, 471 (2014) 381-391.
- [158] W. Li, C. Bian, C. Fu, A. Zhou, C. Shi, J. Zhang, A poly(amide-co-ester) nanofiltration membrane using monomers of glucose and trimesoyl chloride, *Journal of Membrane Science*, 504 (2016) 185-195.
- [159] L. Liu, J.I. Xiaojun, M. Shen, Y. Tong, H. Huang, Serinol: Synthesis and applications, *Chemical Industry and Engineering Progress*, 33 (2014) 2722-2728.
- [160] G.G. Odian, In *Principles of Polymerization*, McGraw-Hill, 1970.
- [161] J. Qin, S. Lin, S. Song, Z. Lin, H. Chen, 4-Dimethylaminopyridine promoted interfacial polymerization between hyperbranched polyesteramide and trimesoyl chloride for preparing ultralow-pressure reverse osmosis composite membrane, *ACS Applied Materials & Interfaces*, 5 (2013) 6649-6656.
- [162] S. Xu, H. Ingmar, K. Bernhard, M. Herbert, S. Wolfgang, Z. Hendrik, The DMAP-catalyzed acetylation of alcohols--a mechanistic study (DMAP = 4-(dimethylamino)pyridine), *Chemistry*, 11 (2005) 4751-4757.
- [163] M. Liu, Y. Zheng, S. Shuai, Q. Zhou, S. Yu, C. Gao, Thin-film composite membrane formed by interfacial polymerization of polyvinylamine (PVAm) and trimesoyl chloride (TMC) for nanofiltration, *Desalination*, 288 (2012) 98-107.
- [164] A.W. Mohammad, Y.H. Teow, W.L. Ang, Y.T. Chung, D.L. Oatley-Radcliffe, N. Hilal, Nanofiltration membranes review: Recent advances and future prospects, *Desalination*, 356 (2015) 226-254.
- [165] A. Hassner, L.R. Krepski, V. Alexanian, Aminopyridines as acylation catalysts for tertiary alcohols, *Tetrahedron*, 34 (1978) 2069-2076.
- [166] A.L. Ahmad, B.S. Ooi, Properties-performance of thin film composites membrane: study on trimesoyl chloride content and polymerization time, *Journal of Membrane Science*, 255 (2005) 67-77.
- [167] C.Y. Tang, Y.N. Kwon, J.O. Leckie, Effect of membrane chemistry and coating layer on physiochemical properties of thin film composite polyamide RO and NF membranes: I. FTIR and XPS characterization of polyamide and coating layer chemistry, *Desalination*, 242 (2009) 149-167.
- [168] C.Y. Tang, Y.N. Kwon, J.O. Leckie, Probing the nano- and micro-scales of reverse osmosis membranes—A comprehensive characterization of physiochemical properties of uncoated and coated

## References

- membranes by XPS, TEM, ATR-FTIR, and streaming potential measurements, *Journal of Membrane Science*, 287 (2007) 146-156.
- [169] H.G. Elias, *Principles of Polymerization*, Springer US, 1977.
- [170] T. Puspasari, N. Pradeep, K.V. Peinemann, Crosslinked cellulose thin film composite nanofiltration membranes with zero salt rejection, *Journal of Membrane Science*, 491 (2015) 132–137.
- [171] B. Tang, Z. Huo, P. Wu, Study on a novel polyester composite nanofiltration membrane by interfacial polymerization of triethanolamine (TEOA) and trimesoyl chloride (TMC) : I. Preparation, characterization and nanofiltration properties test of membrane, *Journal of Membrane Science*, 320 (2008) 198-205.
- [172] H.R. Chae, J. Lee, C.H. Lee, I.C. Kim, P.K. Park, Graphene oxide-embedded thin-film composite reverse osmosis membrane with high flux, anti-biofouling, and chlorine resistance, *Journal of Membrane Science*, 483 (2015) 128-135.
- [173] F. Yan, H. Chen, L. Yang, Z. Lü, S. Yu, M. Liu, C. Gao, Improving the water permeability and antifouling property of thin-film composite polyamide nanofiltration membrane by modifying the active layer with triethanolamine, *Journal of Membrane Science*, 513 (2016) 108-116.
- [174] K. Yoon, B.S. Hsiao, B. Chu, High flux nanofiltration membranes based on interfacially polymerized polyamide barrier layer on polyacrylonitrile nanofibrous scaffolds, *Journal of Membrane Science*, 326 (2009) 484-492.
- [175] T. Wang, Y. Yang, J. Zheng, Q. Zhang, S. Zhang, A novel highly permeable positively charged nanofiltration membrane based on a nanoporous hyper-crosslinked polyamide barrier layer, *Journal of Membrane Science*, 448 (2013) 180-189.
- [176] W. Fang, L. Shi, R. Wang, Mixed polyamide-based composite nanofiltration hollow fiber membranes with improved low-pressure water softening capability, *Journal of Membrane Science*, 468 (2014) 52-61.
- [177] R.J. Petersen, J.E. Cadotte, Thin film composite reverse osmosis membranes, *Handbook of industrial membrane technology*, (1990)307-348.
- [178] D. Li, H. Wang, Recent developments in reverse osmosis desalination membranes, *Journal of Materials Chemistry*, 20 (2010) 4551-4566.
- [179] Y. Zhang, M. Guo, G. Pan, H. Yan, J. Xu, Y. Shi, H. Shi, Y. Liu, Preparation and properties of novel

## References

- pH-stable TFC membrane based on organic–inorganic hybrid composite materials for nanofiltration, *Journal of Membrane Science*, 476 (2015) 500-507.
- [180] W.-P. Zhu, J. Gao, S.-P. Sun, S. Zhang, T.-S. Chung, Poly (amidoamine) dendrimer (PAMAM) grafted on thin film composite (TFC) nanofiltration (NF) hollow fiber membranes for heavy metal removal, *Journal of Membrane Science*, 487 (2015) 117-126.
- [181] D. Emadzadeh, W.J. Lau, M. Rahbari-Sisakht, H. Ilbeygi, D. Rana, T. Matsuura, A.F. Ismail, Synthesis, modification and optimization of titanate nanotubes-polyamide thin film nanocomposite (TFN) membrane for forward osmosis (FO) application, *Chemical Engineering Journal*, 281 (2015) 243-251.
- [182] Q. Zhang, Z. Zhang, L. Dai, H. Wang, S. Li, S. Zhang, Novel insights into the interplay between support and active layer in the thin film composite polyamide membranes, *Journal of Membrane Science*, 537 (2017) 372-383.
- [183] L. Huang, J.R. McCutcheon, Impact of support layer pore size on performance of thin film composite membranes for forward osmosis, *Journal of Membrane Science*, 483 (2015) 25-33.
- [184] A.K. Ghosh, E.M.V. Hoek, Impacts of support membrane structure and chemistry on polyamide–polysulfone interfacial composite membranes, *Journal of Membrane Science*, 336 (2009) 140-148.
- [185] J. Li, M. Wei, Y. Wang, Substrate matters: The influences of substrate layers on the performances of thin-film composite reverse osmosis membranes, *Chinese Journal of Chemical Engineering*, 25 (2017) 1676-1684.
- [186] G.-R. Xu, J.-M. Xu, H.-J. Feng, H.-L. Zhao, S.-B. Wu, Tailoring structures and performance of polyamide thin film composite (PA-TFC) desalination membranes via sublayers adjustment-a review, *Desalination*, 417 (2017) 19-35.
- [187] P.S. Singh, S.V. Joshi, J.J. Trivedi, C.V. Devmurari, R.A. Prakash, P.K. Ghosh, Probing the structural variations of thin film composite RO membranes obtained by coating polyamide over polysulfone membranes of different pore dimensions, *Journal of Membrane Science*, 278 (2006) 19-25.
- [188] N. Misdan, W.J. Lau, A.F. Ismail, T. Matsuura, D. Rana, Study on the thin film composite poly (piperazine-amide) nanofiltration membrane: Impacts of physicochemical properties of substrate on interfacial polymerization formation, *Desalination*, 344 (2014) 198-205.
- [189] R.-X. Zhang, J. Vanneste, L. Poelmans, A. Sotto, X.-L. Wang, B. Van der Bruggen, Effect of the manufacturing conditions on the structure and performance of thin-film composite membranes, *Journal*



## References

- of Applied Polymer Science, 125 (2012) 3755-3769.
- [190] M.F. Jimenez-Solomon, P. Gorgojo, M. Munoz-Ibanez, A.G. Livingston, Beneath the surface: Influence of supports on thin film composite membranes by interfacial polymerization for organic solvent nanofiltration, *Journal of membrane science*, 448 (2013) 102-113.
- [191] R. Zhang, S. Yu, W. Shi, W. Wang, X. Wang, Z. Zhang, L. Li, B. Zhang, X. Bao, A novel polyesteramide thin film composite nanofiltration membrane prepared by interfacial polymerization of serinol and trimesoyl chloride (TMC) catalyzed by 4-dimethylaminopyridine (DMAP), *Journal of Membrane Science*, 542 (2017) 68-80.
- [192] S. Karan, Z. Jiang, A.G. Livingston, Sub-10 nm polyamide nanofilms with ultrafast solvent transport for molecular separation, *Science*, 348 (2015) 1347-1351.
- [193] Z. Jiang, S. Karan, A.G. Livingston, Water Transport through Ultrathin Polyamide Nanofilms Used for Reverse Osmosis, *Advanced Materials*, 30 (2018) 1705973.
- [194] S.-J. Park, W. Choi, S.-E. Nam, S. Hong, J.S. Lee, J.-H. Lee, Fabrication of polyamide thin film composite reverse osmosis membranes via support-free interfacial polymerization, *Journal of Membrane Science*, 526 (2017) 52-59.
- [195] S.-J. Park, W.-G. Ahn, W. Choi, S.-H. Park, J.S. Lee, H.W. Jung, J.-H. Lee, A facile and scalable fabrication method for thin film composite reverse osmosis membranes: dual-layer slot coating, *Journal of Materials Chemistry A*, 5 (2017) 6648-6655.
- [196] Y. Song, F. Liu, B. Sun, Preparation, characterization, and application of thin film composite nanofiltration membranes, *Journal of applied polymer science*, 95 (2005) 1251-1261.
- [197] M. Paul, S.D. Jons, Chemistry and fabrication of polymeric nanofiltration membranes: A review, *Polymer*, 103 (2016) 417-456.
- [198] L. Huang, N.-N. Bui, M.T. Meyering, T.J. Hamlin, J.R. McCutcheon, Novel hydrophilic nylon 6, 6 microfiltration membrane supported thin film composite membranes for engineered osmosis, *Journal of membrane science*, 437 (2013) 141-149.
- [199] N.-W. Oh, J. Jegal, K.-H. Lee, Preparation and characterization of nanofiltration composite membranes using polyacrylonitrile (PAN). II. Preparation and characterization of polyamide composite membranes, *Journal of applied polymer science*, 80 (2001) 2729-2736.
- [200] C. Klaysom, S. Hermans, A. Gahlaut, S. Van Craenenbroeck, I.F.J. Vankelecom,

## References

- Polyamide/Polyacrylonitrile (PA/PAN) thin film composite osmosis membranes: Film optimization, characterization and performance evaluation, *Journal of membrane science*, 445 (2013) 25-33.
- [201] J. Xu, H. Yan, Y. Zhang, G. Pan, Y. Liu, The morphology of fully-aromatic polyamide separation layer and its relationship with separation performance of TFC membranes, *Journal of Membrane Science*, 541 (2017) 174-188.
- [202] N.K. Saha, S.V. Joshi, Performance evaluation of thin film composite polyamide nanofiltration membrane with variation in monomer type, *Journal of Membrane Science*, 342 (2009) 60-69.
- [203] G.-R. Xu, J.-N. Wang, C.-J. Li, Strategies for improving the performance of the polyamide thin film composite (PA-TFC) reverse osmosis (RO) membranes: Surface modifications and nanoparticles incorporations, *Desalination*, 328 (2013) 83-100.
- [204] S.S. Shenvi, A.M. Isloor, A.F. Ismail, A review on RO membrane technology: Developments and challenges, *Desalination*, 368 (2015) 10-26.
- [205] G.Z. Ramon, M.C. Wong, E.M.V. Hoek, Transport through composite membrane, part 1: Is there an optimal support membrane?, *Journal of membrane science*, 415 (2012) 298-305.
- [206] M.J.T. Raaijmakers, N.E. Benes, Current trends in interfacial polymerization chemistry, *Progress in polymer science*, 63 (2016) 86-142.
- [207] N.Y. Yip, A. Tiraferri, W.A. Phillip, J.D. Schiffman, M. Elimelech, High performance thin-film composite forward osmosis membrane, *Environmental science & technology*, 44 (2010) 3812-3818.
- [208] V. Ramachandhran, A.K. Ghosh, S. Prabhakar, P.K. Tewari, Preparation and separation performance studies on composite polyamide membranes using different amine systems and support membranes, *Journal of Polymer Materials*, 26 (2009) 177-185.
- [209] S. Yu, M. Liu, X. Liu, C. Gao, Performance enhancement in interfacially synthesized thin-film composite polyamide-urethane reverse osmosis membrane for seawater desalination, *Journal of Membrane Science*, 342 (2009) 313-320.
- [210] S.H. Kim, S.-Y. Kwak, T. Suzuki, Positron annihilation spectroscopic evidence to demonstrate the flux-enhancement mechanism in morphology-controlled thin-film-composite (TFC) membrane, *Environmental science & technology*, 39 (2005) 1764-1770.
- [211] P.B. Kosaraju, K.K. Sirkar, Interfacially polymerized thin film composite membranes on microporous polypropylene supports for solvent-resistant nanofiltration, *Journal of Membrane Science*,

## References

- 321 (2008) 155-161.
- [212] R. Zhang, S. Yu, W. Shi, J. Tian, L. Jin, B. Zhang, L. Li, Z. Zhang, Optimization of a membrane cleaning strategy for advanced treatment of polymer flooding produced water by nanofiltration, *Rsc Advances*, 6 (2016) 28844-28853.
- [213] D. Rana, T. Matsuura, Surface modifications for antifouling membranes, *Chemical Reviews*, 110 (2010) 2448-2471.
- [214] J.M. Gohil, P. Ray, A review on semi-aromatic polyamide TFC membranes prepared by interfacial polymerization: Potential for water treatment and desalination, *Separation and Purification Technology*, 181 (2017) 159-182.
- [215] W.P. Zhu, J. Gao, S.P. Sun, S. Zhang, T.S. Chung, Poly(amidoamine) dendrimer (PAMAM) grafted on thin film composite (TFC) nanofiltration (NF) hollow fiber membranes for heavy metal removal, *Journal of Membrane Science*, 487 (2015) 117-126.
- [216] T. Wang, H. Qiblawey, E. Sivaniah, A. Mohammadian, Novel methodology for facile fabrication of nanofiltration membranes based on nucleophilic nature of polydopamine, *Journal of Membrane Science*, 511 (2016) 65-75.
- [217] K.Y. Wang, T.-S. Chung, G. Amy, Developing thin-film-composite forward osmosis membranes on the PES/SPSf substrate through interfacial polymerization, *AIChE Journal*, 58 (2012) 770–781.
- [218] B. Tang, Z. Huo, P. Wu, Study on a novel polyester composite nanofiltration membrane by interfacial polymerization of triethanolamine (TEOA) and trimesoyl chloride (TMC) : I. Preparation, characterization and nanofiltration properties test of membrane, *Journal of Membrane Science*, 320 (2008) 198-205.
- [219] S. Xia, L. Yao, Y. Zhao, N. Li, Y. Zheng, Preparation of graphene oxide modified polyamide thin film composite membranes with improved hydrophilicity for natural organic matter removal, *Chemical Engineering Journal*, 280 (2015) 720-727.
- [220] M.R. Hashmet, M. Onur, I.M. Tan, Empirical Correlations for Viscosity of Polyacrylamide Solutions with the Effects of Salinity and Hardness, *Journal of Dispersion Science and Technology*, 35 (2014) 510-517.
- [221] Z. Ismail, A.M. Beddri, Potential of Water Hyacinth as a Removal Agent for Heavy Metals from Petroleum Refinery Effluents, *Water Air and Soil Pollution*, 199 (2009) 57-65.

## References

- [222] I. Asghari, S.M. Mousavi, Effects of key parameters in recycling of metals from petroleum refinery waste catalysts in bioleaching process, *Reviews in Environmental Science and Bio-technology*, 13 (2014) 139-161.
- [223] K.V. Ajayan, M. Selvaraju, K. Thirugnanamoorthy, Growth and Heavy Metals Accumulation Potential of Microalgae Grown in Sewage Wastewater and Petrochemical Effluents, *Pakistan Journal of Biological science*, 14 (2011) 805-811.
- [224] R. Moradi, G. Pirumyan, F. Farahmand, Assessment of heavy metals pollution in wastewater of petrochemical industries, *Research Journal of Pharmaceutical, Biological and Chemical Sciences*, 4 (2013) 279-286.
- [225] J. Wang, W. Yu, N.J.D. Graham, L. Jiang, Evaluation of a novel polyamide-polyethylenimine nanofiltration membrane for wastewater treatment: Removal of  $\text{Cu}^{2+}$  ions, *Chemical Engineering Journal*, 392 (2019) 123769.
- [226] Y.C. Jordan, A. Ghulam, S. Hartling, Traits of surface water pollution under climate and land use changes: A remote sensing and hydrological modeling approach, *Earth-Science Reviews*, 128 (2014) 181-195.
- [227] S. Lee, E. Lee, J. Ra, B. Lee, S. Kim, S.H. Choi, S.D. Kim, J. Cho, Characterization of marine organic matters and heavy metals with respect to desalination with RO and NF membranes, *Desalination*, 221 (2008) 244-252.
- [228] P. Puhlfürß, A. Voigt, R. Weber, M. Morbé Microporous  $\text{TiO}_2$  membranes with a cut off < 500 Da, *Journal of Membrane Science*, 174 (2000) 123-133.
- [229] H. Abu Qdais, H. Moussa, Removal of heavy metals from wastewater by membrane processes: a comparative study, *Desalination*, 164 (2004) 105-110.
- [230] M. Ernst, A. Bismarck, J. Springer, M. Jekel, Zeta-potential and rejection rates of a polyethersulfone nanofiltration membrane in single salt solutions, *Journal of Membrane Science*, 165 (2000) 251-259.
- [231] H. Guo, M. Chen, Q. Liu, Z. Wang, S. Cui, G. Zhang, LbL assembly of sulfonated cyclohexanone-formaldehyde condensation polymer and poly (ethyleneimine) towards rejection of both cationic ions and dyes, *Desalination*, 365 (2015) 108-116.
- [232] P. Li, Z. Wang, L. Yang, S. Zhao, P. Song, B. Khan, A novel loose-NF membrane based on the

## References

phosphorylation and cross-linking of polyethyleneimine layer on porous PAN UF membranes, *Journal of Membrane Science*, 555 (2018) 56-68.

[233] S. Bandehali, F. Parvizian, A.R. Moghadassi, S.M. Hosseini, Copper and lead ions removal from water by new PEI based NF membrane modified by functionalized POSS nanoparticles, *Journal of Polymer Research*, 26 (2019) 211.

[234] M. Li, Z. Lv, J. Zheng, J. Hu, C. Jiang, M. Ueda, X. Zhang, L. Wang, Positively charged nanofiltration membrane with dendritic surface for toxic element removal, *ACS Sustainable Chemistry & Engineering*, 5 (2017) 784-792.

[235] C. Wu, S. Liu, Z. Wang, J. Zhang, X. Wang, X. Lu, Y. Jia, W.-S. Hung, K.-R. Lee, Nanofiltration membranes with dually charged composite layer exhibiting super-high multivalent-salt rejection, *Journal of Membrane Science*, 517(2016) 64-72.

[236] J. Wang, S. Zhang, P. Wu, W. Shi, Z. Wang, Y. Hu, In situ surface modification of thin-film composite polyamide membrane with zwitterions for enhanced chlorine resistance and transport properties, *ACS applied materials & interfaces*, 11 (2019) 12043-12052.

[237] J. Zhu, J. Hou, S. Yuan, Y. Zhao, Y. Li, R. Zhang, M. Tian, J. Li, J. Wang, B. Van der Bruggen, MOF-positioned polyamide membranes with a fishnet-like structure for elevated nanofiltration performance, *Journal of Materials Chemistry A*, 7 (2019) 16313-16322.

[238] C.Y. Tang, T.H. Chong, A.G. Fane, Colloidal interactions and fouling of NF and RO membranes: A review, *Advances in Colloid and Interface Science*, 164 (2011) 126-143.

[239] M.M. Kłosowski, C.M. McGilvery, Y. Li, P. Abellan, Q. Ramasse, J.T. Cabral, A.G. Livingston, A.E. Porter, Micro-to nano-scale characterisation of polyamide structures of the SW30HR RO membrane using advanced electron microscopy and stain tracers, *Journal of Membrane Science*, 520 (2016) 465-476.

[240] D. Miller, D. Dreyer, C. Bielawski, D. Paul, B. Freeman, Surface Modification of Water Purification Membranes: a Review, *Angewandte Chemie International Edition*. 56 (2017) 4662-4711.

[241] J. M. Gohil, P. Ray, A review on semi-aromatic polyamide TFC membranes prepared by interfacial polymerization: potential for water treatment and desalination, *Separation and Purification Technology*, 181 (2017) 159-182.

[242] G. Bargeman, J.B. Westerink, C.F.H. Manuhutu, A. ten Kate, The effect of membrane

## References

characteristics on nanofiltration membrane performance during processing of practically saturated salt solutions, *Journal of Membrane Science*, 485 (2015) 112-122.

[243] Z. Zhang, G. Kang, H. Yu, Y. Jin, Y. Cao, Fabrication of a highly permeable composite nanofiltration membrane via interfacial polymerization by adding a novel acyl chloride monomer with an anhydride group, *Journal of Membrane Science*, 570-571 (2019) 403-409.

[244] Z. Zhai, C. Jiang, N. Zhao, W. Dong, H. Lan, M. Wang, Q. J. Niu, Fabrication of advanced nanofiltration membranes with nanostrand hybrid morphology mediated by ultrafast Noria-polyethyleneimine codeposition, *Journal of Materials Chemistry A.*, 6 (2018) 21207-21215.

[245] Y. L. Liu, X.M. Wang, H.W. Yang, Y. F. Xie, X. Huang, Preparation of nanofiltration membranes for high rejection of organic micropollutants and low rejection of divalent cations, *Journal of Membrane Science*, 572 (2018) 152-160.

[246] C. Jiang, L. Tian, Y. Hou, Q.J. Niu, Nanofiltration membranes with enhanced microporosity and inner-pore interconnectivity for water treatment: Excellent balance between permeability and selectivity, *Journal of Membrane Science*, 586 (2019) 192-201.

[247] Z. Yang, Z.W. Zhou, H. Guo, Z. Yao, X.H. Ma, X. Song, S.P. Feng, C.Y. Tang, Tannic Acid/Fe<sup>3+</sup> Nanoscaffold for Interfacial Polymerization: Toward Enhanced Nanofiltration Performance, *Environmental Science & Technology*, 52 (2018) 9341-9349.

[248] C.Y. Tang, Y.-N. Kwon, J.O. Leckie, Effect of membrane chemistry and coating layer on physiochemical properties of thin film composite polyamide RO and NF membranes: I. FTIR and XPS characterization of polyamide and coating layer chemistry, *Desalination*, 242 (2009) 149-167.

[249] B. Yuan, C. Jiang, P. Li, H. Sun, P. Li, T. Yuan, H. Sun, Q.J. Niu, Ultrathin polyamide membrane with decreased porosity designed for outstanding water-softening performance and superior antifouling properties, *ACS applied materials & interfaces*, 10 (2018) 43057-43067.

[250] A. Fane, C. Tang, R. Wang, *Membrane Technology for Water: Microfiltration, Ultrafiltration, Nanofiltration, and Reverse Osmosis*, *Treatise on Water Science*, 113 (2011) 301-335.

[251] J.J. Bikerman, Surface Roughness and Contact Angle., *The Journal of Physical and Colloid Chemistry*, 54 (1950) 653-658.

[252] H. Zhu, A. Szymczyk, B. Balanec, On the salt rejection properties of nanofiltration polyamide membranes formed by interfacial polymerization, *Journal of Membrane Science*, 379 (2011) 215-223.

## References

- [253] W. Fang, R. Wang, S. Chou, L. Setiawan, A.G. Fane, Composite forward osmosis hollow fiber membranes: Integration of RO-and NF-like selective layers to enhance membrane properties of anti-scaling and anti-internal concentration polarization, *Journal of Membrane Science*, 394 (2012) 140-150.
- [254] R.O. Dunn Jr, J.F. Scamehorn, S.D. Christian, Concentration polarization effects in the use of micellar-enhanced ultrafiltration to remove dissolved organic pollutants from wastewater, *Separation Science and Technology*, 22 (1987) 763-789.
- [255] A. Bera, J.S. Trivedi, S.B. Kumar, A.K.S. Chandel, S. Haldar, S.K. Jewrajka, Anti-organic fouling and anti-biofouling poly(piperazineamide) thin film nanocomposite membranes for low pressure removal of heavy metal ions, *Journal of Hazardous Materials*, 343 (2018) 86-97.
- [256] B.A.M. Al-Rashdi, D.J. Johnson, N. Hilal, Removal of heavy metal ions by nanofiltration, *Desalination*, 315 (2013) 2-17.
- [257] E. Robert, The hydrolysis of cations, 40 (1976).
- [258] B. Tansel, J. Sager, T. Rector, J. Garland, R.F. Strayer, L. Levine, M. Roberts, M. Hummerick, J. Bauer, Significance of hydrated radius and hydration shells on ionic permeability during nanofiltration in dead end and cross flow modes, *Separation and Purification Technology*, 51 (2006) 40-47.
- [259] W.W. Ho, K. Sirkar, Chapter 1: overview, *Membrane Handbook*, Chapman & Hall, New York, London, (1992) 3-15.
- [260] C.-V. Gherasim, P. Mikulasek, Influence of operating variables on the removal of heavy metal ions from aqueous solutions by nanofiltration, *Desalination*, 343 (2014) 67-74.
- [261] J.G. Wijmans, R.W. Baker. The Solution-Diffusion Model: A Review., *Journal of Membrane Science*, 107 (1995) 1-21.
- [262] X. Peng, J. Jin, Y. Nakamura, T. Ohno, I. Ichinose, Ultrafast permeation of water through protein-based membranes, *Nature Nanotechnology*, 4 (2009) 353.
- [263] S. Gao, D. Wang, W. Fang, J. Jin, Ultrathin Membranes: A New Opportunity for Ultrafast and Efficient Separation, *Advanced Materials Technologies*, (2020)1901069.
- [264] S. Karan, Z. Jiang, A.G. Livingston, Sub-10 nm polyamide nanofilms with ultrafast solvent transport for molecular separation, *Science*, 348 (2015) 1347-1351.
- [265] Z.W. Jiang, S. Karan, A.G. Livingston, Water Transport through Ultrathin Polyamide Nanofilms Used for Reverse Osmosis, *Advanced Materials*, 30 (2018) 1705973.

## References

- [266] B. Yuan, P. Li, H. Sun, S. Zhao, P. Li, H. Sun, Q.J. Niu, Novel non-trimesoyl chloride based polyamide membrane with significantly reduced  $\text{Ca}^{2+}$  surface deposition density, *Journal of Membrane Science*, 578 (2019) 251-262.
- [267] S. L. Li, X. Shan, Y. Zhao, Y. Huo, Fabrication of a novel nanofiltration membrane with enhanced performance via interfacial polymerization through the incorporation of a new zwitterionic diamine monomer, *ACS Applied Materials & Interfaces*, 11 (2019) 42846-42855.
- [268] Y. Pan, R. Xu, Z. Lü, S. Yu, M. Liu, C. Gao, Enhanced both perm-selectivity and fouling resistance of poly(piperazine-amide) nanofiltration membrane by incorporating sericin as a co-reactant of aqueous phase, *Journal of Membrane Science*, 523 (2017) 282-290.
- [269] Y. J. Tang, Z. L. Xu, S. M. Xue, Y. M. Wei, H. Yang, Improving the chlorine-tolerant ability of polypiperazine-amide nanofiltration membrane by adding  $\text{NH}_2\text{-PEG-NH}_2$  in the aqueous phase, *Journal of Membrane Science*, 538 (2017) 9-17.
- [270] Y. Li, E. Wong, Z. Mai, B. Van der Bruggen, Fabrication of composite polyamide/Kevlar aramid nanofiber nanofiltration membranes with high permselectivity in water desalination, *Journal of Membrane Science*, 592 (2019) 117396.
- [271] C. Jiang, L. Tian, Z. Zhai, Y. Shen, W. Dong, M. He, Y. Hou, Q. Jason Niu, Thin-film composite membranes with aqueous template-induced surface nanostructures for enhanced nanofiltration, *Journal of Membrane Science*, 589 (2019) 117244.
- [272] Z. Tan, S. Chen, X. Peng, L. Zhang, C. Gao, Polyamide membranes with nanoscale Turing structures for water purification, *Science*, 360 (2018) 518-521.
- [273] Z. Yao, H. Guo, Z. Yang, W. Qing, C.Y. Tang, Preparation of nanocavity-contained thin film composite nanofiltration membranes with enhanced permeability and divalent to monovalent ion selectivity, *Desalination*, 445 (2018) 115-122.
- [274] C. Jiang, L. Tian, Y. Hou, Q.J. Niu, Nanofiltration membranes with enhanced microporosity and inner-pore interconnectivity for water treatment: Excellent balance between permeability and selectivity, *Journal of Membrane Science*, 586 (2019) 192-201.
- [275] R. Zhang, S. Yu, W. Shi, W. Wang, X. Wang, Z. Zhang, L. Li, B. Zhang, X. Bao, A novel polyesteramide thin film composite nanofiltration membrane prepared by interfacial polymerization of serinol and trimesoyl chloride (TMC) catalyzed by 4-dimethylaminopyridine (DMAP), *Journal of*



## References

Membrane Science, 542 (2017) 68-80.

[276] Y. Zhu, W. Xie, S. Gao, F. Zhang, W. Zhang, Z. Liu, J. Jin, Single-Walled Carbon Nanotube Film Supported Nanofiltration Membrane with a Nearly 10 nm Thick Polyamide Selective Layer for High-Flux and High-Rejection Desalination, *Small*, 12 (2016) 5034-5041.

[277] Z. Wang, Z. Wang, S. Lin, H. Jin, S. Gao, Y. Zhu, J. Jin, Nanoparticle-templated nanofiltration membranes for ultrahigh performance desalination, *Nature Communications*, 9 (2018).

[278] X. Yang, Y. Du, X. Zhang, A. He, Z.-K. Xu, Nanofiltration Membrane with a Mussel-Inspired Interlayer for Improved Permeation Performance, *Langmuir*, 33 (2017) 2318-2324.

[279] X. Zhu, X. Cheng, X. Luo, Y. Liu, D. Xu, X. Tang, Z. Gan, L. Yang, G. Li, H. Liang, Ultrathin thin-film composite polyamide membranes constructed on hydrophilic poly(vinyl alcohol) decorated support toward enhanced nanofiltration performance, *Environmental Science & Technology*, 54 (2020) 6365-6374.

[280] S. J. Park, W. G. Ahn, W. Choi, S. H. Park, J. S. Lee, H. W. Jung, J.H. Lee, A facile and scalable fabrication method for thin film composite reverse osmosis membranes: dual-layer slot coating, *Journal of Materials Chemistry A*, 5 (2017) 6648-6655.

[281] C. Jiang, L. Zhang, P. Li, H. Sun, Q.J. Niu, Ultrathin film composite membranes fabricated by novel in situ free interfacial polymerization for desalination, *ACS Applied Materials & Interfaces*, 12 (2020) 25304-25315.

[282] J. Zhu, J. Hou, R. Zhang, S. Yuan, J. Li, M. Tian, P. Wang, Y. Zhang, A. Volodin, B. Van der Bruggen, Rapid water transport through controllable, ultrathin polyamide nanofilms for high-performance nanofiltration, *Journal of Materials Chemistry A*, 6 (2018) 15701-15709.

[283] J. Tian, H. Chang, S. Gao, R. Zhang, How to fabricate a negatively charged NF membrane for heavy metal removal via the interfacial polymerization between PIP and TMC?, *Desalination*, 491 (2020) 114499.

[284] Z. Yang, Z. Zhou, H. Guo, Z. Yao, X. Ma, X. Song, S.-P. Feng, C.Y. Tang, Tannic acid/Fe<sup>3+</sup> nanoscaffold for interfacial polymerization: Toward enhanced nanofiltration performance, *Environmental Science & Technology*, 52 (2018) 9341-9349.

[285] Q. Shi, L. Ni, Y. Zhang, X. Feng, Q. Chang, J. Meng, Poly(p-phenylene terephthamide) embedded in a polysulfone as the substrate for improving compaction resistance and adhesion of a thin film

## References

- composite polyamide membrane, *Journal of Materials Chemistry A*, 5 (2017) 13610-13624.
- [286] L.E. Peng, Z. Yao, Z. Yang, H. Guo, C.Y. Tang, Dissecting the role of substrate on the morphology and separation properties of thin film composite polyamide membranes: Seeing is believing, *Environmental Science & Technology*, 54 (2020) 6978-6986.
- [287] J. Wang, R. Xu, F. Yang, J. Kang, Y. Cao, M. Xiang, Probing influences of support layer on the morphology of polyamide selective layer of thin film composite membrane, *Journal of Membrane Science*, 556 (2018) 374-383.
- [288] X. Li, Q. Li, W. Fang, R. Wang, W.B. Krantz, Effects of the support on the characteristics and permselectivity of thin film composite membranes, *Journal of Membrane Science*, 580 (2019) 12-23.
- [289] A.K. Ghosh, E.M.V. Hoek, Impacts of support membrane structure and chemistry on polyamide-polysulfone interfacial composite membranes, *Journal of Membrane Science*, 336 (2009) 140-148.
- [290] R. Zhang, S. Yu, W. Shi, J. Zhu, B. Van der Bruggen, Support membrane pore blockage (SMPB): An important phenomenon during the fabrication of thin film composite membrane via interfacial polymerization, *Separation and Purification Technology*, 215 (2019) 670-680.
- [291] Z. Yang, P. F. Sun, X. Li, B. Gan, L. Wang, X. Song, H. D. Park, C.Y. Tang, A critical review on thin-film nanocomposite membranes with interlayered structure: Mechanisms, recent developments, and environmental applications, *Environmental science & technology*, 54 (2020) 15563-15583.
- [292] G.Z. Ramon, M.C.Y. Wong, E.M.V. Hoek, Transport through composite membrane, Part 1: Is there an optimal support membrane?, *Journal of Membrane science*, 415-416 (2012) 298-305.
- [293] J. Tian, H. Chang, S. Gao, R. Zhang, How to fabricate a negatively charged NF membrane for heavy metal removal via the interfacial polymerization between PIP and TMC?, *Desalination*, 491 (2020) 114499.
- [294] P.W. Morgan, S.L. Kwolek, Interfacial polycondensation. II. Fundamentals of polymer formation at liquid interfaces, *Journal of Polymer science: Part A: Polymer Chemistry*, 34 (1996) 531-559.
- [295] E.L. Wittbecker, P.W. Morgan, Interfacial polycondensation. I, *Journal of Polymer Science: Part A: Polymer Chemistry*, 34 (1959) 521-529.
- [296] V. Freger, Kinetics of film formation by interfacial polycondensation, *Langmuir*, 21 (2005) 1884-1894.
- [297] B. Yuan, C. Jiang, P. Li, H. Sun, P. Li, T. Yuan, H. Sun, Q.J. Niu, Ultrathin polyamide membrane

## *References*

with decreased porosity designed for outstanding water softening performance and superior antifouling properties, *ACS Applied Materials & Interfaces*, 10 (2018) 43057-43067.

## **Curriculum Vitae**

### **RUIJUN ZHANG**

Date of birth: October 18<sup>th</sup>, 1989

Nationality: Chinese

Gender: Male



### **CONTACT**

Process Engineering for Sustainable Systems (ProcESS)

Department of Chemical Engineering

KU Leuven Chem & Tech

Celestijnenlaan 200F

3001 Heverlee, Leuven, Belgium

Tel: (+86) 18822231917

Email: [ruijun.zhang@kuleuven.be](mailto:ruijun.zhang@kuleuven.be), [zrj@hebut.edu.cn](mailto:zrj@hebut.edu.cn).

## **EDUCATION**

- Nov. 2017-Present      Ph.D in Chemical Engineering  
   KU Leuven, Belgium
- Sept. 2014-Dec. 2018      Ph.D in Municipal Engineering  
   Harbin Institute of Technology, China
- Sept. 2012-Jun. 2014      Bachelor in Civil Engineering  
   Harbin Institute of Technology, China
- Sept. 2008-Jun. 2012      Bachelor in Water Supply and Drainage  
   North China University of Science and Technology, China

## **RESEARCH INTERESTS**

- Synthesis and modification of NF membrane
- Evaluation and characterization of NF membrane
- Application of NF technology in the treatment of industry wastewater
- Analysis of membrane fouling mechanism
- Exploration of membrane cleaning strategy

## **PPUBLICATIONS**

- 1) **Ruijun Zhang**, Jiayu Tian, Shanshan Gao, Bart Van der Bruggen. How to coordinate the trade-off between water permeability and salt rejection in nanofiltration? *Journal of Materials Chemistry A*, 8 (2020) 8831-8847
- 2) **Ruijun Zhang**, Shuili Yu, Wenxin Shi, Wei Wang, Xiaoying Wang, Zhiqiang Zhang, Li Li, Bing Zhang, Xian Bao. A novel polyesteramide thin film composite nanofiltration membrane prepared by interfacial polymerization of serinol and

### *Curriculum Vitae*

trimesoyl chloride (TMC) catalyzed by 4-dimethylaminopyridine (DMAP), *Journal of Membrane Science*, 542 (2017) 68-80.

- 3) **Ruijun Zhang**, Shuili Yu, Wenxin Shi, Junyong Zhu, Bart Van der Bruggen. Support Membrane Pore Blockage (SMPB): An Important Phenomenon during the Fabrication of Thin film Composite Membrane via Interfacial Polymerization, *Separation and Purification Technology*, 215 (2019) 670-680.
- 4) **Ruijun Zhang**, Shuili Yu, Wenxin Shi, Xiaoying Wang, Jun Cheng, Zhiqiang Zhang, Li Li, Xian Bao, Bing Zhang. Surface modification of piperazine-based nanofiltration membranes with serinol for enhanced antifouling properties in polymer flooding produced water treatment, **RSC Advances**, 7(77) (2017) 48904-48912.
- 5) Jiayu Tian, Hailin Chang, Shanshan Gao, Yue Zong, Bart Van der Bruggen, **Ruijun Zhang\***. Direct generation of an ultrathin (8.5 nm) polyamide film with ultrahigh water permeance via in-situ interfacial polymerization on commercial substrate membrane. *Journal of Membrane Science*, 634 (2021) 119450.
- 6) Jiayu Tian, Hailin Chang, Shanshan Gao, **Ruijun Zhang\***. How to fabricate a negatively charged NF membrane for heavy metal removal via the interfacial polymerization between PIP and TMC? *Desalination*, 491 (2020) 114499.
- 7) Shushan Yuan, Jasper Swartenbroekx, Yi Li, Junyong Zhu\*, Frederik Ceysensc, JianLi, **Ruijun Zhang\***, Alexander Volodine, Peter Van Puyvelde, Bart Vander Bruggen. Facile synthesis of Kevlar nanofibrous membranes via regeneration of hydrogen bonds for organic solvent nanofiltration, *Journal of Membrane Science*, 573 (2019) 612-620.
- 8) Zhu Junyong, Hou Jinwei, Yuan Shushan\*, Zhao Yan, Li Yi, **Ruijun Zhang\***, Tian Miaomiao, Li Jian, Wang Jing, Bart Vander Bruggen. MOFs-positioned polyamide

- membrane with fishnet-like structure for elevated nanofiltration performance, *Journal of Materials Chemistry A*, 7 (2019) 16313-16322.
- 9) **Ruijun Zhang**, Wenxin Shi, Shuili Yu, Wei Wang, Zhiqiang Zhang, Bing Zhang, Li Li, Xian Bao. Influence of salts, anion polyacrylamide and crude oil on nanofiltration membrane fouling during desalination process of polymer flooding produced water, *Desalination*, 373 (2015) 27-37.
- 10) **Ruijun Zhang**, Shuili Yu, Wenxin Shi, Jiayu Tian, Limei Jin, Bing Zhang, Li Li, Zhiqiang Zhang. Optimization of a membrane cleaning strategy for advanced treatment of polymer flooding produced water by nanofiltration, *Rsc Advances*, 6(34) (2016) 28844-28853.
- 11) **Ruijun Zhang**, Shengnan Yuan, Wenxin Shi, Cong Ma, Zhiqiang Zhang, Xian Bao, Bing Zhang, Yan Luo. The impact of anionic polyacrylamide (APAM) on ultrafiltration efficiency in flocculation-ultrafiltration process, *Water Science & Technology*, 75(8) (2017) 1982-1989.
- 12) Zhengyang Gu, Shuili Yu, Junyong Zhu, Ping Li, Xuerui Gao, **Ruijun Zhang**. Incorporation of lysine-modified UiO-66 for the construction of thin-film nanocomposite nanofiltration membrane with enhanced water flux and salt selectivity, *Desalination*, 493 (2020) 114661.
- 13) Junyong Zhu, Jingwei Hou, **Ruijun Zhang**, Shushan Yuan, Jian Li, Miaomiao Tian, Penghui Wang, Yatao Zhang, Alexander Volodin, Bart Van der Bruggen. Rapid water transport through controllable, ultrathin polyamide nanofilms for high-performance nanofiltration, *Journal of Materials Chemistry A*, 6 (2018) 15701-15709.
- 14) Xian Bao, Qinglian Wu, Wenxin Shi, Wei Wang, Huarong Yu, Zhigao Zhu, Xinyu Zhang, Zhiqiang Zhang, **Ruijun Zhang**, Fuyi Cui. Polyamidoamine dendrimer

grafted forward osmosis membrane with superior ammonia selectivity and robust antifouling capacity for domestic wastewater concentration, *Water Research*, 153 (2019) 1-10.

## **PATENTS**

- 1) Shuili Yu, **Ruijun Zhang**, Wenxin Shi; One kind of nanofiltration membrane cleaning agent and cleaning method for the treatment of polymer flooding produced water. No. **CN104474905B**.
- 2) Shuili Yu, **Ruijun Zhang**, Wenxin Shi; The fabrication method of a polyestamide thin film composite nanofiltration membrane with strong chlorine resistance and antifouling ability. No **CN106345308B**.
- 3) Jiayu Tian, **Ruijun Zhang**, Feng Xiao, Shanshan Gao, Xiangkun Li; MBR device for wastewater treatment and its operation method. No. **CN111018098B**.

## **CONFERENCE**

- 1) **Ruijun Zhang**, Fabrication and characterization of a novel polyestamide thin film composite nanofiltration membrane via catalyzed interfacial polymerization, The 6th IWA Regional Membrane Technology Conference (IWA-RMTC2018). 10-12 December 2018. Vadodara, Gujarat, India.
- 2) **Ruijun Zhang**, Investigations on membrane fouling mechanisms when treating polymer flooding produced water by nanofiltration, *Engineering With membranes 2015 (EWM2015)*. 6-10 May 2015. Beijing, China.
- 3) **Ruijun Zhang**, Study on Membrane Cleaning Strategy for Advanced Treatment of Polymer Flooding Produced Water by Nanofiltration, *The 8th International Conference on Challenges in Environmental Science & Engineering (CESE2015)*. 28 September-2 October 2015, Sydney, Australia.